



University
of Glasgow

Sutardi, Tata (2019) *The development of coal particle gasification model with application leading to underground coal gasification*. PhD thesis.

<http://theses.gla.ac.uk/75183/>

Copyright and moral rights for this work are retained by the author

A copy can be downloaded for personal non-commercial research or study, without prior permission or charge

This work cannot be reproduced or quoted extensively from without first obtaining permission in writing from the author

The content must not be changed in any way or sold commercially in any format or medium without the formal permission of the author

When referring to this work, full bibliographic details including the author, title, awarding institution and date of the thesis must be given

Enlighten: Theses

<https://theses.gla.ac.uk/>
research-enlighten@glasgow.ac.uk

The development of coal particle gasification model with application leading to underground coal gasification

Tata Sutardi

Submitted in fulfilment of the requirements for the
Degree of Doctor of Philosophy

School of Engineering
College of Science and Engineering
University of Glasgow



University
of Glasgow

February 2019

Abstract

The development of Underground Coal Gasification (UCG) modelling has been carried out for many years and this study is an attempt to improve the mechanisms of thermochemical processes in an existing model. The understanding of the thermochemical behaviour of coal gasification reactions is important because it influences gas production simultaneously with a coal mass reduction.

A coal particle model was developed to investigate the thermochemical processes of gasification for underground coal applications. The chemical reactions were defined with an Eddy Break Up (EBU) model for controlling the reaction mechanisms and the study was particularly focused on identification and roles of the important kinetic parameters. At initial validation, coal particle oxidation based on the combustion experimental results with drop tube furnace, is used for comparison. With regards to the results, the best agreement of coal oxidation is achieved with the pre-exponent factor (A) of 0.002 and 85500, for the reactions, R2 ($C + O_2 = CO_2$) and R3 ($C + 0.5O_2 = CO$), respectively. The gasification reactions are subsequently applied for the thermochemical process investigation and the kinetic parameters for this application are also identified.

A kinetic parameter study was also conducted to identify the difference between bituminous and lignite coals through the comparison parameter of ignition delay time. With seven reaction mechanisms applied to represent coal combustion, this study identified that the ignition delay time difference was significantly affected by the devolatilization reaction. This reaction is important for predicting the ignition delay time of coal particle combustion. For the simulation case, two types of coal, named PSOC 1451 and PSOC 1443, were examined numerically and the results are compared with the experimental data. Existing kinetic parameters for the devolatilization reaction R1 (Coal \rightarrow Coalvolatile + char) underestimate the ignition delay time which is largely influenced by the value of the pre-exponent factor (A) of R1. Results giving the best agreement with

the experiment are obtained with $A = 3.12 \times 10^5$ and 9.36×10^7 for PSOC 1451 and PSOC 1443, respectively.

The UCG application could be friendlier to the environment, since the cavity formed potential to be used as CO₂ storage and the process itself has a promising role on utilising CO₂. For initial investigation, several gasification simulations were conducted by involving the CO₂ at the drop tube furnace as a reactor, and syngas production was investigated. The results showed that the syngas production at the reactor environment's condition with higher CO₂ has better products of H₂, CO and CH₄. When investigating the syngas quality, several gasification simulations with the addition of steam (H₂O) into the reactor were carried out and the results showed that the more concentration of H₂ was obtained at the higher steam condition. However, the study with combining the CO₂ and H₂O in the reactor's environment was also carried out with the results showing a promising indicator in producing the better syngas quality.

This investigation through the simulation performance also identified the gas formation behaviour in the gasification reactions. The production of H₂ and CO is controlled significantly by the level of oxygen concentration via the char reactions. However, their production rates are strongly dependent upon the reaction zones of gasification. For example, CO is produced in both oxidation and reduction reaction zones, while H₂ production dominates the reduction zone. Spatio-temporal distributions of the gas species along with the coal particle temperature provide additional information for further development of UCG modelling. With these results, the model indicates a capability to provide good guidelines with the associated thermochemical processes that can help to develop robust coal gasification technology and lead to improved syngas quality.

The effects of particle size have been identified through the model simulation and experiments. In the results of the simulation, the particle size has a greater effect on the heterogeneous reactions. In the case of CO formation, the smaller particle size has greater products in the unit of mole fraction over the area of generation. However, in the experimental results the effect of particle size variation causes the varieties of coal in the packed bed porosity. The smaller particle size causes less porosity, and therefore a lower rate of gas productions. This is because the porosity contributes to providing access to oxygen to react with coal.

The effects of temperature variation has also been investigated through the model simulation and experimental procedures. The results through the simulation suggest that

the temperature encourages better reactions and therefore more gas products are obtained at the higher temperature either in the results of model simulation or experimental procedures.

Finally, an experiment was also conducted to identify the effect of gas flowrate variations. The air flowrate needs to be injected in order to keep coal reactions occurring simultaneously, because the coal stock moves downstream during the gasification. The results show that a higher flowrate resulted in a greater area of coal surface reactions and also a higher concentration of gas products. It indicates that the greater flowrate need to be presented as more pressure is needed to maintain the reactions occurring at the coal stock which lies further upstream.

Contents

Abstract	i
Contents	iv
List of Tables	vii
List of Figures	viii
Acknowledgement	xii
Declaration	xiii
Publications from this work	xiv
List of Symbols	xvi
List of Abbreviations	xix
Chapter 1 Introduction	1
1.1 History and development.....	2
1.2 Process overview of UCG	5
1.2.1 Linking wells mechanisms	6
1.2.2 Chemical process mechanisms.....	10
1.2.3 Physical parameters which affect the coal seam reactions.....	12
1.3 Purpose of the work.....	17
1.4 The Importance of this research	18
1.5 Thesis outline	18
Chapter 2 Literature review	20
2.1 Introduction	20
2.2 UCG Modelling	21
2.2.1 Packed bed models.....	21
2.2.2 Channel models.....	24
2.2.3 Coal slab models.....	29
2.3 A Review for study development.....	32
Chapter 3 Methodology for the development of a single coal particle model in drop tube furnace	34
3.1 Gasification reaction mechanisms	34
3.1.1 Heterogeneous reaction.....	35
3.1.2 Homogenous reaction	37
3.2 Governing equations.....	37

3.3 Turbulence model.....	39
3.4 Thermal radiation	42
3.5 Reaction-flow	43
3.5.1 Standard EBU	45
3.5.2 Hybrid EBU	45
3.5.3 Kinetic EBU.....	46
3.6 Coal particle properties.....	46
3.7 Numerical procedures.....	48
3.7.1 Modelling space.....	48
3.7.2 Modelling time.....	48
3.7.3 Modelling flow and reactions	48
Chapter 4 Coal particle model development with a kinetic parameter study	50
4.1 Introduction	50
4.2 Coal Particle model development.....	52
4.2.1 The geometry of the model and boundary conditions	52
4.2.2 The grid selection and sensitive study	54
4.2.3 The coal properties.....	57
4.3 Overview of the kinetic parameters.....	58
4.4 Process investigation with validation	61
4.4.1 Investigation of the kinetic parameters of R2 and R3	63
4.4.2 Validation process of coal oxidation	64
4.3 Investigation of other combustion reactions	68
4.4 Model application in various oxygen fractions	72
4.5 Applying the model for lignite coal (PSOC 1443).....	74
4.5 Conclusion.....	78
Chapter 5 Coal particle gasification development to investigate the reactions’ behaviour with applications leading to UCG	80
5.1 Introduction	80
5.2 Investigation of single coal particle gasification processes.....	82
5.2.1 Effect of kinetic parameter variations.....	82
5.2.2 Comparison between combustion and gasification	87
5.2.3 Maintaining char in the coal particle gasification.....	90
5.3 Coal particle gasification.....	91
5.3.1 Effects of coal particle diameters.....	91
5.3.2 Simulation performance in various temperatures	95
5.4 Gasification performance at various environments	98
5.4.1 Study on the effect of steam (H ₂ O).....	99
5.4.2 Study on the effect of CO ₂	101
5.4.3 Study on the effect of combining H ₂ O and CO ₂ with excess oxygen.....	104

5.4.4 Study on the effect of combining H ₂ O and CO ₂ without oxygen	106
5.5 Investigation of UCG processes	108
5.6 Conclusion	113
Chapter 6 Experimental investigation of thermochemical processes of coal particle packed bed	115
6.1. Introduction	115
6.2 Experimental set-up.....	115
6.2.1 Equipment and instrumentations	116
6.2.2. Coal particle properties and preparation	120
6.3 Experimental procedures	121
6.3.1 Test procedures to investigate the effect of particle size variation.....	122
6.3.2 Test procedures to investigate the effect of temperature variation	123
6.3.3 Test procedures to investigate the effect of air flowrate variation	123
6.4 Results and discussion.....	124
6.4.1 Investigation of the effect of particle size variation	124
6.4.2 Investigation of the effect of temperature variation.....	130
6.4.3 Investigation of the effect of air flowrate variation	136
6.5 Possible results that relevant with UCG application	139
6.6 Conclusion.....	140
Chapter 7 Final conclusions and recommendations for future work	143
7.1 Conclusions	143
7.2 Recommendations for future work.....	145
Appendix A Equipment and Instruments.....	146
Appendix B Microanalysis	158
Bibliography	160

List of Tables

Table 1-1. UCG Development from the 1930s to 2000 [5, 7, 9]	2
Table 1-2. Main reactions of gasification process [25].....	11
Table 2-1. Comparison of some essential features in packed bed models [9]	24
Table 2-2. Reaction rate control mechanisms for each research development [9]	24
Table 2-3. Comparison of some essential features in channel models [9].....	28
Table 2-4. Reaction rate control mechanisms for each research development [9]	28
Table 2-5. Comparison of some essential features in slab models [9].....	31
Table 2-6. Reaction rate control mechanisms for each research development [9]	32
Table 3-1. Main gasification reactions [25, 54]	35
Table 4-1. The furnace boundary conditions	53
Table 4-2. Reaction Mechanisms of coal combustion [93, 103].....	53
Table 4-3. Mesh resolution used for study.....	54
Table 4-4. Chemical compositions of coal [105].....	57
Table 4-5. Parameters of chemical kinetics from different studies [53].....	58
Table 4-6. Variation of kinetic parameters value of R2 and R3 [53].....	63
Table 4-7. The ID for combination of Simulation 3 with R4, R5 and R8 in addition to the base case.....	68
Table 4-8. The best fit kinetic parameter values used for combustion	72
Table 4-9. Parameter comparison between the experiments and simulation.....	78
Table 5-1. Kinetic parameter value variations of gasification reactions	82
Table 5-2. Scheme for identification of the kinetic parameters of gasification.....	83
Table 5-3. The kinetic parameter values used in gasification reactions	87
Table 6-1. Gas sensor specification	119
Table 6-2. The chemical and physical properties of charcoal.....	120
Table 6-3. Boundary condition of test with particle size variation	122
Table 6-4. Boundary conditions of test with temperature variation	123
Table 6-5. Boundary conditions of test with flowrate variation	124

List of Figures

Figure 1-1. Schematic diagram of UCG process and utilization (redrawn from <i>Yang et al.</i> [6]).....	1
Figure 1-2. Cavity Formation of UCG (redrawn from <i>Bhutto et al.</i> [5] & <i>Perkins et al.</i> [19]).....	6
Figure 1-3. Linked vertical well method (a) FCL, and (b) RCL (redrawn from <i>Blinderman et al.</i> [21] and <i>Kumar et al.</i> [8])	7
Figure 1-4. CRIP method mechanisms (a) linear and (b) long wall (redrawn from <i>Portman energy</i> [20] and <i>Kumar et al.</i> [8])	8
Figure 1-5. SWIFT path formation mechanisms (redrawn from <i>Portman energy</i> [20])	10
Figure 1-6. Gasification reaction process of underground seam coal (redrawn from <i>Bhutto et al.</i> [5] and <i>Yang L et al.</i> [24])	11
Figure 2-1. Coal block model for cavity formation experiments (redrawn from <i>Shannon et al.</i> [59])	21
Figure 2-2. Channel model illustration (redrawn from <i>Gunn et al.</i> [49])	25
Figure 2-3. Scheme of coal block models (redrawn from <i>Khan et al.</i> [9]).....	29
Figure 3-1. Coal Particle Gasification Process	34
Figure 4-1. Drop tube furnace for coal particle combustion experiments [105]	50
Figure 4-2. The signal outputs transformed to the temperature profiles of coal particle combustion for (a) Bituminous coal (PSOC-1451), and (b) Lignite coal (PSOC-1443) conducted by <i>Levendis et.al</i> [105]	51
Figure 4-3. The furnace illustration (a) Furnace cylindrical shape (b) Axisymmetric model grid	52
Figure 4-4. Grid size variation test for gas temperature along the centre line	55
Figure 4-5. Contour plot of temperature distribution inside the furnace	55
Figure 4-6. Grid size variation test for gas temperature along the radial direction at $x=0.1$ m, $x=0.3$ m, and $x=0.7$ m.....	56
Figure 4-7. The logarithmic value of k variation in R2.....	59

Figure 4-8. The logarithmic value of k variation in R3.....	59
Figure 4-9. The logarithmic value of k variation in R4.....	60
Figure 4-10. The logarithmic value of variation in R5	60
Figure 4-11. The logarithmic value of k variation in R8.....	60
Figure 4-12. The results of Simulation 1 (sub-optimal parameters) and the experiment, to show the discrepancy	62
Figure 4-13. Comparison of T_{cv} obtained in simulations	65
Figure 4-14. Comparison of T_{char} obtained in simulations.....	65
Figure 4-15. Comparison of coal volatile fraction	66
Figure 4-16. Comparison of char fraction profile	66
Figure 4-17. Temperature comparison between experiment and Simulation 3	67
Figure 4-18. Time comparison between experiment and Simulation 3	67
Figure 4-19. The comparison of Simulation 4 and various kinetic parameters of R4, for parameter (a) Char profile, and (b) Temperature profile	69
Figure 4-20. The comparison of Simulation 5 and various kinetic parameters of R5, for parameter (a) Char profile, and (b) Temperature profile	70
Figure 4-21. The comparison of Simulation 8 and various kinetic parameters of R8, for parameter (a) Char profile, and (b) Temperature profile	71
Figure 4-22. The comparison for maximum temperature between experiment and simulation.....	73
Figure 4-23. The comparison for coal volatile burn out time between experiment and simulation.....	74
Figure 4-24. The comparison for char burn out time between experiment and simulation	74
Figure 4-25. Devolatilization reaction process without combustion	76
Figure 4-26. Devolatilization reaction with combustion.....	76
Figure 4-27. The char profile for each simulation	77
Figure 5-1. Process illustration of coal particle gasification model and UCG	80
Figure 5-2. Comparison results for R9 (a) H_2 & CO , and (b) CH_4 & CO_2	83
Figure 5-3. The comparison results for R10 (a) H_2 & CO , and (b) CH_4 & CO_2	84
Figure 5-4. The comparison results for R11 (a) H_2 & CO , and (b) CH_4 & CO_2	85
Figure 5-5. The comparison results for R12 (a) H_2 & CO , and (b) CH_4 & CO_2	86
Figure 5-6. Comparison of combustion and gasification for char in particle fractions ..	87
Figure 5-7. Comparison of combustion and gasification for (a) CO_2 , H_2O and CH_4 and (b) H_2 and CO gas species.....	88

Figure 5-8. Comparison CO ₂ and CO in various oxygen conditions in mass average of mole fraction	89
Figure 5-9. The continuous coal injection for maintaining the char in the reactor	90
Figure 5-10. Molar concentration of H ₂ in a variation of coal particle diameters (μm) (a) 60 (b) 75 (c) 100.....	91
Figure 5-11. Molar concentration of CO in variations of coal particle diameters (μm) (a) 60 (b) 75 (c) 100.....	92
Figure 5-12. Molar concentration of CO ₂ in variations of coal particle diameters (μm) (a) 60 (b) 75 (c) 100	92
Figure 5-13. Mass average mole fraction results for CO and H ₂	93
Figure 5-14. Mass average mole fraction results for CO ₂ and CH ₄	94
Figure 5-15. Molar concentration of H ₂ in various temperatures (K) (a) 1000, (b) 1200, and (c) 1400	95
Figure 5-16. Molar concentration of CO in various temperatures (K) (a) 1000, (b) 1200, and (c) 1400	96
Figure 5-17. Molar concentration of CO ₂ in various temperatures (K) (a) 1000, (b) 1200, and (c) 1400	96
Figure 5-18. The gas products of H ₂ and CO at temperature variations	97
Figure 5-19. Mass average mole fraction of CH ₄ and CO ₂ at temperature variations	98
Figure 5-20. The particle temperature and char profile in H ₂ O environment.....	99
Figure 5-21. H ₂ and CO production under various H ₂ O condition.....	100
Figure 5-22. The comparison result of the addition of H ₂ O for (a) CH ₄ and (b) CO ₂ ..	100
Figure 5-23. Particle temperatures and char mass fraction comparisons.....	101
Figure 5-24. Particle temperature and char mass fraction in CO ₂ variations.....	102
Figure 5-25. CO and H ₂ comparisons in CO ₂ variation.....	103
Figure 5-26. CH ₄ comparison in CO ₂ variations and air.....	103
Figure 5-27. Particle temperature and char mass fraction in the CO ₂ /H ₂ O variations..	104
Figure 5-28. The gas CO and H ₂ productions in some CO ₂ and H ₂ O ratios.....	105
Figure 5-29. The gas CH ₄ production in some CO ₂ and H ₂ O ratios	105
Figure 5-30. Particle temperatures and char fractions' comparison in CO ₂ /H ₂ O ratio variation	106
Figure 5-31. H ₂ and CO comparisons in the CO ₂ /H ₂ O ratio variations	107
Figure 5-32. Comparison of CH ₄ in CO ₂ /H ₂ O background variations, and O ₂ used as a balance when the total concentration of CO ₂ and H ₂ O were not 100%	108
Figure 5-33. Contour plot of reactor temperature	109

Figure 5-34. Contour plot of oxygen inside the reactor	110
Figure 5-35. Contour plot of CO ₂ inside the reactor	110
Figure 5-36. Contour plot of CO inside the reactor	111
Figure 5-37. Contour plot of H ₂ inside the reactor	111
Figure 5-38. Contour plot of CH ₄ inside the reactor	112
Figure 5-39. Coal particle block/bed packed inside the reactor	114
Figure 6-1. Illustration of coal particle bed packed in a reactor	116
Figure 6-2. Schematic diagram for experiments	116
Figure 6-3. Rig as a main reactor with access of air flow	117
Figure 6-4. Ceramic with pores and heater wire	118
Figure 6-5. Thermocouple position in the coal bed area from top and side view	118
Figure 6-6. Equipment installation for coal particle experiment	120
Figure 6-7. The char coal in three different sizes.....	121
Figure 6-8. Schematic process for particle size variation test from the side view	122
Figure 6-9. Schematic process for temperature variation test from side view	123
Figure 6-10. Temperature profile for each channel in bed of coals A, B and C	125
Figure 6-11. The reaction propagation over a certain time period for coals A, B, and C	126
Figure 6-12. Gas products of coal bed reactions for (a) CO ₂ , (b) CO, and (c) CH ₄	128
Figure 6-13. Excess oxygen in gas products	129
Figure 6-14. Reaction propagation of surface coal packed bed for coal C	130
Figure 6-15. Reaction front propagation of surface coal packed bed for coal A	131
Figure 6-16. Reaction front propagation of surface coal packed bed for coal B	132
Figure 6-17. Gas products of coal C in various temperature (a) CO ₂ , (b) CO, and (d) CH ₄	134
Figure 6-18. Gas products of coal A at various temperatures (a) CO ₂ , and (b) CO.	135
Figure 6-19. Gas products of coal B at various temperatures (a) CO ₂ , and (b) CO.....	136
Figure 6-20. Reaction propagation of coal C in different air flowrates	137
Figure 6-21. Gas products of coal C in various flowrates (a) CO ₂ , (b) CO, and (c) CH ₄	138
Figure 6-22. Excess oxygen concentration for each flowrate condition.	139

Acknowledgement

For their insight and encouragement, there are so many people who deserve to be thanked for helping me to complete this PhD, but firstly, I would like to thank Allah for his many blessings and countless favours, and for giving me the health and the patience from the beginning to the end of this research study.

I owe a matchless and sincere gratitude to my supervisors, Dr Manosh C. Paul and Dr Nader Karimi for their help and support. I would like to offer them my deepest thanks for their consistent support, warm encouragement, wise criticisms, insightful suggestions, scientific guidance and inspiring determination in preparing and improving this thesis.

I must acknowledge the Ministry of Research, Technology and Higher Education of Republic Indonesia, for their funding through the Research and Innovation in Science and Technology Project (RISET-Pro). In addition, my deep appreciation goes to my work institution, the Agency for Assessment and Application of Technology (BPPT), Republic of Indonesia, for all their support during my study.

I am delighted to thank all my group members for their support, encouragement and all the good times. In particular, many thanks to Loizos Christodoulou, Linwei Wang, Alexander Elliot, Graeme Hunt, Ainul Nadirah, Ahmed Morsy, Tananop Piemsinlapakunchon, Prashant Ram Kamble, and Skriptyan Noor. Further, thanks to all the members of the academic staff, IT staff, technical staff and administrative staff of the School of Engineering who have helped during the course of this work.

Finally, I am deeply indebted to my parents who dedicated their lives to ensure my success in my academic programme. I am very grateful to them for their moral support and encouragement during my stay abroad. I really owe them much that I cannot express. Most special thanks are to Rinrin, my wife and my children Razan, Masyel and Keyaan for always being here for me. They shared the joy and pain with me. I extend my thanks to my brothers, sisters and relatives who stood by me. I love you.

Declaration

I am aware of and understand the policy of the University of Glasgow regarding plagiarism and I certify that the work in this thesis is my own, except where indicated by referencing, and is in accordance with University and School guidance on good academic conduct.

.....

Tata Sutardi

February, 2019

Publications from this work

Book Chapter

No	Description
1	<u>Ahmed M Salem</u> , <u>Umesh Kumar</u> , <u>Ainul Nadirah Izaharuddin</u> , <u>Harneek Dhami</u> , <u>Tata Sutardi</u> and <u>Manosh C. Paul</u> . Advanced Numerical Methods for the Assessment of Integrated Gasification and CHP Generation Technologies (In: Coal and Biomass Gasification: Fundamentals, Recent Advances and Future Challenge) Springer Publisher, 2017, ISBN 978-981-10-7334-2, pp.307-330.

Journal Articles

No	Description
1	<u>Sutardi, T.</u> , <u>Paul, M. C.</u> , <u>Karimi, N.</u> and <u>Younger, P. L.</u> Numerical Study of the Effects of CO₂ Addition in Single Coal Particle Gasification. (Energy Procedia, Volume 142, 2017, Pages 1306-1311.)
2	<u>Sutardi, T.</u> , <u>Wang, L.</u> , <u>Manosh C. Paul</u> , and <u>Nader Karimi</u> . Numerical simulation approaches for modelling a single coal particle combustion and gasification. (Engineering Letter, Volume 26, Issue 2, 30 May 2018, Pages 257-266)
3	<u>Wang, L.</u> , <u>Nader Karimi.</u> , <u>Sutardi, T.</u> , and <u>Manosh C. Paul</u> . Numerical modelling of unsteady transport and entropy generation in oxy-combustion of single coal particles with varying flow velocities and oxygen concentrations. (Applied Thermal Engineering, Volume 144, 2018, Pages 147-164)
4	<u>Sutardi, T.</u> , <u>Manosh C. Paul</u> , and <u>Nader Karimi</u> . Investigation of Coal Particle Gasification Process with Application Leading to Underground Coal Gasification. (Fuel, V237 (2019) pp1186–1202),
5	<u>Linwei Wang</u> , <u>Nader Karimi</u> , <u>Tata Sutardi</u> , and <u>Manosh C Paul</u> . Combustion characteristics and pollutant emissions in transient oxy-combustion of a single biomass particle-A numerical study , (Energy and Fuel, 2019, Accepted).

Proceedings

No	Description
1	<u>Sutardi, T., Paul, M. C. , Karimi, N. and Younger, P. L. .</u> Identifying Kinetic Parameters for Char Combustion of a Single Coal Particle. (Digital Proceeding for 8th European Combustion Meeting (ECM2017)), Dubrovnik, Croatia, 18-21 April 2017, ISBN 978-953-59504-0-0, pp. 1134-1139
2	<u>Sutardi, T., Paul, M. C. , Karimi, N. and Younger, P. L.</u> Numerical Modelling for Process Investigation of a Single Coal Particle Combustion and Gasification. (Proceeding of World Congress on Engineering 2017 (WCE 2017) Vol.2), Imperial College - London, UK, 5-7 July 2017, ISSN: 2078-0966. pp.946-951.
3	<u>Sutardi, T., Paul, M. C. , and Karimi, N.</u> Numerical Investigation on Kinetic Parameter of Coal Devolatilization Reaction by Identifying Ignition Delay Parameter. (Proceeding of World Congress on Engineering and Computer Science 2018 (WCECS 2018) UC-Berkeley-San Francisco, California USA, 23 – 25 October 2018).

Posters

No	Description
1	<u>Sutardi, T., Paul, M. C. , Karimi, N. and Younger, P. L. .</u> Study on the Thermochemical Processes of Coal Particle Gasification: Application leading to Underground Coal Gasification (Poster Presentation on 29 th edition of the Scottish Fluid Mechanics Meeting, Edinburgh, 20 May 2016)
2	<u>Sutardi, T., Scotchfield, A., Paul, M. C. , Karimi, N. and Younger, P. L.</u> Syngas From Underground Coal Gasification. (Poster was presented in All Energy Conference and Exhibition, Glasgow, 10 – 11 May 2017 and also in Innovation in Gasification and CHP Technology (IGATE), Glasgow, 23 May 2017)

Awards

No	Name
1	Merit Award (for Student) on The World Congress on Engineering (WCE) 2017, International Conference of IAENG, Imperial College – London, UK, 5 – 7 July 2017.
2	Best Student Paper Award of International Conference on Chemical Engineering (ICCE) 2018, in UC-Berkeley, California, USA, 23 – 25 October 2018.

List of Symbols

Roman Symbol

A	Pre- exponential factor (unit vary)
A_{ebu}	EBU rate coefficient A
A_p	Surface area of particle (m^2)
B_{ebu}	EBU rate coefficient B
C_g	Reactant gas concentration (kmol/kg)
D_m	Diffusion coefficient (m^2/s)
E	Total energy (J)
E_a	Activation Energy (J/kmol)
F	External force, vector (N)
G	Filter function that satisfies the normalisation
g_i	Gravitational acceleration
h_s	Heat source ($W/m^2 K$)
H_{rxn}	Low heating value (kJ/kg)
$H_f CV$	Heat of formation of coal volatile
I_λ	Radiative intensity at wavelength λ ($W/(m^2 srm^{-1})$)
$I_{b\lambda}$	Black body intensity at wavelength λ
$I_{pb\lambda}$	Particle blackbody intensity at wavelength λ and current particle temperature
Y_i	Mass fraction of species i
k_i	Reaction rate coefficient of species i
k_{devol}	Reaction rate coefficient for devolatilization reaction
k_m	Mass transfer coefficient
$k_{a\lambda}$	Absorption coefficient at wavelength λ (m^{-1})
$k_{s\lambda}$	Scattering coefficient at wavelength λ (m^{-1})
$k_{pa\lambda}$	Particle absorption coefficient at wavelength λ (m^{-1})
$k_{s\lambda}$	Particle scattering coefficient at wavelength λ (m^{-1})
m	Total mass particle/species (kg)

m_i	Mass fraction
M_i	Molecular weight of species i
M_w	Molecular weight of solid reactant
p_{ij}	Rate exponent of reacting species
h	Enthalpy (kJ/kg)
J_i	The flux of species i
s_b	Stefan-Boltzmann constant ($5.67 \times 10^{-8} W/m^2.K^4$)
S_m	Source of mass (kg)
Sh	Sherwood number
T	Temperature (K)
T_s	Temperature of surface (K)
T_{sur}	Temperature surroundings (K)
Y_i	Mass fraction of species i
YY	Mass stoichiometric coefficient
Y_F	Fuel mass fraction
Y_o	Oxidizer mass fraction
p	Pressure (Pa)
R	Rate of consumption of solid reactant (kg/s)
R_u	Universal gas constant ($8.314 J.K^{-1}mol^{-1}$)
r	Radius/ displacement in radial coordinate (m)
r_F	Rate of fuel depletion (m^3/s)
$C_{\varepsilon 1}; C_{\varepsilon 2}$	Model constant
s_o	Ratio of oxidizer mass coefficient and fuel coefficient
t	Time (s)
x	Distance/displacement in axial coordinate (m)
u	Velocity (m/s)
t_{id}	Ignition delay time (s)
t_{cv}	Coal volatile burnt out time (s)
t_{char}	Char burn out time (s)
T_{cv}	Maximum temperature coal volatile combustion (K)
T_{char}	Maximum temperature char combustion (K)
W_F	Molecular weight of fuel

Greek Symbol

α_i	Particle volume fraction
β	Temperature exponent
β_λ	Extinction coefficient
ϵ	Turbulence dissipation rate
k	Turbulence kinetic energy
τ_{xr}	Stress tensor
ϕ	Ratio of stoichiometric of solid and gas reactant
ρ	Density (kg/m ³)
ρg_x	Gravitational body force
μ, λ	Viscosity coefficient (kg/m.s)
σ	Turbulent Prandtl number
δ	Kronecker delta
μ_t	Turbulent viscosity
μ_B	Bulk viscosity
ω	Field function of k/ϵ
Ω	Solid angle
τ_{turb}	Turbulent time scale (s)

Subscript

p	Particle
x, r, i, j, k	Direction and species or phase
cv	Coal volatile matter
k	Properties of turbulent kinetic energy
ϵ	Properties of turbulent dissipation rate

List of Abbreviations

<i>AERI</i>	Alberta Energy Research Institute
<i>CCS</i>	Carbon Capture Storage
<i>CECEP</i>	Chinese Energy Conservation and Environmental Protection Group
<i>CFD</i>	Computational Fluid Dynamics
<i>CIL</i>	Coal India Limited
<i>CIRI</i>	Cook Inlet Region Incorporated
<i>CMPDI</i>	Central Mine Planning & Design Institute Limited, in India
<i>CRIP</i>	Controlled Retractable Injection Point
<i>CUMTB</i>	Centre of China University of Mining and Technology (Beijing)
<i>DNS</i>	Direct Numerical Simulation
<i>DOM</i>	Discrete Ordinate Method
<i>DTF</i>	Drop Tube Furnace
<i>DTI</i>	Department of Trade and Industry
<i>EBU</i>	Eddy Break-Up
<i>ECM</i>	Eddy Contact Micromixing
<i>EDC</i>	Eddy Dissipation Concept
<i>EPA</i>	Environmental Protection Agency
<i>FCL</i>	Forward Combustion Linking
<i>GIG</i>	Central Mining Institute, in Poland
<i>GTL</i>	Gas to Liquids
<i>HCO</i>	Heat formation of raw coal
<i>HCV</i>	Higher Calorific Value
<i>H_fCV</i>	Heat of formation of coal volatile
<i>HUGE</i>	Hydrogen Oriented Underground Coal Gasification for Europe project
<i>LCV</i>	Lower Calorific Value
<i>LES</i>	Large Eddy Simulation
<i>LFC</i>	Laminar Flame Concept
<i>LLNL</i>	Lawrence Livermore National Laboratories
<i>LVW</i>	Linked Vertical Well
<i>ODE</i>	Ordinary Differential Equation
<i>RANS</i>	Reynold-Averaged Navier-Stokes
<i>RCL</i>	Reverse Combustion Linking
<i>RFCS</i>	Research Fund for Coal and Steel
<i> RNG</i>	Renormalization-Group
<i>RTE</i>	Radiative Transfer Equation

<i>S2S</i>	Surface to Surface
<i>SWIFT</i>	Single Well Integrated Flow Tubing
<i>TCEB</i>	Thar Coal and Energy Board, in Pakistan
<i>TLA</i>	Technology Licence Agreement
<i>UCG</i>	Underground Coal Gasification
<i>US - DOE</i>	US Department of Energy
<i>UTA</i>	Ukrainian Technological Academy

Chapter 1 Introduction

The Survey of Energy Resources was published in 2016 and estimated that the world coal reserves are approximately 890 billion tonnes [1]. The trend for world coal consumption is also likely to increase at an average rate of 0.6% per year, from 6885 million tonnes in 2012 to 8100 million tonnes in 2040 [2]. The top three coal-consuming countries are China, the United States of America and India, which together account for more than 70% of world coal use [3]. It has been suggested that there are greater resources deep underground that could increase the proven coal reserves but these are not mineable with current technology. Underground coal gasification (UCG) is an option to utilise this type of coal reserve [4, 5]. UCG allows the use of coal seams which are technically difficult to exploit (e.g. too thin, too deep, steeply dipping or seams of low ranked coals). Through this process, the coal energy can be extracted as a gas phase, which is known as synthesis gas or syngas. This gas can be used to generate electricity. Furthermore, a cleaning process can be conducted to split CO₂ and increase the calorific value of the fuel-gas. The fuel with gas phase, produces lower emission products than the fuel with solid phase in a combustion process. UCG processes and its utilisation for electricity generation are illustrated in Figure 1-1.

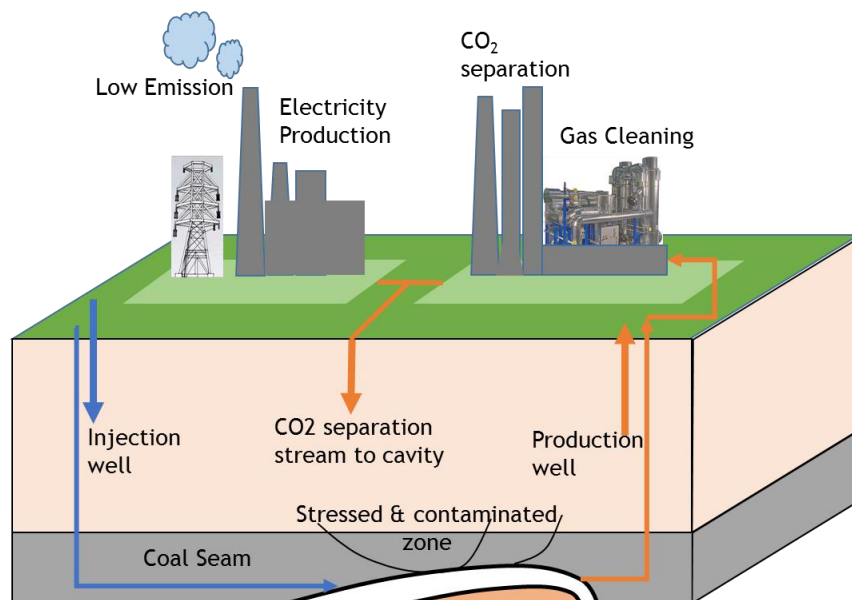


Figure 1-1. Schematic diagram of UCG process and utilization (redrawn from Yang *et al.* [6])

1.1 History and development

The idea of UCG was first mentioned by Sir William Siemens of Great Britain in 1868 [7, 8] and consolidated by the Russian chemist, Dmitri Mendeleev in 1888-1899. Afterwards, the American chemist, A.G. Betts detailed the technical engineering drawing that closely resembles the modern approach, during 1909-1910 [7, 9]. In 1912, the British chemist, Sir William Ramsay expanded the ideas of Betts and the culmination was when he carried out the first UCG experiment at Hett Hill – Durham County in 1912 [7]. UCG technology became commonly available but no further work was done until the 1930s. The global development of UCG from 1930 to 2000 can be seen in Table 1-1.

Table 1-1. UCG Development from the 1930s to 2000 [5, 7, 9]

Site	Country	Start-Up Year	Coal Rank*	Seam Depth (m)	Seam Thickness (m)	Gas Calorific Value (MJ/m ³)
Lisichansk	Russia	1934-36	Bit	24	0.75	3 - 4
Lisichansk		1943-63	Bit	400	0.4	3.2
Gorlovka		1935-41	N/A	40	1.9	6 - 10
Podmoskova		1940-62	SBB	N/A	2	6
Bois-la-Dame	Belgium	1948	A	N/A	1	N/A
Newman Spinney	UK	1949-59	SBB	75	1	2.6
Yuzhno-Abinsk	Russia	1955-89	Bit	128	2.9	9 - 12.1
Angren	Uzbekistan	1965-now	SBB	110	4	3.6
Hanna 1	USA	1973-74	HVC	120	9.1	N/A
Hanna 2		1975-76	HVC	84	9.1	5.3
Hoe Creek 1		1976	HVC	100	7.5	3.6
Hanna 3		1977	HVC	84	9.1	4.1
Hoe Creek 2		1977	HVC	100	7.5	3.4
Hanna 4		1977-79	HVC	100	9.1	4.1
Hoe Creek 3		1979	HVC	100	7.5	3.9
Pricetown		1979	Bit	270	1.8	6.1
Rawlins 1		1979	SBB	105	18	5.6
Rawlins 2		1979	SBB	130-180	18	11.8
Brauy-en-Artois	France	1981	A	N/A	1200	N/A
Thulin	Belgium	1986-86	SA	N/A	860	N/A
Centralia Tono A	USA	1984-85	SBB	75	6	9.7
Centralia Tono B		1984-85	SBB	75	6	8.4
Haute-Deule	France	1985-86	A	880	2	N/A
Thulin	Belgium	1986-87	SA	860	6	N/A
Rocky Mountain	USA	1987-88	SBB	110	7	9.5
El Tremedal	Spain	1997	SBB	600	2	N/A
Chinchilla	Australia	2000	SBB	140	10	6.6

*Bit: bituminous, SBB: sub bituminous, HVC: High volatile, A: Anthracite, SA: Semi-anthracite

From the 1930s to the 1960s, the successful operation of UCG took place on several sites. One of the first commercial-scale UCG plants, which is still working is in Yerostigaz, located in Angren, Uzbekistan. Operational since the 1960s, the plant continuously produces $1,000,000\text{m}^3$ of syngas per day which is piped to the nearby Angren Power Station [5]. After 2000, more countries have been involved in developing UCG. They have identified locations for UCG development and carried out implementation. Some countries that have started to implement the development of UCG are Australia, North America, Europe, Asian and more recently South Africa.

The development of UCG was demonstrated in Australia between 2000 and 2012. Linc Energy, a private company initiated the work and followed by Carbon Energy Ltd. [6]. There was a UCG project carried out by Cougar Ltd in Kingaroy-Queensland in 2006. Unfortunately, in 2010, it detected hydrocarbon contamination in the ground water area near the well and this was believed to be from the UCG development. This project was finally stopped and this affected the development of UCG in Australia. Controlling the effects of UCG on the environment was a challenge for its development in Australia. Nevertheless, Australia still has shown some willingness to undertake the Carbon Capture Storage (CCS) projects involved as a part of UCG development [6].

In North America, the USA and Canada have worked on field trials of UCG for industrial applications and research establishments for many years. The revival in interest of UCG development occurred in about 2005, by Lawrence Livermore National Laboratories (LLNL) when they were funded by the US Department of Energy (DOE) to undertake a review of UCG application [10]. LLNL have continued to research UCG by developing an integrated 3D full simulator for cavity growth [11]. After some projects conducted, controlling the effects of UCG on the environment was a challenge for its development in USA. Meanwhile, the Canadian Company, Laurus Energy, has planned to develop a UCG project at Stone Horn Ridge near the Beluga River in southern Alaska in conjunction with Cook Inlet Region Incorporated (CIRI) which is a native American-owned corporation in Alaska [12]. The project will be designed and developed with the capability for CCS. Currently, the most advanced Canadian UCG development is a pilot project completed by Swan Hills Synfuels with support from the Alberta Energy Research Institute (AERI) [12].

In Poland, the government views UCG as a method to exploit a large amount of their coal reserves for power generation [6]. Since 2007 Poland has begun to re-evaluate UCG activities through new exploratory and field tests. An important EU project undertaken by Central Mining Institute (GIG in Poland) is the Hydrogen Oriented Underground Coal Gasification for Europe project (HUGE, 2007-2010), funded under the Research Fund for Coal and Steel (RFCS) [6]. The main focus was on the theoretical and experimental development of in-situ production of hydrogen-rich gas from coal using underground gasification. This project was extended to HUGE2 project (2011-2014), which focused on the environmental and safety aspects associated with the UCG process, including underground water contamination and potential leakage of toxic gases. Poland also has national funding for a UCG project, which is being constructed in an active coal mine in Upper Silesian Basin [6]. This project aims to produce an industrial plant for UCG.

The UK also has large reserves of indigenous coal - both onshore and offshore - beneath the North Sea and the Irish Sea [4]. An initiative on UCG (2000–2005) led by the UK Coal Authority and supported by the UK Department of Trade and Industry (DTI) investigated the feasibility of UCG in the UK [4]. Since 2008, more than twenty licences have been issued for UCG exploration in offshore locations. In December 2014, Cluff Natural Resources was awarded five licences for offshore sites in Scotland, Wales and Cumbria in England [5, 6, 13, 14]. In October 2015, the Scottish Government announced a moratorium on UCG in Scotland for further assessment and research [15]. However, in October 2016, the final decision to stop UCG implementation in Scotland has been made.

In Asia, UCG development activities have been more progressive. China was the most active and concerned country, not just in Asia but globally. China's proven coal reserves are 114.5 billion tonnes and approximately 50% is unmined [6]. Their interest in UCG was provoked by their commitment to ensure the reduction in emissions from coal-fired power plants. They have run approximately fifteen UCG trials, which were aided by the UCG Research Centre of China University of Mining and Technology (Beijing) (CUMTB) [6]. They have been trying to co-operate with other countries and foreign companies in order to accelerate the development and application of the UCG technology. The most recent projects implemented in China includes "the Key Technology for UCG Industry" under the 863 Programs [16]. China is developing UCG not only for producing fuel, but because they, also, are concerned about gaining chemical stocks and other

derivative products [8, 16]. This shows that, globally, China has the largest number of underground gasification test sites and the most active research. Other Asian countries that are involved in the UCG development are India, Pakistan, and Indonesia. In India, The Central Mine Planning & Design Institute Limited (CMPDI) investigated for five prospective UCG sites [6]. Meanwhile, in Pakistan in December 2009, the Thar Coal and Energy Board (TCEB) collaborated on studying the geological, hydrological, cultural and environmental impact of Thar Coal Mining. And, in Indonesia there were two locations which were assessed for UCG potential; they were in Kalimantan and Sumatera [4].

In South Africa, the energy company Eskom was initiating the investigation of UCG. In 2007, they commissioned a UCG Pilot Plant with a capacity of approximately 3MW and in 2010 the syngas produced was used for co-firing with coal in the Majuba Power Station in Mpumalanga [17]. UCG has a definite role to play in South Africa's future, and this roadmap was assessed for the period of 2016 to 2040 [18].

1.2 Process overview of UCG

UCG has been approached in several different ways [5]. Basically, the coal is gasified in situ using two-vertically drilled wells as the injection and production wells. In brief, the process of UCG utilisation consists of three steps which can be seen in Figure 1-2. In the first step (Figure 1-2(a)), injection and production wells are drilled from the surface to the coal seam and a highly permeable path within the coal seams is established between these two wells, which are injector and producer. The second step is combustion and gasification (Figure 1-2(b)). Understanding the process reactions along the gasification channel is important in this step. After permeable path established, a cavity is formed through further reactions of hot air and coal seam surface. As a result, the gas products are obtained and flow to the downstream or producer well. Gasification occurs when a mixture of air or oxygen and steam is forced into the coal seam through injection well and react chemically with the coal, generating a synthesis gas [5].

The final step is the clean-up and cavity flushing, (Figure 1-2(c)). Once the gasification operations in a section of coal seam have finished, they need to be returned back to their original state. This is achieved by flushing the cavities with steam and/or water to remove gas pollutants from the coal seams and prevent them from diffusing into surrounding

water aquifers. Over time, the water table will return to a level close to that existing prior to the start of gasification [5, 19].

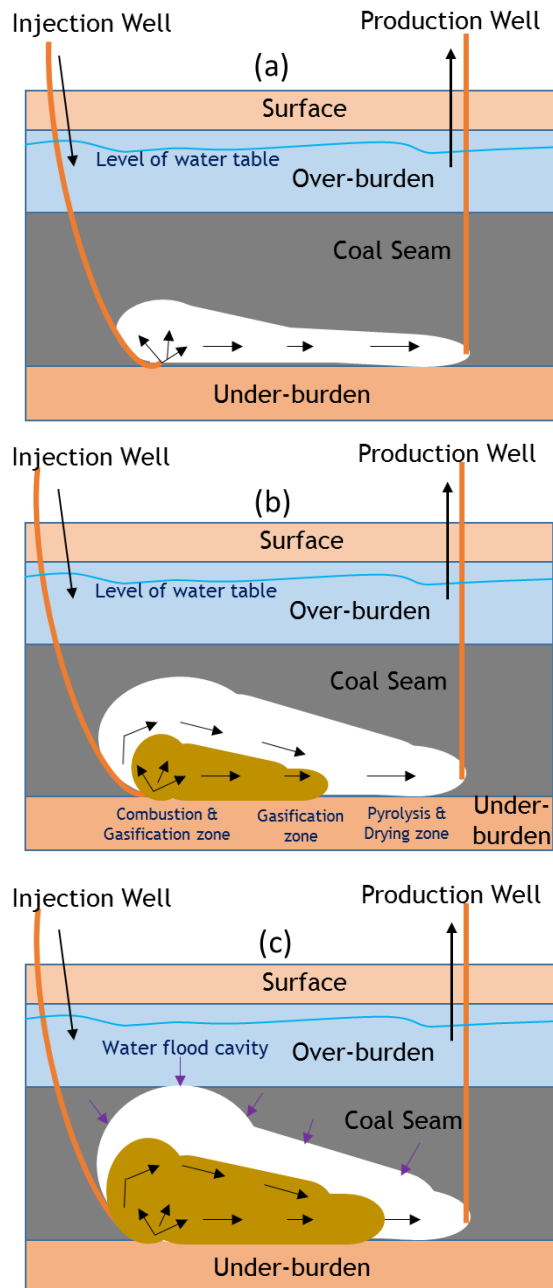


Figure 1-2. Cavity Formation of UCG (redrawn from *Bhutto et al.* [5] & *Perkins et al.*[19])

1.2.1 Linking wells mechanisms

Prior to the process of gasification, a linkage path is created between injector and producer wells. There are several techniques which can be used to provide a path or to link the

injection and production wells; Linked Vertical Well (LVW), Controlled Retractable Injection Point (CRIP) and Single Well Integrated Flow Tubing (SWIFT) [8, 20].

The LVW is the oldest method used for developing paths from injection wells to production wells. Initially, this was implemented in Russia in the 1930s, and applied by using high pressure injection of oxidant to break up the coal seam. The illustration of path formation of LVW can be seen in Figure 1-3.

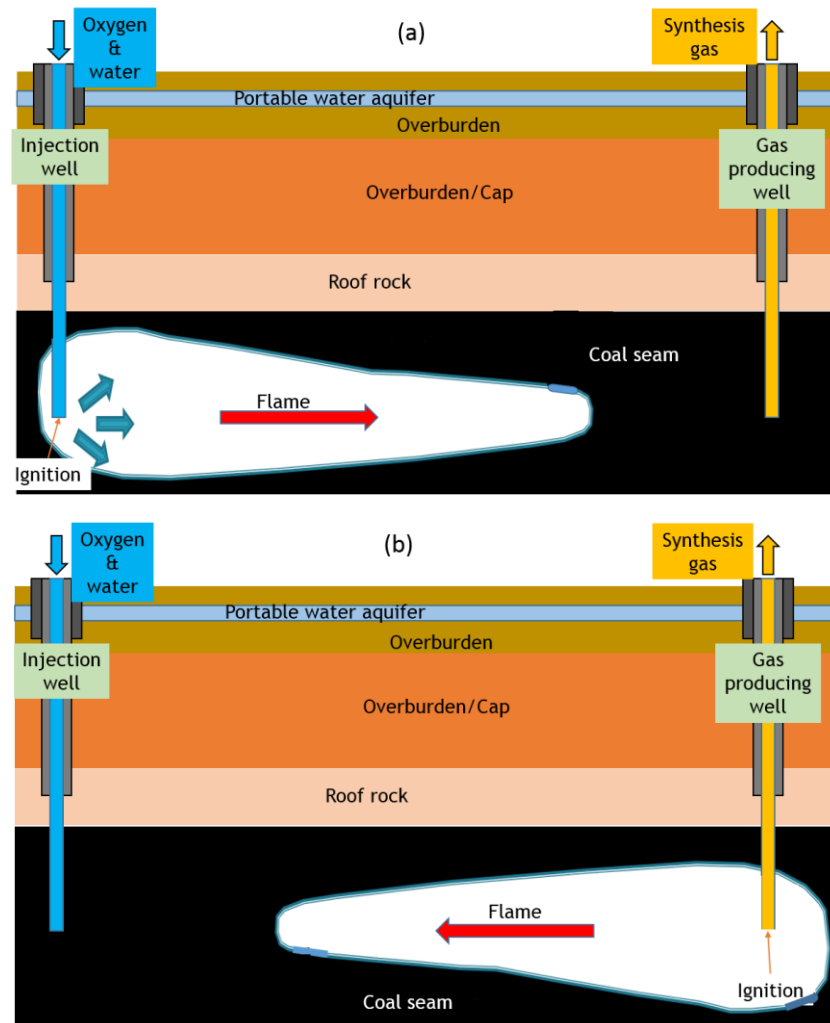


Figure 1-3. Linked vertical well method (a) FCL, and (b) RCL (redrawn from *Blinderman et al.* [21] and *Kumar et al.* [8])

Figure 1-3(a) shows the LVW mechanisms by using the principle of Forward Combustion Linking (FCL), where the flame propagates towards the production well. Another method is Reverse Combustion Linking (RCL) (Figure 1-3(b)). The RCL is a method of linking which includes injection of an oxidant into one well and ignition of coal in the other so that combustion propagates toward the source of oxidant [5, 21]. During forward

gasification, the flame working face gradually moves to the outlet, making the dry distillation zone much shorter. At the moment when forward gasification is nearly complete, the reduction zone also becomes shorter. Flow of oxidant into the injection well is maintained until the fire reaches the bottom of the injection well in the RCL or that of the production well in the FCL. This outcome is accompanied by a significant drop in the injection pressure [21] indicating creation of a low hydraulic resistance link between the wells, which establishes a low hydraulic resistance path between them.

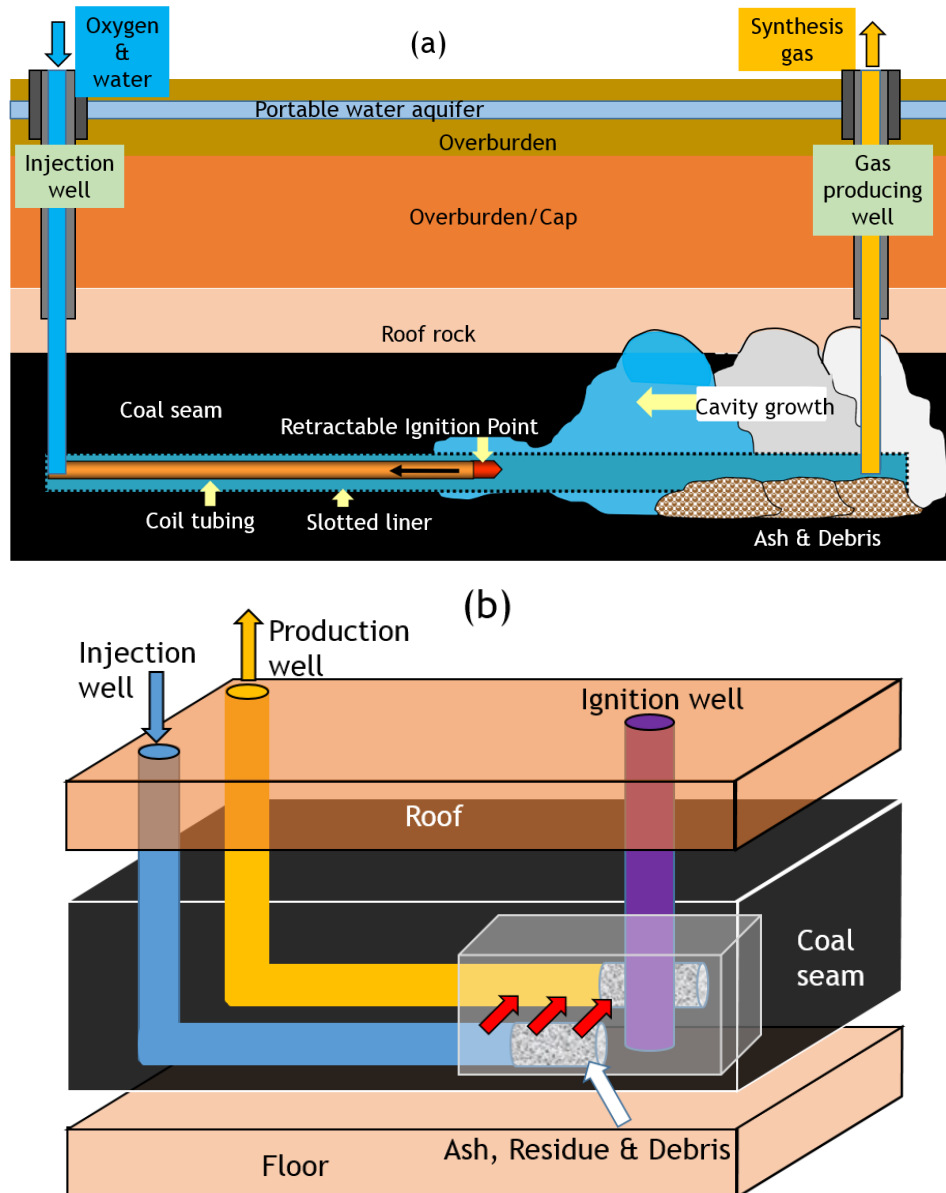


Figure 1-4. CRIP method mechanisms (a) linear and (b) long wall (redrawn from *Portman energy* [20] and *Kumar et al.* [8])

CRIP technique is suitable for thin, deep and wide coal seams[22] (see Figure 1-4). It uses less pressure to ignite the coal seam than LVW does because the ignition point is retractable and oxygen or gasification agents are inserted through the coil tubing. There are two types of CRIP methods, named linear and longwall [8]. In the Linear CRIP, the distance between the channels is shorter and the ignition point comes through injection channel. Meanwhile, the longwall CRIP has a greater space of coal seam between the channels, and therefore it is possible to build an ignition well as a path for inserting the ignition point. Figure 1-4 shows, during the gasification process, the burning zone growing upstream and in contrast the gas flowing in the horizontal (downstream) direction. The CRIP technique produces higher quality gas, results in lower heat loss than the two-vertical well configuration and improves the overall efficiency of the UCG process [23]. Once a successful link has been established the next step is oxidation and this is followed by gasification. Gasification occurred and generating a synthesis gas through the product well. Further cleaning process of syngas can be conducted at the surface for further utilization purposes [24].

More recent technology was announced in May 2012 by Portman Energy, and this was Single Well Integrated Flow Tubing (SWIFT), (see Figure 1-5) [20]. This method uses a single vertical well for both Syngas recovery and oxidant delivery. The design has a single casing of tubing enclosed and filled with an inert gas to allow for leak monitoring, corrosion prevention and heat transfer. A series of horizontally drilled can be extended with lateral oxidant delivery line inside the seam coal. It allows a larger area of coal to be combusted. Meanwhile, a single or multiple syngas recovery pipelines can be used to deliver the products out through the producer well. It describes the processes as they occurred and seen in Figure 1-5. The developers claim this method could increase the syngas production up to ten times previous design approaches [20]. The single well design means that development costs are significantly lower and the facilities and wellheads are concentrated at a single point, reducing surface access roads, pipelines and facilities footprint [25]. The UK Patent Office has advised that the full patent application GB2501074 by Portman Energy was published on 16th October 2013 [8, 20].

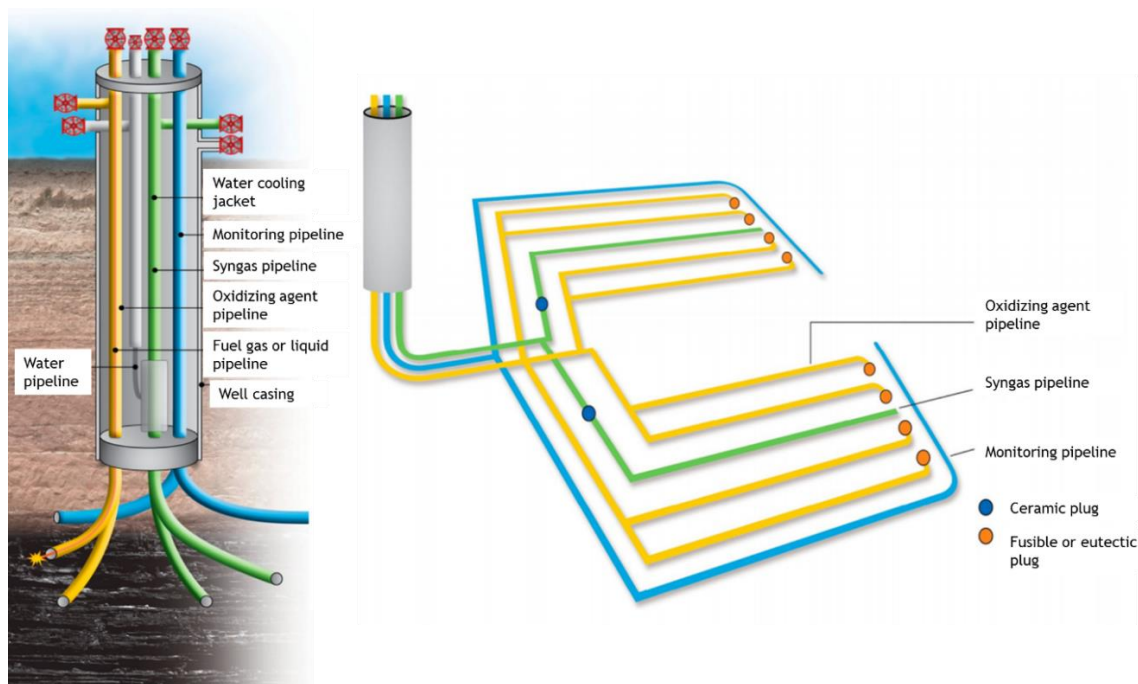


Figure 1-5. SWIFT path formation mechanisms (redrawn from *Portman energy* [20])

1.2.2 Chemical process mechanisms

Underground coal gasification (UCG) is defined as a thermochemical process, which aims to produce gaseous fuel or gas for a wide range of chemical syntheses, carried out in the presence of an air, oxygen or steam, directly in the coal seam. The result of the gasification, called “syngas”, is a mixture of combustible components e.g. CO, H₂, CH₄, with other, less desirable constituents - mainly CO₂, H₂O, N₂. The main chemical processes occurring during coal gasification are drying, pyrolysis/devolatilization, combustion and gasification. The most important chemical reactions taking place during an underground coal gasification are listed in Table 1-2. The heterogeneous reactions take place on the wall plane of the coal seams, while the homogeneous reactions occur in the gaseous phase. The negative sign of enthalpy change indicates exothermic reactions and the positive sign indicates endothermic reactions. The overall UCG process are strongly exothermic and the temperatures in the burn zone are occasionally exceed 900°C [5]. Even after it cools, the syngas flows through the production wells at likely temperatures of 200°C to 400°C. Around the combustion area, the high buoyancy of hot syngas relative to groundwater will tend to lead to large pores getting invaded with bubbles of syngas, which will heat the groundwater and turn it into steam. A dynamic interface between steam and hot groundwater will develop around the burning zone, in which steam will mix with the syngas [14].

Table 1-2. Main reactions of gasification process [25]

Reaction Name	Mechanism	Enthalpy (kJ/mol)
Devolatilization	Raw coal \rightarrow Coal volatile + Char	
Reaction of combustion	$C + O_2 \rightarrow CO_2$	-393
Reaction of combustion	$C + 0.5O_2 \rightarrow CO$	-111
Boudouard reaction	$C + CO_2 \rightarrow 2CO$	+172
Water gas reaction	$C + H_2O \rightarrow CO + H_2$	+131
Methanation reaction	$C + 2H_2 \rightarrow CH_4$	-75
Coal Volatile oxidation	Coal Volatile + $O_2 \rightarrow CO_2 + H_2O + N_2$	
Reaction of combustion	$CO + 0.5O_2 \rightarrow CO_2$	-283
Water formation	$H_2 + 0.5O_2 \rightarrow H_2O$	-242
Water gas shift reaction	$CO + H_2O \rightarrow CO_2 + H_2$	-41
Reforming of methane with steam	$CH_4 + H_2O \rightarrow CO + 3H_2$	+206
Partial oxidation of methane	$CH_4 + 0.5O_2 \rightarrow CO + 2H_2$	-36
Reforming of methane with CO ₂	$CH_4 + CO_2 \rightarrow 2CO + 2H_2$	+247

Overall, the UCG process can be divided into three reaction zones; they are oxidation, reduction and distillation zones [24], as illustrated in Figure 1-6. Through these zones, the gas with the main combustible compositions of CO, H₂ and CH₄ is formed.

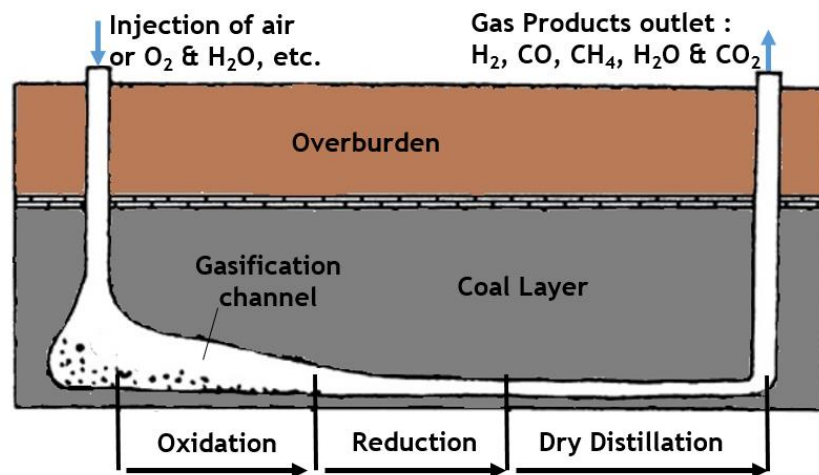


Figure 1-6. Gasification reaction process of underground seam coal (redrawn from *Bhutto et al.* [5] and *Yang L et al.* [24])

These three zones move towards the outlet along the direction of the air flow, which, in turn, ensures the continuous run of the gasification reactions [24]. In the oxidation zone, the multi-phase chemical reactions occur between the oxygen/gasification agent and the carbon in the coal seam. They produce heat and cause the coal seams to become

incandescent and to reach temperatures between 900°C and 1450°C [26]. The moisture content plays a role in allowing the oxygen to propagate through the coal pores and to contribute to the chemical reactions [27]. The O₂ level decreases gradually in the airstream and reaches the reduction zone at a low level. The H₂O and CO₂ are expected to react to form H₂ and CO under the high temperature of the incandescent coal seams in this zone. In the reduction zone, the temperature varies from 600°C to 1000°C, and the channel length could be approximately 1.5 to 2 times longer than the oxidation zone, with the pressure of 0.01 to 0.2 MPa [28]. This reaction zone is dominated by the endothermic reactions, and it causes the gas temperature to drop when completing these reactions. Afterwards, the gas flows into the distillation and dry zones with the temperature at ~200°C to 600°C. At this stage, the gas is still potentially changing through the physical or chemical process, and it depends on the temperature. Dewatering and cracking, as well as absorption and contraction of the coal could occur when the gas temperature is below 100°C. If the temperature is between 100°C and 300°C, only small amounts of paraffin hydrocarbon, water, and CO₂ are separated out. Meanwhile, the slow chemical changes are accompanied by a light polymerization or depolymerisation at temperatures above 300°C. In the meantime, appropriate amounts of volatile and oil-like liquid are separated out which take on a gelatinous state afterwards. When the temperature of the coal seam rises to 350°C to 550°C, a large proportion of tar oil is separated out and a certain amount of combustible gas is yielded. If the temperature of the coal seam continues to rise until over 550°C, the semi-coke remains begin to solidify and contract, accompanied by the yield of H₂, CO₂, and CH₄ [26, 29].

The final product gas consists of hydrogen, carbon monoxide, carbon dioxide, methane and nitrogen. The composition and heating value of the product gas depend on the thermodynamic conditions of the operation as well as on the composition and temperature of the gasifying agent employed [5, 30].

1.2.3 Physical parameters which affect the coal seam reactions

The formation of gas products species on the UCG process has been described by using the chemical reaction mechanisms as were seen in the previous section. Nevertheless, their quality can be affected by the physical conditions of coal seam during the reactions. Some of the parameters are: temperature, coal reactivity, gasifying agents, pressure, heat loss, velocity of combustion front and gas diffusion [5].

The Temperature

Temperature has an important role in determining the continuous and stable production in the process of underground coal gasification. The patterns of variation for the temperature field in the gasifier are closely related to the nature of the gasification process and the changes of cavity [28, 31-34]. In the process of coal gasification, the changes of the temperature in the coal seam are a result mainly of the heat transfer medium of the flame working face, which corresponds to a source of heat [35]. In the process of underground coal gasification, the temperature of coal seams around the gasification channel rises along with the conducted heat. When the coal surface is heated by the hot gas or the neighbouring incandescent coal, its temperature distribution expands toward the coal grains or the interior of the coal seam, which inevitably results in the thermal effects of absorption, desorption, and seepage movement of the dry distillation gas stored in the coal seam [28, 35-37]. *King and Ertekin* [38] show that under non-isothermal conditions, either the absorption-desorption process or the permeation-expansion process is linked to the temperature.

According to the gasification theory [39, 40], the temperature above 1000°C indicates a high-speed diffusion of the water decomposition reaction constituting the fundamental process for the production of a hydrogen rich gas in the course of the UCG steam stage. On the other hand, the temperature drop below 700°C slowed down the reaction speed considerably. For these reasons, special attention was paid to keeping parameters preferable for the production of gas with a high content of the combustible components, mainly hydrogen. The oxidation stage was therefore continued to achieve temperatures in the range between 1100 and 1200°C. According to the simulated calculation results [27], with the increase of the length for the gasification channel, the heating value of the gas improves. However, behind the reduction zone, it increases with a smaller margin. The influence of the temperature field on the heating value for the gas is noticeable. Because of the effect of the temperature, in the high temperature zone, the change of the measured value of the concentration field for the gas compositions is larger than that of the calculated value.

Other studies were conducted to identify the effect of temperature during gasification of UCG process. *Lahne et al.* [41] initiated a study of the process on the chemical reaction by correlating the effect of the gas flow patterns and the distribution of temperature fields

near the flame of the coal seam surface. The effect of high temperature in the channel presented some temperature field forms in the coal layer. This could result in the coal and the rock layers containing has a full of stratification, fractures-soften, melt, cement, and solidify. Accordingly, the internal molecular structure is rearranged and reorganized, which leads to qualitative changes of organizational structure and morphological appearance. Hence, obvious changes take place in the physical and mechanical properties of the coal and rock mass. As a result, its corresponding physical and mechanical properties are no longer constants, but are functions of temperature [35].

When the temperature in the coal seam rises, the desorption rate of the dry distillation gas in the coal seam accelerates. The free dry distillation gas content in the coal increases and the mass of the dry distillation gas, which participates in the seepage, also increases. On the other hand, with the rise in the temperature, the amount of absorbed dry distillation gas in the coal seam drops.

The effect of coal reactivity

The chemical reactivity of the coal is potentially very important for UCG. The reported intrinsic reactivity of low rank coals differs by up to four orders of magnitude when extrapolated to typical gasifier operating temperatures [42]. The coal intrinsic reactivity has a big impact on the distributions in the gasifier and on the final product gas. In particular, high reactivity favours the production of methane via the char and H₂ reaction [5]. Because this reaction is exothermic, the increased reactivity for this reaction can lead to big changes in the final product's gas calorific value.

The effect of gasifying agents

Gasification under different gasifying agents such as air, steam, steam-oxygen, and carbon dioxide has been highlighted in the literature. In general, the gasifier atmosphere determines the calorific value of the syngas produced. When air is used as the gasifying agent, syngas with low heating value is obtained (4 – 7 MJ/Nm³ [43, 44]). This is mainly as a result of the syngas dilution by the nitrogen contained in air. However, if steam or a combination of steam and oxygen is used, a syngas with a medium calorific value is produced (10 – 28 MJ/Nm³ [43, 44]). Adding steam changes the carbon-oxygen system balance to a carbon-oxygen-steam system balance in the combustion process. Oxygen-steam gasification not only utilizes the surplus heat to improve the energy efficiency of

the process, but also increases the gas production volume per tonne of coal and lowers the oxygen consumption volume per tonne of coal [45].

The syngas produced by the UCG process has a low calorific value approximately one-eighth of natural gas if air injection is used and double this figure if oxygen injection is used. Oxygen enriched steam forward gasification has remarkable effects on gas compositions. Under this testing environment, in pure oxygen gasification, the average rising rate for the temperature of the gasified coal seams is approximately 2.10°C/h; in the oxygen-enriched steam forward gasification phase, the high temperature field mainly concentrates around the gasification gallery and the highest temperature in oxidation zone reaches over 1200°C [32].

The air is injected into a gasification channel at a low speed and the flame tends to propagate towards the injection point but if the air flow rate increases, the cavity tends to grow in the downstream direction. It is also known that flame propagation is faster when oxygen is used instead of air. This behaviour is also expected because oxygen-fed flames are hotter and have higher reaction rates [46].

The effect of pressure

Pressure is known to positively impact the performance of coal gasification [47]. At close to atmospheric pressure, the gas calorific value is very low because of the kinetic limitations of the gasification reactions. The changes in operating pressure can provide the underground gasification process to a great extent. Under the cyclically changing pressure condition, heat loss was obviously reduced and heat efficiency and gasification efficiency and the heat value of the product gas were increased greatly. The underground gasifier with a long channel and a big cross-section could improve the combustion and gasification conditions to a large extent, markedly bettering the quality of the product gas and the stability of gas production. Therefore, the large-scale underground gasifier is a condition necessarily met by the industrial production [29].

The effect of heat loss

Heat losses from underground coal gasification are not easy to estimate. If the cavity remains completely in the coal seam, then heat losses to the surrounding strata will probably be small and can be ignored. However, as the overburden is progressively

exposed, irreversible heat loss to the surrounding will increase. It is not easy to estimate this heat loss, because if the overburden undergoes stiffening, some of the energy used to heat it to cavity temperatures may be recovered through preheating the injected gas. The heat loss mechanisms can probably be more easily investigated using a dynamic model, in which cavity growth and heat loss are estimated as simultaneous functions of time [5].

The effect of gas diffusion

In the process of combustion and gasification for the coal seams in the gasifier, the major reactions are multi-phase reactions. At each stage of multi-phase reactions, the gas state reactant spreads to the surface of the solid state reaction by diffusion. Gas diffusion mainly takes two forms; molecular diffusion and convection (eddy) diffusion. The process of the combustion for coal seams depends on the gas diffusion features and the dynamic characteristics for the chemical reactions. According to the diffusion-dynamic theory for combustion [28], under the low temperature conditions, the overall velocity of the combustion and gasification process is mainly determined by the dynamic conditions of the chemical reactions. Under the high temperature conditions, the overall velocity of the combustion and gasification process mostly depends on the speed for oxygen to diffuse from the main current to the carbon surface and the velocity of its product diffusing from the carbon surface to the main current. Seen from the circumstances of the field tests of underground gasification and model experiment, the temperature within the gasifier (the vicinity of the flame working face, in particular) is very high.

Moreover, considering the movement conditions for the fluid, it is possible to conclude that the convection and diffusion for gas is the significant factor influencing the process of the underground gasification. Under high temperatures, molecular diffusion results from the existence of the concentration gradient, temperature gradient and pressure gradient [48]. The diffusion driving force is the composition gradient (expressed through gas component mole fractions) and the driving force for permeation is the total pressure gradient. It was found that the pressure increase influences the speed of the gas front movement more significantly than the temperature increase that is almost negligible.

The effect of velocity of the combustion front

In packed bed gasification, the combustion front moves slowly down the bed parallel to the flow of gases. Hot combustion gases always have intimate contact with the unburned

coal ahead of the combustion zone until the fire breaks through to the production well. In channel gasification, the combustion zone moves outward at nearly right-angles to the flow of air and combustion gases. During UCG a thermal wave is formed which gradually travels through the coal bed toward the gas production well [5]. The shape of the thermal wave tends to change very little. Since the shape of the wave remains unchanged, the processes occurring at each temperature level in the moving wave also remain unchanged in time and an apparent steady-state or pseudo-steady-state condition prevails. Under these conditions in a one-dimensional system, it is possible to transform the mathematical model to a moving co-ordinate system which converts partial differentials to ordinary differential equations, which is a major simplification of the problem [49]. When the physical properties of coal tend to vary widely over short distances even in a single coal seam this makes the task of modelling such as UCG process very complex. Gasification of a typical 9m seam of sub-bituminous coal proceeds at a rate of 0.3 to 0.6m/day consumes all the coal in a swath 12 to 15m wide for a well spacing of approximately 18m [5].

1.3 Purpose of the work

There are still many challenges that need to be overcome in the development of UCG, and therefore, practically, the commercial development of UCG has not yet emerged [50]. In technology terms, the challenges include, obtaining better quality of gas and heating values, high thermal efficiency, high process efficiency, good control on the combustion front, handling the depth of the coal and gas clean-up [51]. However, this underlying technology can be developed through computational modelling work and can be backed up by laboratory-scale experimental work. Relevant to this, this research aims to develop a solid understanding of thermochemical behaviour for UCG application through coal particle model approaches. In particular, this work aims to investigate such aspects as,

1. Developing a robust model of coal particle combustion through the study of kinetic parameters.
2. Expanding the developed model to be a gasification reactions with an aim to improve the reaction mechanisms of the existing model.
3. Developing a solid understanding of the process of coal combustion and gasification, which is important to obtain more efficient processes.

4. Investigating the effects of reaction conditions on coal gasification reaction to increase syngas quality and CO₂ utilisation.
5. Identifying the thermochemical behaviour of gasification reaction mechanisms in UCG application.
6. Introducing a new method of coal block reaction modelling by using coal particle approaches, which are more suited to the mechanisms of the coal reactions.

1.4 The Importance of this research

The study of UCG has been conducted for several years as detailed in the opening section, through the experimental or computational modelling schemes. More developments through the study of UCG are expected to contribute to make UCG technology more viable. Compared to others, this study aims to introduce improved modelling approaches for coal gasification simulations. The coal particle reaction method is introduced, which considers coal as a multi-phase-component of solid-gas as they actually occur in the same process of reactions. Consequently, the coal mass decreasing in the reaction can be identified, as it occurs simultaneously with the gas product formation. Meanwhile, the existing model considers surface reactions with a multi gas-phase, which means that the solid phase is presented in the phase of gas for the reactions. Therefore, this work is important as it provides modelling processes of coal reaction mechanisms that are better suited for gasification application. Furthermore, the success of this model could have a significant contribution on the modelling of the coal seam reactions.

1.5 Thesis outline

The thesis is constructed as follows;

In Chapter 2, an overview of the study of UCG modelling, including some method approaches, is introduced. A description of each method is provided, and a comparison of all approaches is given. Finally, any recent developments with alternative methods are introduced to improve the existing model of simulation.

In Chapter 3, information about the methodology used for model development is introduced. Computational Fluid Dynamics (CFD) modelling techniques with the principal mechanisms applied for the coal gasification development are described.

In Chapter 4, the coal combustion model as an initial stage of gasification reactions is developed. A kinetic parameter study was conducted as the key to the model development, and the results of simulation were verified through comparison with the results of the experiment.

In Chapter 5, the development of coal particle gasification is conducted. This is initiated with the description of the difference between the coal combustion and gasification. Further development of coal gasification is performed including the kinetic parameter study, identifying the parameters that affect the gasification reactions, studying the effects of various gases in the reactor environments and investigating the thermochemical behaviour on coal gasification reactions.

In Chapter 6, the coal particle experiments are conducted and the results are reported. There are three important parameters studied through the experiments; they are the effects of particle sizes or coal block porosity, the effects of temperatures on the reactions' process and the effects of gas flowrate variation injected to reactors.

In Chapter 7, a conclusion of the findings of the study is offered and any future work following any recommendations in the study is described.

Chapter 2 Literature review

2.1 Introduction

Although some of the environmental impacts of UCG are positive ones [52], there are a few potential environmental concerns associated with UCG operations as outlined in Chapter 1. Therefore continuous improvements through the research and technology development are needed to overcome the issues in UCG application. Modern UCG is a new industry to the public and the media. Public acceptance of this technology will depend on more successful research and trials to demonstrate its advantages in terms of both financial and environmental impacts over traditional mining methods. The further challenge of UCG today is to ensure the commercial viability of UCG technology but these hurdles could be overcome by deploying the right policies and arguments to convince public opinion. Government support for this technology may be needed to produce more reliable technical knowledge and an expertise base and more projects need to be implemented in order to test possible UCG approaches. In addition, some field projects could serve as possible locations to develop and test novel monitoring, simulation, advanced drilling techniques and tools, and approaches to confirm the environmental viability of UCG. Collaborating and sharing expertise and knowledge between projects and governments is the key to commercialising and growing the UCG industry.

Although a large number of UCG field trials have been carried out (discussed in Chapter 1), information on the detailed UCG process is still needed. The high cost of extracting data and the difficulty in controlling the operating variables [9] are also believed to be the main reasons. In addition, there is a technical limitation in adjusting control parameters because of the site-specific nature of the UCG performance. Therefore, numerical modelling for UCG development has been an option and is growing as an alternative way to investigate the process of UCG.

2.2 UCG Modelling

Prior to 1975, the development of UCG models was very limited. Over the years, several approaches have been developed for modelling the UCG process, such as packed bed models, channel models and coal slab models [9]. With the progress of computational techniques, recent development of UCG modelling has also helped with CFD or other software tool facilities. Most of the earlier models were one-dimensional (1D); however, with the advancement of computational power, two-dimensional (2D) or even a few three-dimensional (3D) models were developed [39, 41, 53, 54].

2.2.1 Packed bed models

The oldest models of UCG in literature describes the channel reactions process as a packed reactor [9]. The consideration of the coal seam as a packed bed primarily originated from the concept of *Higgins* [55], who considered the creation of a permeable zone between two boreholes either by reverse combustion linking (RCL) or by fracturing the coal seam using pressurized air or chemical explosives [52, 56]. The resultant coal seam resembles a packed bed where coal particles are filled in the reactor. This concept is similar to the major Soviet approach to seam preparation where they included extensive drying of the seam and reverse combustion to obtain a region of enhanced permeability between the boreholes [57]. The packed bed model assumes that coal gasification occurs in highly permeable porous media with a stationary coal bed which is consumed over time [58]. This model can be illustrated with experimental work conducted by *Shannon et al.* [59] from Lawrence Livermore National Laboratory in the USA.

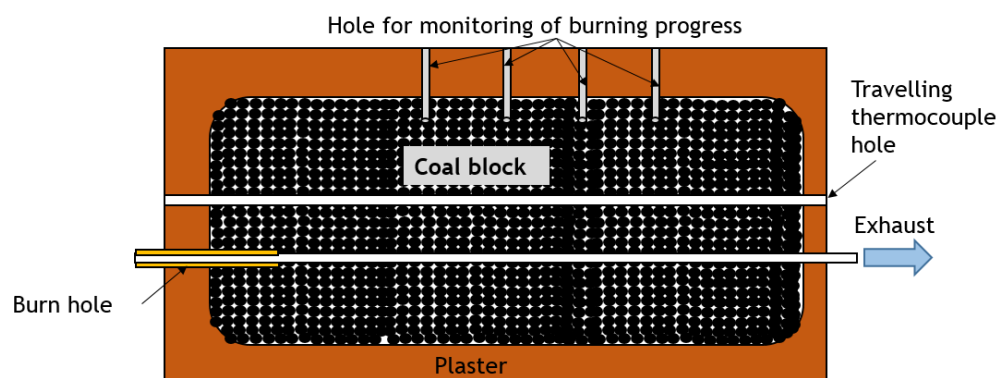


Figure 2-1. Coal block model for cavity formation experiments (redrawn from *Shannon et al.* [59])

Figure 2-1 shows an illustration of combustion experiments for cavity formation in UCG. A packed bed coal is potted in a standard 200 litres drum (0.2 m^3) and then the combustion reactions conducted.

It was in 1976, when the 1D transient packed bed packed models were initially developed by Winslow [60], followed by Thorsness and Rozsa [56], and Thorsness *et al.* [61], with a finite-difference approach based-method which was supported by the Lawrence Livermore National Laboratory (LLNL), USA. However, there is no basic difference between their models. Thorsness and Rozsa [56] provided a detailed description of the laboratory-scale gasification experiment, whereas Thorsness *et al.* [61] provided a detailed description of the development of the physical and chemical models where they made many simplifying physical and chemical assumptions, based on experimental and theoretical comparison and correlation, including, gas permeability, effective thermal conductivity, interphase heat-transfer coefficients, chemical reaction rates, various thermodynamic properties of each species and stoichiometric coefficients. Their models neglected the tar condensation and plugging and gas losses to surrounding of seam layers, water intrusion, heat losses, and coal bed movement as a result of shrinking or swelling during drying and pyrolysis in order to avoid complexity [9]. Meanwhile, Thorsness *et al.* [61] considered all the main reactions for gasification; however, for homogeneous reactions, only the water-gas shift reaction was considered by Winslow [60].

After three decades or so, Khadse *et al.* [58] developed a similar model with pseudo-steady state fluid flow cases. However, their model differed from the model developed by Thorsness *et al.* [61] in the drying and water evaporation/condensation reactions. They did not consider the drying process, and only coal and char were considered for the solid phase. This model gives better performance in analysing the effects of various operating parameters on temperature and gas phase than the previous model did.

Recently, Uppal *et al.* [52] developed another 1D packed bed model adopting the existing model of Thorsness *et al.* [61] with modifications in the model structure and solution strategy. In order to observe the model capability, they developed experiments with more controlled input parameters, especially at the parameters of gas flowrate injection. They varied the gas flowrate and recorded the gas products. In their model, they calculated the exit gas heating values and composition utilising the experimental inlet gas flowrate. In addition, they used non-linear optimisation techniques in order to compensate for the

uncertainty in coal and char by optimising the composition parameters of pyrolysis products. However, a better prediction for the gasification products, because of more parameters controlled identified in the simulation, could provide better results of this model.

The development of 2D models of packed beds was started in 1986 by *Thorsness and Kang* [62]. They assumed an identical gas and solid temperature and incorporated one energy equation for the combination of gas and solids. Considering the negligible difference between the gas and solid temperature obtained by the earlier models [56, 61] the assumption of identical gas and solid temperature seemed to be justified. In their model, they also incorporated diffusion effects, wall transport and char combustion and water-gas shift reaction rates based on the Shell Progressive (SP) and Ash Segregation (AS) reaction model. In the SP model, a core of unreacted solids was assumed to be surrounded by a shell of ash through which the gas phase reactants diffuse. On the other hand, the AS model assumed continuous exposure of unreacted material to the gas stream because of the ash segregation. Although their generalised model was 2D, only one case (steady heat transfer phenomena) was solved using the 2D model. For all other cases, the 1D model was considered. For validation of a UCG model, they calculated gas composition, temperature and carbon fraction considering a steady 1D model with very limited gas species and compared the results with the analytical data obtained from literature.

Abdel-Hadi and Hsu [63] extended previous models by developing pseudo-2D geometry with a moving burn front in the axial direction. A rectangular domain with a length of 1.5m and width of 1m was used in their model. Their governing equations were similar to the equation considered by *Winslow* [60] and *Thorsness and Kang* [62]. However, they included carbon consumption in the reaction zone in order to track the burn front. The conversion rate of the coal seam was found to be fairly constant. In order to gain confidence for this model, they compared their model with the laboratory results reported by *Thorsness and Rozsa* [56] and obtained a good agreement with the experimental data.

Overall, the packed bed models have contributed to the development of UCG and they have validated results with laboratory experiments to some extent. These models agree with the gas composition and were very effective in calculating the heat recovery and gas composition [9]. However, they have limitations to providing the radiation mechanisms,

which occurred in the reaction process of gasification. In addition, as pointed out by Winslow [60], this method requires a fine grid in the vicinity of the reaction front that limits its applicability to field-scale trials.

In summary, the comparison of packed bed models developed by each researcher can be seen in Table 2-1 and 2-2. .

Table 2-1. Comparison of some essential features in packed bed models [9]

Researcher	Dimension and time dependence	Heat transfer			Mass diffusion	Fluid flow	Thermo-mechanical failure	Water influx
		Cond.	Conv.	Rad.				
Winslow[60]	1D & T	x	x			D		
Thorness et.al [61], Thorness and Rozsa[56]	1D & T	x	x			D		
Khadse et.al[58]	1D & PS	x	x			D		
Uppal et.al[52]	1D & PS	x	x			D		
Thorness and Kang[62]	2D & T	x	x		x	D	x	
Abdel-Hadi and Hsu[63]	2D & T	x	x		x			

1D=One-Dimensional, D=Darcy flow, PS=Pseudo-Steady State, T=Transient

Table 2-2. Reaction rate control mechanisms for each research development [9]

Researcher	Drying	Pyrolysis	Char Reaction				Water-Gas shift	Gas and gas reactions		
			R3	R4	R5	R6		R10	R8	R9
Winslow[60]	D	P	K	K	K	K	K			
Thorness et.al [61], Thorness and Rozsa[56]	D	P	K	K	K	K	K	I	I	I
Khadse et.al[58]		P	K	K	K	K	K			
Uppal et.al[52]		P	K	K	K	K	K	I	I	I
Thorness and Kang[62]			K	K	K	K	K	I	I	I
Abdel-Hadi and Hsu[63]	D	P	P	P	P	P				

D=Diffusion-limited, I=Infinite rate, K=Kinetic (power law) and bulk diffusion, P=Power law kinetics, EC=Experiments correlation

2.2.2 Channel models

The channel models were developed in the first decades of modelling. The model assumes that coal is gasified only at the perimeter of the expanding permeable channel [64]. In this approach, the UCG process is represented by an expanding channel where two distinct zones of rubble/char and open channels exist. This approach is considered following observation of the formation of the open channel structure after the gasification phase is

terminated in different field tests of coal seams [65, 66]. The illustration for this method can be seen in Figure 2-2.

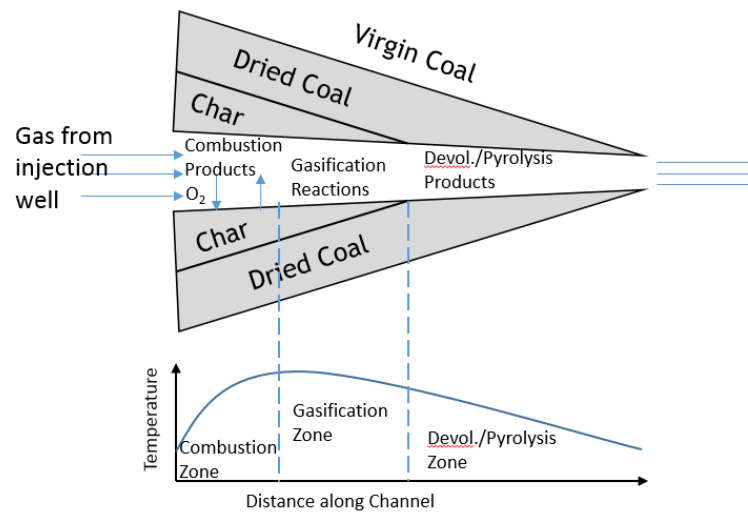


Figure 2-2. Channel model illustration (redrawn from *Gunn et al.* [49])

The basic concept and physics behind this approach is that air or oxygen flows down the central channel and is convected by turbulent flow to the boundary layer along the channel wall. The oxygen diffuses through the boundary layer to the solid surface and reacts. The hot combustion gases diffuse back through the boundary layer to the channel [49], and the channel model is more useful for analysing sweep efficiency.

Dinsmoor et al. [57] developed a steady state, 1D channel model by assuming that the gasifier behaves as an expanding cylindrical cavity in the coal seam with reactions taking place at the walls. For simplicity, no pyrolysis reactions were considered. Heat transfer included conduction for solids only; however, both convection and radiation were included between the wall and gas. Axial heat conduction in the gas phase was neglected. They also considered water influx as evenly distributed along the length of the tube. Char reactions and two gas reactions were considered in their reactions. Forced convection is considered to be a dominant mechanism of mass transfer, and therefore they simulated coal gasification with a forced convection mass transfer correlation. For heterogeneous reaction kinetics, they considered the surface reaction rate constant and wall diffusion resistance. For wall diffusion resistances, the mass transfer co-efficient was calculated from a standard correlation for the turbulent flow of gases in the tube. Char reaction and two gas phase reactions were considered in their model. Because of slow channel evolution, they incorporated a pseudo-steady state assumption for changes associated

with a gas phase. The quality of the predicted products gas observed was inferior to the quality usually obtained in the packed bed model for similar situations. For a constant blast velocity, the reaction rates were observed decreasing with the evolution of the channel as a result of the constant mole fraction of oxygen. As a result, the oxidation zone became longer, and, in turn, was responsible for increased head losses and deterioration of gas quality. Compared to the packed bed combustion front, the oxidation zone was much longer. However, these observations were not supported by any field observation.

Almost at the same time, the conclusion developed by *Dinsmoor et al.* [57] was negated by the work of *Scwhartz et al.*[67] as they found an increase of mass transfer by several orders of magnitude when the natural convection channel was considered as the controlling mechanism of mass transfer instead of forced convection alone. *Scwhartz* was the first investigator to consider natural convection as the controlling mechanism of heat and mass transfer in UCG cavities. In later papers, *Eddy and Schwartz* [68] developed a 2D model and described the evolution of the cavity based on the movement of the cavity wall.

In 2009, *Luo et al.* [69] extended the *Scwhartz et al.* [67] model by including heat transfer and more coal wall and gas phase reactions. Flow inside the cavity was solved based on irrotational fluid flows inside an enclosure which describes velocity potential based on geometric features and enclosure.

Batenburg et al. [65] developed a semi-steady state 2D model for UCG in open channels for developed gasifiers only. Unlike other models, they assumed that oxygen instantaneously reacts with the combustible gases present in the channel instead of reacting with the coal surface. Their interest was only to investigate the process within the channels after the injection gas percolated through the inert permeable rubble zone. They also included the effect of natural convection because of the temperature difference. Their results showed that the effect of pressure on gas composition was negligible, and either natural or forced convection transfer coefficients were in the same order of magnitude and both are important.

Pirlo et al. [70] developed a 2D steady state model by extending the idea of *Batenburg et al.* [65], with two distinct zones. They were a low permeability rubble and ash around the injection point and a high permeability peripheral zone along the wall. After a short

transitory starting phase, those two zones were identified for a thin seam at a great depth. During initial combustion, a cavity was identified partially filled with inert material near the injection hole. Their simulation for this cavity was based on one main parameter - the permeability ratio between the low and high permeability zones. The gasifying agent was assumed to pass through the low permeability zone surrounding the injection point prior to its arrival in the high permeability zone, where reactions with the coal wall occurred. They combined two separate models:

- (1) a flow model for calculation of the flow through the low permeability using Darcy's law and continuity equation; and
- (2) a chemical model for the calculation of the chemical processes occurring between gas and the coal wall in the high-permeability zone using empirical correlations for mass and heat transfer for the packed bed by assuming plug flows in the gas phase.

The coal consumption rate was calculated only on the channel wall. Their model did not consider the details of moisture and volatile matter released by drying and pyrolysis. They assumed that volatile matter is released in the form of water and hydrogen in proportion to the consumption rate of carbon. They concluded that the permeability ratio is one of the main parameters for determining the success of underground coal gasification because of the observation of the increasing final gasifier area, power, and trial duration with the increase in the permeability ratio. According to *Pirlo et al.* [70], the cavity growth and shape obtained from their model were in reasonable agreement with the Pricetown field trials.

Kuyper [66, 71] developed a 2D model to describe UCG process in a cross-section of an open channel for typical western European coal layers of thin seams (1–2m). Field trials of UCG indicated growth of the cavity upwards and radially outwards around the injection well as gasification proceeds. As a result, for thin seams, the top wall was exposed to rock material and failure of the overburden is apparently expected. However, the main focus of their work was to obtain an insight for heat and mass transfer because of the double diffusive turbulent natural convection in which both the temperature and concentration gradients played a role in the transport process.

Perkin and Sahajwalla [72] considered a thick coal seam and expanded *Kuyper's* model by including an ash layer at a lower part of the channel. They developed a 2D

axisymmetric model by using Ansys-Fluent (a commercial CFD software) to investigate double diffusive natural convection along with relevant reactions in a partially filled cavity.

Briefly, the channel models discussed in this section with their essential features and reactions rate control mechanisms are outlined in Table 2-3 and 2-4.

Table 2-3. Comparison of some essential features in channel models [9]

Researcher	Dimension and time dependence	Heat transfer			Mass diffusion	Fluid flow	Thermo-mechanical failure	Water influx	Heat loss
		Cond.	Conv.	Rad.					
<i>Dinsmoor et al.</i> [57]	2D & T	x	x	x		P		x	
<i>Eddy & Schwarz</i> [68]	1D & T	x	x	x	x	M	x	x	x
<i>Luo et al.</i> [69]	2D & T	x	x		x				
<i>Batenburg et al.</i> [65]	1D & SS	x	x	x		D			
<i>Pirlot et al.</i> [70]	2D & S	x	x		x	D		x	
<i>Kuyper</i> [66, 71]	2D & PS	x	x	x	x	NS			
<i>Perkin and Sahajwalla</i> [72]	2D & T	x	x	x	x	NS			

D=Darcy flow, P=Plug flow, M=Mixed flow, NS=Navier-Stokes, S=Steady state, SS=Semi-Steady state, PS=Pseudo-Steady State, T=Transient

Table 2-4. Reaction rate control mechanisms for each research development [9]

Researcher	Drying	Pyrolysis	Char reaction				Water-Gas shift	Gas & gas reactions		
			R2	R4	R5	R6		R10	R8	R9
<i>Dinsmoor et al.</i> [57]			K	K	K			P	P	
<i>Eddy & Schwarz</i> [68]			P	P	P	P	P	P	P	P
<i>Luo et al.</i> [69]				E	E	E	E		E	
<i>Batenburg et al.</i> [65]				E	E	E	E	E	E	E
<i>Pirlot et al.</i> [70]				D				M		
<i>Kuyper</i> [66, 71]				P				M		

D=Diffusion-limited, E=Equilibrium, K=Kinetic (power law) and bulk diffusion, M=Turbulent mixing limited, P=Power law kinetics

The consideration of natural convection has been found to be one of the main phenomena in the channel model development. Natural convection plays an important role in the mixing of injected blast gas and the gases coming from the channel wall. The channel model is found to better calculate sweep efficiency. However, most of the channel models neglected drying and pyrolysis which are considered to be very important in the coal block model. In order to determine cavity shape and size, the channel model is preferred.

2.2.3 Coal slab models

Another model describes the UCG coal seam as a coal slab. This approach examines the process by movement of various defined regions in a coal slab perpendicular to the flow of the injected blast gas. These regions usually include the gas, ash layer, char region, dried coal and virgin coal. The existence of different regions is caused by the slow heating rate of the UCG. At a very high heating rate, there is a possibility of the coincidence of a drying front with a combustion front [73]. The framework of these models in general can be seen in Figure 2-3.

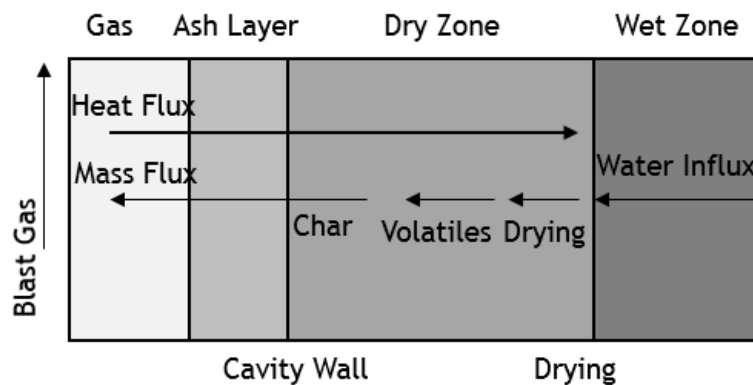


Figure 2-3. Scheme of coal block models (redrawn from *Khan et al.* [9])

Tsang [73] was the first to use this approach considering the observation of the development of drying, pyrolysis, and gas-char reactions zones around the most permeable path in the coal seam. In addition, the profiles of temperature and saturation, as well as the direction of heat and mass transfer, were exhibited from the pyrolysis experiment. In that experiment, a constant heat was applied to the coal surface and career gas was supplied along the length of the cylinder. The evaporation of water is assumed to take place entirely at the retreating drying front. Thus, the model following this approach must be a moving boundary value problem with phase change which is known as the “Stefan” problem [9]. In this approach, as can be speculated from Figure 2-3, there is an efflux of steam, devolatilized materials, and “self-gasification” products from the wall to the cavity, while there is a counter-current flux of heat towards the cavity wall. “Self-gasification” is considered as the reaction of the gases (steam and devolatilized gases) with hot char while they pass through before flowing into the cavity. Because of the consideration of different layers, unlike other types of models, for each layer separate mass and energy balances are usually considered. As a result, the governing equations for

mass and energy balances are of split boundary types. The mass flux is considered to be diffusion dominant.

As stated earlier, *Tsang* [73] was a pioneer of the approach and developed a 1D unsteady UCG model considering the two regions of a coal block which are the wet and the dry zone. *Massaquoi and Riggs* [74, 75] extended *Tsang's* 1D model by including the combustion of char and volatiles at the boundary while solving a steady-state case. As well as the zones shown in Figure 2-3, they included another zone of bulk gas that was composed of water vapour, CO₂, O₂, and some inert gases outside the gas film. This developed model was used to describe the simultaneous combustion and drying of a wet Texas lignite coal. The flow of gases in the porous dry coal was modelled by Darcy's law, and heat transfer was considered by both conduction and convection. Radiation heat transfer was also considered between the edge of the ash and the bulk gas. However, heterogeneous combustion was considered unstable because of the decrease of the coal face temperature with the increasing bulk gas temperature for a constant oxygen concentration. In contrast, homogenous combustion was considered stable because of the experimental observation reported in the literature [76-78]. In addition, *Massaquoi and Riggs* [74, 75] concluded that the burn rate would be nearly linear with the increase in the concentration of oxygen when the flame front is located in the char face, and the burn rate increases when the flame is located in the gas film.

Park and Edgar [79] developed an unsteady 1D model with a moving burning front based on the work of *Massaquoi and Riggs* [74, 75] to describe lateral cavity growth in UCG. However, unlike the assumption of *Massaquoi and Riggs* [74, 75], they did not consider having the same velocity for the cavity wall and drying front during the early stages. As well as char gasification, they included coal shrinkage as an effect of drying and pyrolysis, as well as the "self-gasification" of drying and pyrolysis products (steam and CO₂) in the region between the cavity wall and the drying front in order to consider the additional movement of the cavity wall. The cavity wall movement was determined by the rate of the removal of coal by chemical reactions and the physical movement of the cavity wall because of the shrinkage of the coal. In their simulation, an increase of the cavity growth was noticed during the transient period as a result of the shrinkage of the coal. However, the cavity growth with, and without, considering the shrinkage eventually merged into one rate when the steady state was reached. However, *Park and Edgar* [79] suggested that the movement of the cavity wall as a result of shrinkage is only important in

laboratory-scale processes and can be neglected in larger-scale processes. Their results indicate that cavity growth is controlled by the rate of oxygen transfer to the cavity wall, when the flame is located at the char surface.

Perkins and Sahajwalla [19, 42] also developed a 1D transient coal block model with an extension of *Tsang's* [73] study by including a multi-component diffusion and the random pore model to account for changes of heterogeneous reaction rates with conversion. For multi-component diffusion, Stefan-Maxwell equations and the bi-dispersed dusty gas model were used for the gas film and dried coal matrix, respectively. They proposed that cavity growth occurs at the reduction condition, so, therefore, only heterogeneous gasification reactions are solved, and required heat was provided by defining a constant temperature at char surface. The char surface was allowed to participate in radiation heat exchange with its surroundings. For pyrolysis, they followed the work of *Tsang*. The movements of the drying front and char front were assumed to be equal under pseudo-steady state conditions. They assumed that solid and gas phases are in thermal equilibrium and bulk gas has a fixed composition that is representative of the product gas.

The special feature of coal slab model is in tracking the drying and combustion front movement. This model can successfully demonstrate the drying and devolatilization behaviour of large coal particles. However, this model is yet to be validated using UCG trial data. Because of the assumption of semi-infinite coal slab, it is possible to speculate that this model is only good for a thick coal layer. All the models developed so far by considering the coal slab are 1D, therefore information of cavity formation cannot be obtained. In summary, the comparison for each research development can be seen in Table 2-5 and 2-6.

Table 2-5. Comparison of some essential features in slab models [9]

Researcher	Dimension & time dependence	Heat transfer			Mass diffusion	Fluid flow	Thermo-mechanical failure	Water influx	Heat loss
		Cond.	Conv.	Rad.					
<i>Tsang</i> [73]	1D & T	x	x	x	x			x	
<i>Massaquoi and Riggs</i> [74, 75]	1D & S	x	x			D			x
<i>Park and Edgar</i> [79]	1D & T	x	x			D			
<i>Perkin and Sahajwalla</i> [19, 42]	1D & PS	x	x	x	x	NS	X	x	

D=Darcy flow, NS=Navier-Stokes, S=Steady state, PS=Pseudo-Steady State, T=Transient

Table 2-6. Reaction rate control mechanisms for each research development [9]

Researcher	Drying	Pyrolysis	Char reactions				Water-gas shift	Gas-gas reactions		
			R2	R4	R5	R6		R10	R8	R9
<i>Tsang</i> [73]	H	P		P	P		K			
<i>Massaquoi and Riggs</i> [74, 75]	H	P		P	P		E	I	I	
<i>Park and Edgar</i> [79]	H	P	D	P	P			I	I	
<i>Perkin and Sahajwalla</i> [19, 42]	H	P		P	P	P	E			I

D=Diffusion-limited, E=Equilibrium, H=Heat transfer limited, I=Infinite rate, K=Kinetic (power law) and bulk diffusion, P=Power law kinetics

2.3 A Review for study development

All models aforementioned have identified the reaction mechanisms of coal gasification with the application in UCG. Without doubt, each model has a contribution on the UCG modelling development. However, they still have a limitation to provide a particular reaction in the gasification mechanisms. It was described that the packed bed model has limitation to provide the radiation process, meanwhile the channel method could not provide the process of drying and pyrolysis reactions, and coal slab method has a limitation on identifying the cavity formation. Therefore, further study need to be attempted to improve the model development.

An improvement was attempted by *Shirazi et.al* [80], by combining the method of packed bed and channel to improve the gasification reaction mechanisms. *Shirazi* developed a small scale 3D packed bed model (3cm x 1.5cm x 2cm) for shrinking coal seams using a CFD software. The model was developed by fulfilling the set of governing equations, such as momentum and energy conservation, transport of species, equation of state, and heat transfer mechanisms. The model assumes the gas and solid from the porous media, and they were in thermal equilibrium condition at each cell. The cavity development was tracked by the decrease of porosity because of thermal effects. Porosity increases as the solids are consumed by reactions or species' transfer from the solid phase to gas phase following the thermal effects. The coal seam was considered to be a porous medium with a defined initial porosity and permeability. However, the porous media presented in this model does not allow for solid species to participate in reactions. That is why no separated mass conservation equation was solved for the solid phase.

With almost similar procedures, *Zogala et al.* [54] from the Central Mining Institute (GIG), Poland, developed the UCG model as a coal block (2.6m x 0.7m x 0.7m) and

gasification channel (2.6m x 0.05m x 0.05m) as a porous medium to perform the gasification reactions. They were more concerned about the syngas formation under the effects of steam in gasification agent parameters. However, they have similar limitation with the model of Shirazi to provide coal mass conservation.

The existing of UCG model developed by *Shirazi* and *Zogala* has limitations in performing coal mass shrinkage, because they could not provide the coal mass conservation due to the reactions. As was highlighted earlier, the seam coal in the gasification channel was presented as a porous medium, but in the modelling application its properties were presented as a liquid or fluid. The coal itself consists of multi-phase component species dominated by solids. They have devolatilization/pyrolysis reaction mechanisms, in which the volatile material is released from the solid coal. These reactions were also limited when presented in *Shirazi's* and *Zogala's* model application. Therefore, this study improves the reaction mechanisms that were more reliable for coal and also includes the coal mass shrinkage that occurs in the UCG application.

The model offered through this study presents coal as a multi-phase component material, and therefore Lagrangian or multi-phase component reaction mechanisms can be performed in the reaction. A similar mechanisms model was developed but with multi-phase reactions in devolatilization reactions. Meanwhile, a governing equation was set up similar to the model of *Shiraz* and *Zogala*, with considering the coal mass conservation equation. In further application, this model will be applied into coal particle bed packed to form a block coal. Therefore, currently, the main purpose of this study is to explore the reliability of coal performance in the gasification reaction mechanisms.

Chapter 3 Methodology for the development of a single coal particle model in drop tube furnace

The research and development of UCG modelling, involving various previous studies, were explained in the previous chapters. This chapter focuses on a numerical method for developing the coal particle model of gasification. The particle model approach is offered because it can provide a more reliable process of coal to present in the reactions. It is also based on understanding that the coal reaction mechanisms are regardless of size, and therefore this research initiates its development from the particle level.

3.1 Gasification reaction mechanisms

The coal gasification process consists of several stages; drying, devolatilization/pyrolysis, oxidation, and reduction [40]. In the UCG application, the process is ended by the gas drying and distillation before exiting through the production well [9], as was illustrated in Figure 1-6 (Chapter 1). This study offers the particle approach for UCG application, and the gasification process is further illustrated in Figure 3-1.

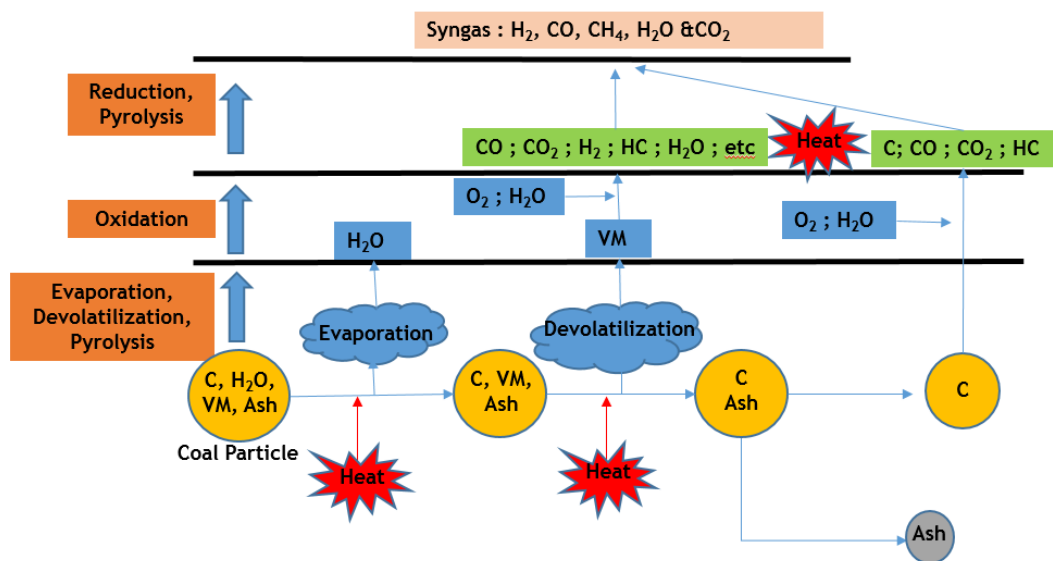


Figure 3-1. Coal Particle Gasification Process

The initial process of coal gasification is drying or evaporation, in which liquid (water) leaves the coal particle as a steam. This is followed by devolatilization, or the pyrolysis process, which relates to the process of releasing gas-matter from the coal particle because of heat or a reaction process in the absence of oxygen. The gas is named coal volatile/volatile matter and the species remaining in the coal particle is called char. The further reaction of the coal particle is oxidation, where the coal reacts with oxygen to produce CO₂, H₂O, and CO. The final stage of the gasification reaction is reduction, which is intended to cause all gas products to be in the form of syngas [40]. The chemical reactions of Figure 3-1 can be expressed with the mechanisms as seen in Table 3-1.

Table 3-1. Main gasification reactions [25, 54]

No	Reaction Name	Mechanism	Enthalpy (kJ/mol)
R1	Devolatilization	Raw coal \rightarrow (YY)Coal volatile + (I-YY) Char	
R1	Char oxidation	$C + O_2 \rightarrow CO_2$	-393
R3	Char oxidation	$C + 0.5O_2 \rightarrow CO$	-111
R4	Boudouard reaction	$C + CO_2 \rightarrow 2CO$	+172
R5	Water gas reaction	$C + H_2O \rightarrow CO + H_2$	+131
R6	Methanation reaction	$C + 2H_2 \rightarrow CH_4$	-75
R7	Coal Volatile oxidation	Coal Volatile + O ₂ \rightarrow CO ₂ + H ₂ O + N ₂	
R8	Oxidation	$CO + 0.5O_2 \rightarrow CO_2$	-283
R9	Water formation	$H_2 + 0.5O_2 \rightarrow H_2O$	-242
R10	Water gas shift reaction	$CO + H_2O \rightarrow CO_2 + H_2$	-41
R11	Reforming of methane with steam	$CH_4 + H_2O \rightarrow CO + 3H_2$	+206
R12	Partial oxidation of methane	$CH_4 + 0.5O_2 \rightarrow CO + 2H_2$	-36
R13	Reforming of methane with CO ₂	$CH_4 + CO_2 \rightarrow 2CO + 2H_2$	+247

Chemical reactions in Table 3-1 are commonly used in the application of UCG modelling [9, 54, 80]. Thirteen chemical reactions [54, 81] have been applied. The reactions R1 – R6 are heterogeneous reactions, and in the UCG application they take place on the wall plane of coal seams between the gas and solid coal. Meanwhile, other reactions occur in the channels or reactors, between gas species and are known as homogeneous reactions.

3.1.1 Heterogeneous reaction

The gasification reactions in Table 3-1 are considered as devolatilization reactions for the initial stage, and are then followed by the homogenous and heterogeneous reactions that

occur simultaneously. Heterogeneous reactions involve at least two different phases of species in the reactants. As in the initial reaction, in the devolatilization reaction or pyrolysis, the coal is converted to volatile matter and char as an effect of external heat in the absence of oxygen [53]. The devolatilization reaction is written as [82].



Here s and g denote solids and gas respectively, while YY is the stoichiometric coefficient. In the first order rate method, the reaction rate coefficient k_{devol} (1/s) is expressed in the Arrhenius form,

$$k_{devol} = AT^\beta \exp\left(\frac{-E_a}{R_u T}\right) \quad (1)$$

where, A is the frequency factor or pre-exponential factor, T is the temperature (K), β is the temperature exponent, E_a is the activation energy, and R_u is the universal gas constant.

The devolatilization rate of coal is given by

$$\frac{dm_i}{dt} = -k_{devol}\alpha_i m \quad (2)$$

where, α_i is the particle volume fraction for species i , m is the total mass of particle/species.

Particle reactions begin when the volatile fraction of raw coal has completely evaporated, and they could consist of multiple solids. In this study, the particle is dominated by the char as a carbon element. As shown in Table 3-1, the heterogeneous reaction is initiated by the coal particle (char) oxidation to form carbon dioxide [83] (R2), and is then followed by the other four reactions (R3-R6). The rate of coal particle reaction is determined by the combined effect of the Arrhenius-type reaction kinetics and gas-reactant diffusion rates to the particle surface. Since char is dominant, the reaction rate co-efficient can be presented by the char reaction (the first order rate method) [82], with the reaction rate coefficient of char, k_{char} (1/s), in the Arrhenius form being given by

$$k_{char} = AT^\beta \exp\left(\frac{-E_a}{R_u T}\right) \quad (3)$$

the rate of consumption of the solid component (char) is determined by

$$\frac{dm_i}{dt} = -\frac{k_m k_{char}}{k_{char} + k_m} \phi C_g M_w A_p, \quad (4)$$

where,

$$k_m = \frac{Sh D_m}{d}. \quad (5)$$

In the above equations, ϕ is the stoichiometric ratio of solid and gas reactant, C_g is the reactant gas concentration ($kmol/kg$), M_w is the molecular weight of solid reactant, A_p is the surface area of particle (m^2), Sh is the Sherwood number, d is particle diameter, and finally D_m is the diffusion coefficient [82].

3.1.2 Homogenous reaction

The homogeneous reactions (R7 – R13) occur between the gas species in the channel of UCG or reactors of the gasification, as defined in Table 3-1. The rate of j th reaction (R_j) in the homogeneous reactions, as a function of the composition and the rate constant, is determined by the following equation

$$R_j = -k_j \prod_{all\ reactants} \left(\frac{\rho Y_i}{M_i}\right)^{p_{ij}}. \quad (6)$$

where, k_j is the reaction rate coefficient of reaction j , ρ is the density, Y_i is the mass fraction of species i , M_i is the molecular weight of species i , and p_{ij} is the exponent for species i in reaction j .

3.2 Governing equations

The state of mass and species in the gasification simulation change over time. The governing equations consist of the equation of continuity, momentum, chemical species transport, and conservation of energy. The simulation under consideration uses an

axisymmetric model and, therefore, the governing equation is presented in the axial and radial directions. For the continuity equation, it is written as [84]:

$$\frac{\partial \rho}{\partial t} + \frac{\partial(\rho u_x)}{\partial x} + \frac{\partial(\rho u_r)}{\partial r} + \frac{\rho u_r}{r} = 0, \quad (7)$$

where, u is the velocity (m/s), t is time (s), x is the axial coordinate, r is the radial coordinate, and the subscript x and r indicates a direction.

The axial direction of the momentum conservation is expressed as:

$$\begin{aligned} & \frac{\partial(\rho u_x)}{\partial t} + \frac{1}{r} \frac{\partial(r \rho u_x u_x)}{\partial x} + \frac{1}{r} \frac{\partial(r \rho u_r u_x)}{\partial r} \\ & = -\frac{\partial p}{\partial x} + \frac{1}{r} \frac{\partial}{\partial x} \left[r \mu \left(2 \frac{\partial u_x}{\partial x} - \frac{2}{3} (\nabla \cdot \vec{u}) \right) \right] \\ & + \frac{1}{r} \frac{\partial}{\partial r} \left[r \mu \left(\frac{\partial u_x}{\partial r} - \frac{\partial u_r}{\partial x} \right) \right] + \rho g_x \end{aligned} \quad (8)$$

In the meantime, the equation for the radial direction of momentum conservation is expressed as:

$$\begin{aligned} & \frac{\partial(\rho u_r)}{\partial t} + \frac{1}{r} \frac{\partial(r \rho u_x u_r)}{\partial x} + \frac{1}{r} \frac{\partial(r \rho u_r u_r)}{\partial r} \\ & = -\frac{\partial p}{\partial r} + \frac{1}{r} \frac{\partial}{\partial x} \left[r \mu \left(\frac{\partial u_r}{\partial x} - \frac{\partial u_x}{\partial r} \right) \right] \\ & + \frac{1}{r} \frac{\partial}{\partial r} \left[r \mu \left(2 \frac{\partial u_r}{\partial r} - \frac{2}{3} (\nabla \cdot \vec{u}) \right) \right] - 2 \mu \frac{u_r}{r^2} \\ & + \frac{2}{3} \frac{\mu}{r} (\nabla \cdot \vec{u}) \end{aligned} \quad (9)$$

where, $\nabla \cdot \vec{u} = \frac{\partial u_x}{\partial x} + \frac{\partial u_r}{\partial r} + \frac{u_r}{r}$, μ is the viscosity coefficient, p is the pressure, and ρg_x is the gravitational body force.

The concentration of species can be expressed in terms of the mass fraction, $m_i(x, r, t)$, or the concentration of species $C_i = m_i \rho$, which is defined as the mass of species per unit volume. The conservation law of chemical species is represented as [84],

$$\frac{\partial}{\partial t} (\rho m_i) + \nabla \cdot (\rho m_i V + J_i) = R_i, \quad (10)$$

where, R_i is the account for the production or consumption of the species by chemical reaction, J_i is the molecular mass flux of species i , and V is a gas velocity.

The energy equation in this simulation may be written as [84]:

$$\frac{\partial(\rho E)}{\partial t} + \nabla \cdot (u(\rho E + p)) = -\nabla \cdot \left(\sum_j h_j J_j \right) + h_s \quad (11)$$

In this equation, E is the total energy, and h_s as heat generation includes the heat of the chemical reaction, any inter-phase exchange of heat and any other user-defined volumetric heat source.

The gas state condition is an important parameter in the study of gasification. The equation state for ideal gas is considered to perform as the gas reactant and product behaviour in the reactor. This is expressed as,

$$pV = nR_u T \quad (12)$$

This equation connects the thermodynamic correlation of gas properties such as, p , ρ , and T [84].

3.3 Turbulence model

Most existing flows, and in engineering practice, are turbulent. These are identified by an unstable condition at above a certain Reynolds number [85]. Therefore numerical studies need various approaches and methods for performing the effect of turbulence in a fluid flow. The numerical approaches of turbulence can be divided into two groups; simulations and modelling. In simulations, the calculation is based on the actual or real size of the flow, and in modelling, instead of calculating the actual size of the flow, the problem is recast as a system of equations for mean flow quantities, such as mean velocity and pressure and Reynolds stresses [84]. Indeed, various approaches of numerical methods can be used to perform simulation and modelling. They are the Direct Numerical Simulation (DNS) and the Large Eddy Simulation (LES) methods for simulation, and the Reynold-averaged Navier-Stokes (RANS) method for modelling. This study uses modelling with the RANS method to perform the effect of turbulence in the flow, since

it is more suitable for a system with complex equations and reactions [84, 86]. And, RANS also has the benefit of giving the lowest computational cost.

To obtain the Reynolds-Averaged Navier-Stokes equations, each solution variable φ in the instantaneous Navier-Stokes equations is decomposed into its mean, or averaged, value $\bar{\varphi}$ and its fluctuating component φ' :

$$\varphi = \bar{\varphi} + \varphi' \quad (13)$$

where, φ represents velocity components, pressure, energy, or species concentration.

After applying the Favre-time-averaging procedure, the RANS equations are as follows:

$$\begin{aligned} \frac{\partial(\rho u_x)}{\partial t} + \frac{\partial(\rho u_x u_r)}{\partial r} = \\ -\frac{\partial(p)}{\partial x} + \frac{\partial}{\partial r} \left[\mu \left(\frac{\partial}{\partial r} u_x + \frac{\partial}{\partial x} u_r - \frac{2\partial}{3\partial x_k} u_k \delta_{i,j} \right) - \rho \overline{u'_x u'_r} \right] \end{aligned} \quad (14)$$

These equations are not solved because the component Reynold stress tensor, $-\rho \overline{u'_x u'_r}$ is unknown and cannot be expressed directly as a function of u and p . Therefore, additional transport equations are required to solve this equation.

A number of approaches have been proposed to solve this equation. Amongst them, the most popular models are $k - \epsilon$ and $k - \omega$ [87-91]. Basically, these methods come up with a solution with two additional transport equations. A common method employs the *Boussinesq* hypothesis [92] used in these turbulence models:

$$-\rho \overline{u'_i u'_j} = \mu_t \left(\frac{\partial}{\partial x_j} u_i + \frac{\partial}{\partial x_i} u_j \right) - \frac{2}{3} \delta_{i,j} \left(\mu_t \frac{\partial}{\partial x_k} u_k + \mu_B \right) \quad (15)$$

Where, μ_t is the turbulent viscosity and μ_B is the bulk viscosity and is also known as volume viscosity, which expresses the resistance of the fluid against the rapid changes in volume. In the case of $k - \epsilon$, the two additional transport equations provide a solution for the turbulence kinetic energy k and the turbulence dissipation rate ϵ , and μ_t is computed as a function of k and ϵ . In addition, in the case of $k - \omega$ model the term ω is basically a field function of k/ϵ . Both methods have been proven to give good results for different turbulent flow regimes and have been commonly used with gas and coal combustion models for the simulation [93]. The $k - \epsilon$ models have been used in this work. This is

because they are more reliable for dealing with the free-stream flow which occurred in the area of inlet boundary conditions at internal flows [86].

There are three $k - \epsilon$ models available; standard, RNG (renormalization-group) [94], and realizable [95] models. The RNG model has a similar form to the standard $k - \epsilon$ model, and was developed by *Yakhot and Orszag* [94] in response to the empirical nature of the standard $k - \epsilon$ model. The Realizable $k - \epsilon$ model contains a new transport equation for the turbulent dissipation rate ϵ [96] and a critical coefficient of the model C_μ which is expressed as a function of mean flow and turbulence properties, rather than being assumed to be constant as in the standard model. This procedure lets the model satisfy certain mathematical constraints on the normal stresses consistent with the physics of turbulence (realizability). The concept of a variable C_μ is also consistent with experimental observations in boundary layers. This model is substantially better than the Standard $k - \epsilon$ model for many applications and can generally be relied upon to give answers that are at least as accurate. Therefore, this model is considered to use Realizable $k - \epsilon$.

The k model is the transport equation for turbulent kinetic energy and may be represented as

$$\frac{\partial(\rho k)}{\partial t} + \text{div}(\rho k \vec{u}) = \text{div} \left[\left(\mu + \frac{\mu_t}{\sigma_k} \right) \text{grad } k \right] + G_k - \rho \epsilon \quad (16)$$

where, G is the filter function that satisfies the normalisation condition.

While, the ϵ model is the transport equation for viscous dissipation (the rate at which the kinetic energy of small scale fluctuation is converted into heat by viscous friction) and is represented as,

$$\frac{\partial(\rho \epsilon)}{\partial t} + \text{div}(\rho \epsilon \vec{u}) = \text{div} \left[\left(\mu + \frac{\mu_t}{\sigma_\epsilon} \right) \text{grad } \epsilon \right] + C_{\epsilon 1} P_k \frac{\epsilon}{k} - C_{\epsilon 2} \rho \frac{\epsilon^2}{k} \quad (17)$$

In this simulation the constants used for the equation above are: $C_{\epsilon 1} = 1.44$; $C_{\epsilon 2} = 1.9$; $\sigma_k = 1$; $\sigma_\epsilon = 1.2$ [84].

3.4 Thermal radiation

Thermal radiation is the emission of electromagnetic waves from all matter that has a temperature greater than absolute zero. The net thermal motion of charged particles results in charge-acceleration and dipole oscillation. This behaviour drives the electrodynamic generation of coupled electric and magnetic fields, which cause the emission of thermal radiation [97]. The energy of radiation will be transported from this high temperature to cooler surroundings. The thermal radiative heat flux from a blackbody to isothermal surroundings is given as

$$Q_r = s_b(T_s^4 - T_{sur}^4) \quad (18)$$

where, $s_b = 5.67 \times 10^{-8}$ (W/m².K⁴) is the Stefan-Boltzmann constant, T_s is the temperature of particle surface, and T_{sur} is the temperature surroundings. The radiative flux is proportional to T^4 , and therefore it becomes significant at high temperature compared to the heat transfer following convection or conduction. The radiative flux is also affected by the composition of the surrounding species that have been passed through by the radiation. For example, mainly CO₂ and H₂O absorb and emit a significant amount of radiation in the thermal spectrum. In contrast, diatomic gases as N₂ and O₂ have no significant absorption bands, and, therefore, the radiative flux propagates fast as under vacuum condition.

There are two approaches that can be considered to calculate the intensity of electromagnetic waves propagation; surface to surface (S2S) and a participating media radiation method. In the case of gasification, gas products are present, and therefore this study uses the participating media radiation approach. The effect of media participation can be approached by using the Discrete Ordinate Method (DOM) which simulates thermal radiation exchange between diffuse or specular surfaces forming a closed set [97-99]. The surface radiative properties are quantified in terms of emissivity, specular and diffuse reflectivity, transmissivity, and radiation temperature. These properties do not depend on direction.

The medium that fills the space between the surfaces can also absorb, emit or scatter radiation. Therefore, the amount of radiation that each surface receives and emits depends on this effect, as well as the optical properties of the surface and the thermal boundary

conditions that are imposed on it. As radiation travels through a medium, the intervening material absorbs and increases its radiant intensity, I in the Ω direction. The radiative transfer equation (RTE) governs this process and can be written in terms of radiant intensity for a specific wavelength λ as,

$$\frac{dI_\lambda}{ds} = -\beta_\lambda I_\lambda + k_{a\lambda} I_{b\lambda} + \frac{k_{s\lambda}}{4\pi} \int_{4\pi} I_\lambda \Omega d\Omega + k_{pa\lambda} I_{pb\lambda} + \frac{k_{ps\lambda}}{4\pi} \int_{4\pi} I_\lambda \Omega d\Omega \quad (19)$$

where, I_λ is the radiative intensity at wavelength λ ($W/(m^2 srm^{-1})$), β_λ is the extinction coefficient, $k_{a\lambda}$ is the absorption coefficient at wavelength λ (m^{-1}), $I_{b\lambda}$ is the black body intensity at wavelength λ , $k_{s\lambda}$ is the scattering coefficient at wavelength λ (m^{-1}), Ω is the solid angle, $k_{pa\lambda}$ is the particle absorption coefficient at wavelength λ (m^{-1}), $I_{pb\lambda}$ is the particle blackbody intensity at wavelength λ and current particle temperature, and $k_{s\lambda}$ is the particle scattering coefficient at wavelength λ (m^{-1}).

3.5 Reaction-flow

The reaction mechanisms and governing equations that are present in the reactions were introduced in Sections 3.1 and 3.2. In the reacting flow, the effects of species-reactions need to be considered in the modelling procedures. There are several methods provided in the StarCCM software for this purpose; Complex Chemistry, Eddy Contact Micromixing (ECM) and Eddy Break-Up (EBU) [100].

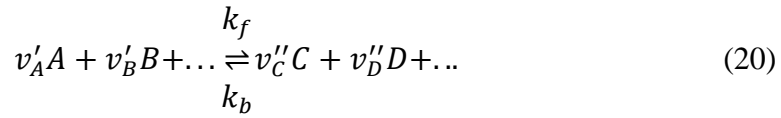
Complex Chemistry problems are solved by using a stiff ODE (Ordinary Differential Equation) solver to integrate the chemical source terms. In calculating the turbulence effects in combustion, the method of Laminar Flame Concept (LFC) model or the Eddy Dissipation Concept (EDC) model should be considered. The Complex Chemistry model is suitable for introducing detailed chemistry information to the CFD simulation. This model can solve thousands of reactions among hundreds of species — hence the term complex chemistry - and is a preferred method used to perform these homogeneous reactions.

The Eddy Contact Micromixing (ECM) method is used when solving the reaction rates of the reacting flow by expressing them in a molecular form and, therefore, it is named

micromixing. This method is suitable for performing liquid-liquid reactions. Liquids have low diffusivity, and the reaction is limited by the diffusion rate of the liquid interface.

The Eddy Break-Up model is intended to carry out the reacting flow with fast chemistry. The reaction rate is determined by the rate at which turbulence causes mixing of the reactants and heat. This model is applicable perform both to homogeneous and heterogeneous reactions.

Of all these transport mechanisms the EBU method is preferable for this study. This is because the EBU can be used to perform the multi-phase (Lagrangian) reactions flow. The description of EBU model is initiated from the general reaction as in eq.(20),



where, the stoichiometric coefficients v with superscript ' and " indicate a reactant and product, respectively; k_f is the rate constant of the forwards reactions, and k_b is the rate constant of the backwards reaction. The production or consumption rate, r_i of species i , depends on the reaction rates and the species' concentration in the reactions. The total net rate of all reactions, in which species i participates, is expressed in eq.(21)

$$r_i = \frac{d[A]}{dt} = \sum_{j=1}^{N_j} v_{ij} \left[k_{f,j} \prod_i [A]^{v'_{j,i}} - k_{b,j} \prod_i [A]^{v''_{j,i}} \right] \quad (21)$$

where, net stoichiometric coefficient v_{ij} gives the total number of moles of species i that are produced or consumed by the reaction, j .

The EBU models solve individual transport equations for mean species concentrations on the computational grid [101]. The reaction rates that are used in the transport equations are calculated as functions of the mean species concentrations, turbulence characteristics and, depending on the specific model that is used, temperature. A mean enthalpy equation is solved in addition to the species transport equations. The mean temperature and density are then calculated knowing the mean enthalpy and species concentrations. In the EBU approach, the kinetic reaction source term for each species i , is obtained by multiplying the rate from eq.(21), with the molecular weight W_i . The species source term, S_i is

assumed as a function of chemical reaction rates and is a characteristic of timescales. EBU considers several methods for assuming these value functions such as the standard EBU, Hybrid EBU, and Kinetics EBU [101].

3.5.1 Standard EBU

The Standard EBU model assumes that species are mixed and immediately burnt. The chemical source term is calculated from the mixing time scale. For the reaction in eq.(20), the rate of fuel depletion is assumed to be:

$$r_F = -\frac{\rho}{W_F} \left(\frac{1}{\tau_{turb}} \right) A_{ebu} \min \left[Y_F, \frac{Y_O}{S_O} \right] \quad \text{moles}/(m^3s) \quad (22)$$

where, r_F is rate of fuel depletion (m^3s), ρ is fuel density (kg/m^3), τ_{turb} is turbulent time scale (s), A_{ebu} is EBU rate coefficient A, W_F is the molecular weight of fuel in a cell, Y_F is fuel mass fraction, Y_O is oxidizer mass fraction, and S_O is the ratio of oxidizer mass coefficient and fuel coefficient ($v_O m_O / v_F W_F$). When consider the products rate, the reaction can be seen:

$$r_F = -\frac{\rho}{W_F} \left(\frac{1}{\tau_{turb}} \right) A_{ebu} \min \left[Y_F, \frac{Y_O}{S_O}, B_{ebu} \left(\frac{Y_{P1}}{S_{P1}} + \frac{Y_{P2}}{S_{P2}} + \dots + \frac{Y_{Pj}}{S_{Pj}} \right) \right] \quad (23)$$

where, B_{ebu} is EBU rate coefficient B, while subscript p and j indicate a specific products. The *min* operator on the right-hand side indicates that the concentration of the limiting reactant is used to determine a mass fraction scale when calculating the reactant consumption rate. Eq.(23) is an optional modification of eq. (22) for premixed flames in which fuel and oxidizer are already mixed in the molecular scale. The reaction rate is determined by the rate at which the products are mixed with reactants.

3.5.2 Hybrid EBU

The Hybrid EBU model assumes that the minimum value of mixing and chemical kinetic time scale is rate-limiting and calculates the source term using eq. (21) multiplied by the molecular weight W_i of species i .

This model is expressed as:

$$r_i = -\min(|r_{i,kin}(\rho, Y_1, Y_1, Y_1, \dots, Y_N, T)|, |r_{i,mix}|) \quad (24)$$

3.5.3 Kinetic EBU

The Kinetics EBU model assumes that the reaction rate is dictated by finite-rate chemical kinetics. The source term is calculated by eq.(25), and the reaction rate is calculated by eq.(21).

$$\omega_i = \rho f \left(\frac{Y_i^* - Y_i}{\tau} \right) \quad (25)$$

Where, ω_i source term for i 'th species, f is the mean reaction rate multiplier, and τ is time integration for unsteady simulation. Basically this method is similar to complex chemistry but it can be used for a heterogeneous reaction by using the stiff reaction with a certain amount of kinetic parameter values.

As aforementioned, the EBU methods suit to be used for solving the multiphase-component reactions such in this case. In the standard and hybrid EBU, the role of time scale in mixing is very important to affect the reactions rate. Meanwhile, in kinetics EBU, the role of value of kinetic parameters dominate to control the reactions. The gasification process proceeds over a relatively long period of time, and the kinetic model provides the information about reaction mechanisms in an intermediate state [53]. Therefore, this study prefer to develop the model with kinetic EBU. It is also supported with the availability of data for the simulations, and therefore it more beneficial to use this approach [101].

3.6 Coal particle properties

The equation of motion for the particle is defined as,

$$m_p \frac{d\overline{u_{i,j,k}^p}}{dt} = \sum \overline{F}. \quad (26)$$

where, m_p is particle mass, $\overline{u_{i,j,k}^p}$ is average velocity of particle at direction i, j, k , and \overline{F} is a force vector. As the particle size used in this simulation is small, the lift force of the particle is neglected. However, the effects of the drag and gravity forces have been included since they have influence on the parameters being investigated.

A coal particle consists of multi-phase components, and, in the simulation, is composed of four constituent components; raw coal, char, ash, and H₂O. Raw coal consists of the volatile matter and char (fixed carbon). The multi-component coal material or the multi-component solid can be chosen from the Lagrangian Phase Models in StarCCM software. Choosing coal combustion will activate the three mass transfer models - namely Coal Devolatilization, Char Oxidation and Coal Moisture Evaporation. It is important to have the multi-component gas active in the gas-phase continuum with mandatory components involved in the reaction mechanisms as in Table 3-1, such as O₂, CO, CO₂, H₂, H₂O, CH₄ and coal volatile.

In order to provide coal performance in the combustion or gasification, information about the coal particle is needed, such as proximate analysis, ultimate analysis, calorific value (Higher Calorific Value (HCV) or Lower Calorific Value (LCV)), heat specific, and particle density. The proximate analysis is used to define the fuel composition in the injector. It also used with ultimate analysis results to define the species composition of raw coal and volatile matter, which is very important in performing the species balance in the reaction.

In order to have the correct heat release rate and flame temperature of coal combustion or gasification, it is important to calculate the heat formation of raw coal (H_{f-coal}). It can be calculated from the difference between the heat of the reaction for coal and the heat of formation for the products from coal combustion according to,

$$H_{f-coal} = \text{Sum} [H_f(\text{products})] - H_{rxn} \quad (27)$$

where, H_{rxn} is the LCV of the coal, and $H_f(\text{products})$ is the heat of formation of the products from coal combustion products (CO₂ and H₂O). After H_{f-coal} is obtained, then the heat of formation of coal volatile (H_fCV) can be obtained from the following formula:

$$H_fCV = H_{f-coal}/YY \quad (28)$$

YY is the mass stoichiometric co-efficient (volatile yield) for devolatilization based on proximate analysis, or it can also be seen in R1 in Table 3-1.

More detail of the coal particle properties development for simulation in StarCCM software can be seen in Ref. [102].

3.7 Numerical procedures

The coal particle gasification model was initially developed based on the reactions of combustion mechanisms [93, 103, 104]. The simulations were carried out using the CFD package StarCCM, and developed by considering several procedures:

3.7.1 Modelling space

The interior volume of the furnace needs to be constructed by using computational meshes as required in the CFD simulations. This simulation considers a two-dimensional axis-symmetric domain to present the cylindrical shape of the reactor, in this case is drop tube furnace. All meshes were constructed by using directed mesh procedures. The cells are concentrated at the centreline where the coal reaction is located and, as a result, large gradients in flow properties exist. Therefore, more cells are concentrated here to provide more accuracy in resolving the gradients. The growth ratio of the distance between cell nodes has been used and the cells size affects the accuracy of simulation. Therefore, the mesh independence study is required to perform this effect to the simulation.

3.7.2 Modelling time

The Implicit Unsteady model is used in the simulation with the segregated flow, fluid energy and species models. This model allows the simulation of the object based on iteration or time-step. The second-order scheme is used for discretization, with the criterion of convergence being set to 10^{-6} for energy and radiation, and 10^{-4} for the other terms of the transport equations.

3.7.3 Modelling flow and reactions

The coal particle simulation is conducted under a quiescent gas condition in the furnace and it is set by turning off the hot air flows at ten seconds prior to the particle injection. This treatment supports the creation of a homogeneous furnace gas temperature at around 1400K. Gas chemical species reactions are defined and Eddy Break Up (EBU) model with the kinetic control parameter is implemented in order to control the reaction mechanisms. The kinetic properties of each reaction have an important role in controlling the reaction mechanisms and the values can be found in the literature sources [53, 54].

The interaction of coal particles with the fluid is dealt with through the Lagrangian multi-phase model. Coal particle properties are defined and an injector is set up in order to control the particle injection into the furnace. The interactions of these species, and heat or energy in the fluid region, are governed through the transport equations already described in section 3.2. The model of numerical simulation is developed based on the experimental condition and then this result is validated. In the numerical simulation, coal particle behaviour inside Drop Tube Furnace (DTF) is represented as a single coal particle injected into the furnace. The injector can also be set for injecting coal particles continuously into the reactor. Some parameters, such as combustion time, species component fraction and temperature profile, can be identified through the simulation and then compared to the experimental result.

Chapter 4 Coal particle model development with a kinetic parameter study

4.1 Introduction

A coal particle gasification model was developed based on the reaction mechanisms presented in Table 3-1. Several references for the study of coal combustion modelling also refer to some of the reactions in this table [93, 103, 104]. In other words, the mechanisms of coal gasification can be developed with the reactions of coal combustion and other reactions to complete the syngas products formation.

The study initiates the development of this model intending to investigate the behaviour of gasification reactions at the oxidation stage. The model is used for initial validation, with data sourced from a number of reference papers on coal particle combustion. Of particular relevance is the experimental study of coal particle combustion conducted by *Levendis, and Khatami et.al* [105-108], (see Figure 4-1).

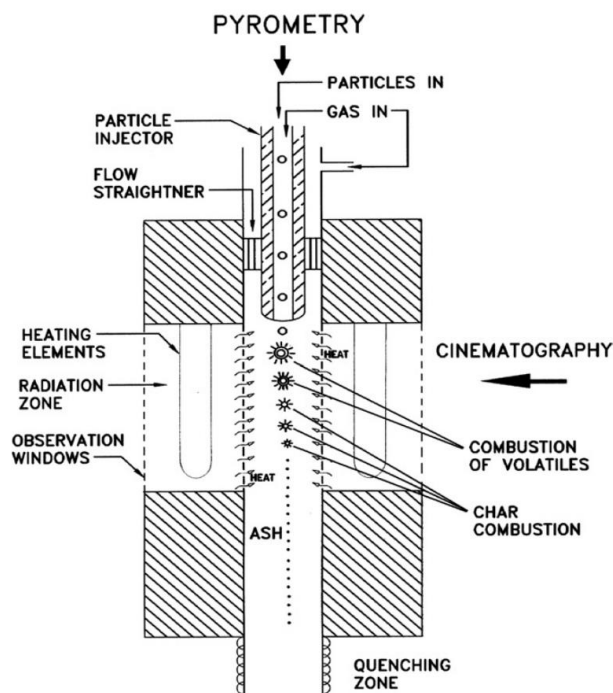


Figure 4-1. Drop tube furnace for coal particle combustion experiments [105]

The drop tube furnace used for the coal combustion experiment of *Levendis et.al* was equipped with a pyrometer and cinematography to track the coal particle temperature and also to capture the particle's behaviour. An electrical heater was used to heat up the reactor and it was maintained at a constant wall temperature of 1400K. (*Khatami and Levendis* in Ref.[109]) This study was concerned with the results of temperature measurements. The temperature was measured by using three signals in a voltage output of the pyrometer, and they were converted into the temperature profiles (See Figure 4-2).

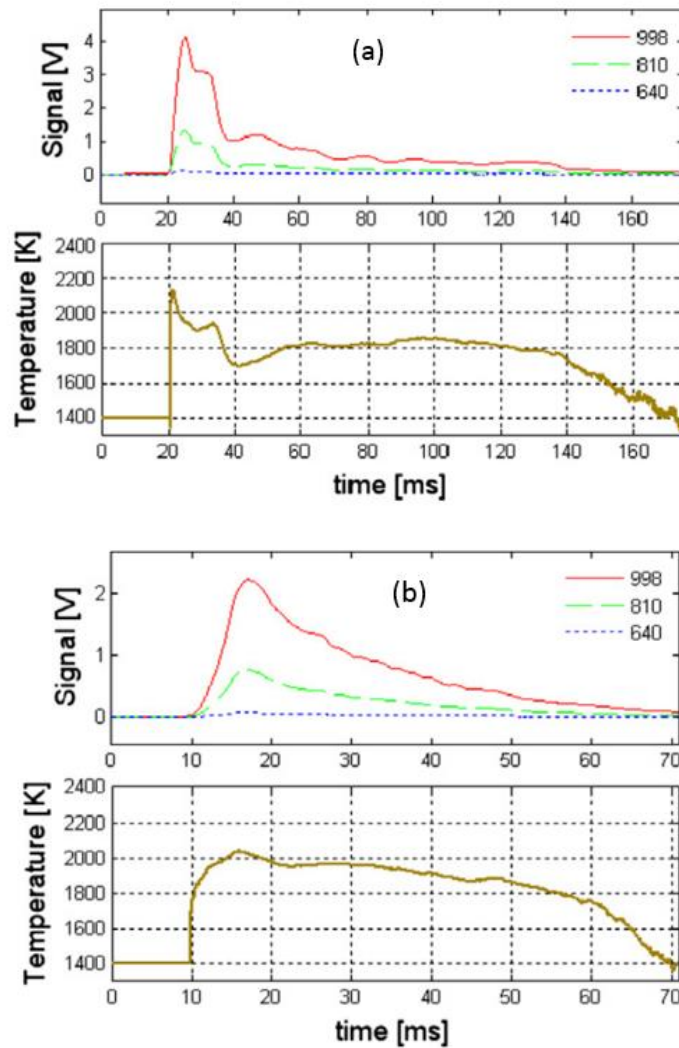


Figure 4-2. The signal outputs transformed to the temperature profiles of coal particle combustion for (a) Bituminous coal (PSOC-1451), and (b) Lignite coal (PSOC-1443) conducted by *Levendis et.al* [105]

The profiles of single coal particles of PSOC-1451 and PSOC-1443 were observed during combustion, as shown in Figure 4-2. At the top entry of each frame, the radiation intensity traces are displayed, which are expressed as voltage signals S_n , for three wavelengths of

the pyrometer ($n = 1, 2, 3$). At the bottom entry, corresponding temperature profiles are shown [105]. The temperature profile identifies the behaviour of each coal combustion process. It is therefore important to understand these behaviour as they directly relates to the combustion reactions study carried out in this chapter. Additionally, the coal particle combustion model will be used to identify the parameters affecting the combustion reactions. One of the crucial parameters examined are the kinetic properties.

4.2 Coal Particle model development

4.2.1 The geometry of the model and boundary conditions

The geometric model, as illustrated in Figure 4-3(a), is considered to be a cylindrical furnace (Drop Tube Furnace (DTF) shape) with an internal diameter of 7cm. The heated wall section of the furnace was 25cm measured from the inlet, and coal particle injection starts from the centre of the inlet. An axisymmetric model was used for the simulation, and in Figure 4-3(b), the grid distribution with the boundary conditions used is shown.

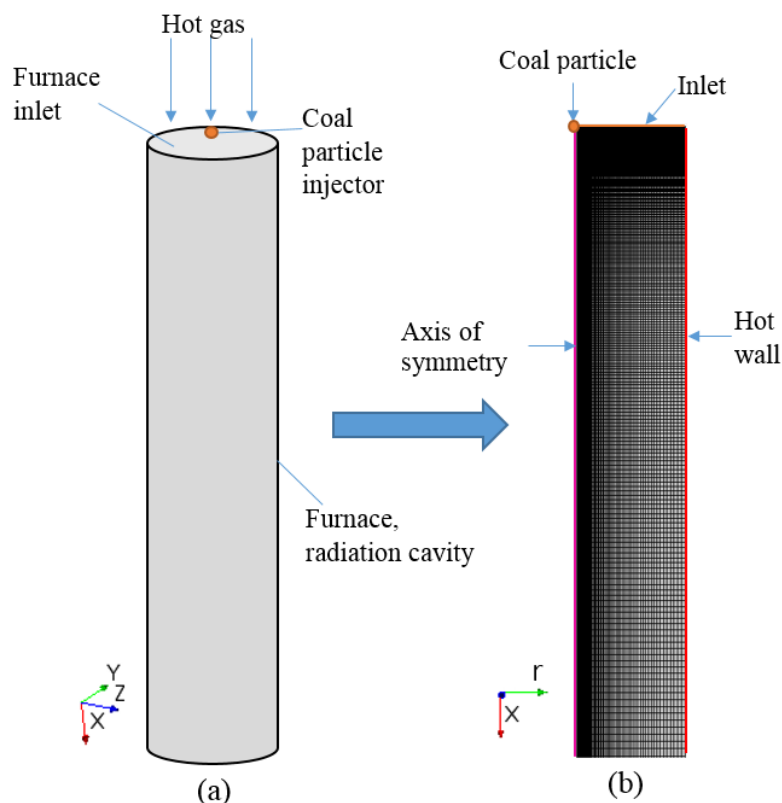


Figure 4-3. The furnace illustration (a) Furnace cylindrical shape (b) Axisymmetric model grid

From the experimental data [105], the initial boundary condition for the simulation is defined (see Table 4-1). The furnace was initially heated up with hot air at 1200K before the coal was injected, while the furnace wall temperature was maintained at 1400k. The inlet air velocity was 0.045m/s. The simulation was run to establish a fully-developed flow and, in order to accommodate the development region, the furnace wall was extended to 75cm and this portion kept adiabatic.

Table 4-1. The furnace boundary conditions

Parameter	Value
Hot gas velocity (ms ⁻¹)	0.045
Hot gas temperature (K)	1200
Furnace diameter (m)	0.07
Hot wall temperature (K)	1400
Coal particle diameter (mm)	0.075
Hot wall length (m)	0.25

The coal particle was injected into the furnace from the top. The simulation uses a single coal particle injection. Raw coal transformation and gas component production are investigated through the simulation. In the modelling, the reaction mechanisms of coal combustion are governed by the following set of chemical equations (Table 4-2).

Table 4-2. Reaction Mechanisms of coal combustion [93, 103]

No	Reaction Name	Mechanism	Enthalpy (kJ/mol)
R1	Devolatilization	Raw coal \rightarrow (YY)Coal volatile + (I-YY)Char	
R2	Char oxidation	$C + O_2 \rightarrow CO_2$	-393
R3	Char oxidation	$C + 0.5O_2 \rightarrow CO$	-111
R4	Boudouard reaction	$C + CO_2 \rightarrow 2CO$	+172
R5	Water gas reaction	$C + H_2O \rightarrow CO + H_2$	+131
R7	Coal Volatile oxidation	Coal Volatile + $O_2 \rightarrow CO_2 + H_2O + N_2$	
R8	Oxidation	$CO + 0.5O_2 \rightarrow CO_2$	-283

Note that Table 4-2 only shows the seven selected reactions, taken from the complete set of gasification mechanisms already presented in Table 3-1, to perform the combustion modelling. That is because these reactions lead to the development of the process of combustion of coal particles inside the furnace/reactor.

4.2.2 The grid selection and sensitive study

The interior volume of the furnace needs to be constructed by using computational meshes as required in the CFD simulations. The dimensions used for meshes are shown in Figure 4-3(b), with the centreline being aligned by the x -axis. The meshes were constructed by using a directed mesh procedure in StarCCM software. This operates by sweeping a mesh from the surfaces of a geometry through its volume onto a facing target surface. Directed meshing is ideal for meshing fluid flow simulations as it provides a structured mesh in the axial direction. As shown in Figure 4-3(b), the cells are concentrated at the centreline and also upstream of the furnace in order to provide better numerical stability while resolving the large gradients of the flow properties. The growth ratio between cell nodes has been used with an initial distance of 0.1 mm, and a number of divisions 308 and 68, along the axial and radial directions, respectively. For the purposes of the sensitivity study, initial mesh with a number of mesh cells of 20,944 was chosen with an identify (ID) of Mesh A. Another three differences of grid density were developed, with increases of approximately 5% of division numbers for each direction, and they were designated as Mesh B, C, and D. In addition, a mesh independence study was performed to investigate their effect on the simulated results with the aim of establishing a combination of mesh that is best suited for simulation performance. The number of cells for each mesh ID can be seen in Table 4-3.

Table 4-3. Mesh resolution used for study

Mesh	Number of cells
A	20,944
B	23,760
C	29,925
D	35,916

The mesh independent test was conducted in the hot air flow conditions and before the coal injection. The gas temperature was used as a parameter of comparison at steady state or fully developed condition, or at around 30s after it was injected. The effects of the grid size variation are presented by the gas temperature variation of each grid size along the axis (x – direction) and along the radial directions at certain distances from the inlet. The temperature variation along the axis can be seen in Figure 4-4, and the contour plot of furnace temperature can be seen in Figure 4-5.

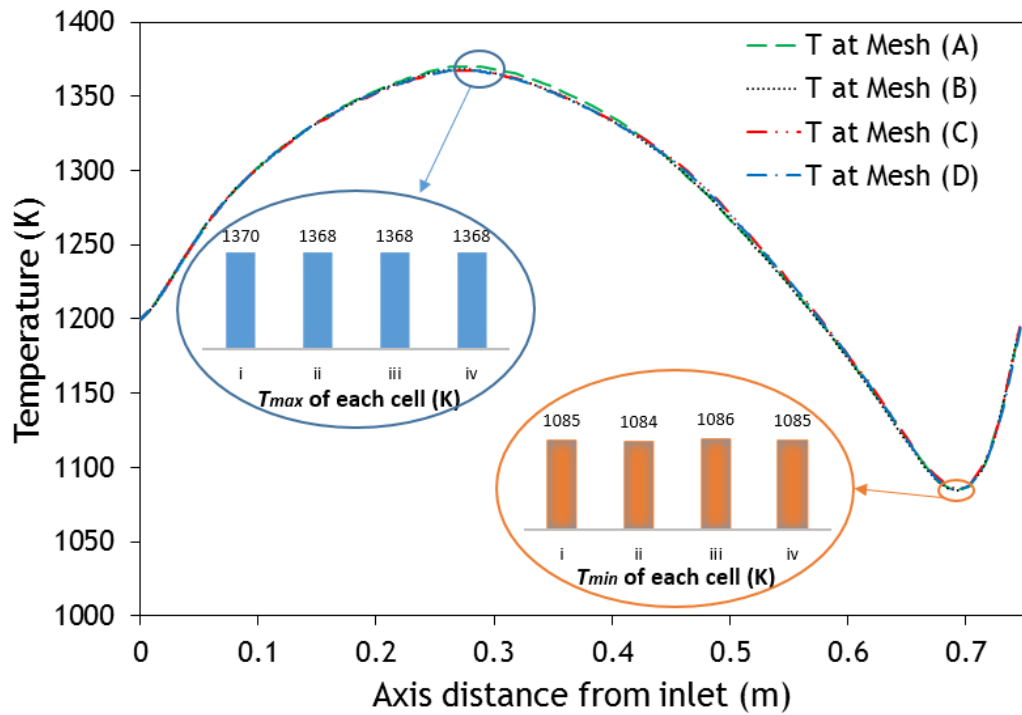


Figure 4-4. Grid size variation test for gas temperature along the centre line

Figure 4-4 shows the gas temperature along the axis for each mesh-size, and they are almost similar. The temperature difference at the maximum and minimum points is very small and therefore can be ignored. The contour plot of furnace temperature also can be considered to identify any possible impacts of varying mesh resolution in the entire domain (See Figure 4-5). This has been further explored through a set of direct comparative plots of the temperature distribution in the radial direction at several distances along the axis (see Figure 4-6). Again, as clearly seen in both the figures that the results predicted by the chosen meshes have similarity. This therefore indicates that the grid size variation implemented has no significant issue in these simulations.

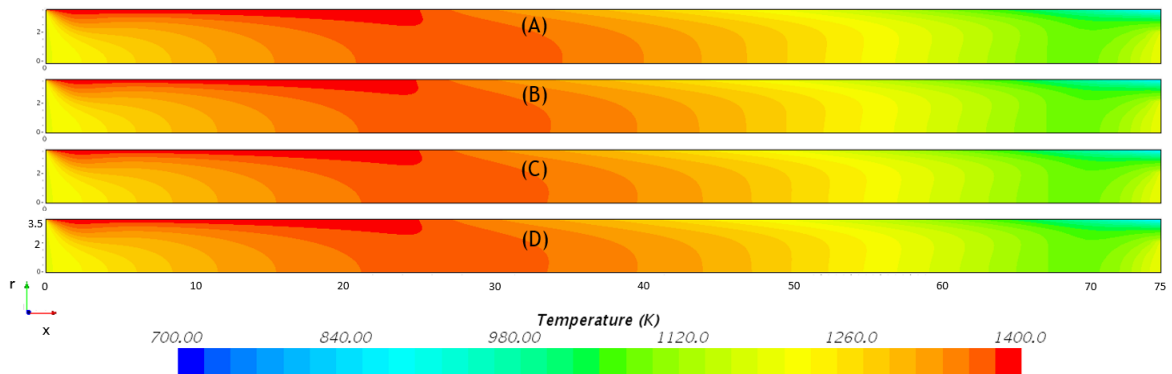


Figure 4-5. Contour plot of temperature distribution inside the furnace

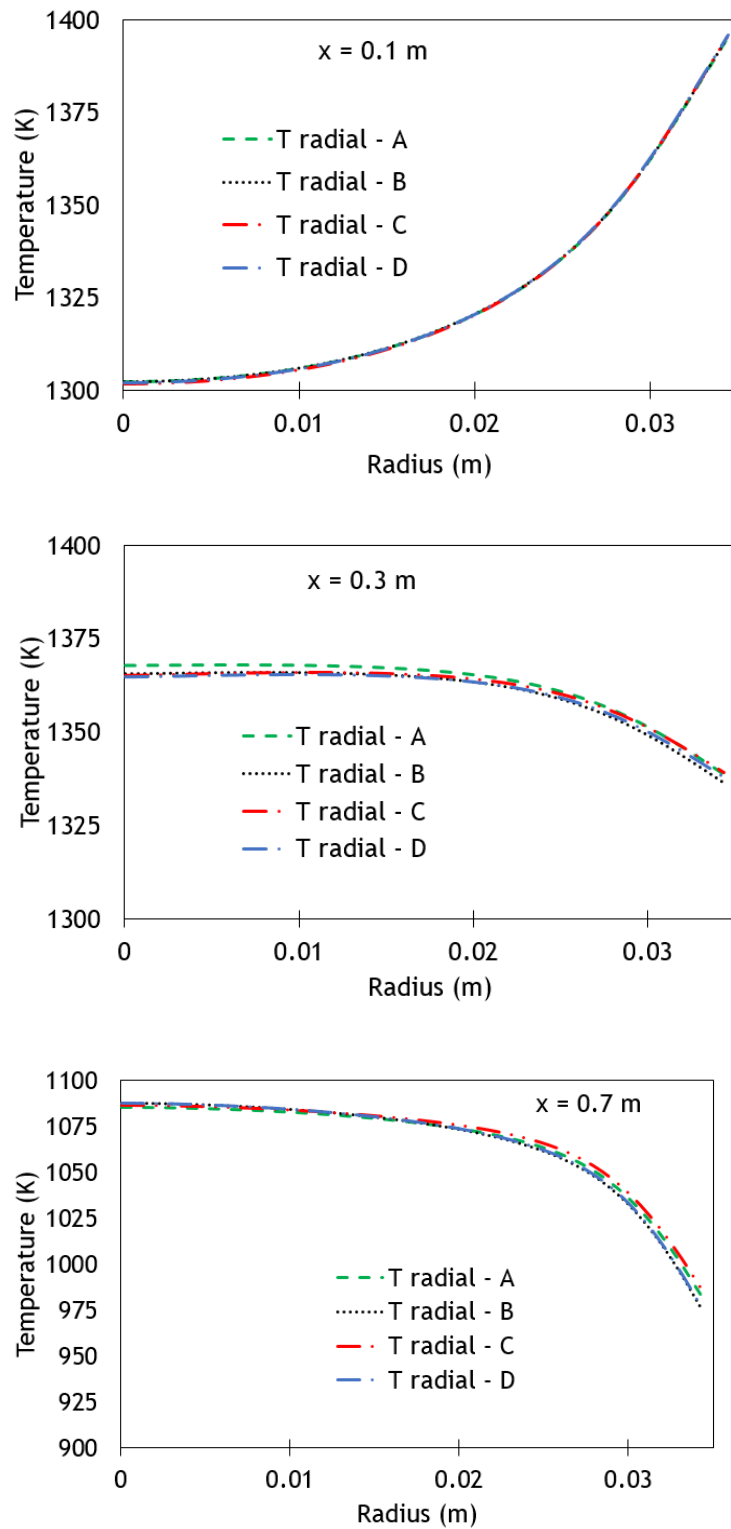


Figure 4-6. Grid size variation test for gas temperature along the radial direction at $x=0.1$ m, $x=0.3$ m, and $x=0.7$ m

However, to avoid any potential issue with numerical stability, this study has considered the grid size with 29,925 cells in order to perform all the numerical simulations. The results of simulation will also be further validated with the experimental data.

4.2.3 The coal properties

Simulation of coal particles is carried out with bituminous and lignite samples of PSOC 1451 and PSOC 1443, respectively; for detailed properties, such as its proximate and ultimate analyses, see Table 4-4 [105].

Table 4-4. Chemical compositions of coal [105]

	PSOC 1451	PSOC 1443
Proximate Analysis as received		
Moisture (%)	2.5	18.6
Volatile matter (%)	33.6	50.3
Fixed Carbon (%)	50.6	13.7
Ash (%)	13.3	17.4
Ultimate Analysis (dry basis)		
Carbon (%)	71.9	56.8
Hydrogen (%)	4.9	4.1
Oxygen (%) (by diff.)	6.9	15.8
Nitrogen (%)	1.4	1.1
Sulphur (%)	1.4	0.7
Sodium (%)	0.06	0.04
Ash (%)	13.7	21.4
Heating value dry fuel (MJ/kg)	31.5	23.0

The table gives important information that can be used to define the chemical compounds of coal and its volatile contents as was highlighted in the methodology chapter (Chapter 3). Since the focus is only on the combustion and gasification process, sulphur (S) elements from the ultimate Dry-Ash Free (DAF) analysis are neglected. Further, based upon the proximate and ultimate correlations, the PSOC 1451 and PSOC 1443 coal volatile compositions are defined as $\text{CH}_{2.7} \text{O}_{0.248} \text{N}_{0.058}$ and $\text{CH}_{1.2255} \text{O}_{0.2952} \text{N}_{0.0235}$, respectively. The YY value of 0.29 and 0.7068, for PSOC 1541 and 1443, respectively, are stated in the reaction balance (R1). However, the PSOC 1451 will be further investigated, and afterwards the PSOC 1443 will be taken for comparison and further investigation will be carried out on the devolatilization reactions.

In the experimental study, the coal particle freely falls into the reactor. Therefore, the coal particle simulation was conducted under a quiescent gas condition in the furnace. It was

set by turning off the hot air flows a few seconds prior to the particle injection. This treatment supports the creation of a homogeneous furnace gas temperature at around 1400K. The coal particle diameter used is $75\mu\text{m}$, which is the size commonly used in pulverized coal power plants and modelled as a spherical particle.

4.3 Overview of the kinetic parameters

The kinetic parameters, such as the pre-exponent factor (A), activation energy (E_a), and temperature exponent (β), are needed to develop the numerical modelling of reaction applications. These values are obtained through the experiments [110], such as from the entrained flow reactors test facilities [111].

Table 4-5. Parameters of chemical kinetics from different studies [53]

Reaction no	Kinetic parameters			Ref.
	A (unit vary)	E_a (J/kmol)	β	
R1	3.12E+05	7.40E+07	0	<i>Blaid et.al</i> [93]
R2	0.002	7.90E+07	0	<i>Blaid et.al</i> [93]
	322	9.01E+07	0	Tomeczek [112]
	1225	9.98E+07	0	<i>Li et.al</i> [113]
	11000	1.13E+08	0	<i>Boiko et.al</i> [114]
R3	0.052	1.33E+08	0	<i>Blaid et.al, Silaen 09 et.al</i> [93, 115]
	0.002	7.90E+07	0	<i>Chen et.al</i> [116]
	3.3	6.11E+07	0	<i>Silaen 10 et.al</i> [117]
	85500	1.40E+08	0.84	<i>Watanabe et.al</i> [118]
R4	4.4	1.62E+08	1	<i>Blaid et.al , Silaen10 et.al</i> [93, 117]
	0.0732	1.13E+08	0	<i>Silaen 09 et.al</i> [115]
	6.94E+04	1.85E+08	1	Tomeczek [112]
	242	2.75E+08	0	<i>Chen et.al</i> [116]
	7.38E+03	1.38E+08	0	<i>Li et.al</i> [113]
	8.55E+04	1.40E+08	0.84	<i>Watanabe et.al</i> [118]
	7.90E+05	2.14E+08	0	<i>Boiko et.al</i> [114]
R5	1.33	1.47E+08	1	<i>Blaid, Silaen 10, Mayers</i> [93, 117, 119]
	7.82E-02	1.15E+08	0	<i>Silaen 09 et.al</i> [115]
	4.26E+02	3.16E+08	0	<i>Chen et.al</i> [116]
	1.60E+04	1.81E+08	0	<i>Boiko et.al</i> [114]
	5.96E+04	2.08E+08	0	Tomeczek [112]
R7	8.55E+04	1.40E+08	0.84	<i>Watanabe et.al</i> [118]
R7	2.12E+11	2.03E+08	0	<i>Blaid et.al</i> [93]
R8	1.30E+11	1.26E+08	0	<i>Blaid et.al , Howard et.al</i> [93, 120]
	2.20E+20	1.67E+07	0	<i>Chen et.al</i> [116]
	2.20E+12	1.67E+08	0	<i>Silaen 10, Watanabe</i> [117, 118]
	1.10E+10	1.33E+08	-0.75	Tomeczek [112]

With the growth of the computational modelling technique, literature sources that provide the information of kinetic parameter values getting exposed. As a result, a variety of

values can be found for the kinetic parameter for a certain type of reaction [53]. At some points, it gives some benefits, but it also requires some prudence in the application. Therefore, this study is concerned with the investigation of the kinetic value varieties, and to identify the possible effects of the variation on the reaction mechanisms. As shown in Table 4-5, the values of kinetic parameters for R2, R3, R4, R5 and R8 have more than one value, according to their sources.

To indicate the variation, the logarithmic value of the kinetic rate coefficient (k) of each reaction was plotted against the temperatures. The results of R2, R3, R4, R5 and R8 can be seen in Figure 4-7 to 4-11, respectively.

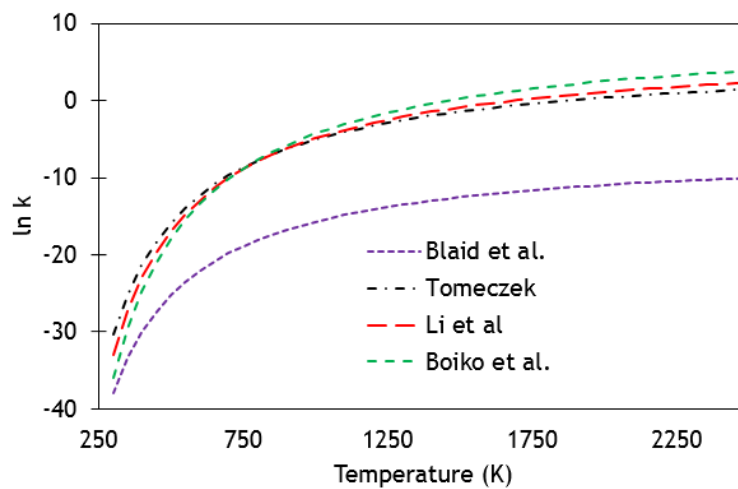


Figure 4-7. The logarithmic value of k variation in R2

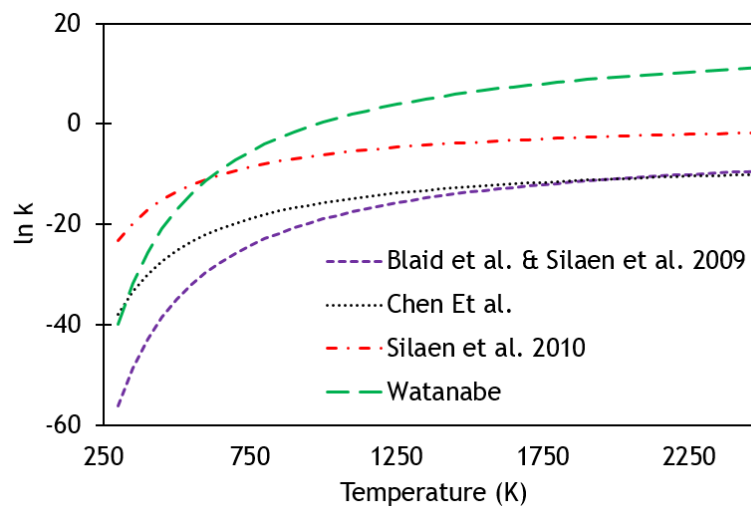


Figure 4-8. The logarithmic value of k variation in R3

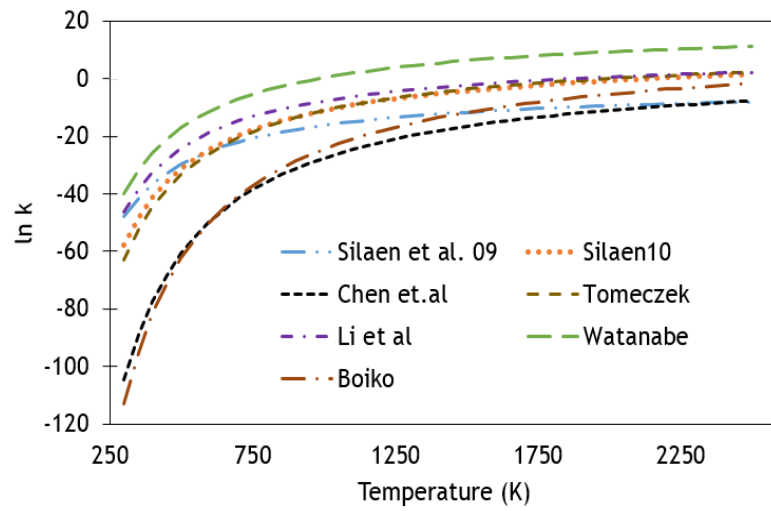


Figure 4-9. The logarithmic value of k variation in R4

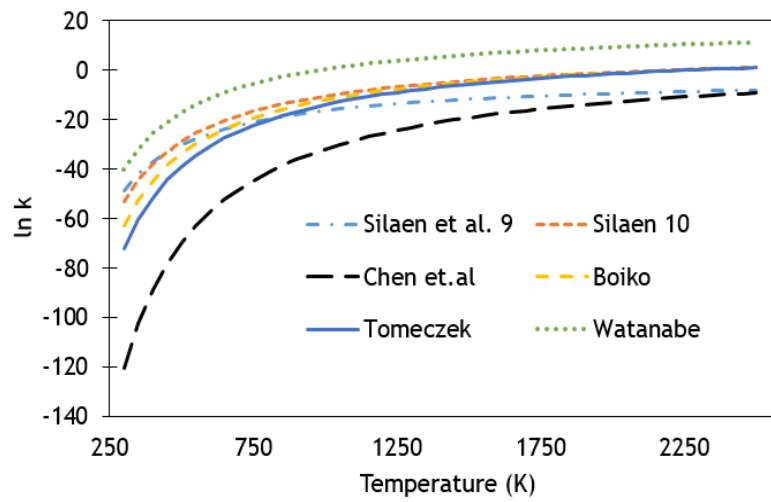


Figure 4-10. The logarithmic value of variation in R5

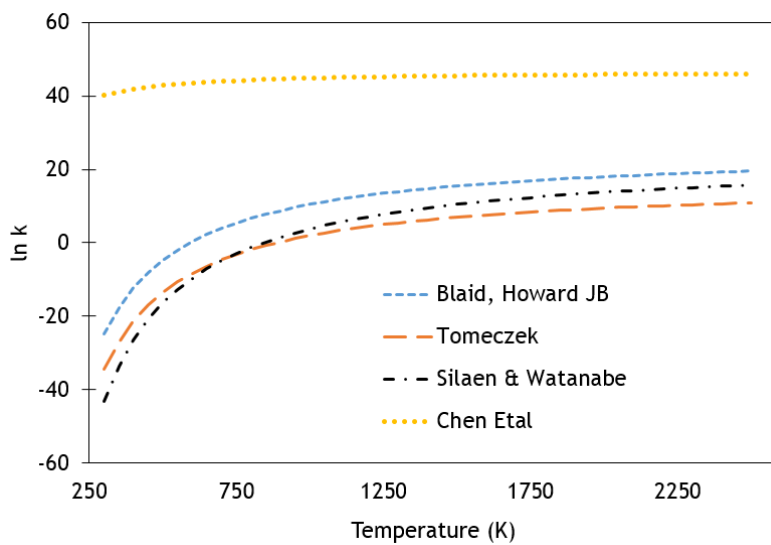


Figure 4-11. The logarithmic value of k variation in R8

Figure 4-7 to 4-11 show the variation in logarithmic values of the rate constant for each reaction. These indicate a disparity in the results of the kinetic rate coefficient (k), affected by the variety of parameter values. This disparity potentially causes the differences in the species rate reactions of all the mechanisms because they occur simultaneously. As a result of these differences, unsatisfactory results could be obtained from the simulation when unsuitable properties are applied. This clarifies the importance of finding suitable values for model application. Therefore, the kinetic study needs to be a major part of the investigation to identify the effect of the variation on these mechanisms through reactions' comparison. It also will identify the valid value of kinetic parameters when they use the results of experiments as a reference in the process of validation.

4.4 Process investigation with validation

The process of validation was conducted along with the comparison of critical parameters in the experiment and simulation. Some parameters, such as combustion time, species component fractions and temperature profiles, can be identified through the simulation and then compared to the experimental results. As mentioned in the previous section, the kinetic parameters have an important role in controlling the reaction mechanisms. Table 4-5 already provided the reference values of kinetic properties that can be considered for each reaction [53].

The validation is applied for the coal oxidation stage with the aim of finding the most suitable set of kinetic properties for this model simulation. For this purpose, the experimental result of coal particle combustion [105, 106, 121] was used as a reference for coal particle oxidation. In the simulation, coal particles' interaction with the fluid region was dealt with through the Lagrangian multiphase model [122]. Coal particle properties were defined and an injector was set up for controlling the particle injection into the furnace. The interaction of these species and heat or energy in the fluid region were governed through the transport equations already described in Chapter 3.

There are several numbers of kinetic values in the literature cited, but for an initial simulation the set of kinetic values from *Blaid et al.* was used [93]. For identification purposes, it was called Simulation 1. The results of Simulation 1 and the experiment are plotted in Figure 4-12, for identification.

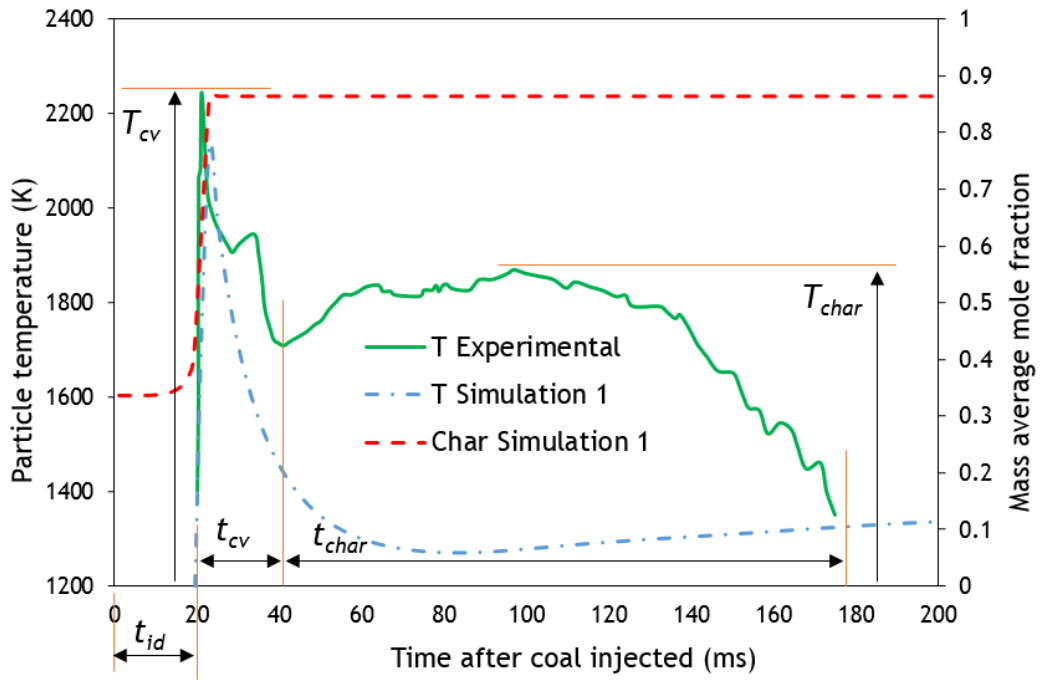


Figure 4-12. The results of Simulation 1 (sub-optimal parameters) and the experiment, to show the discrepancy

The results of the experiment are presented with a green line in Figure 4-12, and this consistently exhibited two peaks in the temperature profile: an exceedingly strong first peak followed by a significantly less pronounced second peak [105]. The first peak is attributed to the volatile matter burning homogeneously with air, which typically lasted for ~ 20 ms (milliseconds) after the ignition delay time (t_{id}) and it was identified as the burning out time for the volatile matter (t_{cv}). The second peak is attributed to the heterogeneous combustion of char residue which lasted for ~ 140 ms (t_{char}).

Simulation 1 shows the temperature and char mass fraction profiles, as demonstrated by the blue dash-dot and red dashed lines, respectively. The blue line shows that the coal particle increases the temperature rapidly to ~ 2200 K (T_{cv}) within ~ 20 ms after the coal injection, and that indicates a clear agreement for the ignition delay time and also for the maximum temperature of the coal volatile combustion (T_{cv}) with the experimental result. From this point, the particle temperature, as in the experimental result, drops and increases again from ~ 40 ms, but this was not shown in the temperature profile of Simulation 1. Instead, the particle temperature of Simulation 1 (the blue line) shows a sharp drop to its minimum at ~ 80 ms and then finally reaches ~ 1400 K. This temperature drop further indicates an absence of char combustion, as was also evidenced by the result of the char fraction (the red line), which remained stable at a value of around 0.85.

Clearly, there were no char reactions and this is considered to be a limitation of the set kinetic values utilised in the four reactions of char combustion (R2 to R5), in Table 4-2. R2 and R3 represent the exothermic reactions and the others are endothermic. Simulation 1 failed to model the coal particle burning that would lead to the production of heat and, subsequently, to increase the particle temperature. Therefore, it is essential to initially focus the investigation on the exothermic reactions which potentially might have caused this issue, followed by an investigation into the other relevant reactions.

4.4.1 Investigation of the kinetic parameters of R2 and R3

The reaction rate coefficient (k) is affected by the set of kinetic parameters as they are governed by the Arrhenius equation. The effects of the kinetic parameter values of R2 and R3 on the reaction rates as a function of temperature were already illustrated in Figure 4-7 and 4-8.

Table 4-6. Variation of kinetic parameters value of R2 and R3 [53]

Reference sources for R2	Reference sources for R3	ID of combination
Blaid, et al. 2015,[93]	<i>Blaid Alganash et al.</i> [93], <i>Silaen & Wang, 2009</i> [115]	Simulation 1
	<i>Silaen & Wang, 2010</i> [117]	Simulation 2
	<i>Watanabe & Otaka, 2006</i> [118]	Simulation 3
Tomeczek, 1992 [112]	<i>Chen Et al, 2012</i> [116]	Simulation 4
	<i>Silaen & Wang, 2009</i> [115]	Simulation 5
	<i>Silaen & Wang, 2010</i> [117]	Simulation 6
	<i>Watanabe & Otaka, 2006</i> [118]	Simulation 7
Li et al, 2003 [113]	<i>Chen Et al, 2012</i> [116]	Simulation 8
	<i>Silaen & Wang, 2009</i> [115]	Simulation 9
	<i>Silaen & Wang, 2010</i> [117]	Simulation 10
	<i>Watanabe & Otaka, 2006</i> [118]	Simulation 11
Boiko & Pachkovskii, 2004 [114]	<i>Chen Et al, 2012</i> [116]	Simulation 12
	<i>Silaen & Wang, 2009</i> [115]	Simulation 13
	<i>Silaen & Wang, 2010</i> [117]	Simulation 14
	<i>Watanabe & Otaka, 2006</i> [118]	Simulation 15

Also, as mentioned previously, the initial Simulation 1 used the set of kinetic values based on the study by *Blaid et al.* [93], and their coefficient rates have been presented using the purple line in Figure 4-7 and 4-8. Both R2 and R3 in this case have the lowest k result compared to the other results, and it is understood that these rates are slow compared to the other reactions and, so the char remained unaffected. Kinetic values of R2 and R3 from the several other references were sourced and, subsequently, applied to the simulation model to examine the char reaction rates. Using the kinetic parameter values

of R2 and R3 as presented in Table 4-5, a combination of fifteen different simulation models was generated and their simulation IDs can be seen in Table 4-6.

4.4.2 Validation process of coal oxidation

For validation purposes, the parameters to be compared between the experimental and simulation results were

- the maximum temperature of coal volatile combustion (T_{cv}),
- the maximum temperature of char combustion (T_{char}),
- the ignition delay time (t_{id}),
- the coal volatile matter burning out time (t_{cv}), and
- the char burning out time (t_{char}).

As shown in Table 4-6, fifteen IDs of simulations have been defined for the investigation. Their set of kinetic properties used in the simulation, and the results of each parameter mentioned above, are compared with the experimental results. The best agreement between them will be identified and their set kinetic parameter values will be considered as the best fit values for the coal particle combustion.

The first comparison was of the parameters of the maximum temperature of coal volatile combustion (T_{cv}). The results of simulation compared with the results of the experiment can be seen in Figure 4-13. The experimental result of T_{cv} is ~2250K [105, 106]. The study allows for deviation of experimental results at ~116K or ~5%, [105, 109]. The comparative plot shows that almost all of them are within the acceptance range, except for Simulations 7, 11, and 15. This indicates that the kinetic parameter values of simulation within the acceptance range can be considered as the values for further simulation.

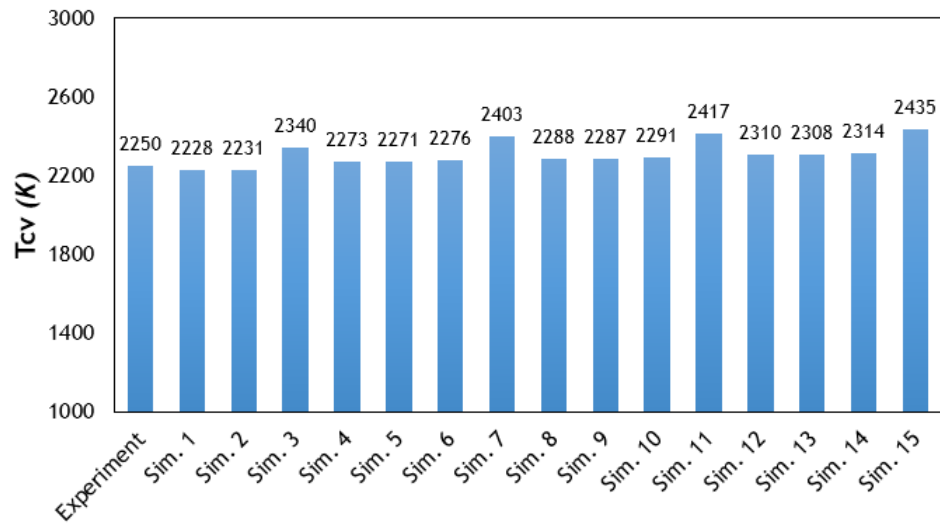


Figure 4-13. Comparison of T_{cv} obtained in simulations

However, considering the maximum temperature of char combustion ($\sim 1860\text{K}$ [105]) presented in Figure 4-14, it clearly indicates that the set of kinetic parameters used in Simulation 3 have produced the results that give the best agreement of T_{char} with the experimental result.

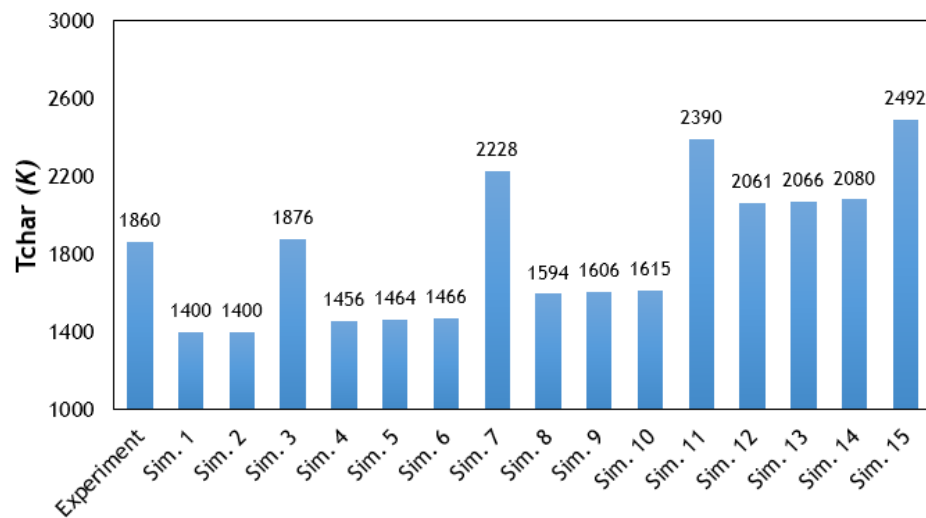


Figure 4-14. Comparison of T_{char} obtained in simulations

Other parameters of comparison are the ignition delay time (t_{id}) and coal volatile matter burning out time (t_{cv}). The comparison of these parameters can be seen in Figure 4-15. This figure shows all the results which agree with the experiments, in the tolerance range 10 to 20ms for the ignition delay time (t_{id}), and another of 10 to 20ms, for the coal volatile matter burning out time (t_{cv}) [105, 106].

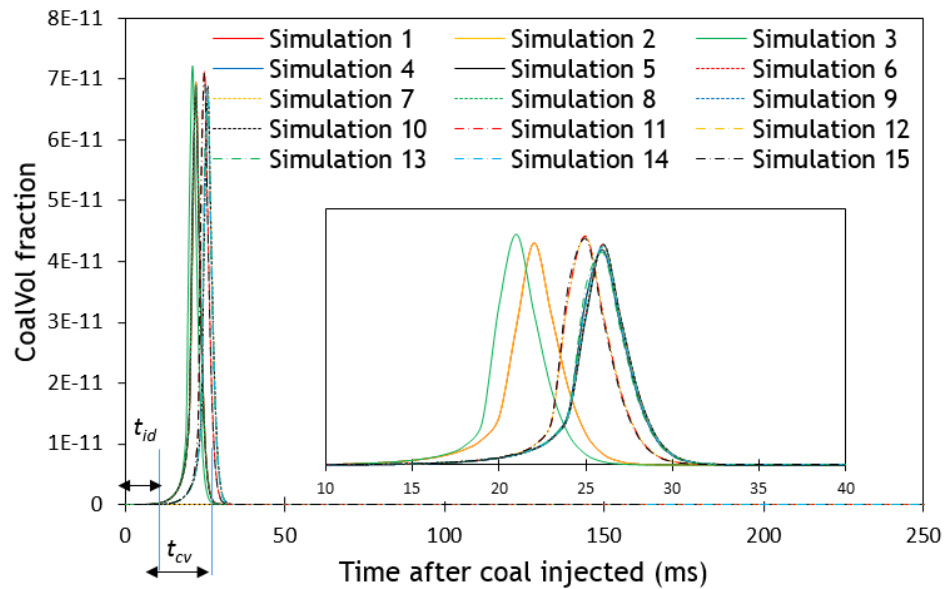


Figure 4-15. Comparison of coal volatile fraction

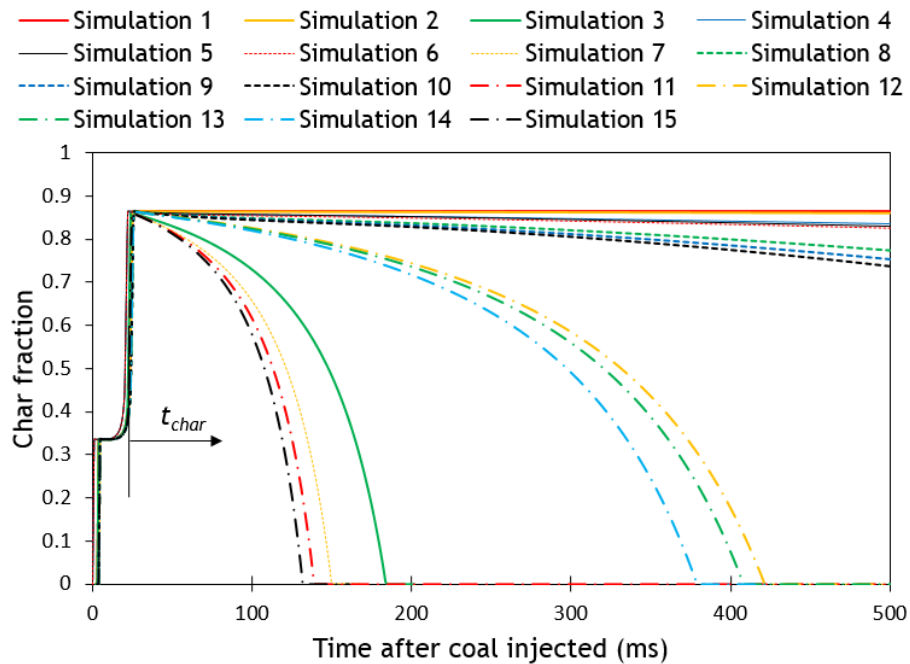


Figure 4-16. Comparison of char fraction profile

Although the simulation results of t_{id} and t_{cv} in Figure 4-15 show that all the kinetic parameters provided accurate results but the char burning out time (t_{char}) was clearly predicted to be different (Figure 4-16). It should be noted that the char burn out time is determined by calculating the interval of time taken to completely burn the char i.e. the time between the maximum and minimum/zero fractions of char. The experimental results suggest that the burn out time for char (t_{char}) is ~ 140 ms while the burning out time of coal particles is ~ 180 ms [105]. As shown in Figure 4-16, only Simulation 3 achieved

the burning out time of coal particles within ~180ms and also the burning out time of char ~140ms. Other simulations predicted the burning out time of char to be more than 500ms, or much shorter than the experimental value. Therefore, this validation exercise further confirmed that the set of kinetic parameters of R2 and R3 used in Simulation 3 for the coal particle oxidation was best suited for this model. Thus, this set of values should be considered for further development and investigation for gasification.

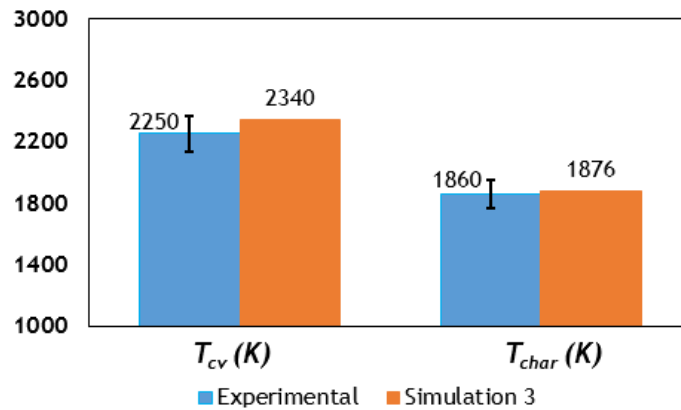


Figure 4-17. Temperature comparison between experiment and Simulation 3

Figure 4-17 shows a summary of all the comparative results for parameters of temperature from Simulation 3 and associated experiments. The deviation allowed for the maximum particle temperature of coal volatile and char combustion are about 116K and 59K, respectively [105], and therefore the results are in the range of tolerance.

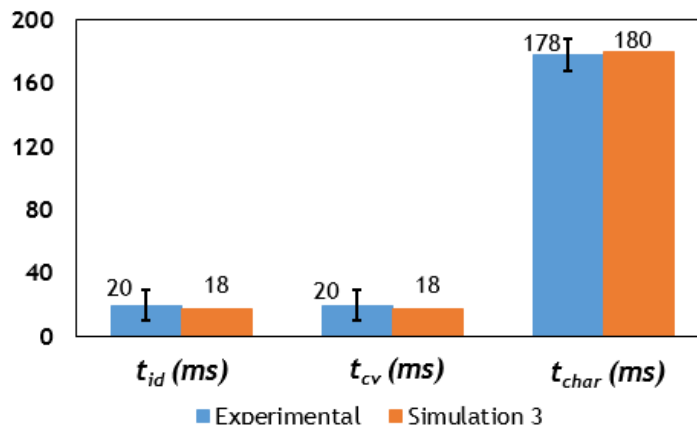


Figure 4-18. Time comparison between experiment and Simulation 3

Figure 4-18 shows a summary of the reaction times from Simulation 3 compare to the experimental values [105]. The simulation results are within the limit of tolerance from the experimental values of *Levendis et. al* [105].

Nevertheless, it is necessary to re-consider other reactions as well and to investigate their potential effects on coal oxidation.

4.3 Investigation of other combustion reactions

As described in the previous section, the validation procedures initially considered only the exothermic process of char reactions as they performed in R2 and R3. This initial validation has identified a good agreement and this was presented in Simulation 3. There are other reactions with several kinetic parameter values; R4 and R5 present as endothermic and heterogeneous reactions, and R8 presents as an exothermic and homogeneous reaction. These reactions have more than one value of kinetic parameters and need to be investigated by performing the simulation. This further simulation is developed to identify the effects of variation and to find more satisfactory results. Simulation 3 is taken as a reference point and then the other set of kinetic parameters values for R4, R5, and R8 are examined, taking into account the various available data sourced from the literature as shown in Table 4-7 with their individual Simulation ID.

Table 4-7. The ID for combination of Simulation 3 with R4, R5 and R8 in addition to the base case

Combination		Kinetic parameters			Ref	ID
		A (unit vary)	E_a (J/kmol)	β		
Simulation 3	R4	0.0732	1.13E+08	0	[115]	Simulation 3A-R4
		6.94E+04	1.85E+08	1	[112]	Simulation 3B-R4
		242	2.75E+08	0	[116]	Simulation 3C-R4
		7.38E+03	1.38E+08	0	[113]	Simulation 3D-R4
		8.55E+04	1.40E+08	0.84	[118]	Simulation 3E-R4
		7.90E+05	2.14E+08	0	[114]	Simulation 3F-R4
Simulation 3	R5	7.82E-02	1.15E+08	0	[115]	Simulation 3A-R5
		4.26E+02	3.16E+08	0	[116]	Simulation 3B-R5
		1.60E+04	1.81E+08	0	[114]	Simulation 3C-R5
		5.96E+04	2.08E+08	0	[112]	Simulation 3D-R5
		8.55E+04	1.40E+08	0.84	[118]	Simulation 3E-R5
Simulation 3	R8	2.20E+20	1.67E+07	0	[116]	Simulation 3A-R8
		2.20E+12	1.67E+08	0	[117] [118]	Simulation 3B-R8
		1.10E+10	1.33E+08	-0.75	[112]	Simulation 3C-R8

The parameter of investigation in this section is limited to the char burn out time (t_{char}) and the maximum char temperature (T_{char}), since the significant effect to be identified is on the char reaction. The results of simulation for coal particle combustion of various

kinetic parameter values in R4, R5, and R8 are provided in Figure 4-19, 4-20 and 4-21 respectively.

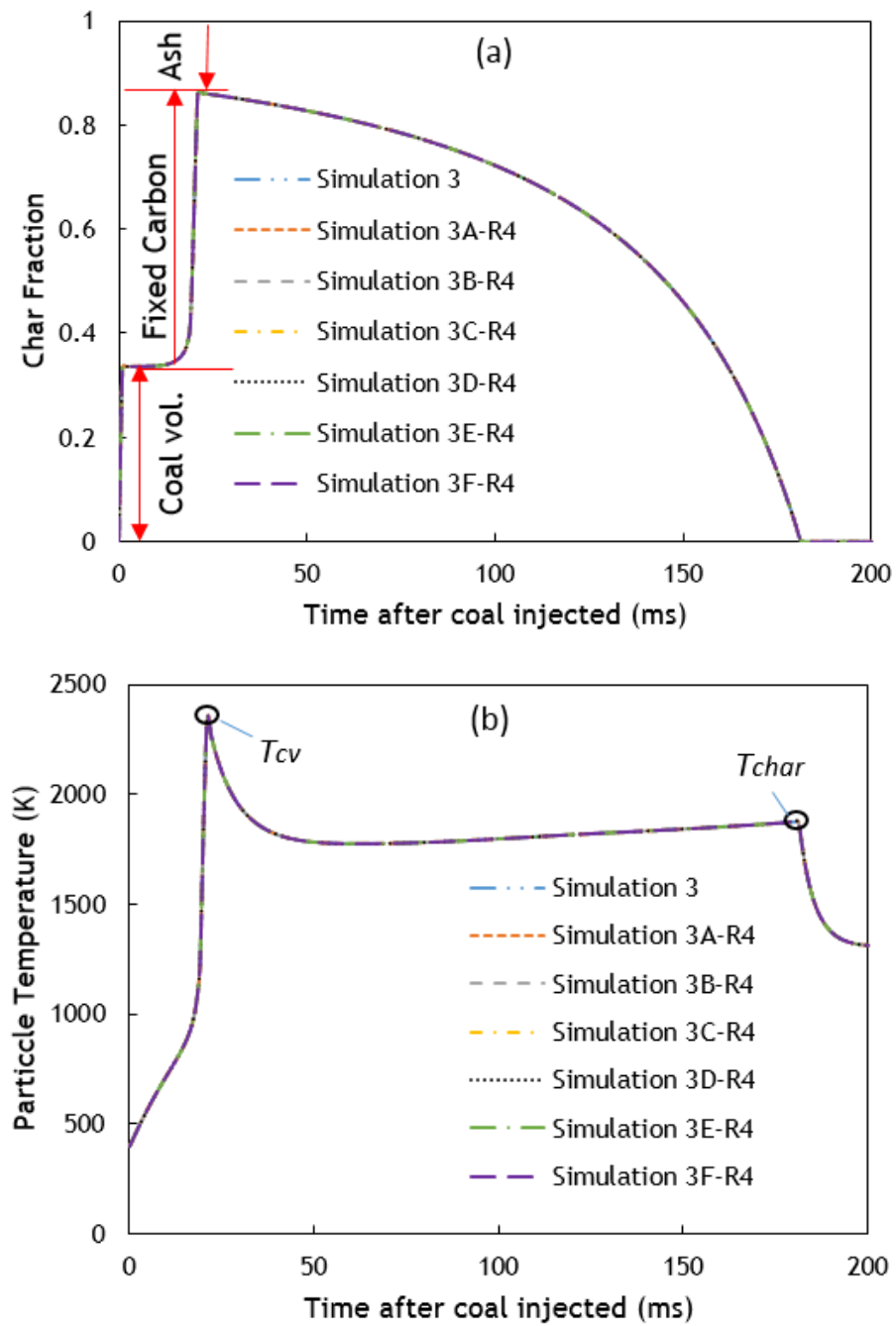


Figure 4-19. The comparison of Simulation 4 and various kinetic parameters of R4, for parameter (a) Char profile, and (b) Temperature profile

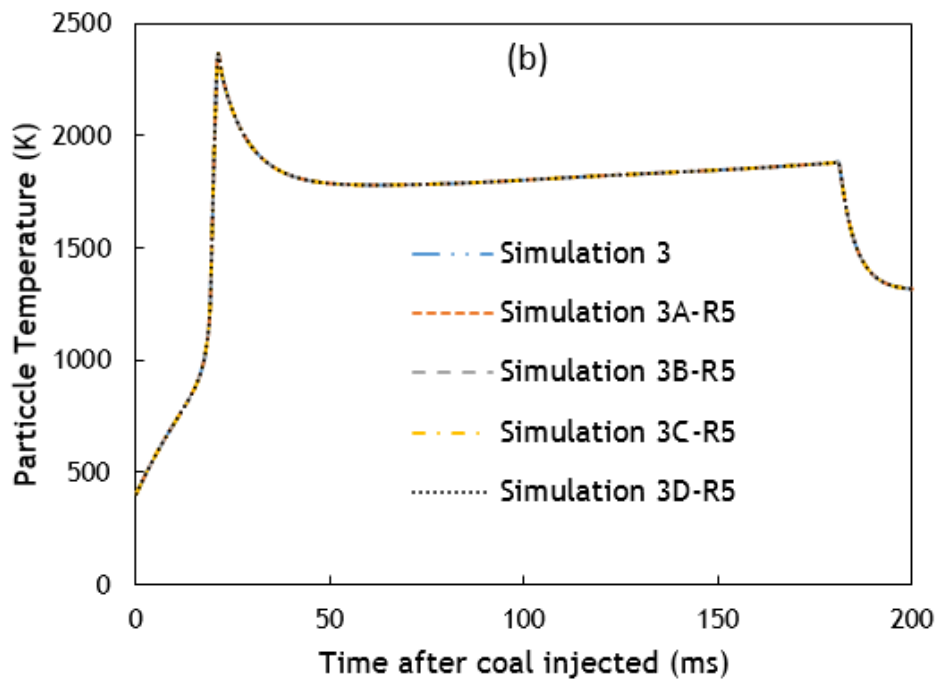
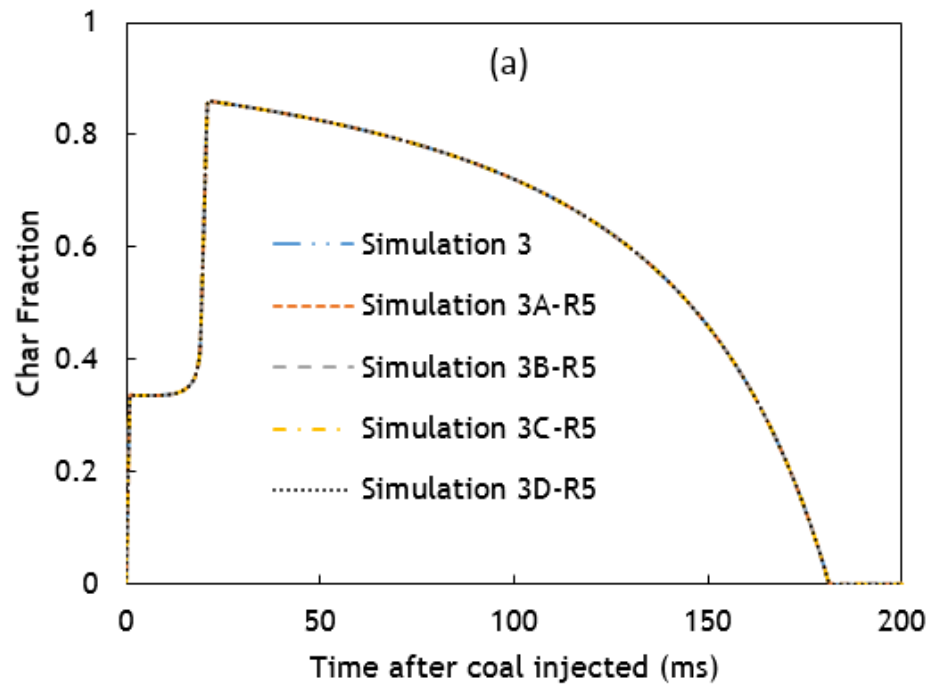


Figure 4-20. The comparison of Simulation 5 and various kinetic parameters of R5, for parameter (a) Char profile, and (b) Temperature profile

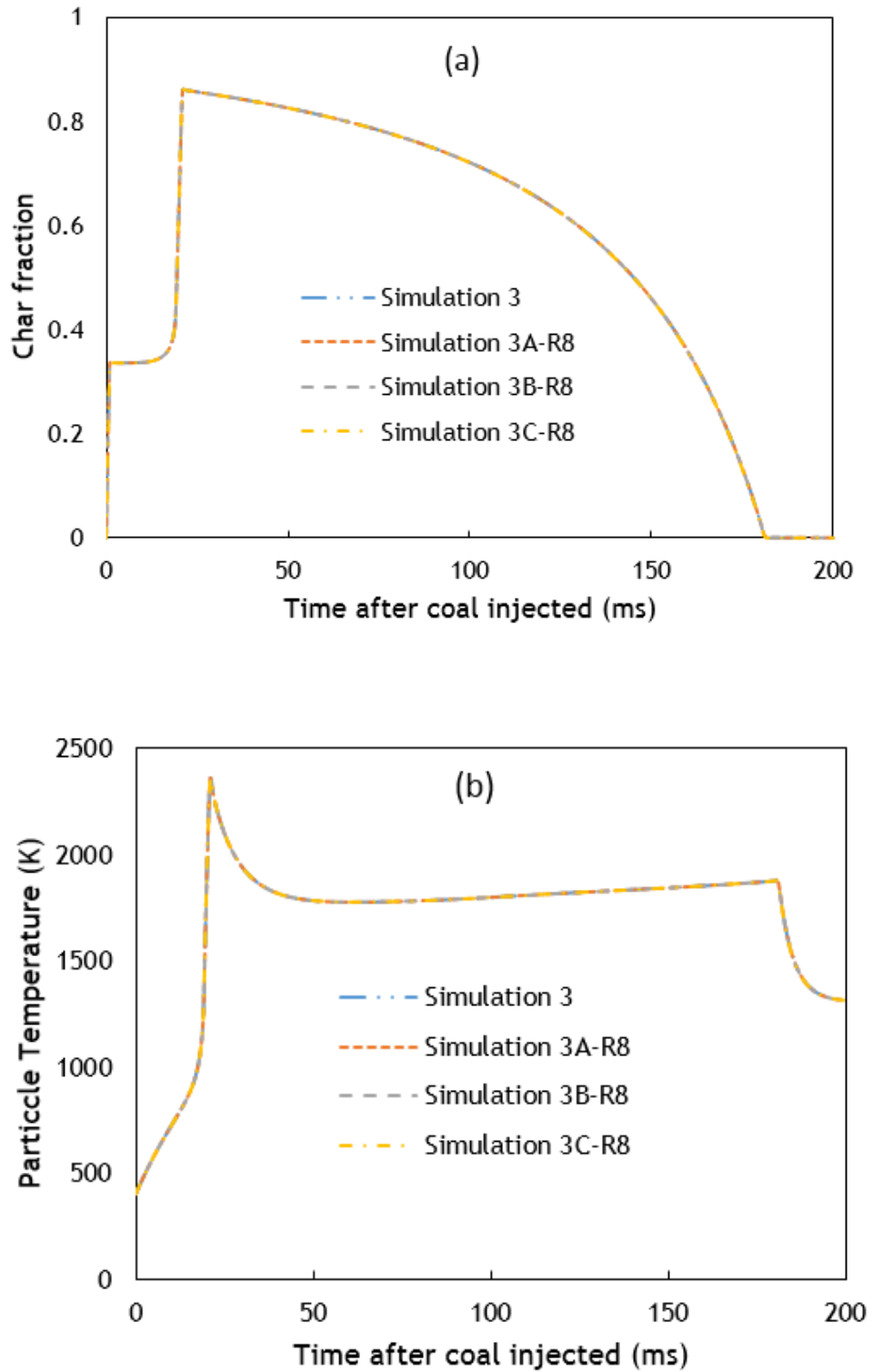


Figure 4-21. The comparison of Simulation 8 and various kinetic parameters of R8, for parameter (a) Char profile, and (b) Temperature profile

Figure 4-19 (a) shows the char fraction behaviour during coal particle reaction for the base case (Simulation 3) and at the variations of R4. The coal particle consists of about

34% of coal volatile, 51% of fixed carbon, and 13% of ash (see Table 4-4). At initial stage of coal particle reaction, the coal volatile release and therefore the fraction of char in the particle increases. Char reaction begin after about 20ms as seen in Figure 4-19 (a), and due to the reactions, its fraction drop, meanwhile the ash fraction increases. Figure 4-19 (b) shows the temperature profile of coal particle during the reactions for the base case condition and the variations of R4. However, Figure 4-19 (a) and (b) show the profile of char fractions and temperatures of coal particle are the same at the base case condition and at the variations of the kinetic parameters of R4. This, therefore, indicates that these variations do not have any significant effect on the char decomposition process. Figure 4-20(a)-(b) and 4-21(a)-(b) also show the same results which are unaffected by the variation in the kinetic parameters of R5 and R8. They all agree with the results of simulation 3, or in other words, confirm that all the kinetic parameter values for R4, R5 and R8 (i.e. Simulation 3 case) can be considered as the best fit with the experimental results and the kinetic parameter values of this simulation can be used for the development of coal particle combustion and gasification.

As a summary, the best fit kinetic parameter values obtained from the simulation and which will be used further in this study are outlined in Table 4-8.

Table 4-8. The best fit kinetic parameter values used for combustion

No	Kinetic parameters			Ref.
	A (unit vary)	E_a (J/kmol)	β	
R1	3.12E+05	7.40E+07	0	Alganash et.al [93]
R2	0.002	7.90E+07	0	Alganash et.al [93]
R3	85500	1.40E+08	0.84	Watanabe et.al [118]
R4	4.4	1.62E+08	1	Alganash et.al [93] & Silaen [117]
R5	1.33	1.47E+08	1	Alganash et.al [93], Silaen [117], Howard [120]
R7	2.12E+11	2.03E+08	0	Alganash et.al [93]
R8	1.30E+11	1.26E+08	0	Alganash et.al [93], Howard [120]

4.4 Model application in various oxygen fractions

The best fit value of the kinetic parameters have been obtained and they performed the simulations in good agreement with the experimental study [105]. Further assessments with another set of experimental studies [106, 108] are carried out to ensure that these values are strongly valid and suitable. The results of the new experimental papers

provided data for coal particle combustion in various oxygen fractions. They were compared with the simulation for several parameters; maximum coal particle temperature, coal volatile burn out time, and char burn out time. In this comparison, both the experiment and simulation used the PSOC 1451 coal, with diameter $50\mu\text{m}$ used in the furnace (DTF). The comparative results of each parameter, between the experiment and simulation, can be seen in Figure 4-22 to 4-24.

With tolerable deviation of temperature about 5%, or equal to 157K [106], as seen in Figure 4-22, the maximum temperature of combustion simulation showed having good agreement with the experiment. The coal volatile and char burn out time also seem to agree well with each other, since the maximum difference between the experimental and simulation results less than 5ms [106]. This therefore further indicates that the kinetic parameter values that have been selected in this study are definitely suitable for the simulation.

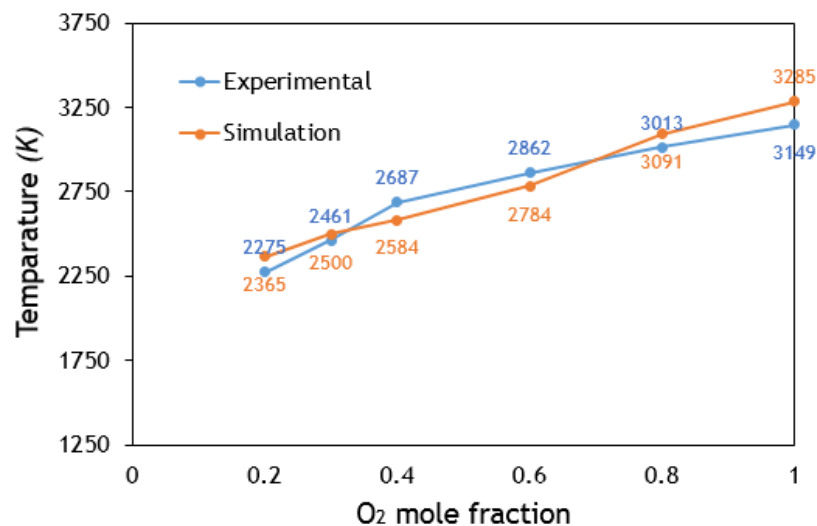


Figure 4-22. The comparison for maximum temperature between experiment and simulation

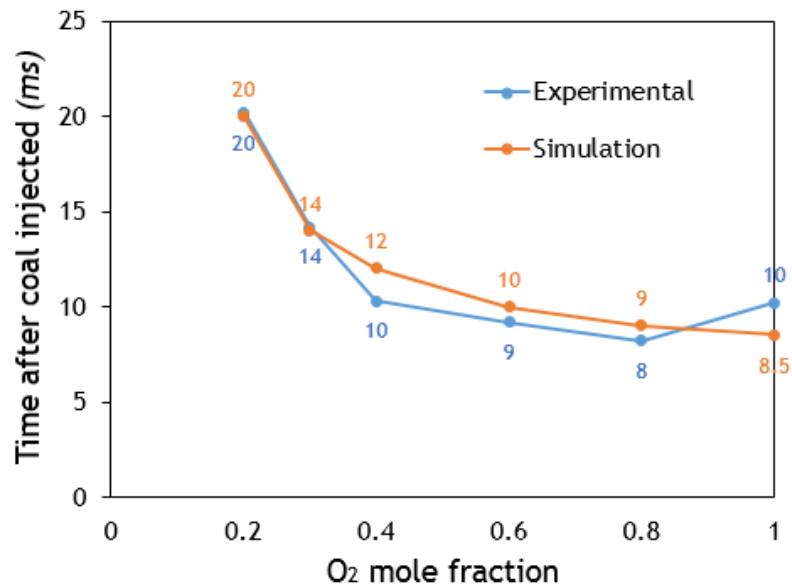


Figure 4-23. The comparison for coal volatile burn out time between experiment and simulation

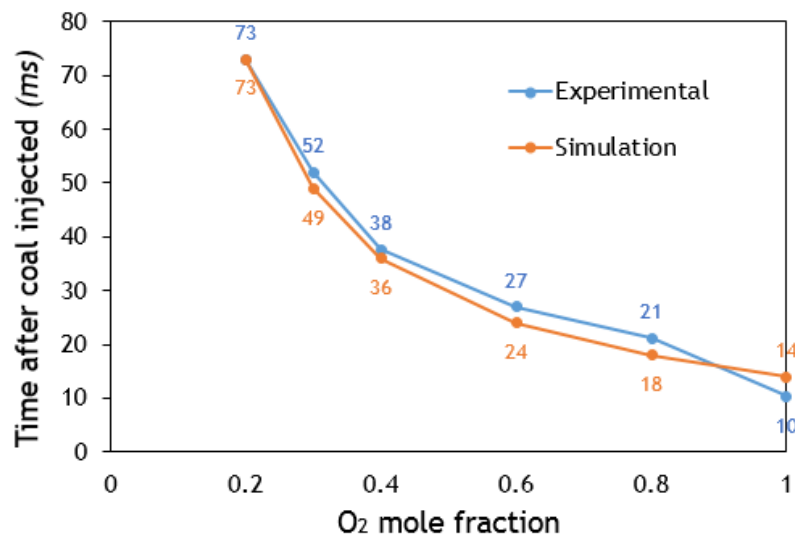


Figure 4-24. The comparison for char burn out time between experiment and simulation

4.5 Applying the model for lignite coal (PSOC 1443)

Many studies have been performed to investigate the combustion behaviour for different types of coal [123], as each of them is unique in terms of their combustion process. Recent studies have demonstrated this in various ways, either through experiment [124] or numerical simulation [125], with the aim of better understanding as well as characterising the processes of coal utilisation. One of the important parameters is ignition delay and this was introduced in section 4.4.2. This characteristic is very

important for designing coal combustion systems as it has significant roles in the prediction of spontaneous ignition and in the production of stable flames [126].

In the experimental study by *Levendis et al.* [105, 121] reported that the lower rank (lignite) coal has the shorter ignition delay time (t_{id}) compared to the higher rank (bituminous) coal [105]. This result generally agrees with the studies of several other authors [126-128], and further indicates that the ignition delay time increases from a lower to higher rank coal. In addition, *Young et al.* [129] reported that lignite coal is more reactive than other types of coal.

The ignition delay was the lapse of time after the coal was injected until the burning occurred. However, the devolatilization reaction of coal initiates the process of combustion [40, 130], therefore potentially linking with the ignition delay. Numerical studies of bituminous coal particle combustion have been performed in this study [131-133]. The numerical model has been validated by the experimental study by *Levendis et al.* [105], which was specifically based on the results of the ignition delay time (t_{id}), char burn out time (t_{char}), maximum temperature of coal volatility combustion (T_{cv}), and maximum char temperature (T_{char}) [133, 134]. This section investigates the devolatilization reaction and how it influences the ignition delay time. A comparison of the ignition delay time was carried out between bituminous and lignite coals, representing, respectively, a high and low ranked coal since they have significantly different chemical compositions. Results could give a better understanding of the devolatilization reaction for further modelling applications.

By using the same procedures, the combustion model of lignite coal (PSOC 1443) in the DTF reactor is developed and the ignition delay time between the results of simulation and experiment is assessed. The devolatilization reaction process is simulated initially with the kinetic parameters of R1 in Table 4-8. This model simulation allows the process of devolatilization to be simulated either by including, or excluding, the process of combustion of coal volatile species. Therefore, the devolatilization process can be simulated independently, or even simultaneously with the other reactions referred to Table 4-2. For identification, the simulation process of PSOC 1443 (lignite coal) combustion with the kinetic parameters in Table 4-8, is named as Simulation A. Other simulations, named respectively accordingly as Simulations B, C and D, are developed

as a part of the investigation. The simulation results of the model devolatilization process can be seen in Figure 4-25, where they do not have any combustion of coal volatile matter.

As part of the investigation, the same process of each simulation with the coal volatility matter burning can be seen in Figure 4-26.

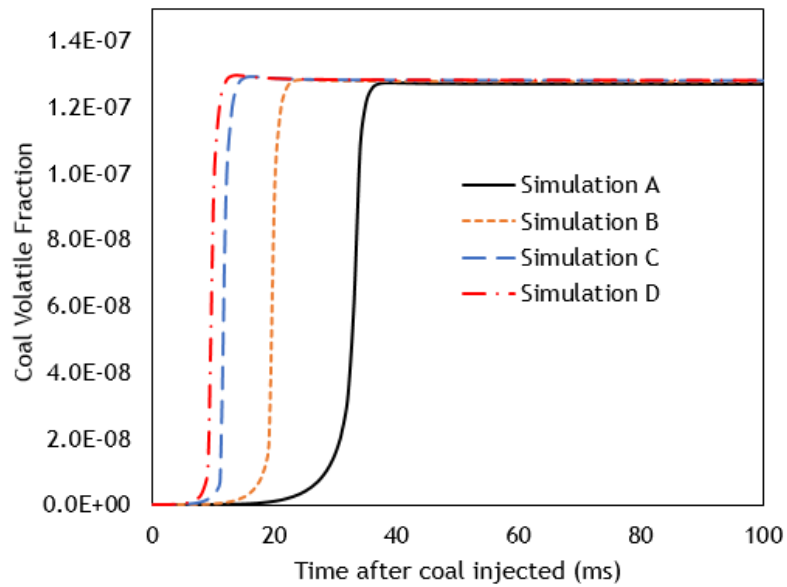


Figure 4-25. Devolatilization reaction process without combustion

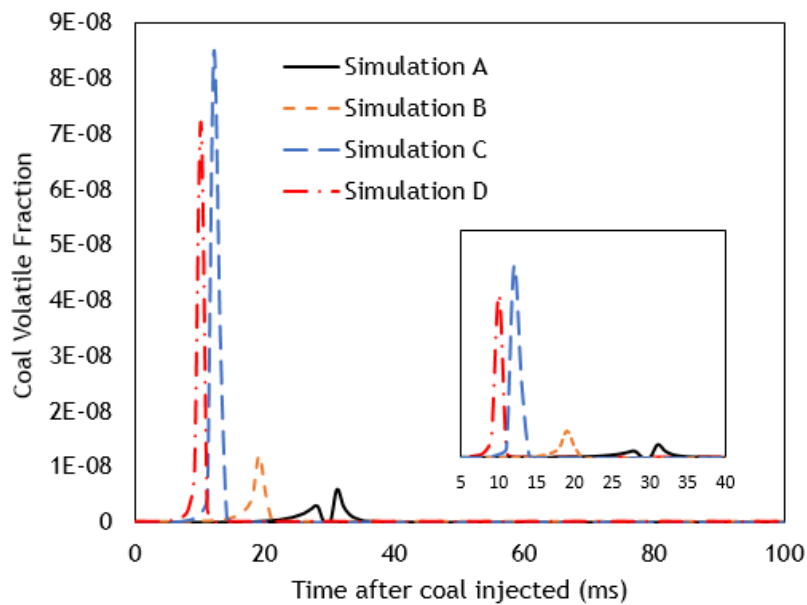


Figure 4-26. Devolatilization reaction with combustion

Figure 4-25 and 4-26 show the process of devolatilization in terms of the coal volatile fraction profile. Figure 4-25 presents the devolatilization process without volatile

combustion while Figure 4-26 presents it with combustion. The devolatilization process of Simulation A lasts between ~ 20 and ~ 40 ms with the most rapid coal volatility release occurring at ~ 30 ms, as seen in Figure 4-25. If it is performed with combustion, as in Figure 4-26, the peak of coal volatile profile occurs also at ~ 30 ms, but then it goes down, which indicates its burning out. However, the coal volatile combustion initiates the combustion of coal particles, so at the time when the most rapid combustion occurred, the temperature of the coal particle increased rapidly and initiated its burning. The period between the particle injection and the particle starting to burn is the ignition delay time. Therefore, the ignition delay of Simulation A is determined as ~ 30 ms after the coal injection, but this result does not agree with the experiment [105, 106], and therefore Simulation B, C and D are developed by systematically increasing the pre-exponent factor (A). It should be noted that the reactor condition is the same for each simulation (heat rate and temperature), so the activation Energy (E_a) and temperature exponent (β) are assumed to be the same. The value of the pre-exponent factor of Simulations B, C, and D is increased 10, 100 and 300 times that of Simulation A, respectively. Finally, the results indicated that the best fit result of the ignition delay time was that obtained by Simulation D. Simulation D took ~ 10 ms, which agrees with the ignition delay time for the lignite coal PSOC 1443 in the experiment [105]. This further indicates that the kinetic parameter value of Simulation D is suitable for the lignite coal combustion. The comparison of PSOC 1443 coal particle in a char fraction for each simulation can be seen in Figure 4-27.

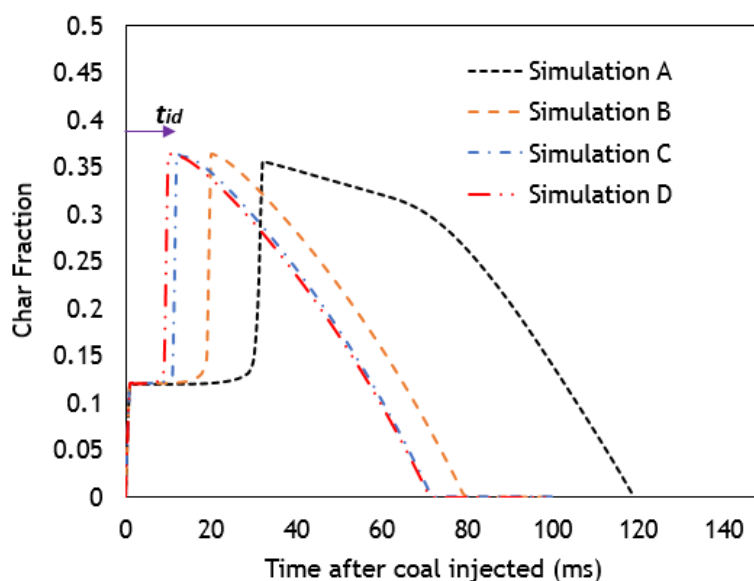


Figure 4-27. The char profile for each simulation

Figure 4-27 further shows that, from simulation A to Simulation D, the ignition delay time decreases. This is because of the increase in the kinetic parameter of devolatilization reaction. Simulation D agrees best with the experiment and it indicates the best fit value of kinetic parameters for PSOC 1443 coal particle combustion.

A comparison between the results of experiments and simulation for coal PSOC 1443 can be seen in Table 4-9.

Table 4-9. Parameter comparison between the experiments and simulation

PSOC 1443	Max Temperature (K)	t_{id} (ms)	Total Burn out (ms)
Experimental	2000	10	72
Deviation [105, 106]	93	-	15
Simulation	2042	10	71

Table 4-9 shows all parameters of simulation results are in the limit of tolerance according to the references [105].

4.5 Conclusion

The comparison results of simulation have been validated with the experiments through the process of identifying the kinetic parameter values of coal combustion. The best fit kinetic parameter values of bituminous coal particle (PSOC 1451) are provided in Table 4-8.

Through the same procedures, the investigation with validation of lignite coal (PSOC 1443) has been performed and obtained good agreement results with the experiment. In the case of PSOC 1443, the increment of pre-exponent factor (A) of devolatilization ($R1$) as shown in Table 4-8 needs to be increased 300 times to achieve the agreement with the experimental result.

The process investigation shows how important kinetic parameters are for developing the model in this study. Their value is specific, especially in the coal particle combustion and, therefore, validation of the experimental results needs to be performed. This model could be considered as a tool for finding the best fit kinetic parameter value for coal particle combustion cases.

The single coal particle model of combustion has been further developed to investigate the effect of devolatilization reaction on the ignition delay of bituminous and lignite coal combustion. Based on the numerical investigation, the ignition delay of coal combustion is most affected by the devolatilization reaction in the process of modelling.

The coal particle model for combustion application has been performed, and now further application for gasification is needed to achieve the purposes of the study. The next chapter will describe the development of coal particle gasification whilst still based on the kinetic parameter study. The performance of coal gasification through the particle model approach is important, since the model provides more appropriate mechanisms for the coal reaction procedures.

Chapter 5 Coal particle gasification development to investigate the reactions' behaviour with applications leading to UCG

5.1 Introduction

A coal particle model has been developed and validated in both combustion and oxidation stages as an initial development of gasification reactions. The coal particle gasification reactions have also been developed by the inclusion of the pyrolysis and reduction reactions into the coal combustion mechanisms, as seen in Table 3-1. The aim of the study in this chapter is to investigate the coal particle gasification process with applications leading to UCG, as illustrated in Figure 5-1.

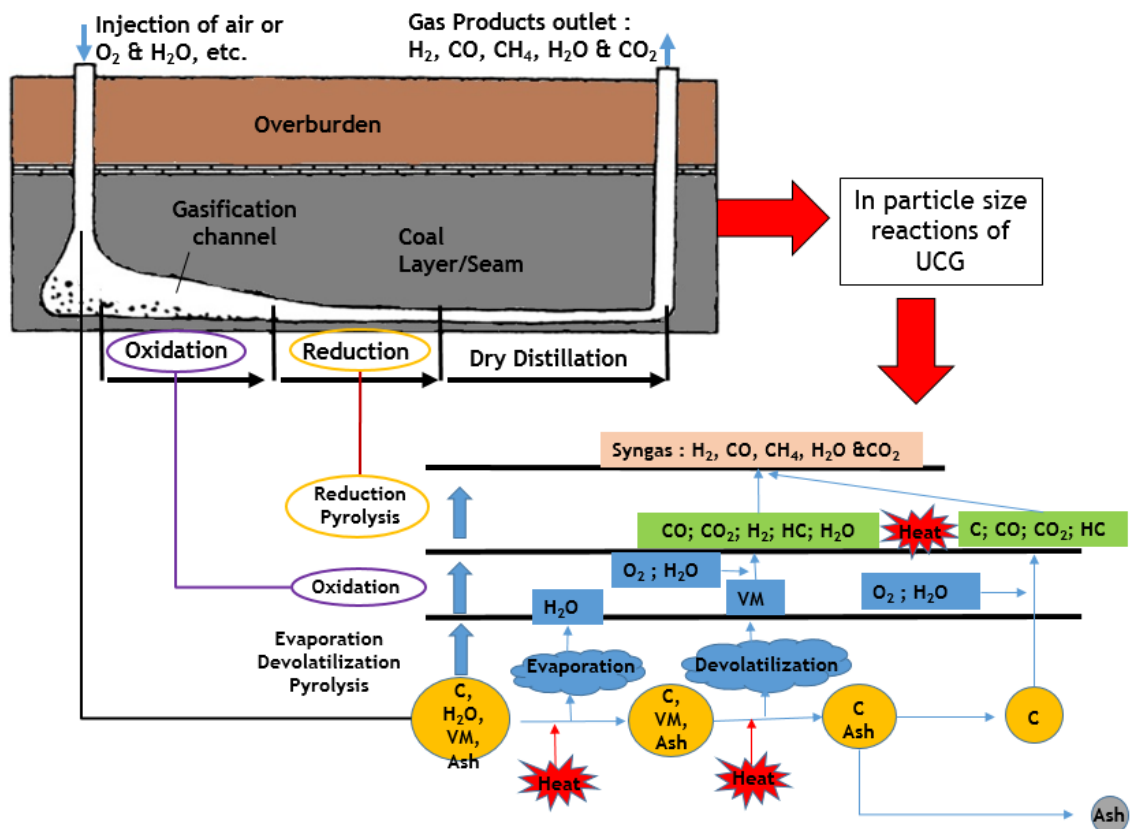


Figure 5-1. Process illustration of coal particle gasification model and UCG

Figure 5-1 presents the gasification processes of UCG and how each of these is directly linked to the gasification of a coal particle, which is considered to be a microscale coal block from deep underground. As clearly identified in this figure, the reaction mechanisms of coal gasification, irrespective of the scaling of the model, are essentially the same and mainly consist of the processes of devolatilization and/or pyrolysis, oxidation, and reduction [125]. Therefore, the proposed particle based computational model provides an opportunity to investigate the fundamental aspects of the thermochemical physics which usually occur in UCG. This also provides an additional flexibility to identify the effects of various relevant operating and boundary conditions on gasification. A full scale UCG simulation model, on the other hand, may be developed. However, without any doubt, it would be highly cumbersome and computationally expensive to run each model based on the parametric optimisations which are planned. Moreover, the particle based modelling approach allows for the prediction of the coal mass release during the reactions, which remains very difficult with the surface reaction model [41, 54]. In the UCG process, the contact area between the coal seam surface and hot gas changes over time result in a dynamic boundary condition at the interface. The propagation of combustion front also causes coal mass loss and results in gas products. Therefore, the coal mass loss causes the boundary layer propagation or displacement of the contact area. The particle model will address this challenging issue of defining a dynamic boundary condition which is encountered in the computational modelling of UCG.

Initially, the study is focused on the investigation of the thermochemical reaction processes using the UCG reaction mechanisms sourced from Żogała and Janoszek [54]. Then, the processes will be kinetically controlled and their effect on the gasification will be investigated, with the aim of predicting the best possible gasification conditions that would lead to the best quality gas products. Various operating parameters, including fuel composition, kinetics properties and gasification agents, are also the subject of investigation in this work. This study uses bituminous coal, PSOC 1451 with its properties shown in Table 4-4 for this investigation throughout the gasification simulation.

5.2 Investigation of single coal particle gasification processes

The coal particle gasification reactions are developed by inclusion of the pyrolysis and reduction reactions (R6, and R9 to R13) into the coal combustion mechanisms as shown in Table 4-2. Similar to the combustion, selected reactions for gasification have more than one set of kinetic parameter values as shown in Table 5-1, and therefore, an in-depth investigation focusing on the sensitivity of the selective kinetic parameters is needed to discover the suitable values for the gasification application [53].

Table 5-1. Kinetic parameter value variations of gasification reactions

Type of reaction	Reaction no	Kinetic parameters			Ref.
		A (unit vary)	E_a (J/kmol)	β	
Devolatilization	R1	3.12E+05	7.40E+07	0	[93]
Heterogeneous	R2	0.002	7.90E+07	0	[93]
Heterogeneous	R3	85500	1.4E+08	0	[118]
Heterogeneous	R4	4.4	1.62E+08	1	[93, 117]
Heterogeneous	R5	1.33	1.47E+08	1	[93, 117, 119]
Heterogeneous	R6*	1000	1.13E+08	0	[114]
Coal volatile oxidation	R7	2.12E+11	2.03E+08	0	[93]
Homogenous	R8	1.30E+11	1.26E+08	0	[93, 120]
Homogenous	R9*	1.50E+13	2.85E+07	0	[112]
		5.00E+10	1.68E+08	0	[116]
		6.80E+15	1.68E+08	0	[118]
Homogenous	R10*	4.20E+07	1.38E+08	0	[114]
		2.75E+02	8.38E+07	0	[117]
		2.75E+10	8.38E+07	0	[118]
Homogenous	R11*	4.40E+11	1.68E+08	0	[118]
		4.40E+03	1.68E+08	0	[116]
Homogenous	R12*	3.00E+08	1.26E+08	-1	[118]
		4.00E+03	1.26E+06	-1	[116]
Homogenous	R13*	4.60E+11	3.12E+08	0.3	[135]

(*added for gasification processes)

5.2.1 Effect of kinetic parameter variations

The reactions of gasification with more than one kinetic parameter value are shown in R9* to R12*. The simulation of coal particle gasification is needed to perform the effect of the variation in the respective kinetic properties. Valid coal particle combustion is used as a base case (Simulation 3 from the previous chapter), and a combination of the simulation models generated with their respective simulation ID can be seen in Table 5-2.

Table 5-2. Scheme for identification of the kinetic parameters of gasification

Type of reaction	Reaction no	Kinetic parameters			Ref	ID
		A (unit vary)	E_a (J/kmol)	β		
Simulation 3	R6	1000	1.13E+08	0	[114]	
	R9	1.50E+13	2.85E+07	0	[112]	GA-R9
		5.00E+10	1.68E+08	0	[116]	GB-R9
		6.80E+15	1.68E+08	0	[118]	GC-R9
	R10	4.20E+07	1.38E+08	0	[114]	GA-R10
		2.75E+02	8.38E+07	0	[117]	GB-R10
		2.75E+10	8.38E+07	0	[118]	GC-R10
	R11	4.40E+11	1.68E+08	0	[118]	GA-R11
		4.40E+03	1.68E+08	0	[116]	GB-R11
	R12	3.00E+08	1.26E+08	-1	[118]	GA-R12
		4.00E+03	1.26E+06	-1	[116]	GB-R12
	R13	4.60E+11	3.12E+08	0.3	[135]	

The simulations were conducted, and the results presented, in terms of mole fractions of CO, H₂, CO₂ and CH₄ as the main products of gasification. The comparison results for R9 to R12 are presented in Figure 5-2 to 5-5.

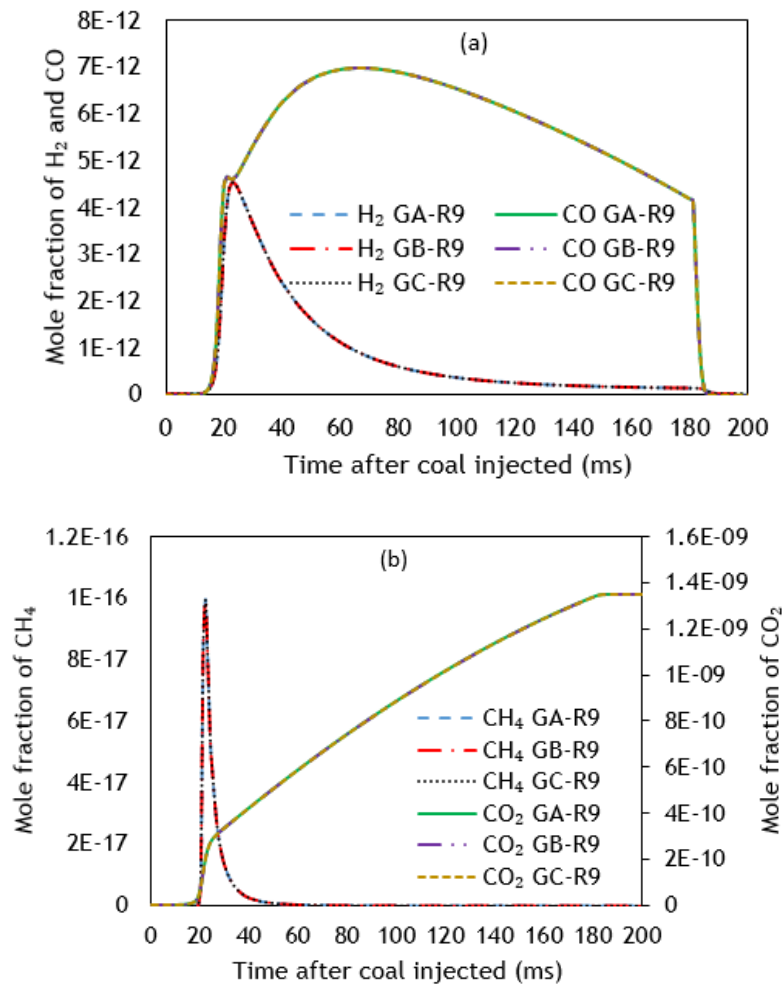
Figure 5-2. Comparison results for R9 (a) H₂ & CO, and (b) CH₄ & CO₂

Figure 5-2 (a) and (b) represent the kinetic value variations of R9 on the gas products H_2 and CO , and CO_2 and CH_4 respectively. The simulations result in a similar fraction of the gas products for each variation implemented and indicate that all the variations in the kinetic parameters for this reaction have a negligible effect on gas production.

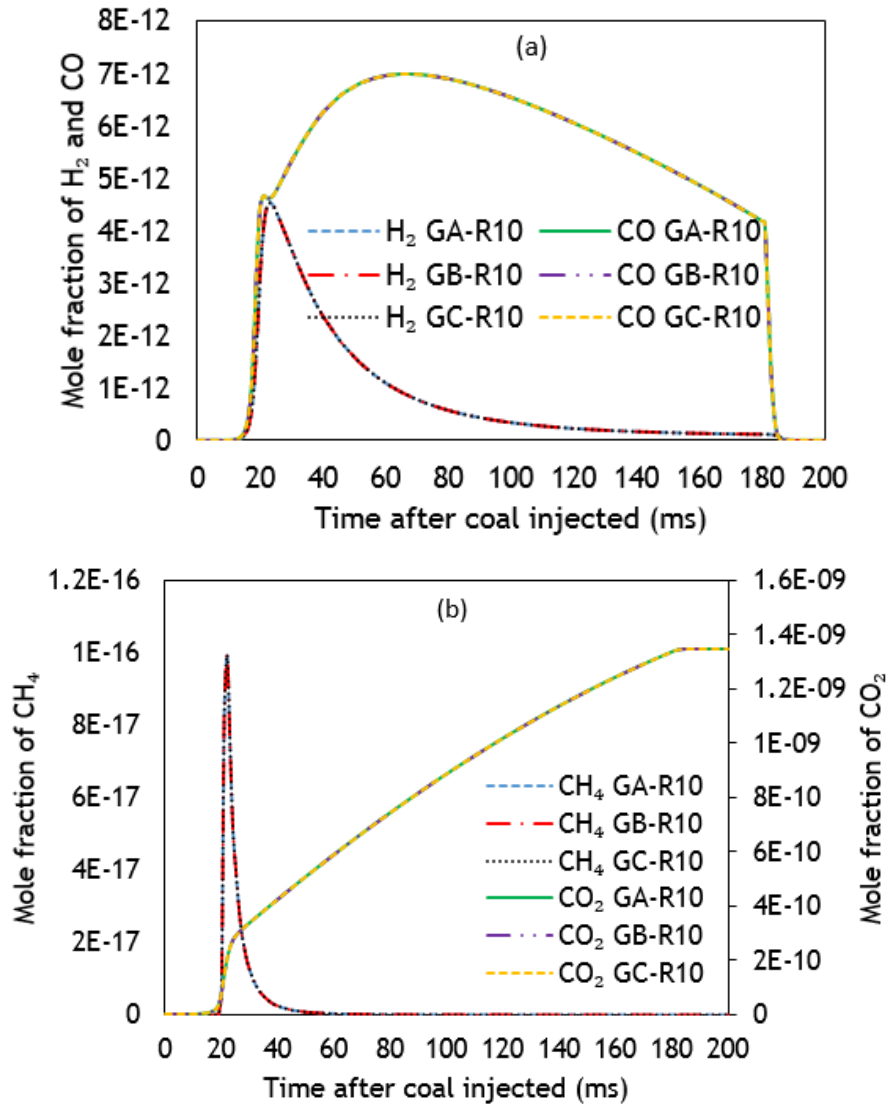


Figure 5-3. The comparison results for R10 (a) H_2 & CO , and (b) CH_4 & CO_2

Other results can be seen in Figure 5-3, which presents the effects of the kinetic value variations of R10 on the gas products H_2 and CO , and CO_2 and CH_4 , respectively. The result shows these gas products are similar, thus confirming that all the variations in the kinetic parameters for this reaction have also a negligible effect on the gas production.

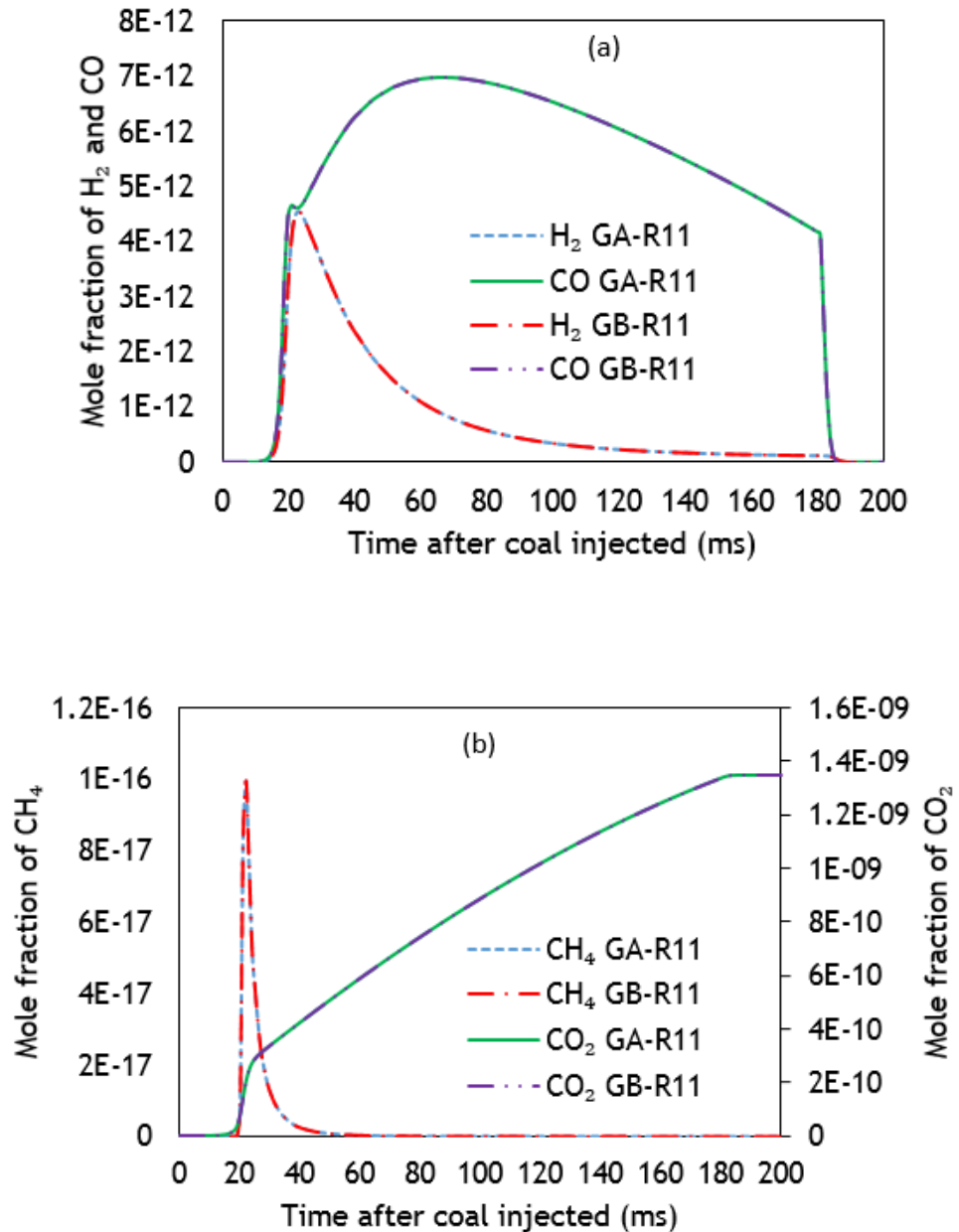


Figure 5-4. The comparison results for R11 (a) H_2 & CO , and (b) CH_4 & CO_2

The same behaviour of simulation results can be seen for the other reactions, R11 and R12, as shown in Figure 5-4 and 5-5, respectively. They also show the same profile for the gas products, and further confirm that the variation of the kinetic parameters does not have any significant effect on the gasification reactions results for the gas products.

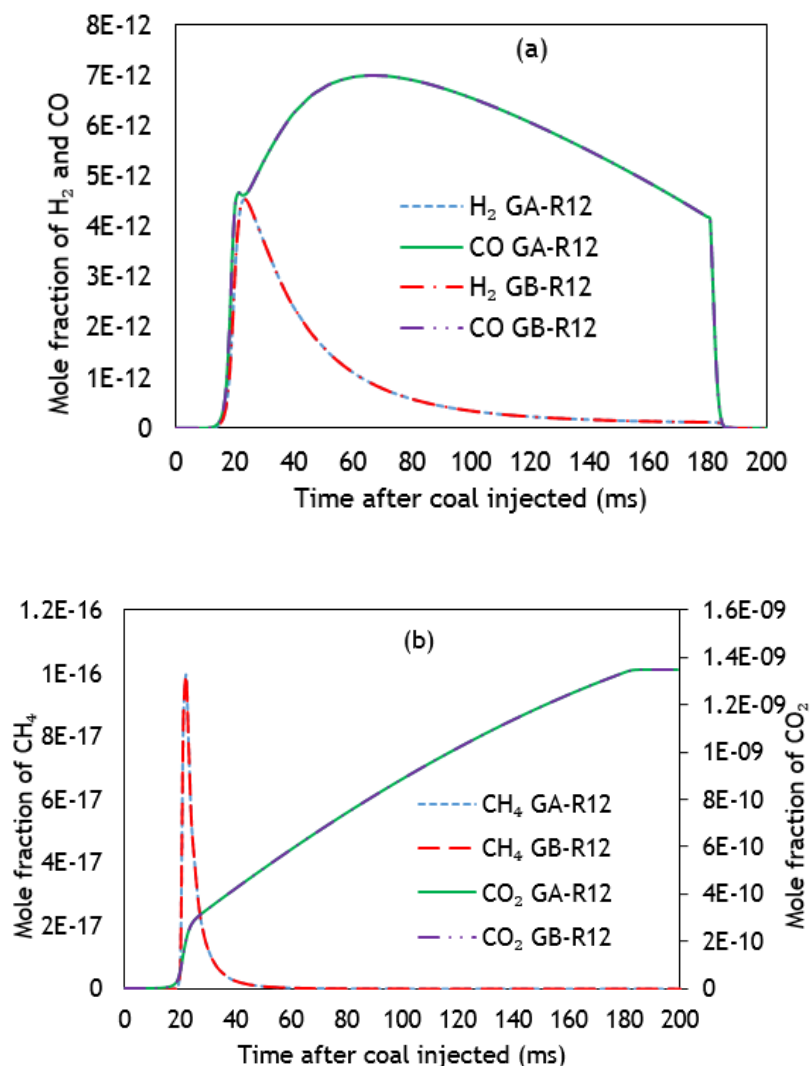


Figure 5-5. The comparison results for R12 (a) H_2 & CO , and (b) CH_4 & CO_2

All the variations of the kinetic parameter values of R9 to R12 have been simulated as previously mentioned. The results of simulation indicate that all the sets of the kinetic parameters can be considered for the coal gasification simulation. However, only one value of various kinetic parameters is needed and used for each reaction in the gasification mechanisms. Therefore, this study needs to decide these values.

The kinetic parameter studies have been conducted in Chapter 4, and the results informed the best agreed value of R1 to R5, R7 and R8 as shown in Table 4-8. Further study on the reaction kinetics added to the gasification mechanisms are carried out in this chapter. This study considers the additional reactions of gasification taken from Table 5-2, and the value as identified with “A” letter IDs used when the reaction has a variation. As a quick

summary, the kinetic parameter values of the gasification reactions are shown in Table 5-3.

Table 5-3. The kinetic parameter values used in gasification reactions

Type of reaction	Reaction no	Kinetic parameters			Ref.
		A (unit vary)	E_a (J/kmol)	β	
Devolatilization	R1	3.12E+05	7.40E+07	0	[93]
Heterogeneous	R2	0.002	7.90E+07	0	[93]
Heterogeneous	R3	85500	1.40E+08	0.84	[118]
Heterogeneous	R4	4.4	1.62E+08	1	[93, 117]
Heterogeneous	R5	1.33	1.47E+08	1	[93, 117, 120]
Heterogeneous	R6	1000	1.13E+08	0	[114]
Coal volatile oxidation	R7	2.12E+11	2.03E+08	0	[93]
Homogenous	R8	1.30E+11	1.26E+08	0	[93, 120]
Homogenous	R9	1.50E+13	2.85E+07	0	[112]
Homogenous	R10	4.20E+07	1.38E+08	0	[114]
Homogenous	R11	4.40E+11	1.68E+08	0	[118]
Homogenous	R12	3.00E+08	1.26E+08	-1	[118]
Homogenous	R13	4.60E+11	3.12E+08	0.3	[135]

5.2.2 Comparison between combustion and gasification

The value of the set kinetic parameters for each reaction identified can now be applied to the simulation of coal particle combustion and gasification processes. It is important to see this difference through the model of simulation for understanding the process. The initial comparison to be made is on the char fraction of the coal particle and the results of simulation can be seen in Figure 5-6.

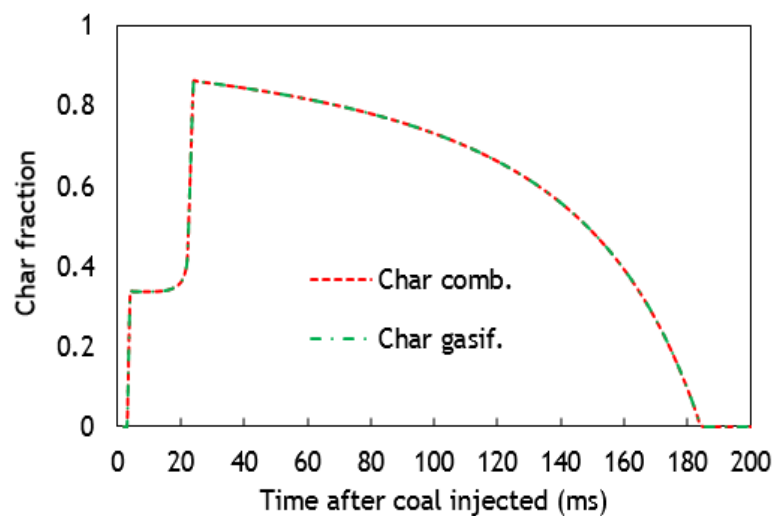


Figure 5-6. Comparison of combustion and gasification for char in particle fractions

Figure 5-6 shows that the char reaction has similar behaviour at the combustion and gasification reactions. This indicates that the char has a similar reaction rate in both processes. Other parameters need be examined to identify any effects on the gas products. These results are presented in Figure 5-7.

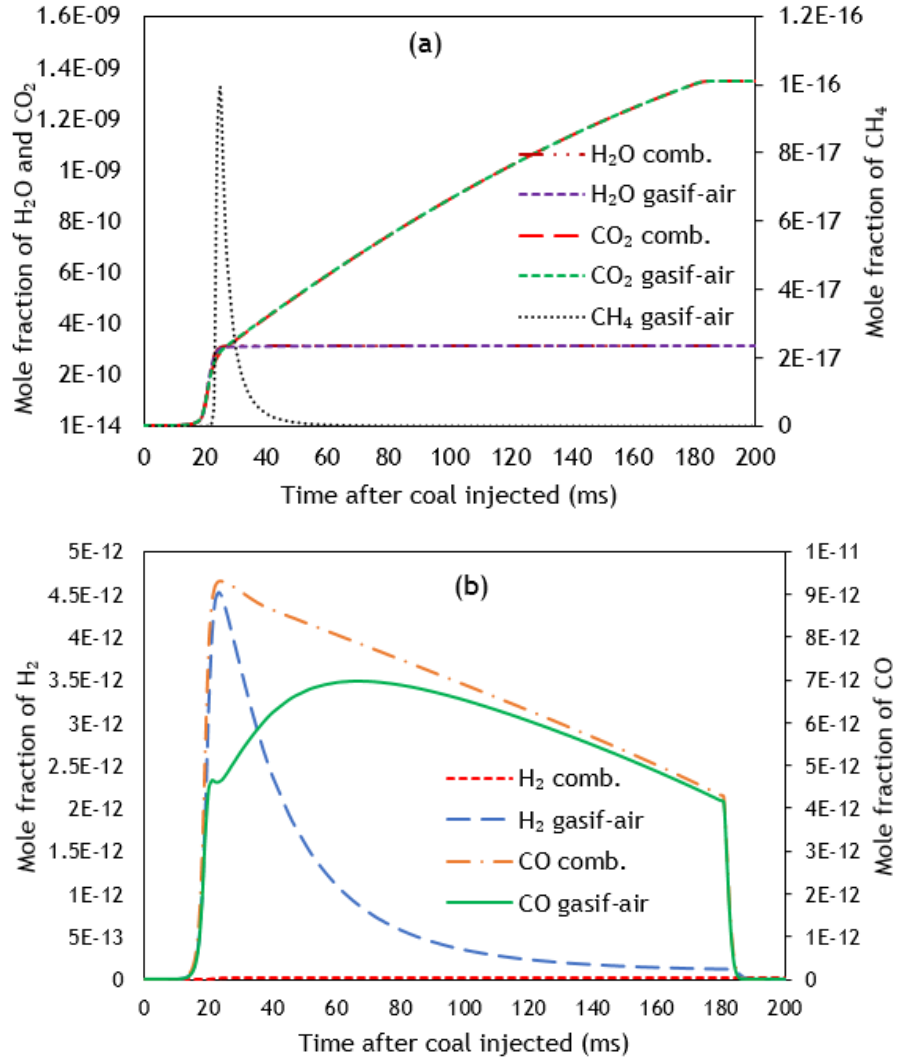


Figure 5-7. Comparison of combustion and gasification for (a) CO₂, H₂O and CH₄ and (b) H₂ and CO gas species.

Figure 5-7 (a) shows the results of CO₂ and H₂O, although trending, to be similar and only the gasification process produces CH₄. Meanwhile, Figure 5-7(b) shows the H₂ and CO production of the coal particle combustion and gasification and the difference in the results is clearly identified by the two different processes utilised. In particular, H₂ from the gasification process is much higher than that from the combustion process. Specifically, when comparing the CO production, it is shown that the gasification produces lower CO than the combustion, whereas the CO₂ production is similar (See

Figure 5-7(a)). This result is unexpected, as through the gasification process more CO and less CO₂ should be obtained. Hypothetically, it occurred because of the excess oxygen condition inside the reactor

To investigate whether this hypothesis is true, further gasification simulations with reduced oxygen concentrations are developed. The results of CO₂ and CO are compared, as seen in Figure 5-8.

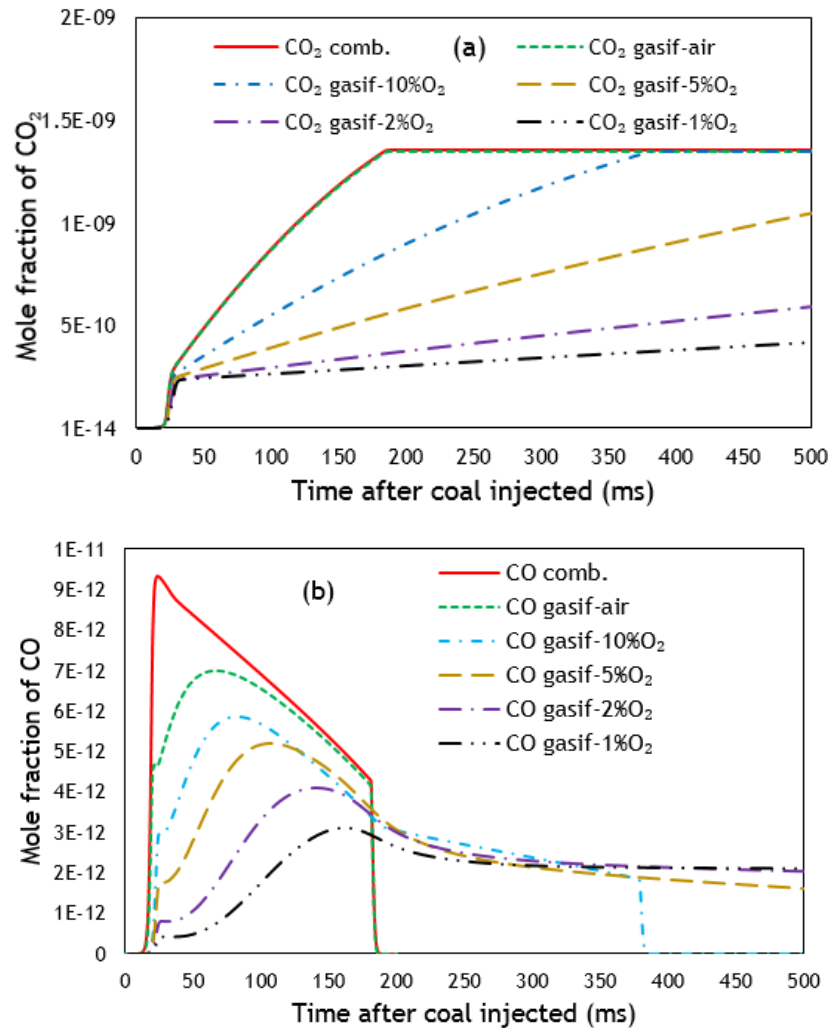


Figure 5-8. Comparison CO₂ and CO in various oxygen conditions in mass average of mole fraction

Figure 5-8(a) shows that the CO₂ products of gasification decreased after the reduction of oxygen concentration inside the reactor. This reduction was expected to occur in the gasification process. Figure 5-8(b) shows how the CO production lasts longer after the oxygen reduction, which means the carbon conversion slows down in the condition of less oxygen. This behavior agrees with the experiments conducted by *Yoshiie et al* [136],

to distinguish between the process of combustion and gasification. Their experiment results observed that the coal reaction rates at gasification were much lower than at combustion.

Overall, Figure 5-8 confirms the importance of having the oxygen control in the gasification process.

5.2.3 Maintaining char in the coal particle gasification

The observation of Figure 5-6 and 5-7(b) indicates a strong correlation between the char and the production of CO and H₂. This shows that the CO and H₂ production occurs when the coal particle or char exists in the reactor and they decay (dropped) after the coal particles or char burns out. One way of maintaining the char can be by injecting the coal particles continuously into the reactor. To perform these procedures, a coal particle is injected every 50ms and the system reaches steady-state after 20s and the results of CO and H₂ productions are presented in Figure 5-9.

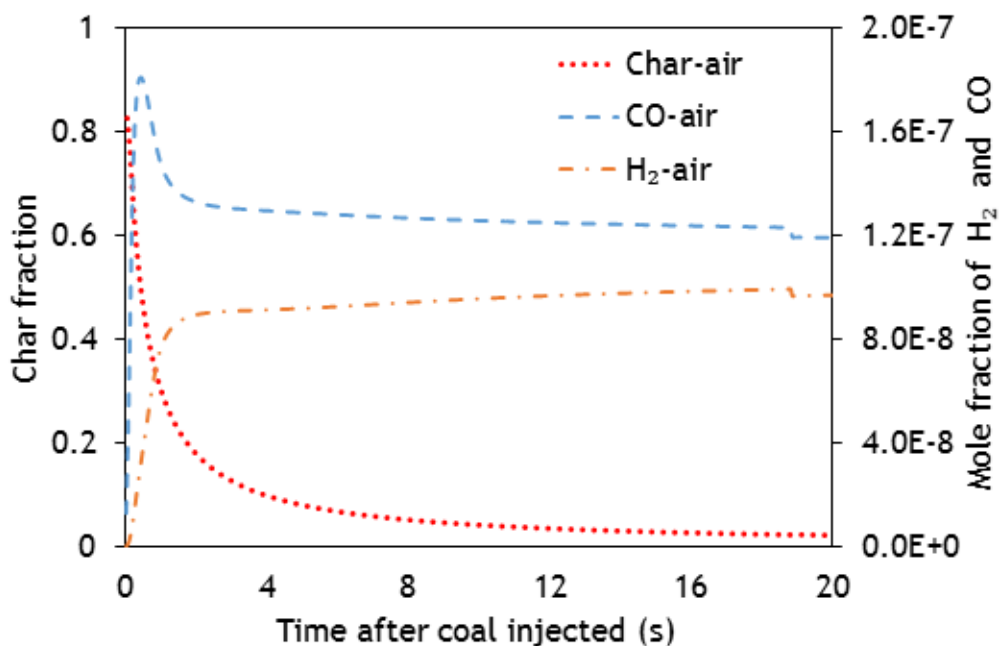


Figure 5-9. The continuous coal injection for maintaining the char in the reactor

Figure 5-9 shows that continuous coal injection maintains the production of CO and H₂, and this was expected for the investigation. Because of this, the study is concerned with the process of syngas production and further simulation is mostly performed with

continuous injection of coal particles. This is designed to maintain the gasification process and then the investigation can begin.

5.3 Coal particle gasification

A model for simulation of coal particle gasification has been developed. Further investigation is carried out with the aim of identifying the effects of the coal particle size and reactor temperature on the gasification products.

5.3.1 Effects of coal particle diameters

The simulation is applied with three different coal diameters (60 μm , 75 μm and 100 μm). Each is performed by injecting the coal particle every 50ms into the reactor with air temperature $\sim 1400\text{K}$. The comparison results of syngas production, as a contour plot of the H_2 molar concentration, can be seen in Figure 5-10.

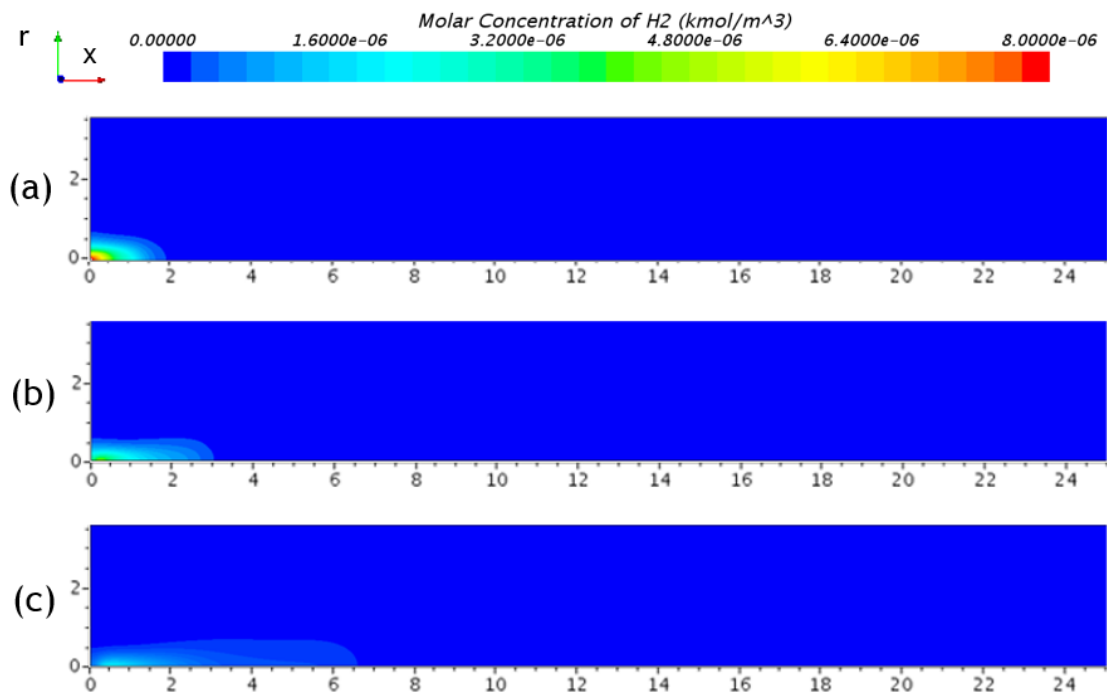


Figure 5-10. Molar concentration of H_2 in a variation of coal particle diameters (μm) (a) 60 (b) 75 (c) 100

Figure 5-10 shows that the bigger coal particle has the greater area of gas distribution in the contour plot, but the level of concentration seems lower. This is because the bigger coal particle has more gravity forces and causes the free-fall particle to move faster inside

the reactor. The gas products then fill the space along the particle displacement and finally develop a greater area with lower concentration. It is possible that the H_2 product further reacted with oxygen or char to obtain CH_4 and H_2O according to the reaction mechanisms as shown in Table 3- 1, and therefore the concentration seems weaker along the gas stream (axis direction). On the other hand, the smaller particles accumulated the production of H_2 in a smaller area of the reactor and, therefore, they have a higher concentration level.

Other species of syngas products, such as CO and CO_2 , can also be presented to identify the effect of particle size as shown in Figure 5-11 and Figure 5-12, respectively.

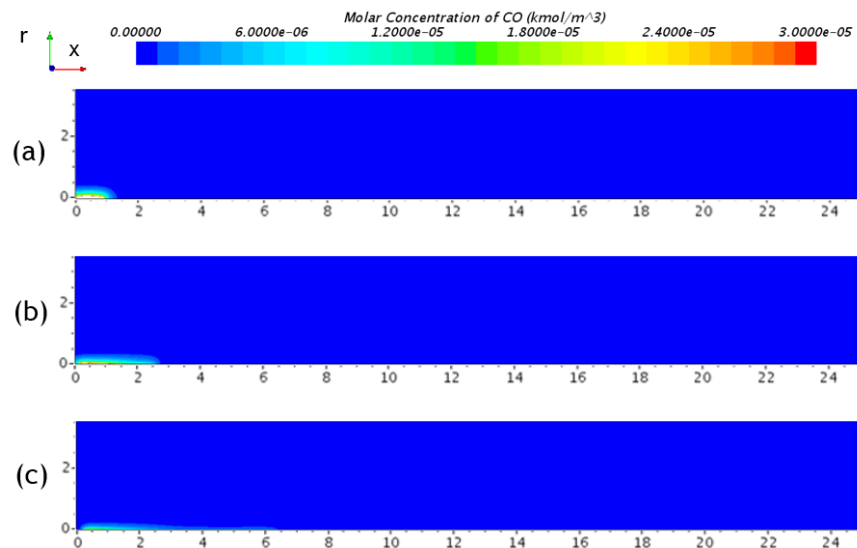


Figure 5-11. Molar concentration of CO in variations of coal particle diameters (μm) (a) 60 (b) 75 (c) 100.

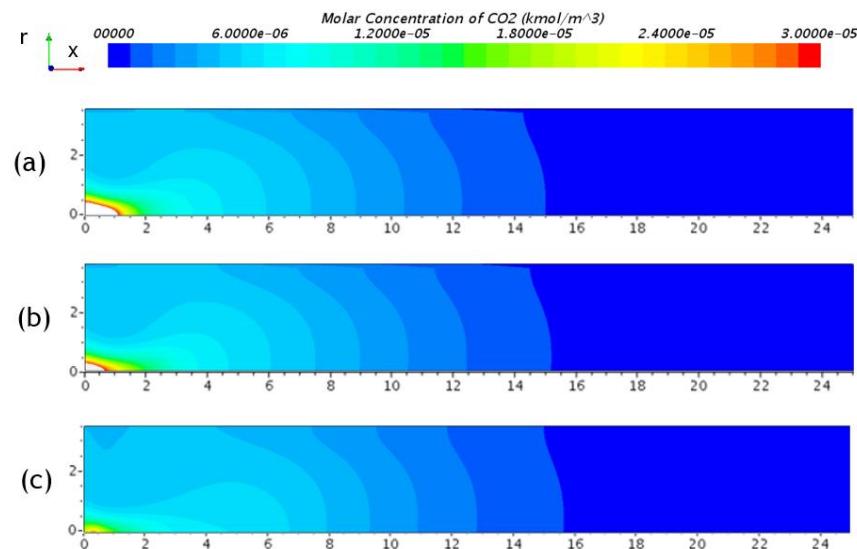


Figure 5-12. Molar concentration of CO_2 in variations of coal particle diameters (μm) (a) 60 (b) 75 (c) 100

Figure 5-11 and 5-12 show that both CO and CO₂ have a trend similar to H₂, i.e. the bigger particle size covers a greater area in the reactor but with a lower level of gas concentration. For CO, as shown in Figure 5-11, the concentration also seems to be weaker along the particle flow, and it is possible that CO has further reacted with oxygen to produce CO₂ as defined in Table 3-1. Having the same trend as CO and H₂, the distribution area of CO₂ concentration looks greater in the reactor, as shown in Figure 5-12. This indicates the production of CO₂ is much more than other gases in this simulation. It is understandable since, at this stage, according to the gasification mechanisms defined in Table 3-1, the simulation has excess oxygen or it has been undertaken at lean combustion conditions.

The contour plot results present information about the mole gas concentration over the volume of the reactor. It is helpful to clarify the gas product distribution of each coal particle and gasification inside the reactor. However, as a comparison value of gas concentration produced over the area of generation by each particle size, see Figure 5-13 and 5-14.

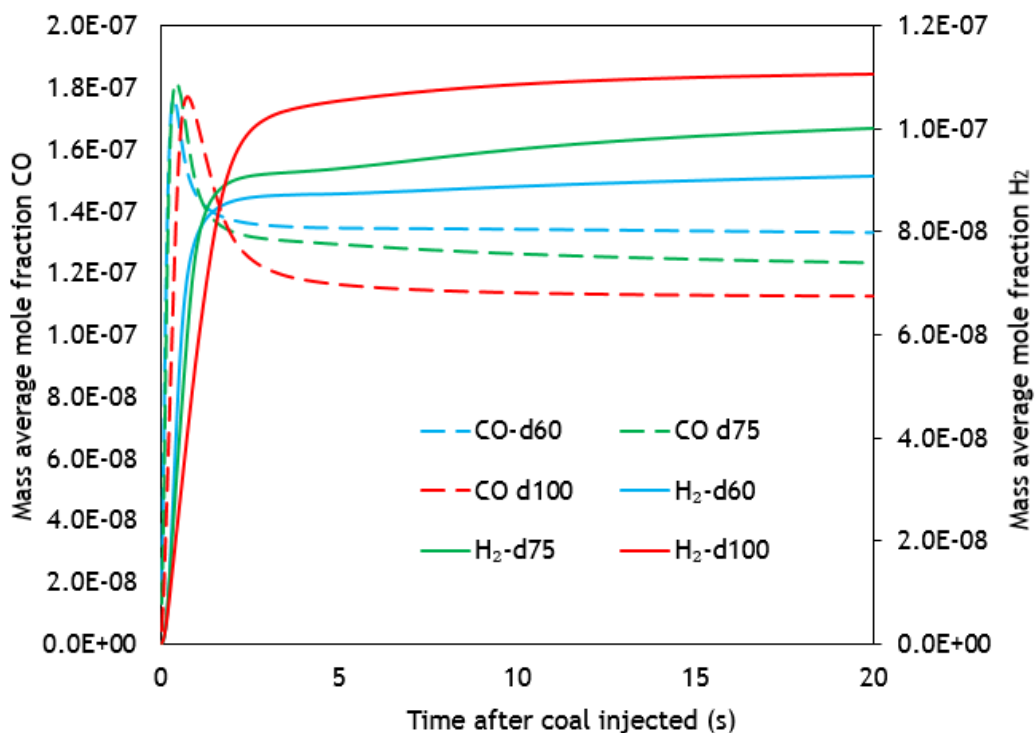


Figure 5-13. Mass average mole fraction results for CO and H₂

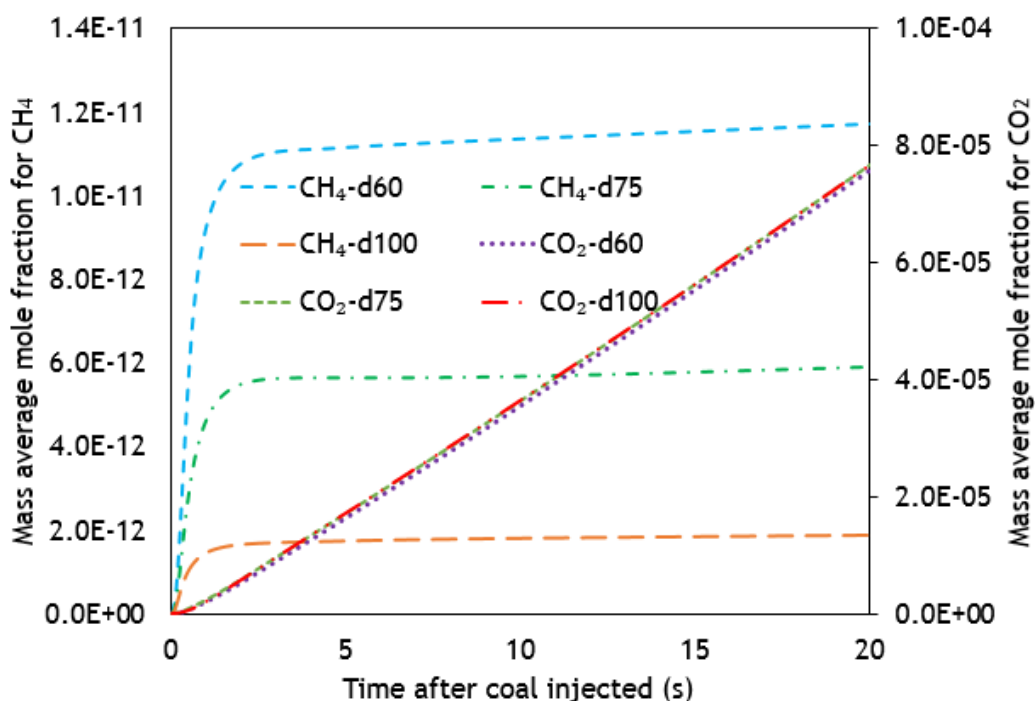


Figure 5-14. Mass average mole fraction results for CO₂ and CH₄

Figure 5-13 and 5-14 show the comparison of gas products CO & H₂, and CH₄ & CO₂, respectively in the parameters of mole fractions over the area of the products generated. Figure 5-13 shows that the larger size of particle produces the more H₂, and the less CO after steady state condition. The greater H₂ production can be explained because the increasing particle diameter causes an increase in the reactants' mass (i.e. char fraction and coal volatile), and this causes an increase in mass products as well. In addition, H₂ is produced dominantly from homogeneous reactions (see Table 3-1), which is not affected by particle size. In contrast, CO is mostly produced from heterogeneous reactions, and therefore the effect of particle size is significant.

Figure 5-14 further shows that the higher coal particle size has a slightly higher CO₂, and lower CH₄. The increase in the reactant's mass increases the product of reactions, as in CO₂. Although the CO₂ is produced dominantly from heterogeneous reactions, the effect of additional coal mass gives greater significance to the products' formation. Meanwhile, CH₄ behaviour indicates a similarity with the CO. This because the CH₄ formation (as shown in Table 3-1) is obtained from heterogeneous reactions, which indicates that they are affected by the particle size. The smaller particle size potentially produces more products.

5.3.2 Simulation performance in various temperatures

The influence of temperature on the gasification reactions was studied to identify performance behaviour. For this purpose, the three temperature conditions of the reactor are set for gasification performance and they are at the temperature of 1000K, 1200K and 1400K. These values refer to the temperature variation condition application according to *Bhutto et al.* [5]. The coal is injected and the gas products are identified. Similar boundary conditions are set; the coal particle diameters used 75 μm , and air was considered as gasification agent. The simulation is performed for 20s.

The contour plots of the H_2 molar concentration products in three different reactor temperatures are presented in Figure 5-15.

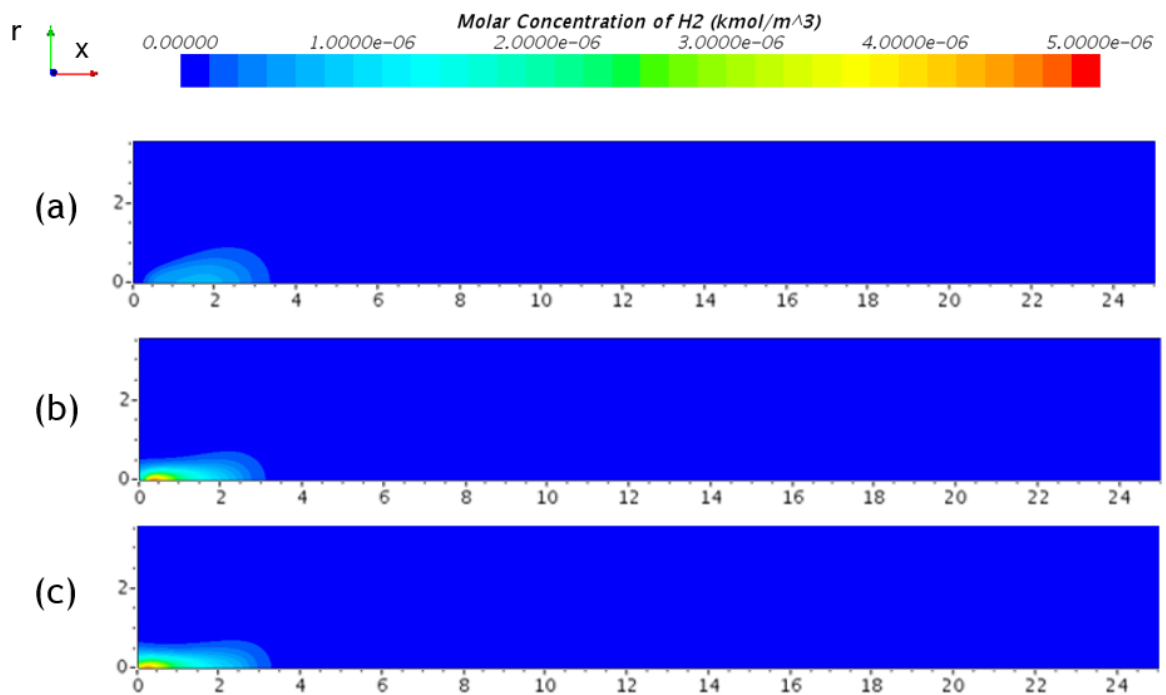


Figure 5-15. Molar concentration of H_2 in various temperatures (K) (a) 1000, (b) 1200, and (c) 1400

Figure 5-15 shows that the increase in reactor temperatures in the gasification process could affect the H_2 formation, and the higher temperature process could produce an earlier H_2 formation. As evidence, this can be seen at the temperature of 1400K, the H_2 formation starts closer to the inlet of coal injection, and the lower temperature is produced further from the inlet region. This also indicates that the higher temperature of reactor obtains a

greater production of H_2 , and, as is shown, their molar concentration of H_2 is greater and/or longer in the contour plot area of reactor. For further identification, the same process of comparison can be performed for molar concentration of CO and CO_2 inside the reactor. Their contour plot can be seen in Figure 5-17 respectively.

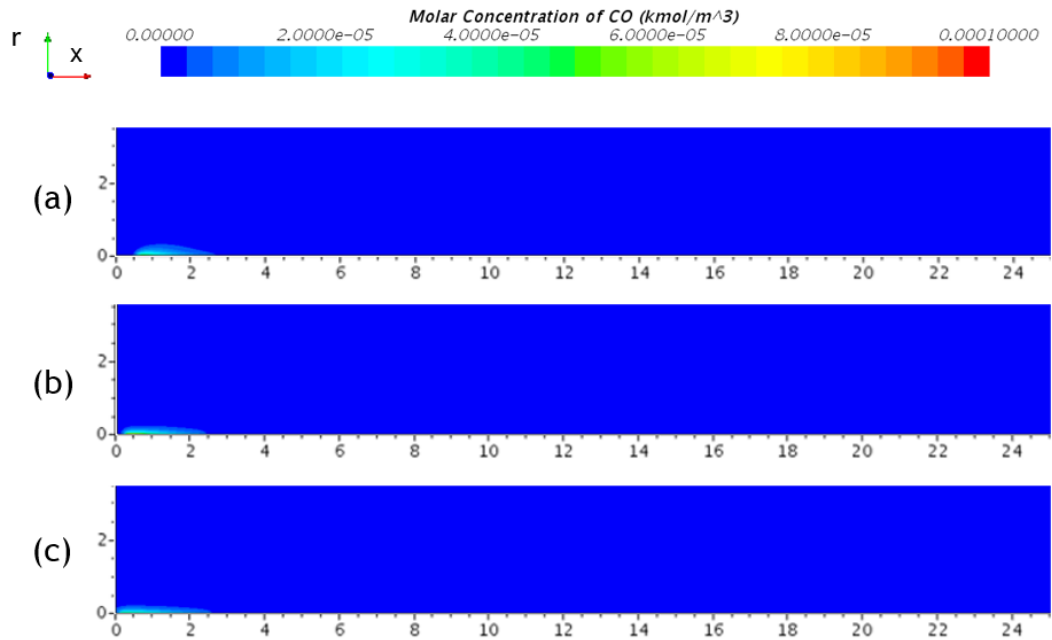


Figure 5-16. Molar concentration of CO in various temperatures (K) (a) 1000, (b) 1200, and (c) 1400

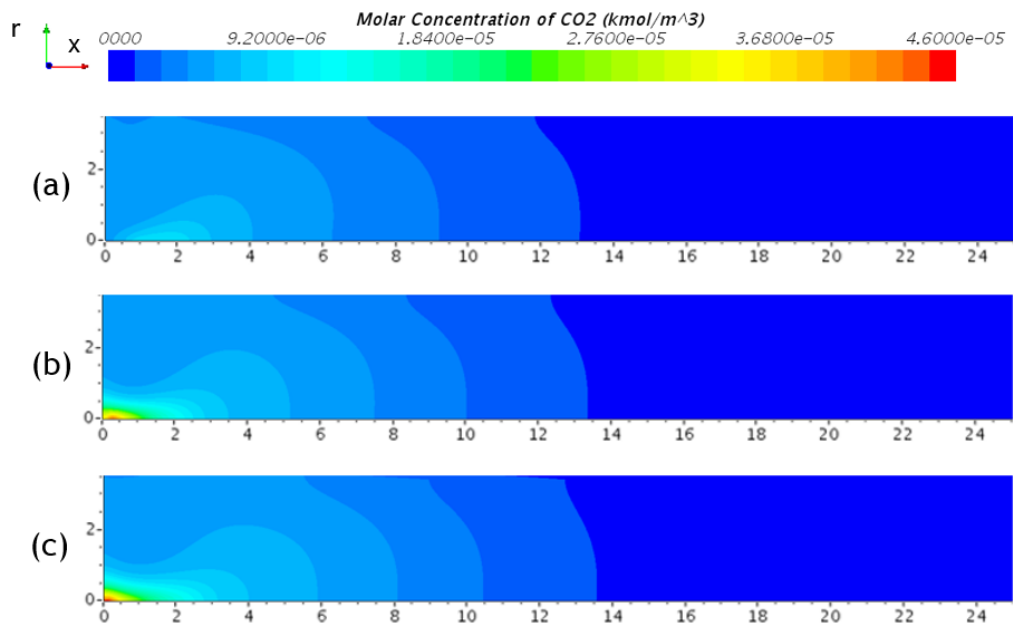


Figure 5-17. Molar concentration of CO_2 in various temperatures (K) (a) 1000, (b) 1200, and (c) 1400

Figure 5-16 show the distribution area of CO and CO₂ in the contour plot of the reactor. Gas CO formation behaviour in Figure 5-16 is similar to the H₂ behaviour in Figure 5-15. The higher reactor temperature has the greater plot area, which indicates the greater CO production obtained in the reactor at 1400K. Meanwhile, CO₂ production is greater at the higher temperature of the reactor as shown in Figure 5-17. These results clarify that the gas production obtained was greater at the higher temperature of the reactor.

Those results are described qualitatively and in order to see the comparison better, this is shown in Figure 5-18.

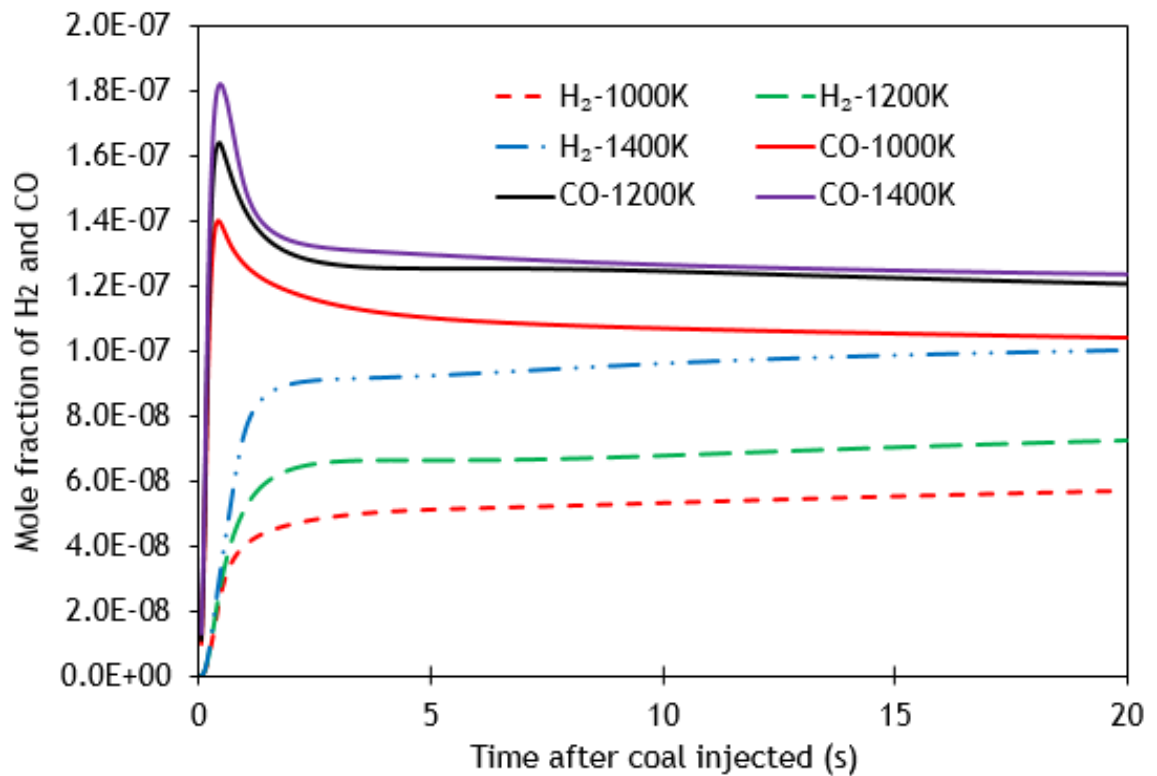


Figure 5-18. The gas products of H₂ and CO at temperature variations

Figure 5-18 shows the comparison in earlier contour plot results and this confirms that the results show higher temperature as more H₂ and CO are produced. Other parameters are CO₂ and CH₄, as shown in Figure 5-19.

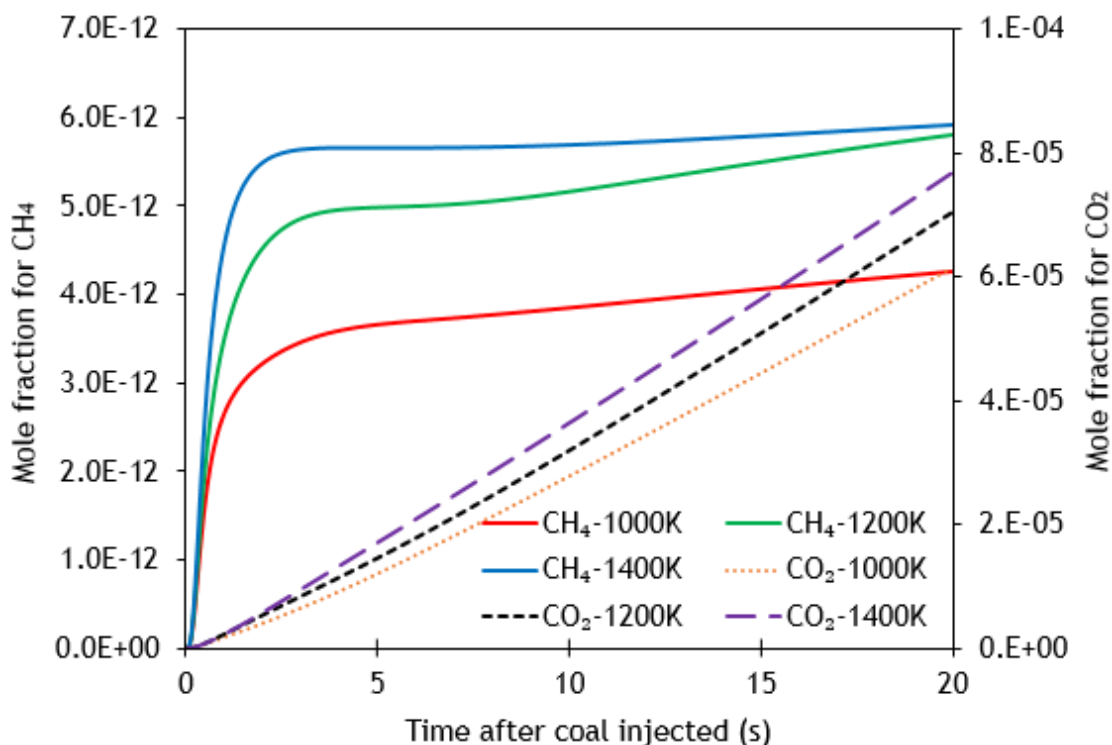


Figure 5-19. Mass average mole fraction of CH₄ and CO₂ at temperature variations

Figure 5-19 confirms these results, and shows that, at a higher temperature, greater CH₄ and CO₂ production is obtained. Those results have identified the important role of temperature in gasification performance. A high temperature is required for gasification reactions in order to provide a better condition of coal conversion into gas products and most gas-gas reactions occur at a high temperature to produce the required gas products or syngas.

5.4 Gasification performance at various environments

The effects of particle size and temperature have been simulated with this model and they have been identified through the results of the gas products. In this section, the investigation is performed with the addition of H₂O and CO₂ in the environment of the reactions. The addition of H₂O is designed to find better syngas products and the addition of CO₂ is to investigate the potency of the CO₂ involved in the reactions in response to the environmental issue of coal utilisation through the gasification process [137, 138]. It is also possible to identify the effect when both gases are added into the reactor at a certain fraction to see the gas products' behaviour.

The simulation and the description of results obtained are provided in the sections below.

5.4.1 Study on the effect of steam (H₂O)

The three simulation cases were carried out to present various steam (H₂O) additions in the reactor, with the percentage for each case being 20%, 40%, and 60% (with 20% of O₂ and the rest is N₂). Other boundary conditions are similar, with particle diameters used being 75 μm , injected every 50ms, and the simulation performed for 20s. The simulation performance with air is also presented for reference. The results of each simulation performance for the parameter of coal particle temperature and char fraction are seen in Figure 5-20.

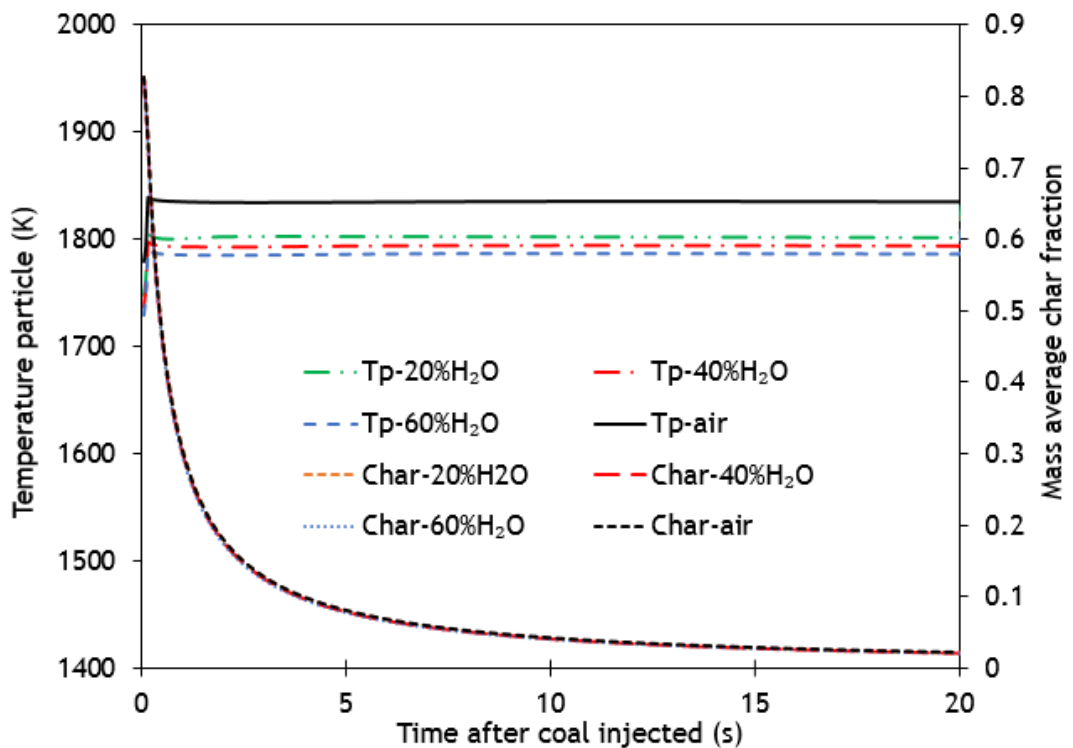


Figure 5-20. The particle temperature and char profile in H₂O environment

Figure 5-20 shows that the higher particle temperature occurred at a lower fraction of H₂O; meanwhile the char fraction profile was almost similar for every condition. This indicates that the additional steam into the gasification reactor potentially dropped the coal temperature but it had no significant effect on char reactions. As mentioned in Section 5.3.2, the temperature also had an effect on the gasification reaction; therefore it was possible to identify this issue on the gas products' formation.

The results of CO and H₂ products in various H₂O fractions can be seen in Figure 5-21.

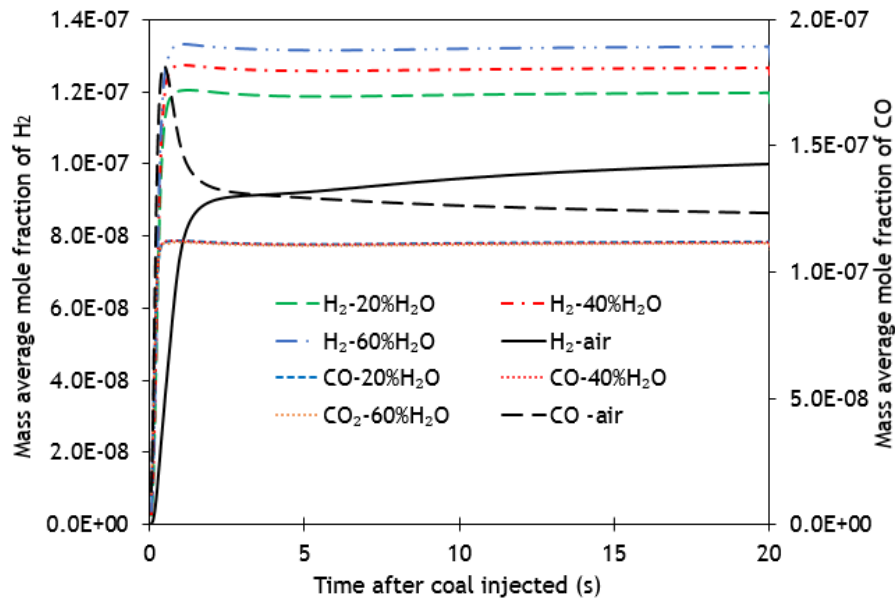


Figure 5-21. H₂ and CO production under various H₂O condition

Figure 5-21 shows that supplying steam (H₂O) into the reactor potentially increases gas H₂ production, and it has no significant effect on CO formation. However, the CO formation in the environment of H₂O is lower than in the condition with only air. This indicates that the addition of steam helps to obtain more H₂ in the gasification products, but it can also decrease the temperature which is also important for the gasification process. Other gas product results are CH₄ and CO₂ production. The comparison of these gases can be seen in Figure 5-22.

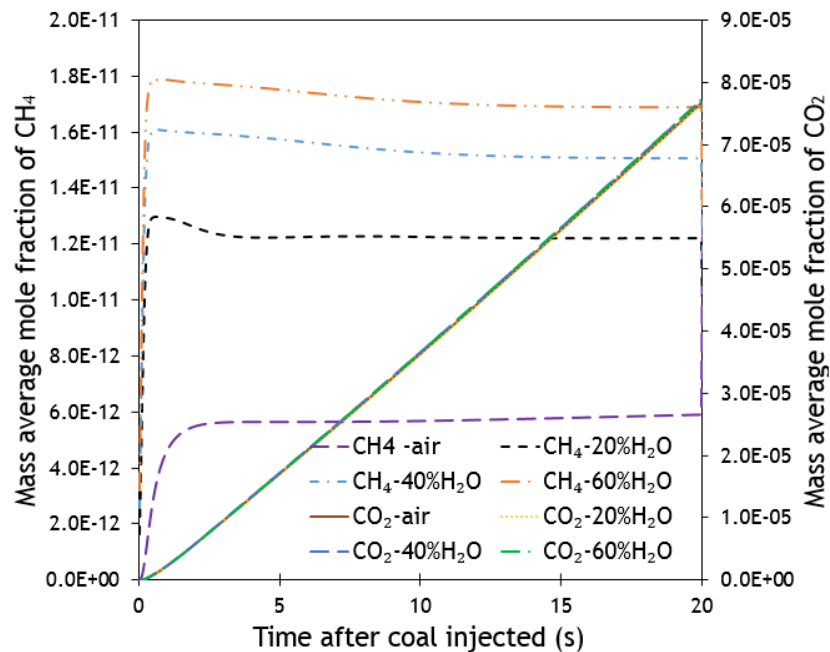


Figure 5-22. The comparison result of the addition of H₂O for (a) CH₄ and (b) CO₂

Figure 5-22 shows CH_4 and CO_2 production under various fractions of H_2O , with air as a reference case. CH_4 increases with the addition of steam and the CO_2 has no significant effect in any case. This indicates that the addition of H_2O into the reactor of gasification potentially increases the CH_4 production.

This section describes the potency of the benefits of the gasification process with additional steam into the environment of reactions as these can increase the syngas quality, especially for H_2 and CH_4 products. However, any unexpected effect also needs to be considered, such as the decrease in coal temperature. Therefore, the process optimisation needs to be considered to achieve any benefit.

5.4.2 Study on the effect of CO_2

An initial simulation was performed in a single coal particle performance in order to identify the potency of CO_2 additions in the environment of gasification reactions. There are two conditions for the comparison; they are air (20% of O_2 and 80% of N_2) and air with the addition of CO_2 (20% of O_2 , 60% of N_2 , and 20% of CO_2) respectively. These are applied to the reactor to perform the simulation. The result of gas products for the parameters of CO and H_2 can be seen in Figure 5-23.

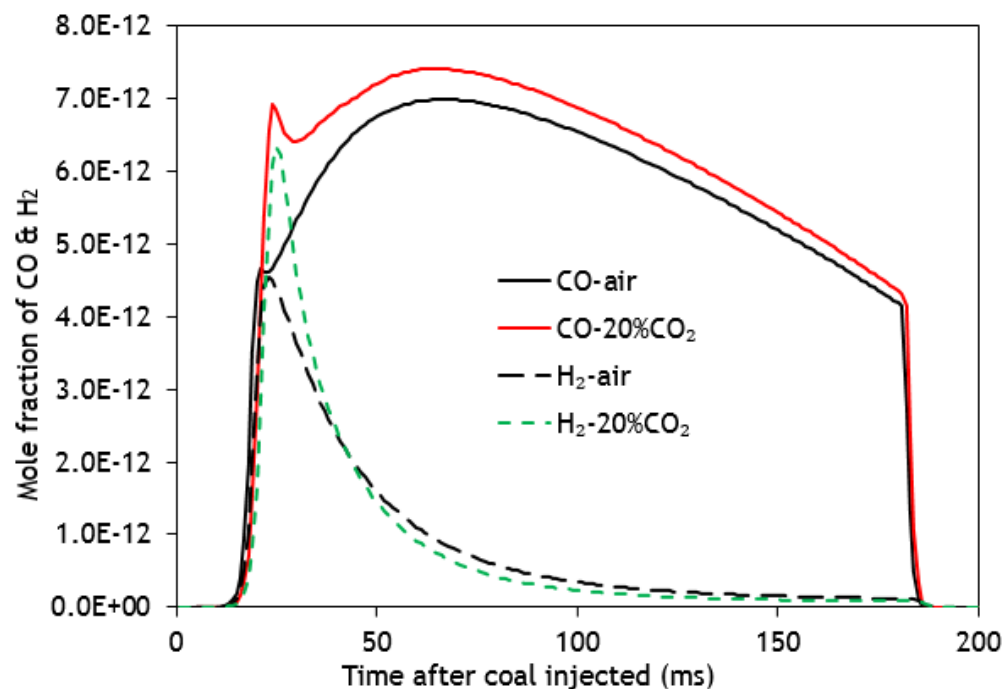


Figure 5-23. Particle temperatures and char mass fraction comparisons

Figure 5-23 shows that the maximum value of CO and H₂ with the addition of CO₂ in the environment of the reactor is higher than with air, but after approximately 50ms the H₂ at air is slightly higher than with the addition of CO₂. However, it is still an indication of the potency of the addition of CO₂ to provide a better H₂ and CO formation.

In order to produce more evidence and results, further investigation was performed with continuous coal injections. The three cases were developed with CO₂ added into the reactor at 20%, 40%, and 60% of CO₂ (with 20% O₂ and the rest is N₂), respectively and the performance with air, as a reference case, was also shown. Other similar boundary conditions were also set with the coal diameter of 75 μm injected every 50ms, until a steady condition was reached in the reactor (~20s). The simulation results for the particle temperature and char mass fraction can be seen in Figure 5-24.

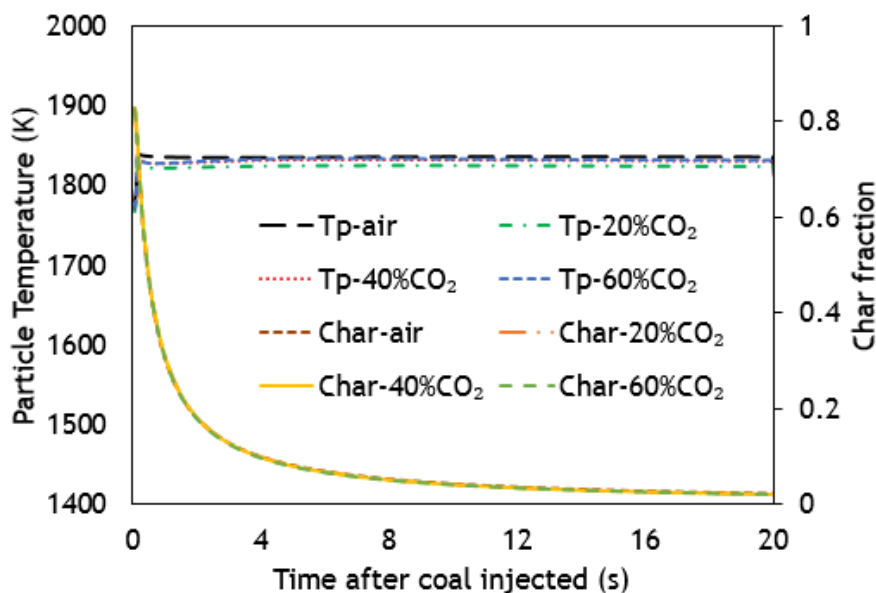


Figure 5-24. Particle temperature and char mass fraction in CO₂ variations

Figure 5-24 shows that the temperature of the coal particles, with the addition of CO₂ are slightly lower than at the condition with air, but there is almost no difference in the char percentages. This indicates that the addition of CO₂ potentially reduces the temperature and has no significant effect on the char reaction.

Other results on the gas CO and H₂ products in various fractions with the addition of CO₂ can be seen in Figure 5-25.

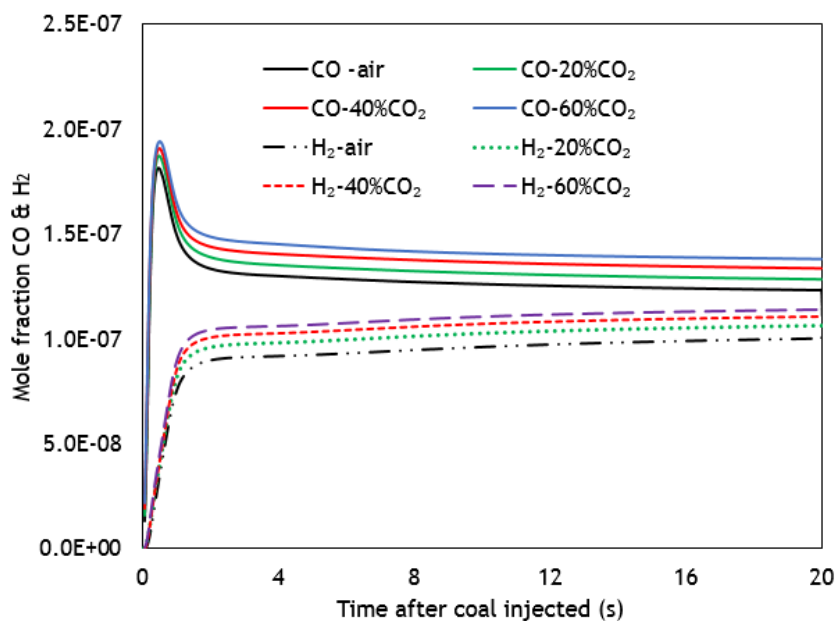


Figure 5-25. CO and H₂ comparisons in CO₂ variation

Figure 5-25 shows that the addition of CO₂ in the reactor has the power to increase the quality of syngas products. This shows that the products of CO and H₂ in the environment with the addition of CO₂ are higher than on the environment with air only. This gives greater evidence of the power of adding CO₂ as obtained in the single coal particle model.

The last syngas product for comparison is CH₄ and the results can be seen in Figure 5-26.

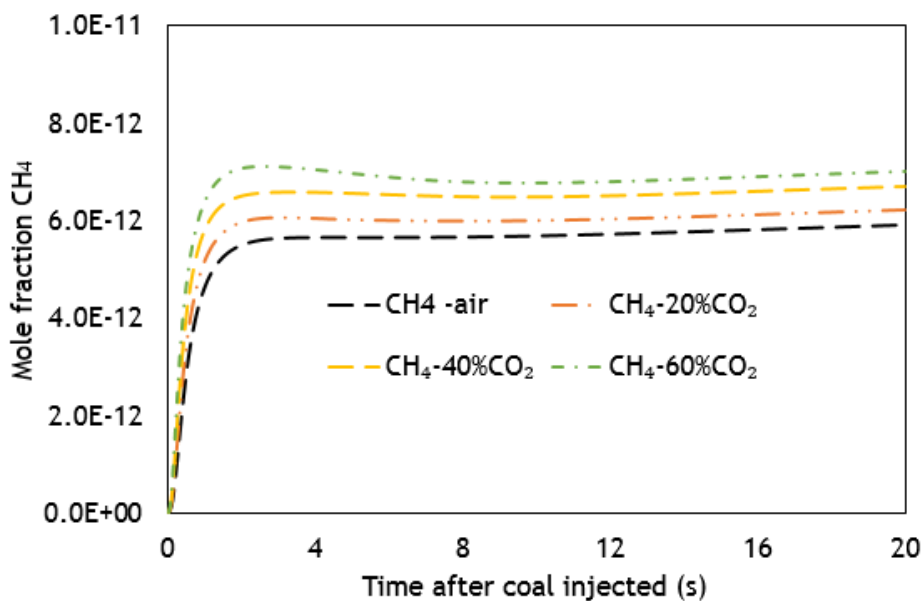


Figure 5-26. CH₄ comparison in CO₂ variations and air

Figure 5-26 shows the impact of adding CO₂ for increasing gas CH₄. It shows that CH₄ increases with the addition of CO₂ in the reactor. Again, it is a good indication of the

gasification process, since all syngas products show an increase through the addition of CO_2 in the environment of the reactions.

5.4.3 Study on the effect of combining H_2O and CO_2 with excess oxygen

A simulation in the condition with additional H_2O and CO_2 has been performed, and it is necessary to investigate the effect of mixing (combining) both H_2O and CO_2 in the reactor. To provide the simulation, the reactor is set with gas consisting of CO_2 and H_2O at a certain ratio, and 20% of O_2 is set constant for each performance to allow the coal oxidation reactions to take place. The simulations performed in the ratio of CO_2 and H_2O are 20/60, 30/50, 40/40, 50/30 and 60/20, respectively. Other similar boundary conditions are set with the coal diameter of $75 \mu\text{m}$, injected at every 50ms, for about $\sim 20\text{s}$, and the gas products of the reaction are compared.

The results of the simulation for the parameters of the particle temperature and char fraction are seen in Figure 5-27.

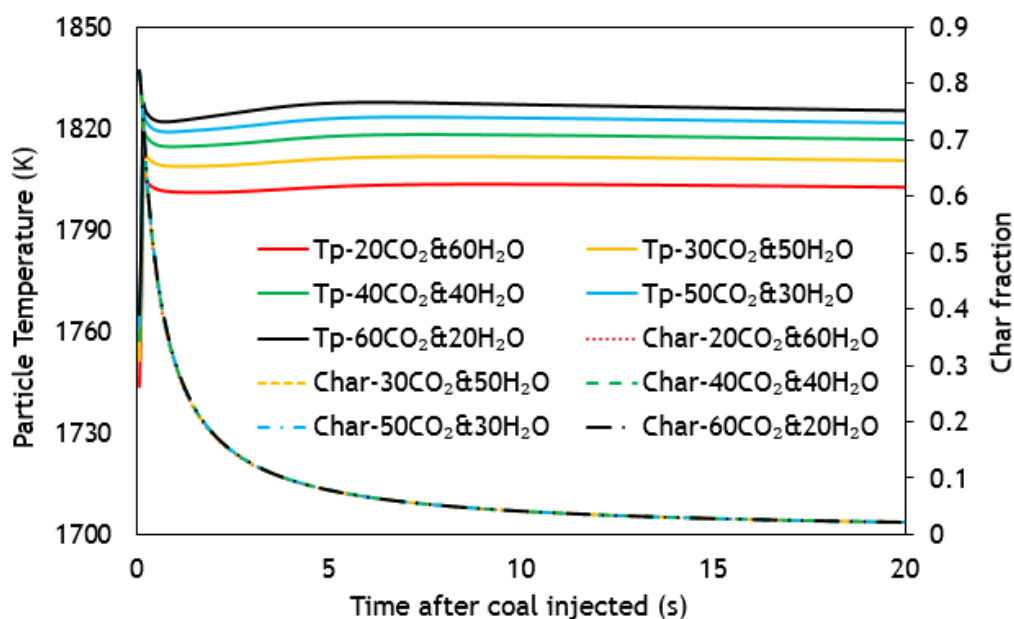


Figure 5-27. Particle temperature and char mass fraction in the $\text{CO}_2/\text{H}_2\text{O}$ variations

Figure 5-27 shows that the increase in the ratio of $\text{CO}_2/\text{H}_2\text{O}$ potentially increases the particle temperature, and the char fraction looks similar for each case. This indicates that the increase of CO_2 has a greater effect on the increase in the temperature rather than H_2O , while the changes in both CO_2 and H_2O have no significant effect on the char

reactions. It can also be seen from the figure that the temperature profile slightly fluctuates. This could have occurred due to the continuous injection of coal particle. When it occurred, the coal volatile and char can be burnt simultaneously. Since they have different maximum temperature of combustion, so a slight fluctuation of coal particle can be obtained.

The results of simulating the CO and H₂ products can be seen in Figure 5-28 and for CH₄ products in Figure 5-29.

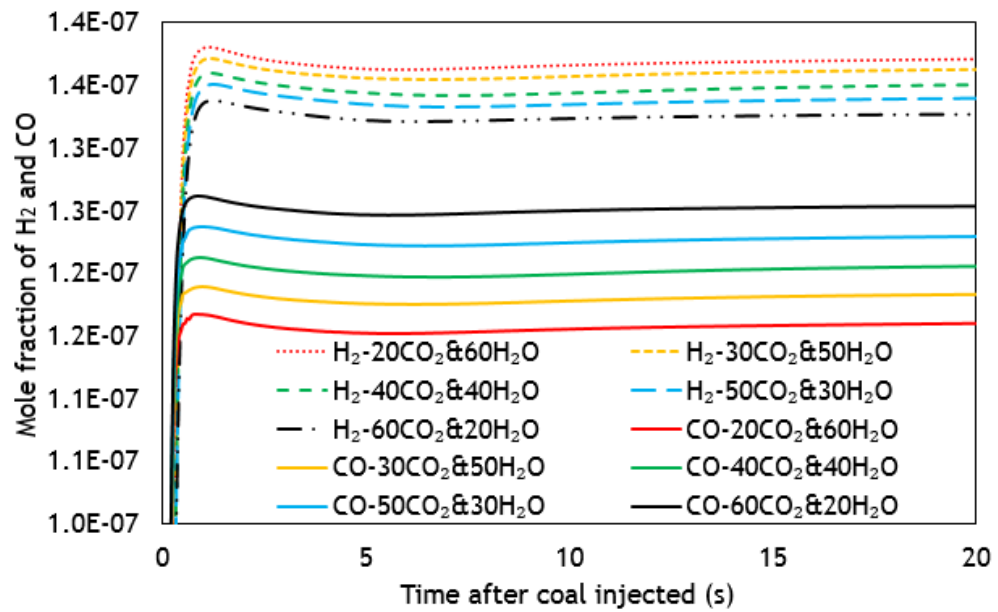


Figure 5-28. The gas CO and H₂ productions in some CO₂ and H₂O ratios

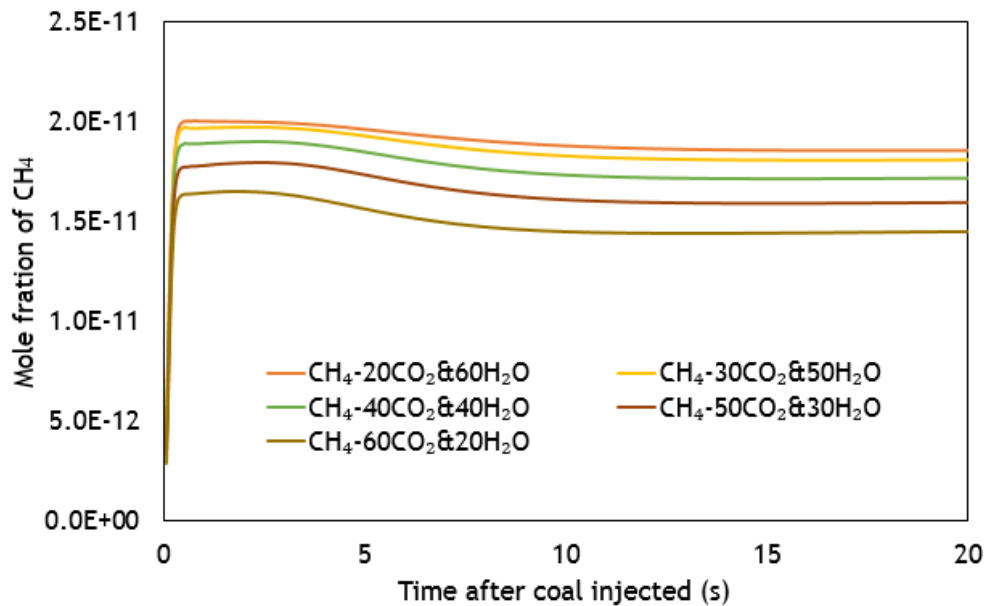


Figure 5-29. The gas CH₄ production in some CO₂ and H₂O ratios

Figure 5-28 shows that the increasing ratio of CO_2 and H_2O provides more CO , but fewer H_2 products. This indicates that the addition of CO_2 has a greater effect on CO formation, and the addition of H_2O has a greater effect on H_2 formation. Meanwhile, Figure 5-29 shows that the increase in the ratio of CO_2 and H_2O potentially produces less CH_4 . This indicates that the CH_4 formation is more influenced by H_2O rather than CO_2 .

5.4.4 Study on the effect of combining H_2O and CO_2 without oxygen

The condition when CO_2 and H_2O are combined in the absence of oxygen potentially occurs in the gasification process. Particularly in the UCG application, the condition occurs mostly in the reduction zone. Therefore, it is important to investigate the behaviour due to this condition. In the present investigation, the simulation performs similar procedures to the previous section, but without of oxygen fractions. The reactor is filled with CO_2 and H_2O at certain ratios; 20/80, 40/60, 50/50, 60/40 and 80/20. Other boundary conditions are similar for each case of simulation.

The simulation results for the parameters of particle temperature and char fraction can be seen in Figure 5-30.

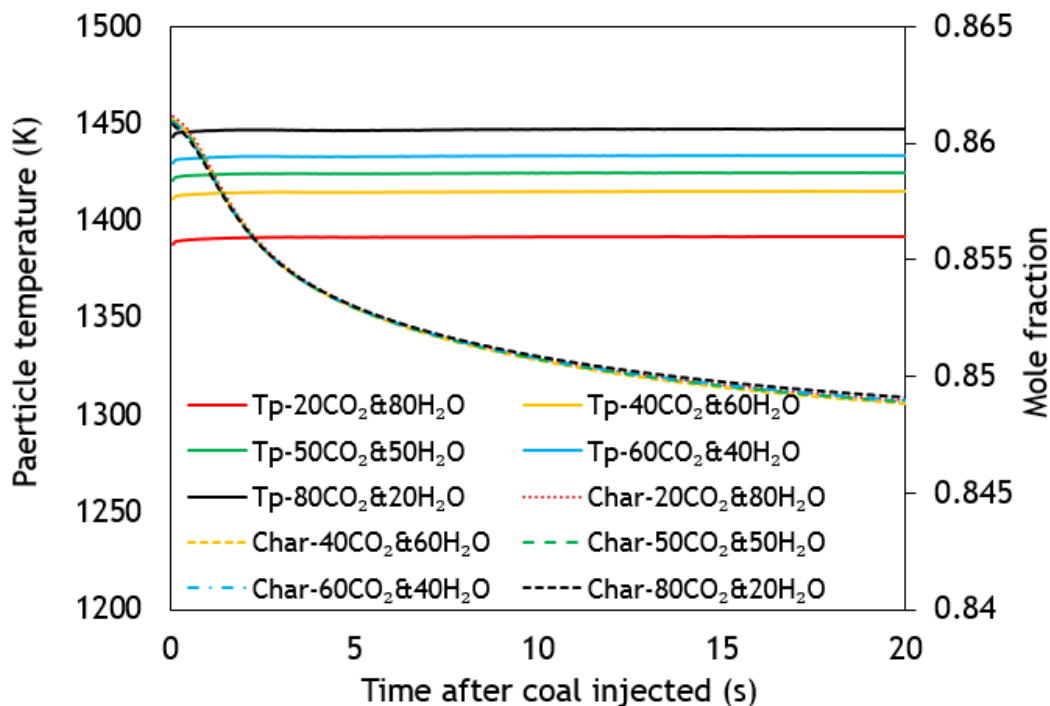


Figure 5-30. Particle temperatures and char fractions' comparison in $\text{CO}_2/\text{H}_2\text{O}$ ratio variation

Figure 5-30 shows that the increase on the CO_2 and H_2O ratio affects the increase in particle temperatures. More CO_2 produces higher temperature than an increase in H_2O . However, the maximum temperature being relatively low compares with the presence of oxygen (see Figure 5-27) because of the absence of oxygen. In addition, the trend of the particle reaction is very slow and is almost insignificant. An almost similar trend of char reaction showed for each fraction level.

Other parameters were H_2 and CO , and the comparison for each fraction level can be seen in Figure 5-31.

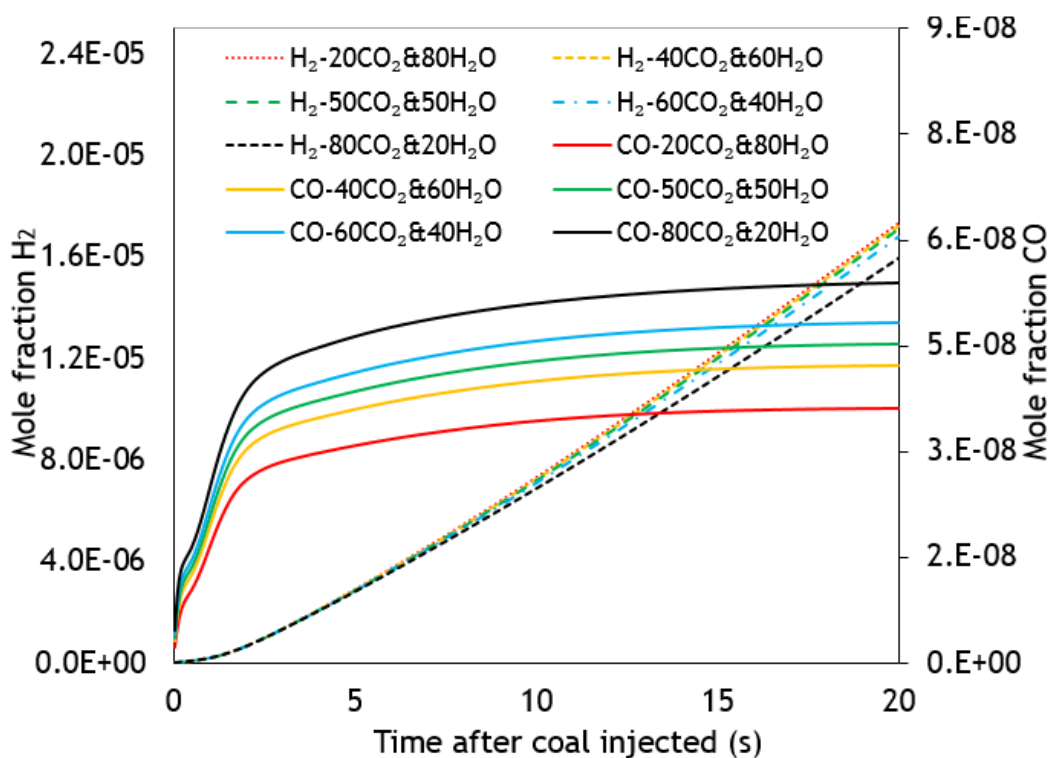


Figure 5-31. H_2 and CO comparisons in the $\text{CO}_2/\text{H}_2\text{O}$ ratio variations

Figure 5-31 shows that the increase in CO_2 and H_2O ratio increases the CO production, but decreases H_2 . However, the CO formation in the absence of oxygen is slower than the reaction in the presence of oxygen (see Figure 5-28 for comparison). On the other hand, the H_2 production in this figure keeps increasing, with the level of concentration being also higher than the H_2 production with oxygen inclusion (see Figure 5-28). This indicates that this condition is preferable for H_2 formation rather than CO .

The other comparison parameter is CH_4 . In order to provide a more comprehensive analysis, the results are more inclusive with the condition of the oxygen being present

(Figure 5-29). The results of both conditions, with their trends for each condition, can be seen in Figure 5-32.

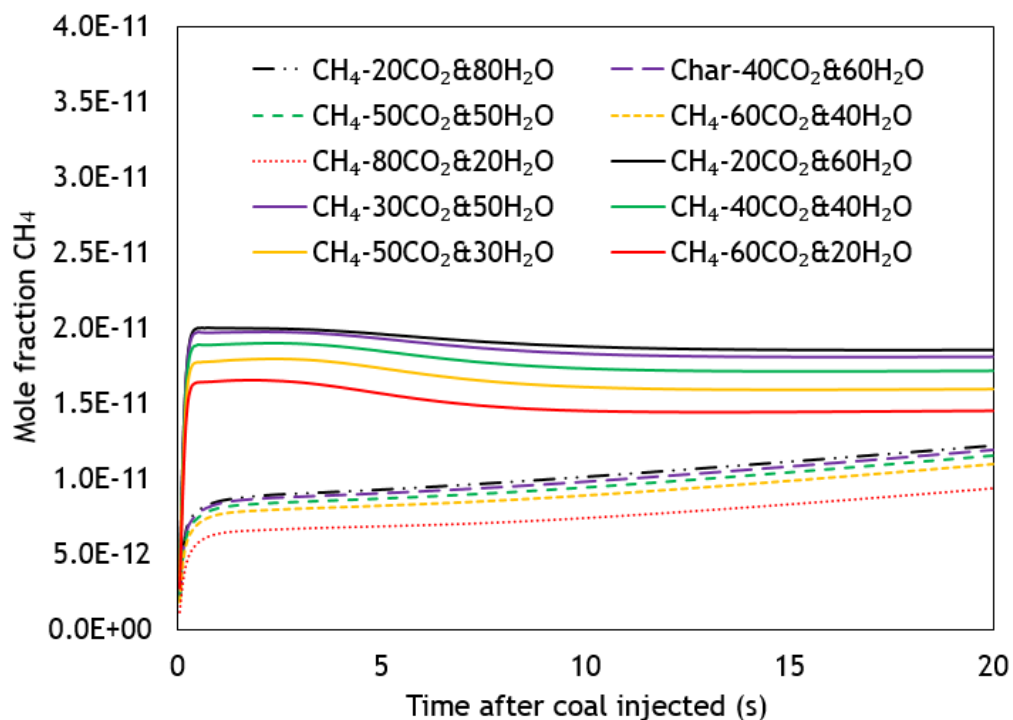


Figure 5-32. Comparison of CH₄ in CO₂/H₂O background variations, and O₂ used as a balance when the total concentration of CO₂ and H₂O were not 100%

Figure 5-32 shows a range of information such as the comparison of the effect of the CO₂ and H₂O ratios on CH₄ formation, and the effect of oxygen. The first issue has already been described in the previous section and Figure 5-32 confirms it. It clears that CH₄ is more affected by H₂O than CO₂ and the increase in CO₂ and H₂O ratios causes the decrease in CH₄. With regard to the existence of oxygen, Figure 5-32 shows that CH₄ production is higher and more stable in the condition with oxygen, but the trend of CH₄ formation in the condition without oxygen is consistent with an increase. However, the simulation results show that CH₄ formation occurred in both conditions, with or without oxygen.

5.5 Investigation of UCG processes

The most important reason for developing coal gasification through the particle approach is to examine the behaviour of the reactions. The particle method has been supplied with proper gasification mechanisms, and the modelling approach will now be used for UCG

reaction investigation. The illustration figure was introduced in Figure 5-1, and this section describes the behaviour of the reactions. In a UCG process, coal gradually burns up through the oxidation process and the resulting products flow downstream where the reduction processes occur and finally the product gases are collected through a bore hole. In the simulation, continuously injected coal particles flow through the channel under a quiescent gas condition and the oxidation reaction is propagated downstream because of the presence of air. The reduction process reactions occur simultaneously in the spot at behind the oxidation reaction of the coal stream (after the flame front in the coal particles stream). The process described is an analogue of the reactions that occur in the channel of UCG, and it presents similar reaction zones but in the reverse direction. In the model, the coal flows in a quiescent gas, meanwhile in the UCG, the gas flows through a static surface of coal seam. Therefore, the coal particle reactions model can be utilised to identify the reaction behaviour of coal gasification.

The previous simulation was dominated by the excess oxygen reaction, therefore the zone of reactions to be identified are slightly different. A further simulation is developed by providing a greater coal mass to be injected into the reactor to perform more clear reactions in a contour plot of the reactor. In this model, the mass flow-rate of the coal particle was increased by 500 and the temperature of the reactor after several occurrences of the reaction's process can be seen in Figure 5-37.

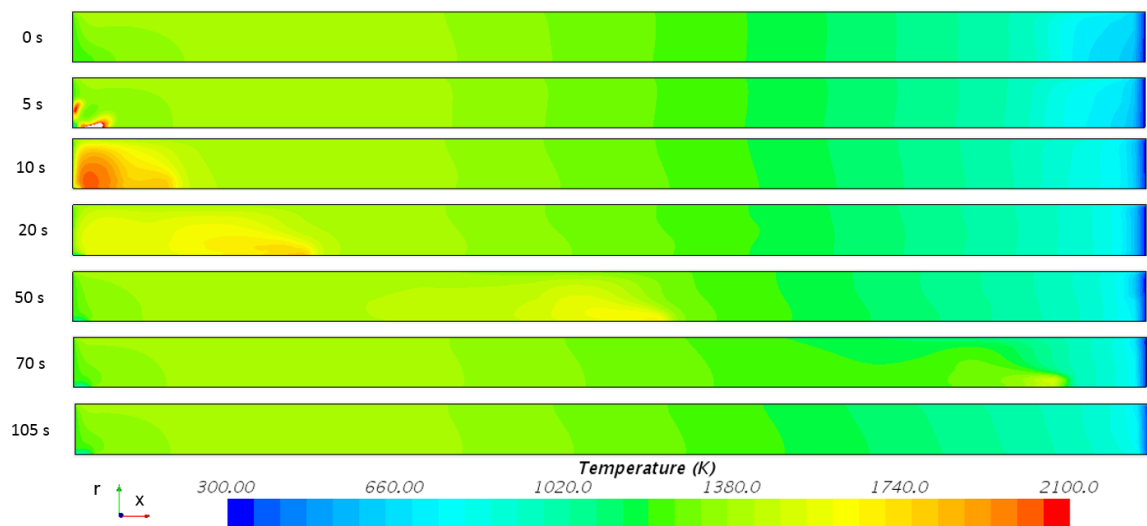


Figure 5-33. Contour plot of reactor temperature

Figure 5-33 shows the reactor's temperature plot inside the reactor and some spots show the coal and oxygen reaction as identified by the high temperature. The figure shows a

sequence of time in order to identify the process over that period. It can be seen the coal particles were burned and because of gravity they flow along the axis. The reaction process can be performed with the contour plot of oxygen concentration inside the reactor, as seen in Figure 5-34.

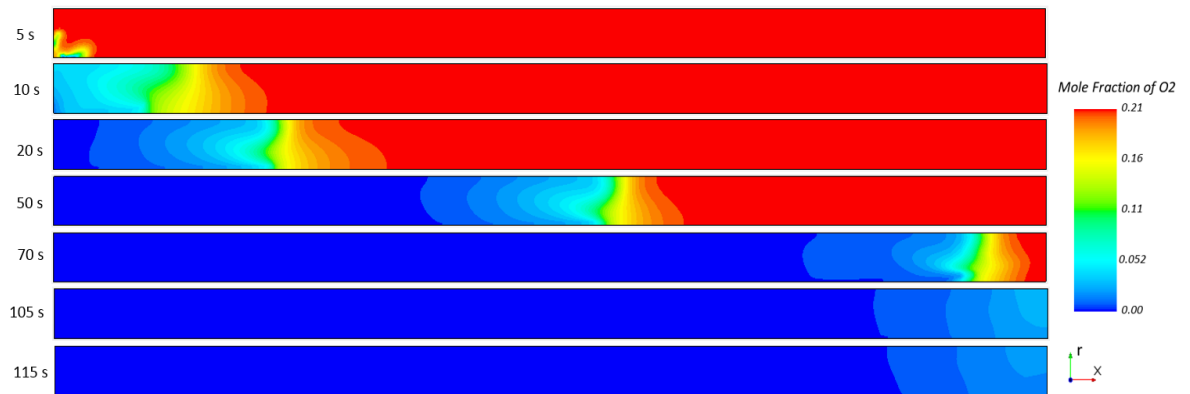


Figure 5-34. Contour plot of oxygen inside the reactor

Figure 5-34 shows the oxygen level of the reactor in time-sequences after coal injections. It identifies the coal reactions with oxygen conversion by seeing their level in area of reactor. The spot with gradation of colour identified the oxygen and coal reactions, it occurred at front stream of coal reactions. The colour changing indicates the reactant to products. To identify the products of the reactions, Figure 5-35 to 5-37 show the gas products; CO_2 , CO , and H_2 .

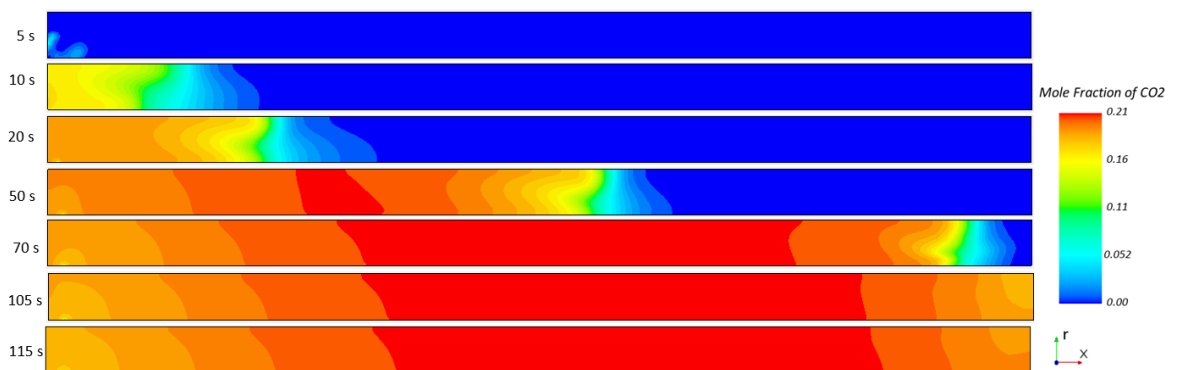


Figure 5-35. Contour plot of CO_2 inside the reactor

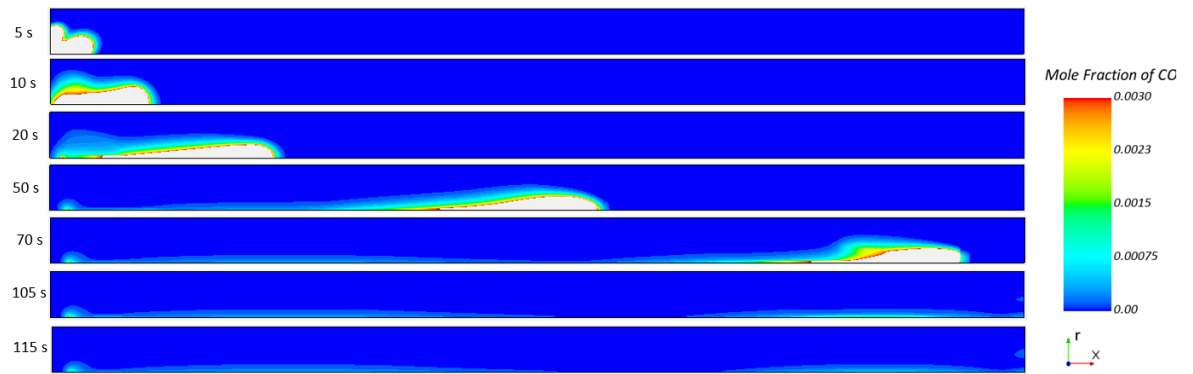


Figure 5-36. Contour plot of CO inside the reactor

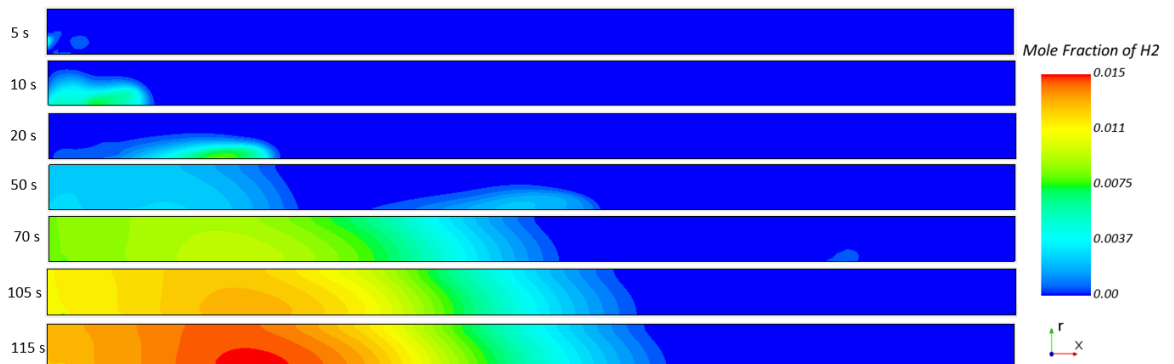


Figure 5-37. Contour plot of H₂ inside the reactor

Figure 5-37 shows the contour plots inside the reactor of gases CO₂, CO, and H₂, respectively at different times up to the period of 115s. In Figure 5-34, the oxygen concentration dominants in the reactor are from the time when the coal particle was injected. Over that period, oxygen concentration upstream decreases and finally disappears. In terms of process reactions, this behaviour aligns with the process in UCG but in a reverse direction [5, 9]. In UCG the gas is flowing downstream, therefore the excess oxygen occurred upstream, but in this simulation the coal is downstream, therefore the excess oxygen occurred downstream.

On the other hand, the effect of CO₂ production is shown in Figure 5-37. The CO₂ concentration initially is at its minimum (zero), but over the time of the oxidation reactions, its magnitude increases and finally becomes dominant in the reactor as seen at ~105 s after the coal particles have been injected. These are also identified in Figure 5-35, where the more gradation colour occurred in the CO₂ products area and were identified as a reaction. This indicates that more reactions occurred between CO₂ and other species

inside the reactor. Because of its location near the inlet, at the spot of the coal injection, it is identified that the reaction occurred between the CO_2 and the coal particles.

This confirms the decrease of CO_2 at the area near the inlet and, co-incidentally, it was at that spot that the CO formation occurred. Figure 5-36 shows the spots of CO formation. There are at least two spots of CO formation and they are at the oxygen reaction area and at the coal injection spot area. However, the greater production occurred at the oxygen reaction's area and the smaller spot indicates where the CO_2 reacted with solid carbon and coal particles. This clarifies the CO formation process, which the simulation showed mostly came from coal and oxygen reactions.

Other gas products' behaviour can be seen in Figure 5-37 which shows the H_2 production in the reactor. Initially, the H_2 production occurs in the area of oxygen reaction and it can be seen that the colour gradation of H_2 formation follows the coal and oxygen reaction spot. Over this period, it can be seen that the spot decreases and a new spot appears in the area of less (or zero) oxygen. Its production was developed and was greater in the absence of oxygen. This further indicates that this gas is potentially better produced in this zone (the less oxygen area). In a UCG application, the downstream area has less, or possibly zero, the oxygen concentration. This area is the reduction zone (see Figure 5-1), and the investigation of H_2 formation as shown in Figure 5-37 clarifies the behaviour in the reduction zone of UCG.

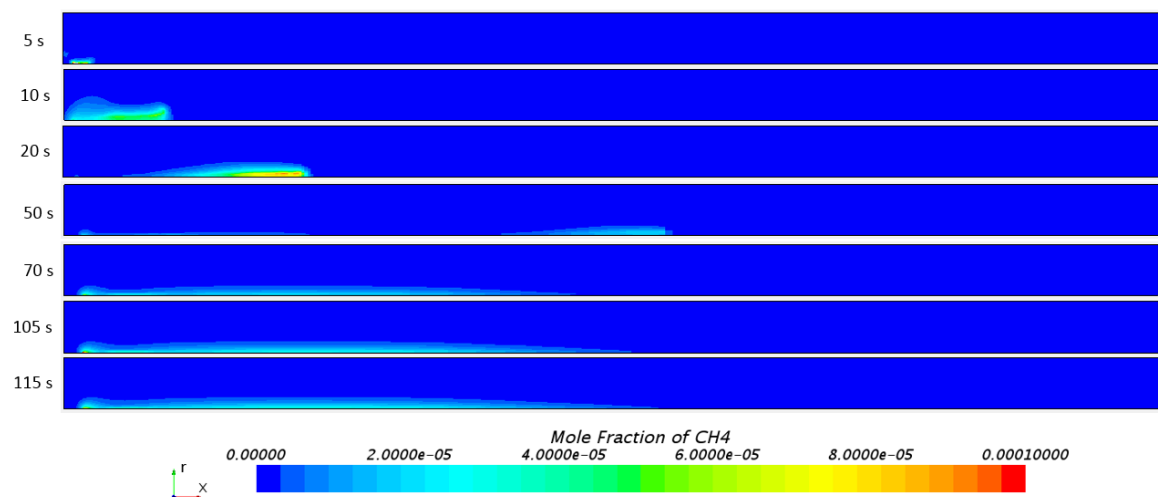


Figure 5-38. Contour plot of CH_4 inside the reactor

Another important gas product in the gasification process is CH_4 . Figure 5-38 shows the behaviour of CH_4 formation based on the result of simulation. The spot of formation CH_4 products is similar to the contour plot of H_2 formation (see Figure 5-37), but the area is smaller. This indicates the correlation between the CH_4 and H_2 formation, which is relevant to the reaction mechanism defined in Table 3-1. The results also show that, if the CH_4 decreases in the downstream area, this was possibly caused by its reaction and distribution through the reactor.

The gas production behaviour, as explained earlier, describes the thermochemical process of chemical reaction mechanisms as defined for coal gasification. It was developed to clarify the process behaviour in UCG. Generally, this behaviour agrees with the UCG mechanism as described in reference [5]. The simulation results have clarified the gas production in each stage and correlation among the species in the reaction has also identified. However, it occurred in the reverse direction to the UCG gas flow, since the model uses the flowing coal and quiescent gas or air inside the reactor. Nevertheless, all the oxidation and reduction zones of reactions in UCG are now understood and the gas production has been seen clearly in the simulation performance.

5.6 Conclusion

A simulation model of coal particle gasification has been carried out to investigate the gasification reactions and simplify the understanding of complex thermochemical reaction mechanisms. The aim of the development is for UCG application and at this time the focus is on the reaction's behaviour. The simulation has delivered greater understanding of the complex reactions in UCG as shown in the results. This understanding is important in obtaining better syngas production and will be used further to develop a more robust method of modelling.

The coal particle model can be applied to support the investigation of thermochemical behaviour of each species in the gasification reactions. As a result, the behaviour of char reaction, gas reaction, and syngas production in the gasification process can be seen. The single coal particle simulation results show that the syngas production stops after the char burns out, and this indicates the important role of char in the gasification reactions.

The simulation results also showed the importance of controlling oxygen to obtain better syngas production. In the case of single coal particle simulation, the excess oxygen

appears along the reaction and the fuel equivalence ratio used is very small (~ 0.0000041). The increase in coal mass injection into the reactor provided the increase in the fuel equivalent ratio, and showed some expected gas products of gasification. The performance of simulation also made it clearer for the investigation of coal gasification.

The thermochemical process of coal gasification can be described through the coal particle model simulation. The performance of the simulation has identified the oxidation and reduction process that occurred in the UCG zone. Control plot results illustrated the behaviour through the magnitude level of the species. Investigation of performing the gasification simulation under various gases has given clues for better operational conditions for better gasification process.

The UCG reaction mechanisms based on the references have been used to present the thermochemical behaviour of UCG throughout the simulation model. This is an initial development to correlate the gas production and coal mass consumption in the UCG application. Some studies on UCG modelling are concerned with the gas production [54] or cavity formation as an effect of coal's porous nature [80]. This study makes a distinction between both effects; they are reactions and coal mass loss that cause the cavity formation. In the modelling, this can be presented as a particle bed packed model study with reaction mechanisms. Therefore, a further study will consider the development of accumulated particles in a packed bed inside the reaction to perform these gasification reactions. An illustration for further study can be seen in Figure 5- 39

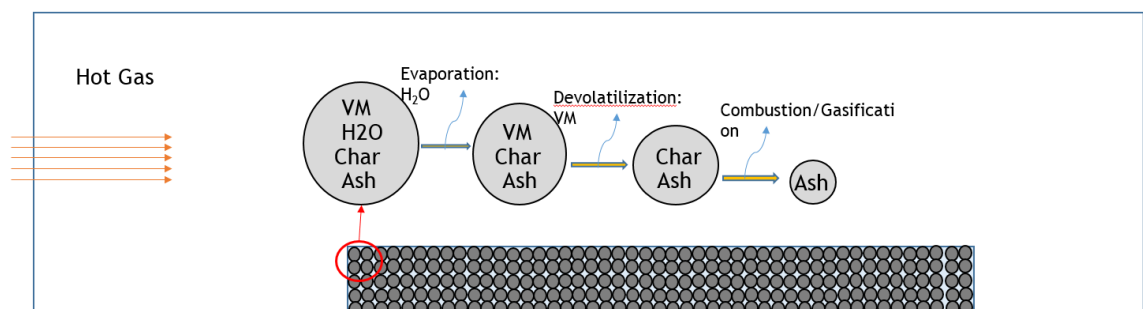


Figure 5- 39. Coal particle block/bed packed inside the reactor

Overall, these simulation results offer a good guideline for obtaining better quality syngas production, and initiate a new model approach for controlling the seam coal reaction mechanisms as a part of UCG modelling development.

Chapter 6 Experimental investigation of thermochemical processes of coal particle packed bed

6.1. Introduction

An initial development of a coal particle gasification model has been performed and its results investigated. It has clarified the thermochemical behaviour of gasification reaction mechanisms and can be considered as an assessment tool to obtain better gas products from gasification. Further development of a study on coal particle gasification for UCG application can be implemented through the particle packed bed reactions' development. A number of coal particles packed and collected into a bed to form a coal block are then set up for a reaction process to investigate the coal block gasification behaviour. The reactions can be performed either through experimental or computational simulation. This chapter initiates the study of coal particle block reactions in a packed bed, through experimental study. This way is preferable because the initial model needs to be confirmed experimentally, although the confirmation will not be a direct quantitative comparison. Strong agreement of behaviour obtained between the results of model simulation and experimental development would be sufficient information obtained from the initial study.

6.2 Experimental set-up

An experiment was set up to perform the reactions of a coal particle packed bed inside an optically accessible reactor. In the numerical modelling, the coal particles flow in a quiescent hot gas, and in the experiment, they were set packed in a static bed inside the reactor. The hot gas flows through the bed, and the coal reaction's process was investigated. The reaction behaviour was investigated by measuring the gas products and bed temperatures. The schematic process of the experiment can be seen in Figure 6-1.

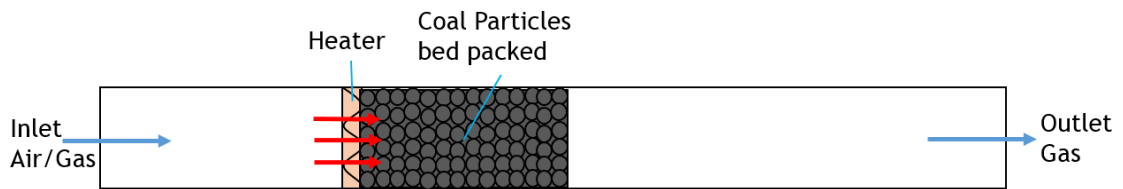


Figure 6-1. Illustration of coal particle bed packed in a reactor.

Figure 6-1 shows the heated gas flowing through the coal particles packed in a bed (as a coal block), and the products of the reactions obtained can be observed. It was necessary to set up the experiment with equipment and instrumental control to achieve the aim of the test. Therefore, the installation of equipment to accommodate the experimental performance needs to be prepared.

6.2.1 Equipment and instrumentations

The equipment consists of a rig as a main reactor and equipped with some instruments to control and observe the process of coal particle reactions inside the reactor. The schematic process of the installation for the experimental setup can be seen in Figure 6-2.

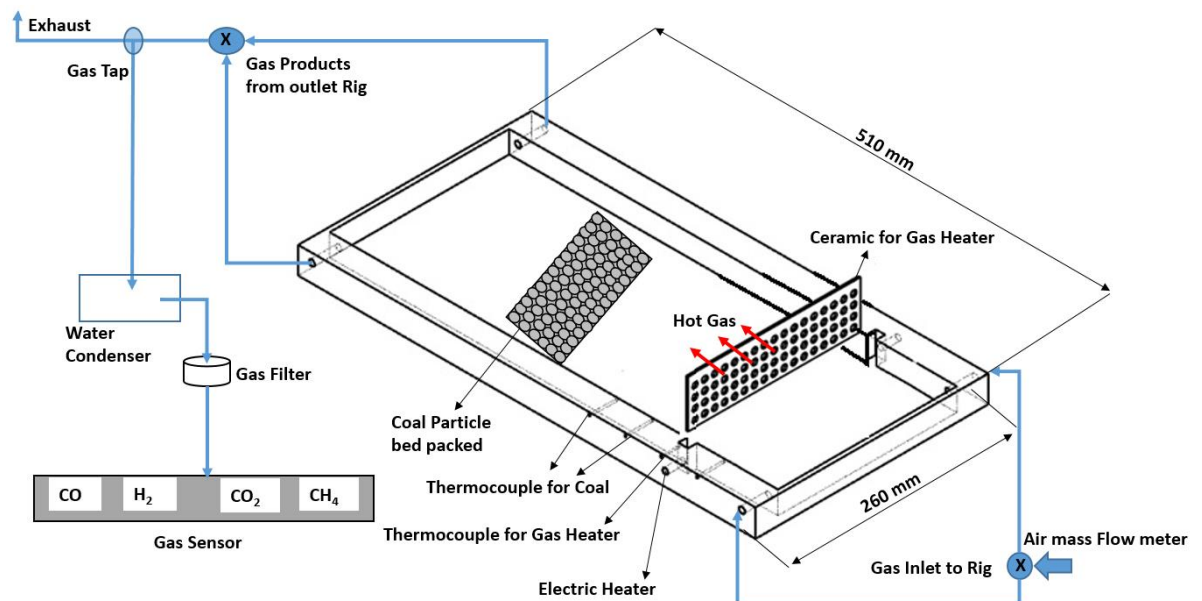


Figure 6-2. Schematic diagram for experiments

The rig as a main reactor was made from a mild steel or low carbon material to provide formability properties in the machining process but still resists a high temperature. The inner dimension of the reactor was $500 \times 200 \times 25 \text{ mm}^3$ (length x width x height). The optical access made from quartz glass was provided to observe the coal bed reactions. Air

was supplied through two inlet accesses and another two outlets provided for gas products flow out the reactor. The schematic design of the rig or main reactor can be seen in Figure 6-3.

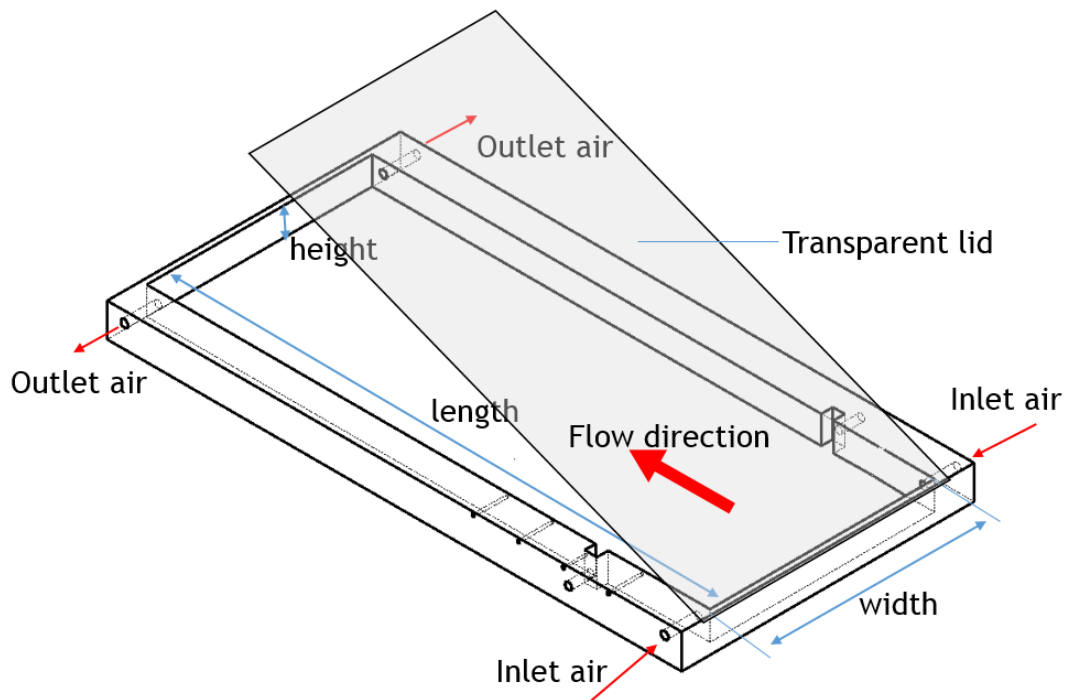


Figure 6-3. Rig as a main reactor with access of air flow

Air was injected into the reactor and controlled with a gas flowmeter with a range of 0 – 20 slpm. The unit measured was in a standard condition of gas (1atm and 25°C). The valve of the air flowrate control was set as a single direction valve to avoid the back pressure because of the temperature differences. Detail specification and its picture provided in Appendix A.

An electric heater was provided with a wire heater and twisted in the ceramic material with pores. The pores passed and contacted by air flow, therefore the air temperature increases. The wire has a resistance of $\sim 3.90 \text{ hm/m}$ with a length approximately of one metre and supplied with DC current $\sim 7.5\text{A}$. The experiment was performed with two electric wire-heaters in order to heat air temperatures up to $\sim 400^\circ\text{C}$, at which point ignition of coal particles takes place. There were another three ceramics pores without heater, and used as a boundary between the ceramics with heaters. Therefore, in total five ceramics with pores used in this experiments. The schematic of a single ceramic pores with heater attached can be seen in Figure 6-4.

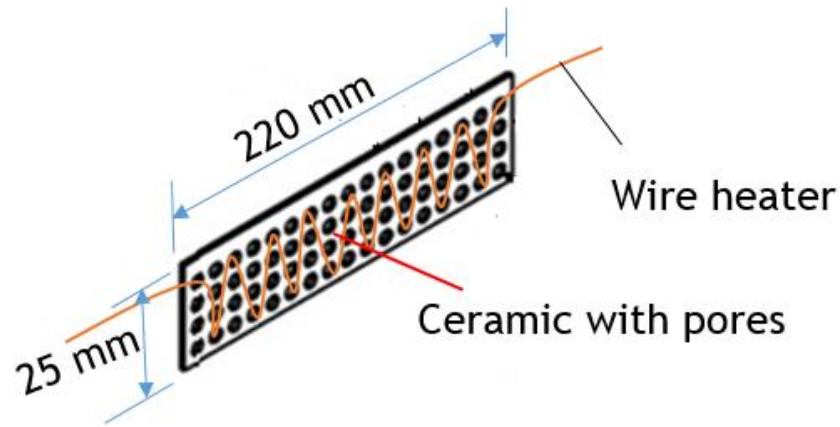


Figure 6-4. Ceramic with pores and heater wire

The packed bed of coal particles lies after the ceramic with heater, toward to the rig downstream. In schematic figure, the coal bed is at the area of thermocouples as seen in Figure 6-5. The detail information of ceramic and heater, with also the spot area of coal bed in the reactor also provided in Appendix A.

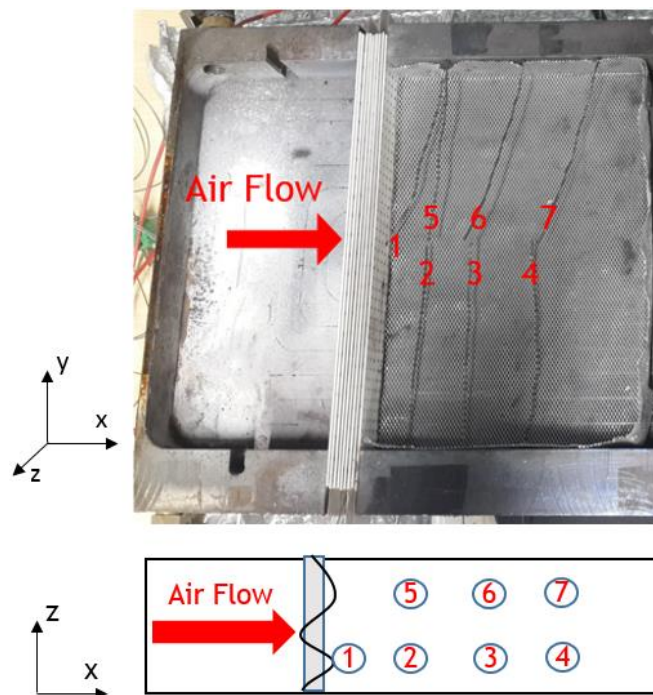


Figure 6-5. Thermocouple position in the coal bed area from top and side view

Thermocouple used as an instrument to observe the coal reactions process. Seven channels of thermocouple type K were placed in the coal bed area to record the temperature propagation of the packed particles. Channel 1 was used to measure the heated air at the inlet of the reactor or the coal packed bed. Channels 2, 3 and 4 were used to measure the lower side of the coal bed, and channels 5, 6, and 7 to measure the upper

side of the coal bed area. The thermocouple position in the centre bed reactor is as seen in Figure 6-5. The coal reactions were identified with the heat propagation over the time. Therefore, the sensor was put along the bed to record and obtain the temperature profile for further investigation. The heat propagation was expected to be in line with the gas flow. It started at the coal near to the heater, identified with channel 1 and then continues to channels 2 and 5 and so on. All data of temperature measurements were logged through the thermocouple hub and recorded in the computer's memory.

In order to measure the gas products of the gasification reactions, the equipment was set up to use four gas sensors as seen in Figure 6-2. However, because of the sensor availability and the fact that the focus of the current investigation was on the char performance, the test was applied to measure the gas products consisting of char and carbon reactions; CO₂, CO, and CH₄. To identify the availability of the excess air of reactions, an O₂ sensor was used. The specification of the gas sensors used in the experiment can be seen in Table 6-1.

Table 6-1. Gas sensor specification

Parameter	Range of measurements (%)	Manufacturer
CO ₂	0 – 100	Edinburgh Instruments
CO	0 – 100	Edinburgh Instruments
CH ₄	0 – 30	Edinburgh Instruments
O ₂	0 - 25	Anton Instrument

The sensor measures the gas products' concentration and the information was logged into the computer's memory. In order to prevent the sensor contact with water, because it produced in the charcoal reactions, the water trap was provided. It was consisted of the glass container with the ice bath, and they work as a condenser system.

The picture of equipment setup on the experimental desk can be seen in Figure 6-6. However, the specifications and more detail pictures of each equipment and instrument for this setup are provided in Appendix A. Meanwhile, the certificate of calibration and analysis of laboratory are also provided in Appendix B.

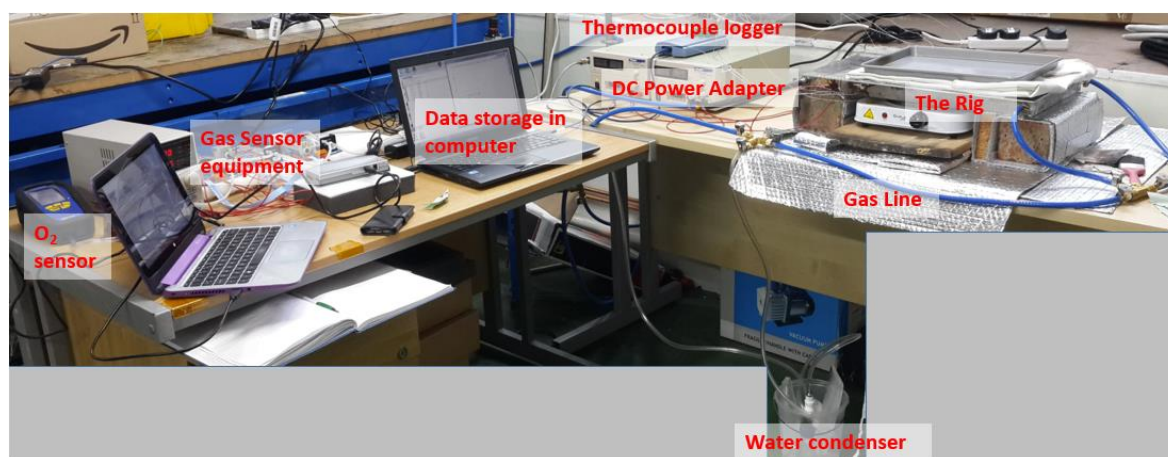


Figure 6-6. Equipment installation for coal particle experiment

6.2.2. Coal particle properties and preparation

The fuel sample used in the experiments was a charcoal, which dominated by carbon element. Coal volatile matter was not considered in this experiment, because the focus was on char reactions as the model simulation showed its important effect on gasification reactions.

Table 6-2. The chemical and physical properties of charcoal

Chemical Composition for Coal A, B, and C			
Elements	unit	Composition	
		Test 1	Test 2
Carbon	%	66.21	65.95
Hydrogen	%	3	2.89
Nitrogen	%	1.04	0.98
Oxygen, (by difference)	%	29.75	30.18
Physical properties (coal size)			
Coal ID	unit	screen size	status
Coal A	mm ²	1 x 1	passed
Coal B	mm ²	1 x 1	not passed
		2 x 2	passed
Coal C	mm ²	2 x 2	not passed
		4 x 4	passed

For investigation purposes, the charcoal particle is classified into three different sizes based on the screening dimension, and they are named as Coal A, B, and C. The ID of A, B, and C have been identified for the coal particles that could pass the screening with a size of 1 x 1 mm²; 2 x 2 mm²; and 4 x 4 mm², respectively. The detail information of chemical and physical properties of the charcoal can be seen in Table 6-2. This table shows the chemical composition measurement through micro analysis equipment test,

and conducted with repetition. As seen in this table that the results of laboratory analysis of test 1 and 2 have no significant difference. Meanwhile, the physical property of charcoal sample for each size as described in Table 6-2, visually can be seen in Figure 6-7.



Figure 6-7. The char coal in three different sizes

Figure 6-7 shows that, from coals A to C, the particle size increases but their chemical properties were similar. In the experiment, the amount of mass used was 120 grams for each test and it fully covers the bed volume up to thermocouple 3 and 6. Sensor temperature number 4 and 7 were not fully covered with the coal particles and therefore they can be used to measure the temperature of gas outlet or additional heater.

6.3 Experimental procedures

The data collection of the experiment was conducted after thermal equilibrium in the reactor was reached. Therefore, initially, the hot air flow to heat up the reactor until the coal ignition temperature was achieved and the distribution became steady. Then the packed bed coal particles fed into the reactor for the process reactions. These reactions occurred and were identified by rapid increments in the sensor temperature initiated by Sensor no 1. The temperature changes in the sensor spot and gas products' concentration level were recorded. A picture of flame front propagation or ash formation can be captured through the optical access in sequences of time. However, almost during the test, the transparent lid was covered with an isolator (fire blanket) to minimise the heat loss through the lid.

To achieve its purpose, the experimental procedures should be developed. There are two parameters which were studied in the simulation model; the effects of particle sizes and

temperature variations. And, another test was to investigate the effect of air flowrate on the coal bed packed reactions. Each test has a slightly different procedure, and they were described in the section below.

6.3.1 Test procedures to investigate the effect of particle size variation

In the case of particle size variation, each coal, named A, B, and C, was packed and put on the bed of reactor. The experiment was performed in conditions without an additional heater and with the bottom of the reactor well insulated. Schematic process of the test can be seen in Figure 6-8.

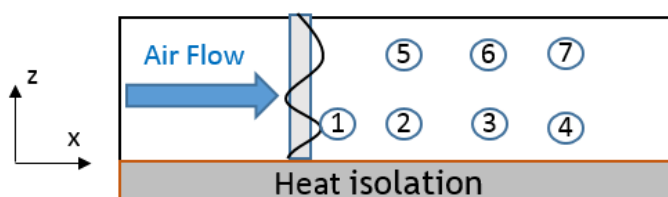


Figure 6-8. Schematic process for particle size variation test from the side view

Each coal was packed into a bed inside the reactor, and seven thermocouples arranged as in Figure 6-8 in the middle of bed. The performance was identified through the pattern of temperature profiles and the pictures captured at sometimes during the test. The information collected from gas products was also needed to clarify the reactions' behaviour. The results obtained from the experiments will be elaborated with the results from the simulation model (effects of particle diameter in section 5.3.1). This experiment was performed for each coal and with the same boundary conditions. The boundary condition of the test performance can be seen in Table 6-3

Table 6-3. Boundary condition of test with particle size variation

Parameter	Coal variation		
	Coal A	Coal B	Coal C
Coal ID /size (mm ²)	x	x	x
Initial air temperature, T1 (°C)	400		
Air Flowrate variation (slpm)	2 - 3.5		
Time of test performance (s)	10000		
External heater	No available		

X: the test conducted

6.3.2 Test procedures to investigate the effect of temperature variation

The second performance of the experiment was to investigate the effects of temperature variation. To perform the test, an additional heater was supplied at the rear part of the coal packed bed area and this could be adjusted to control the temperature level. The schematic process of the test can be seen in Figure 6-9.

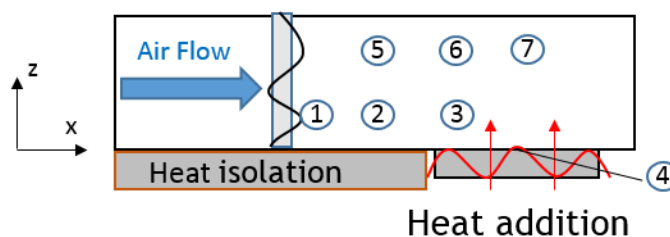


Figure 6-9. Schematic process for temperature variation test from side view

The heater was controlled for several temperature conditions, and they were heater off at 135°C, 200°C, 275°C and 350°C. These tests were performed with coal C, and an additional performances were used to confirm the behaviour with coal A and B. Figure 6-9 shows the additional heater position and channel 4 was used to monitor the temperature level of the heater (outside reactor). The test was performed at an air flowrate of 2 slpm, with the variation of temperature level indicated in channel 4. In a summary, the boundary condition of each test performance for temperature variation can be seen in Table 6-4.

Table 6-4. Boundary conditions of test with temperature variation

Parameter	Temperature variations (°C)				
	Heater off	135	200	275	350
Coal A (with external heater)	x		x		x
Coal B (with external heater)	x		x	x	x
Coal C (with external heater)	x	x	x	x	x
Initial air temperature, T1 (°C)	400				
Air flowrate (slpm)	2				
Time of test performance (s)	4000				

X: the test conducted

6.3.3 Test procedures to investigate the effect of air flowrate variation

Another test was performed in the experiments, even though it was not used in the simulation model. It was the investigation of the effect of air flowrate variation on the

reaction's performance. A particle packed bed of coal C was prepared for the test, and set up with a block of coal in the reactor bed to perform the reaction. The schematic process of experiment set up was similar with the temperature variations tests, as shown in Figure 6-9. The temperature of external heater (channel four) set constant at 350°C, and the test was performed for 4000s. In summary, the boundary conditions of each test performance can be seen in Table 6-5.

Table 6-5. Boundary conditions of test with flowrate variation

Parameter	Air flowrate variation (slpm)			
	1.5	2	3	4
Coal C	x	x	x	x
Initial air temperature, T1 (°C)	400			
Time of test performance (s)	4000			
External heater (°C)	350			

X: the test conducted

The four tests were carried out and pictures were taken in order to identify the reaction front propagation. The gas sensors were used to identify the process of reactions through the gas products. After around 60minutes, the picture and gas product measurements of each test were compared in order to identify the behaviour.

6.4 Results and discussion

6.4.1 Investigation of the effect of particle size variation

The temperature distribution in the coal bed for the reactions of coals A, B, and C can be seen in Figure 6-10. This shows the pattern of temperature profile recorded by seven thermocouples. The maximum temperature reached by each coal bed was 624°C, 582°C, and 569°C, for A, B, and C respectively. For this parameter, coal A had the highest bed temperature, while the lowest occurred with coal C. This indicates that the bed with smaller particles obtained the higher temperature. The different particle size in the coal bed caused the difference in porosity for each coal bed. The smaller particle forms less porosity than the bigger particle size. The less porosity causes the heat transfer to take place more through the particle (conduction) than the porous material (convection). With the property of the heat capacity higher than gas, the particle reserves more heat than the gas. As a result, the coal bed with less porosity has a higher temperature than the bed with higher porosity.

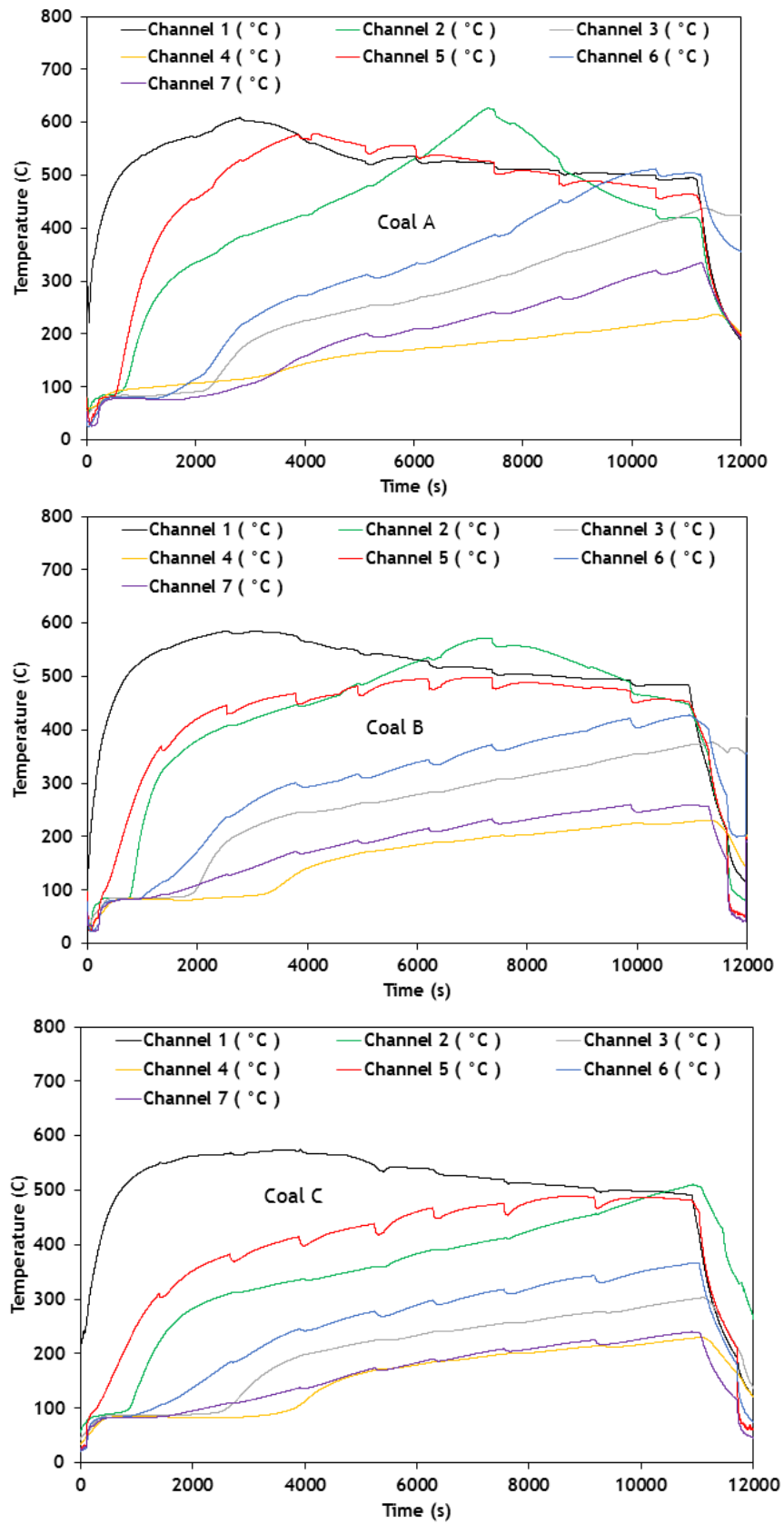


Figure 6-10. Temperature profile for each channel in bed of coals A, B and C

From Figure 6-10, it can also be seen that the temperature gradient (dT/dt) of the bed with smaller particle size was higher – as can be seen in each channel of temperature measurement. To achieve the maximum temperature at channels 1, 2 and 5, the bed with coal A was earlier than the bed with coals B and C; and the bed with coal B was earlier than the bed with coal C. Another indicator was the heat propagation rate, which can be identified by measuring the time interval of maximum temperature (peak temperature) between the two sensor temperature channels along the gas flow. One sample case was the time interval of heat propagation from channel 1 to 2, at each coal bed. Figure 6-10 shows that the time needed for the heat to propagate (reach peak temperature) from channel 1 to 2 was ~4600s, ~4700s, and 8300s, for coal A, B and C, respectively. This indicates that heat propagation was faster in the bed with a smaller size of coal particle. Thus, this clarifies that the porosity has an important role in heat propagation in the coal block.

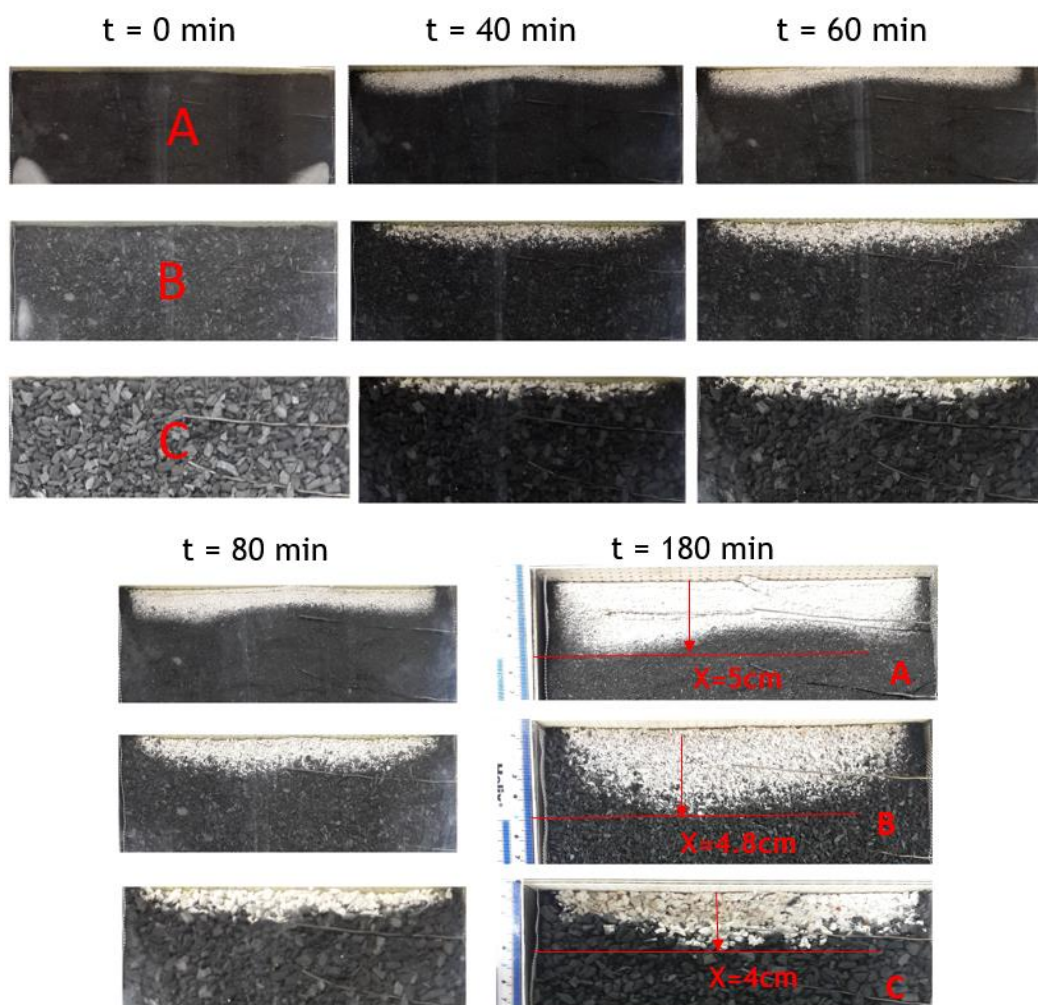


Figure 6-11. The reaction propagation over a certain time period for coals A, B, and C

Another method that can be used to investigate these reactions was with visual observation. The angle of picture taken was from the top of the reactor or particle bed. The pictures over several time frames of coals A, B and C can be seen in Figure 6-11. This figure shows that the reaction process started with the same condition at minute zero. Over this time, the reaction fronts propagate and were indicated by the ash formation (white colour). The ash gets wider over the time of reactions in line with the gas flow direction. The final length of ash formation was compared for each coal after 180 minutes. The results show that the distance was approximately 5cm, 4.5cm and 4cm for the bed with coal A, B, and C, respectively. This indicates that the smaller particle size has a longer distance from the inlet side of the coal bed. Therefore, the picture presented for observing the reactions' propagation was the surface area of the coal bed. This area has direct contact with the transparent lid and there was a gap between the coal bed surface and the lid. This notice was important in order to develop an understanding about the process observation of coal reactions.

Gas sensors were used to measure the gas products and this was important for the study of the gasification process. The gas measurement results of the test can be seen in Figure 6-12. This figure shows the results of gas CO_2 , CO and CH_4 for coals A, B, and C. The test was performed for approximately 10,000s (~180 minutes), and as seen in Figure 6-12(a) the air flowrate increased gradually to maintain the reactions as they occurred.

The measurement results in Figure 6-12(a) and (b) show that the trend in gas production of CO_2 and CO is similar. At the initial stage, they increase and then become stable, which indicates the stability of the reactions. However, the gap of gas CO products resulted as seen in the figure were quite significant, especially for coal A. Meanwhile, the gas CO_2 products still can be seen the level different, even though their different quite slightly.

Slightly different, the gas production of CH_4 as seen in Figure 6-12(c), shows that they initially increase and then decrease, after sometimes they finally dropped. This indicates an unstable supply of element to support of CH_4 formation. The obtained results had a similar trend with the conditions of CH_4 formation in the case of a single particle model. However, Figure 6-12 shows that the gas products (CO_2 , CO and CH_4) obtained were higher with the bigger size of coal particle. These results need to be clarified to develop a strong understanding with the results shown in Figure 6-10 and Figure 6-11. It is provided after all measurement data observed.

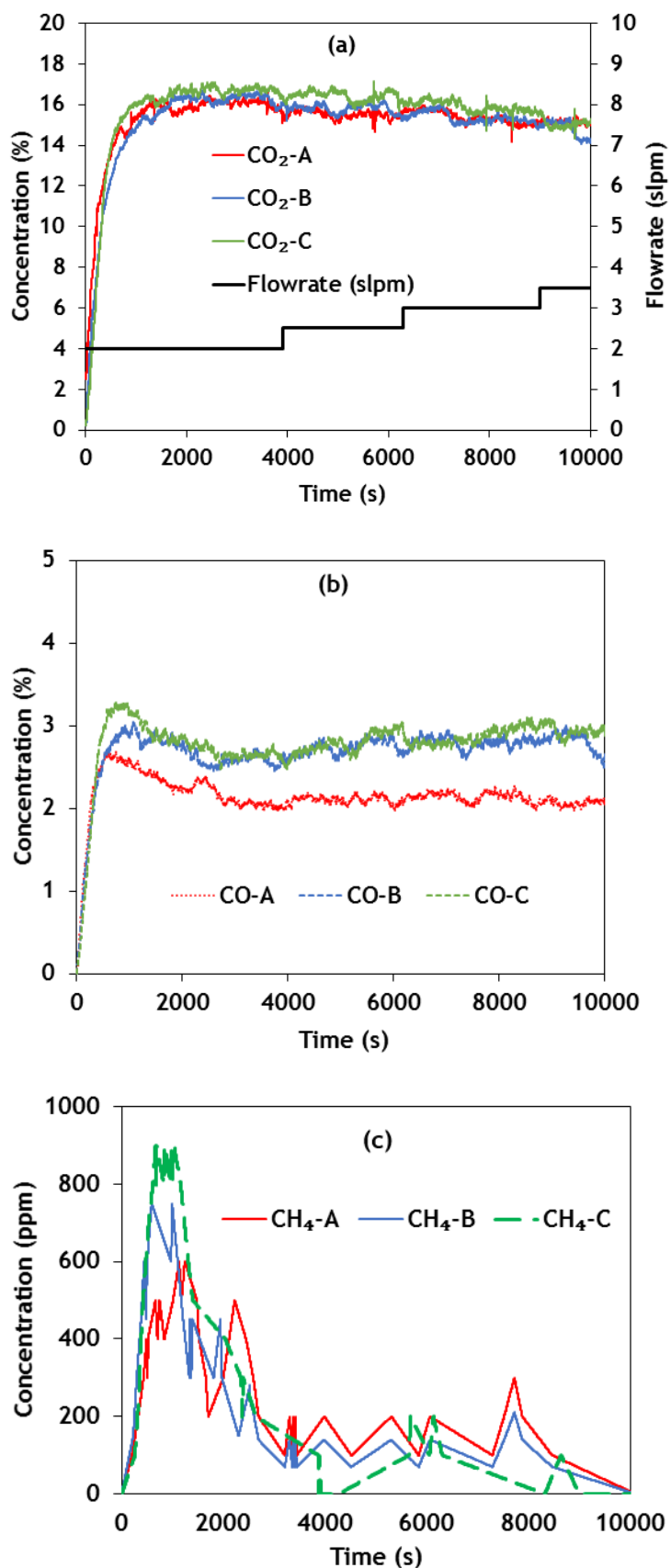


Figure 6-12. Gas products of coal bed reactions for (a) CO₂, (b) CO, and (c) CH₄

Another parameter of measurement needs to be observed to find the correlation between the result of temperature and gas products. The parameter was excess oxygen and measured with the oxygen sensor. The results of oxygen in the excess air for each test can be seen in Figure 6-13.

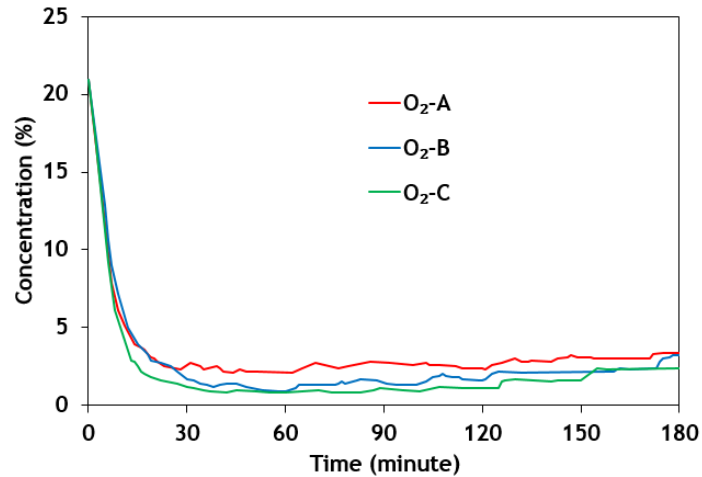


Figure 6-13. Excess oxygen in gas products

Figure 6-13 shows that the result of the excess oxygen measurement was slightly different for each test. The bed reactions with smaller coal size have more excess oxygen. This indicates that less oxygen reacts with charcoal, and therefore fewer products of CO₂ and CO occurred in that case.

The smaller reaction of char coal and oxygen was caused by less porosity. In the coal packed bed, the air flows through the porous material and reacts with the coal surface to produce these gas products. The bigger particle size provides more porosity, and therefore there was more space available for char and oxygen to react. This confirms the results obtained in Figure 6-12, and confirms that the coal packed bed with bigger porosity produces more gas products.

This looks slightly contradictory to the results explained in Figure 6-11 and Figure 6-12 about the effects of particle size on the reaction rate. It needs to be noted that the main factor causing the reaction propagation is the interaction between the coal and air. Ideally, the more space provided, the more air potentially reacts with coal. In the case taken from Figure 6-11, the smaller particles exist on the surface of the coal bed and there was a gap between the bed and the transparent lid. This gap possibly provides more air on the

surface, and therefore the heat propagation was faster in the smaller coal particle on this case.

6.4.2 Investigation of the effect of temperature variation

An investigation of the effect of temperature on the coal particle reactions was performed in the modelling and now the study continues through the experimental test. The aim, at this moment, is to identify the reaction behaviour by developing an understandable correlation between the modelling and the experiment.

The test performance was initiated for coal C, and the pictures taken during the test are shown in Figure 6-14.

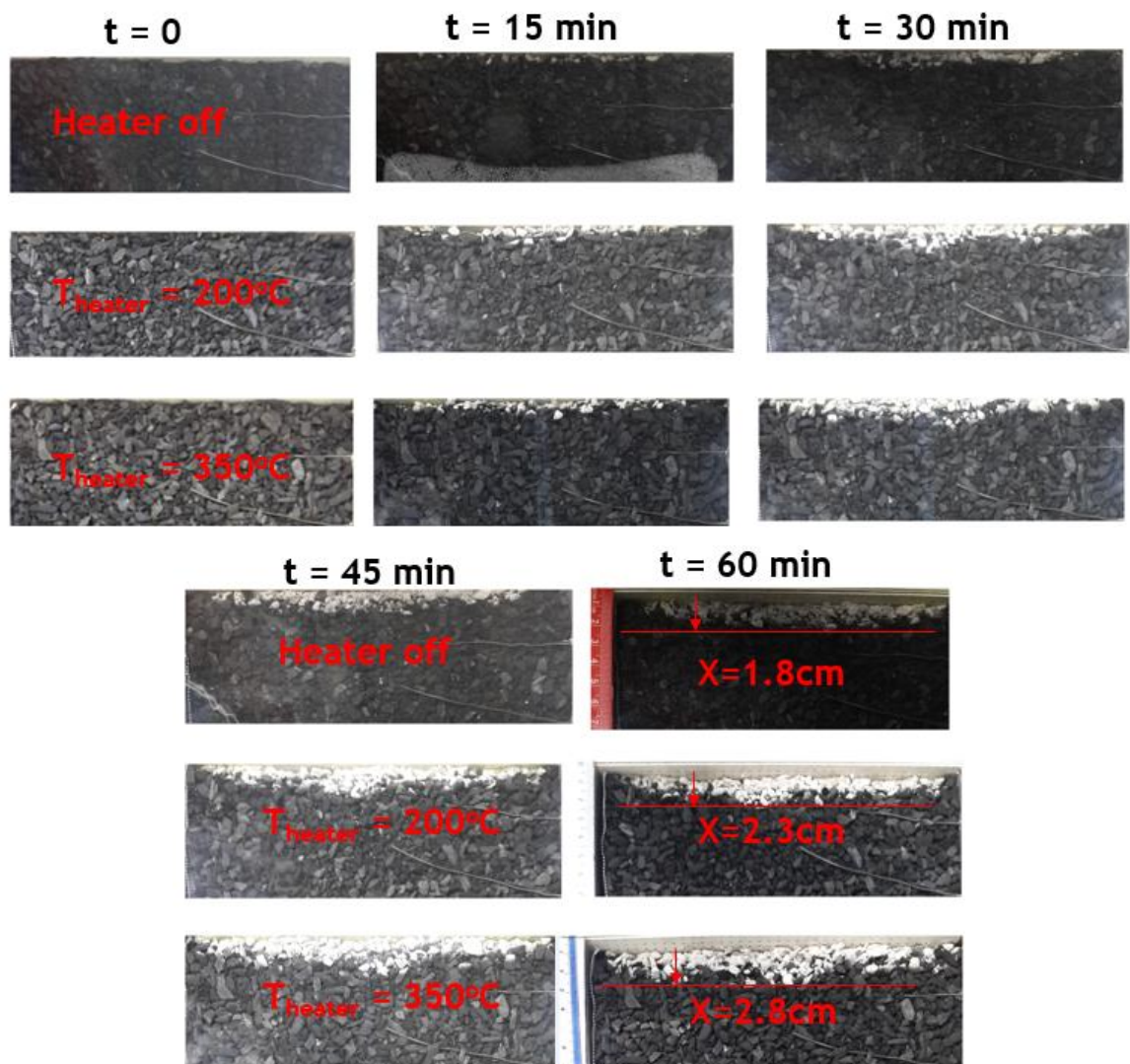


Figure 6-14. Reaction propagation of surface coal packed bed for coal C

Figure 6-14 shows the reaction front propagation identified with the ash products, and these were taken at three different temperatures; they were at heater off, at heater temperature set off, 200°C and 350°C. The test was conducted for 4000s or about 60minutes and a picture was taken every 15 minutes. The initial results were shown at minute zero and, over time, the length of ash formed by the reaction got longer. After 60 minutes, the distance between the inlet bed and the boundary of coal and ash was measured. The maximum distances obtained were 1.8cm, 2.3cm, and 2.8cm, for the condition of the heater at off, 200°C, and 350°C, respectively, as shown in the figure. The result indicates that a particle bed with a higher temperature has a longer distance of reaction propagation, or they propagate faster. It can be understood, because with the same boundary condition the charcoal at higher reactor temperature will achieve their ignition temperature faster. The ignited charcoal produces heat and transfer to another spot, therefore the propagation of reaction front occurred faster.

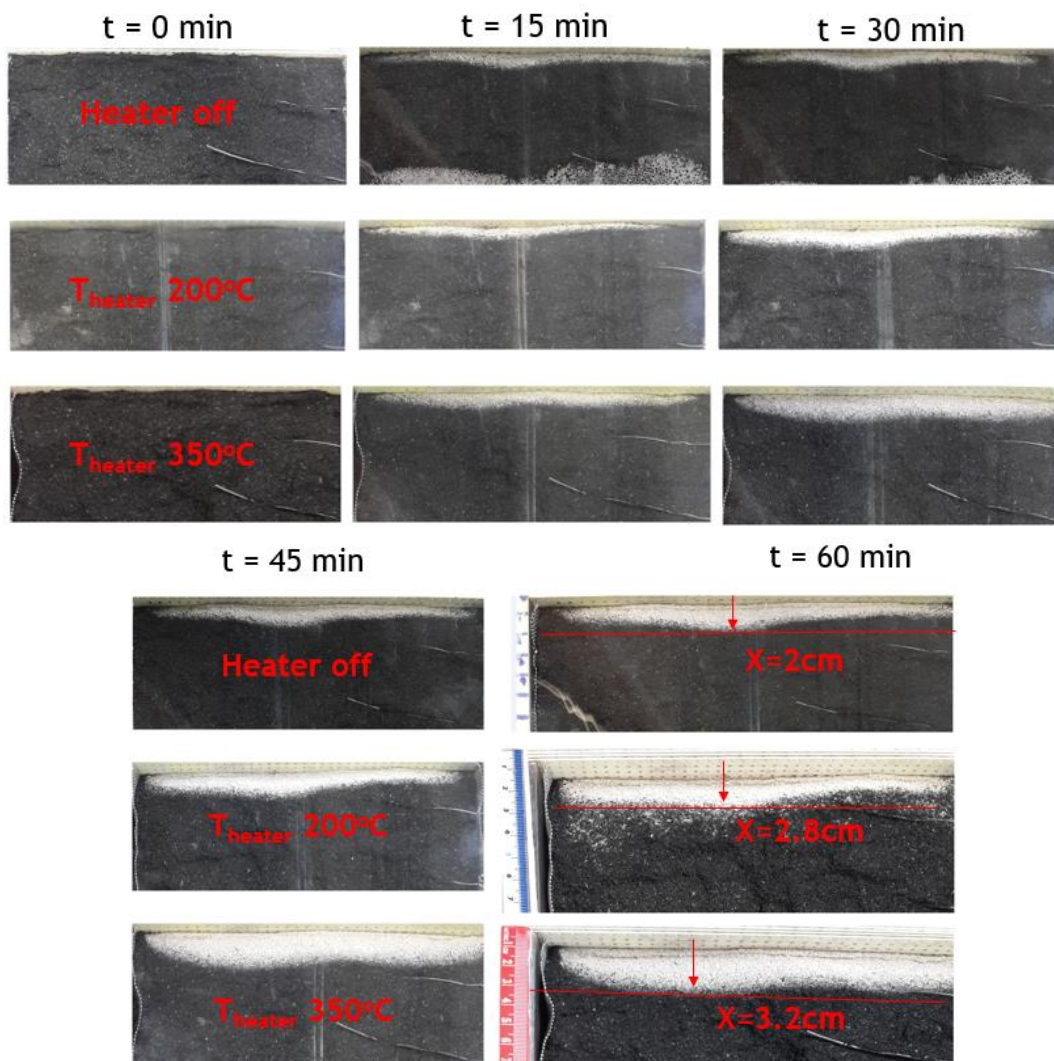


Figure 6-15. Reaction front propagation of surface coal packed bed for coal A

The repetition scheme was conducted on the bed with coal A and B to confirm the results obtained. The same procedures, and boundary conditions as in Table 6-4 were applied. The picture was captured on the test performance of coal A and B at several times in various temperatures, and these can be seen in Figure 6-15 and Figure 6-16, respectively.

Figure 6-15 shows the reaction front propagation presented with ash products on the bed with coal A. It has a similar trend to what happened with coal C. They were initiated at time zero and over time the length of ash formed by the reaction got longer. After 60 minutes, the distance between the inlet bed and the boundary of reaction front was measured. It showed that the maximum distances were 2cm, 2.8cm, and 3.2cm, for the temperature heater at off, 200°C, and 350°C, respectively.

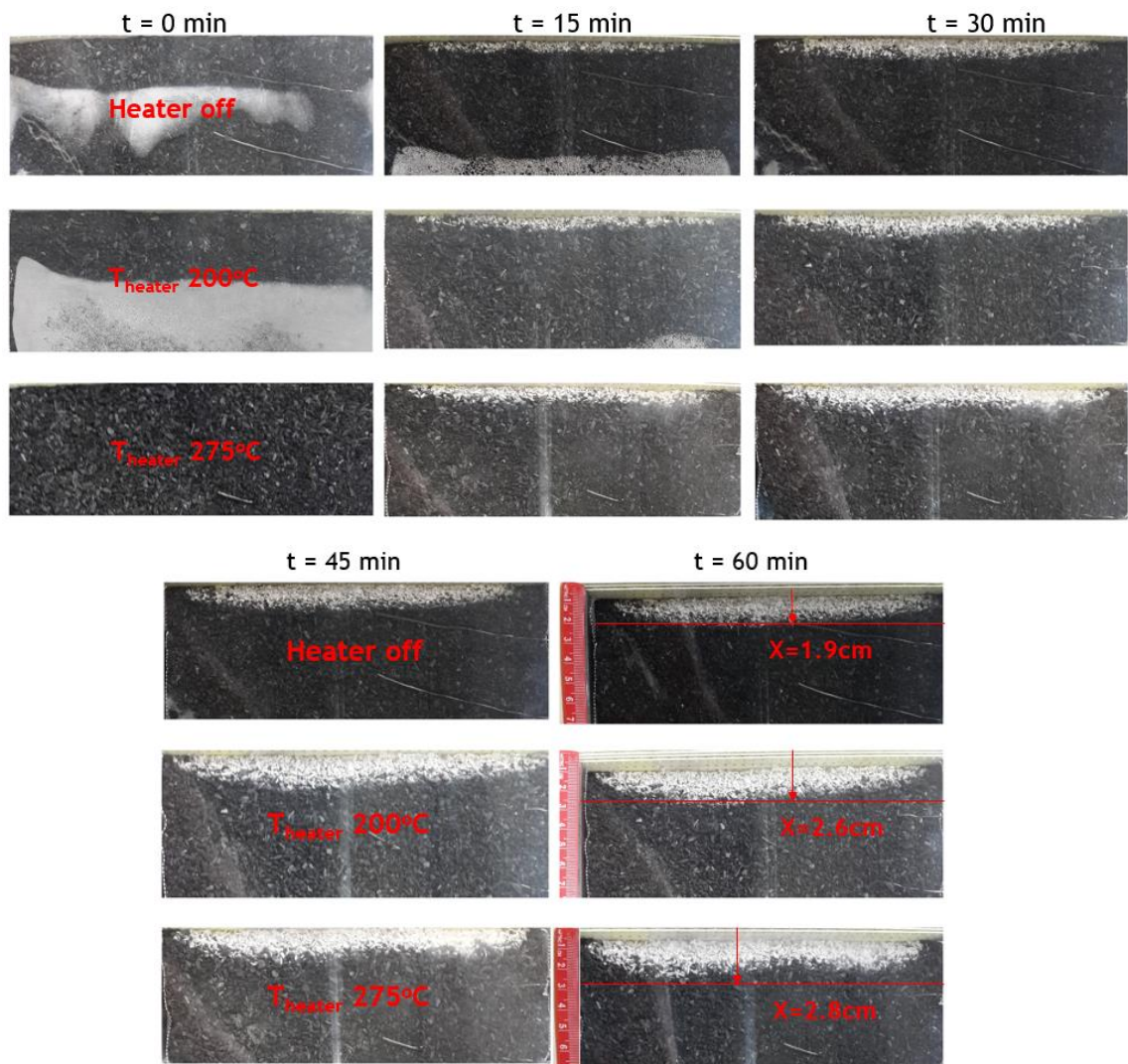


Figure 6-16. Reaction front propagation of surface coal packed bed for coal B

Meanwhile, Figure 6-16 shows the reaction front propagation on the bed with coal B. The test performed, and the bed reactor was captured every 15 minutes. After 60 minutes, it showed that the maximum distances were 1.9cm, 2.6cm, and 2.8cm, for the temperature of external heater at off, 200°C, and 275°C, respectively.

The test results obtained with coal A, B, and C have the same trend, which was on the parameter of reaction front propagation. The particle bed with the higher temperature has a longer distance of reaction front propagation. However, further observation can be conducted to identify the combination between coal particle size and temperature effect. At the same level of temperature heater set, for example at heater off, the length of reaction front propagation for coal A, B, and C, were 2cm, 1.9cm, and 1.8cm, respectively. And, when temperature heater set at 275°C, the length of reaction front for coal A, B, and C, were 2.8cm, 2.6cm, and 2.3cm, respectively. All results identify that coal A had a maximum length of reaction front propagation greater than the results of coal B and C, at the same level of temperature heater. And, coal B had greater of reaction front length than coal C. It again affirms of the effects coal particle size as described in section 6.4.1.

The coal reaction behaviour was also identified through the monitoring of gas products. The results of the measurement of gas CO₂, CO and CH₄ can be seen in Figure 6-17. This figure shows the gas products' measurement of coal C in the bed reactions at various heater temperatures. The test was performed at five different temperature levels in order to investigate the difference. For gas products of CO₂ and CO, they had a similar trend. Initially they increase then become stable at some point, while CH₄ had initially increased and then dropped. The gas CH₄ dropped possibly caused by the lack supply of hydrogen element, and its trend similar with the model simulation, section 5.2.2. However, all gas products indicated have more gas products at higher reactor temperatures.

More tests were conducted for coals A and B, but only at three temperature levels to confirm obtained results. The results for gas CO₂ and CO can be seen in Figure 6-18 and Figure 6-19 for coals A and B, respectively.

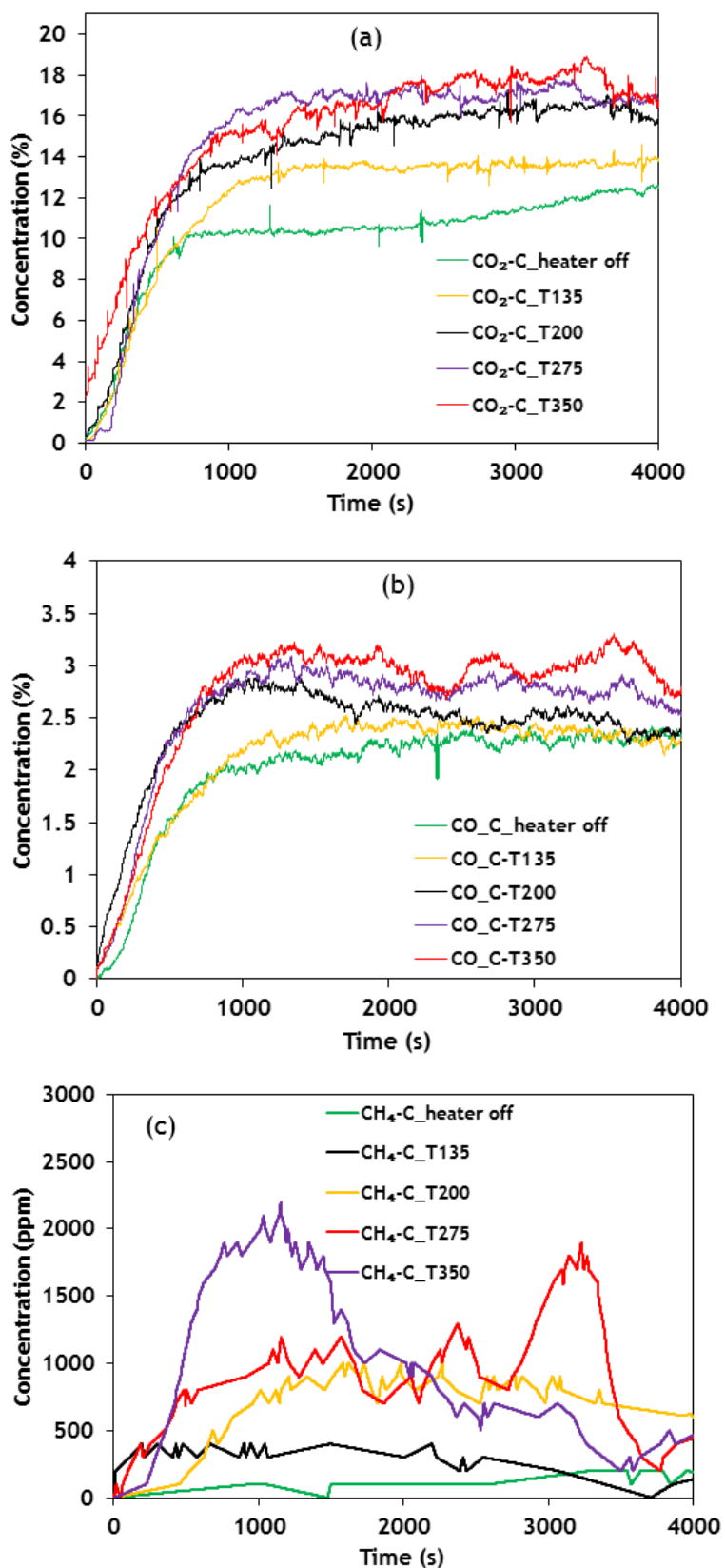


Figure 6-17. Gas products of coal C in various temperature (a) CO₂, (b) CO, and (d) CH₄.

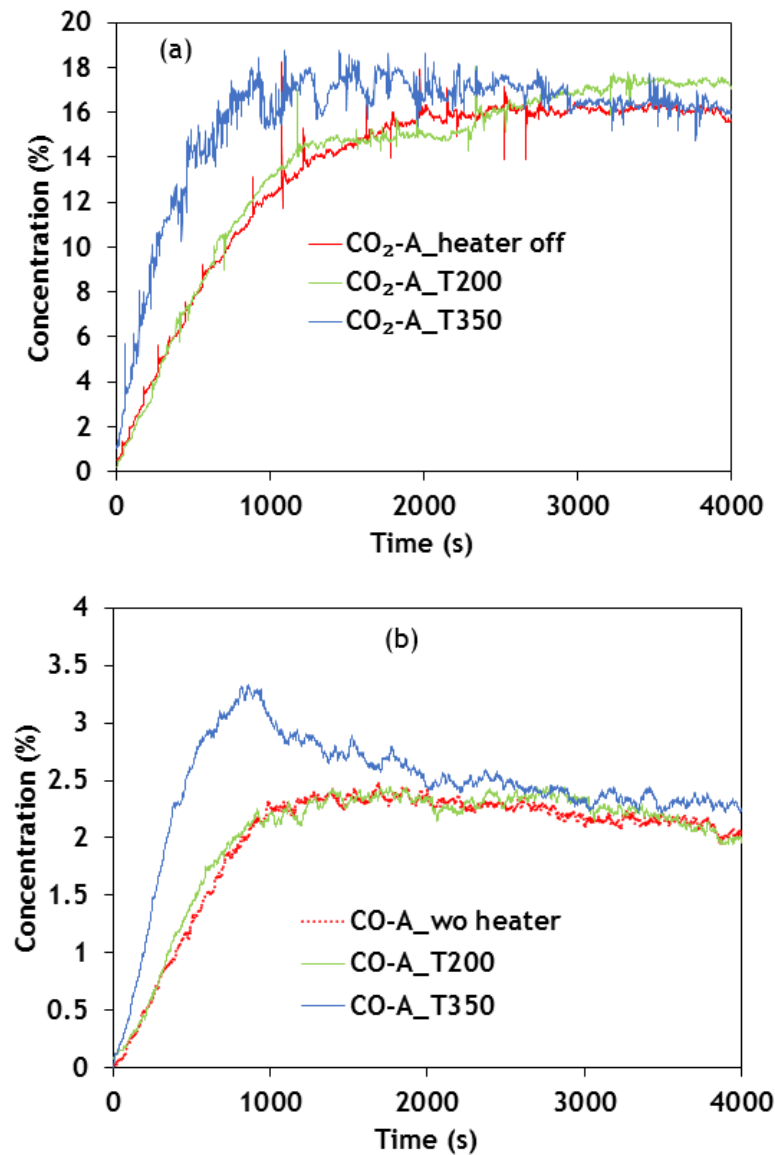


Figure 6-18. Gas products of coal A at various temperatures (a) CO₂, and (b) CO.

Figure 6-18 and Figure 6-19 show a similar trend, during which they initially increase and stabilise after a certain period of time. The gas products' level was higher for the coal reactions at a higher temperature. Again, these results confirm the behaviour that the higher temperature could affect the coal reaction for producing more gas products.

However, the results of gas production in the experiments show a similar trend to the modelling in section 5.3.2 simulation performance in various temperature. This was a good indication for an initial development of a coal particle model for gasification reactions.

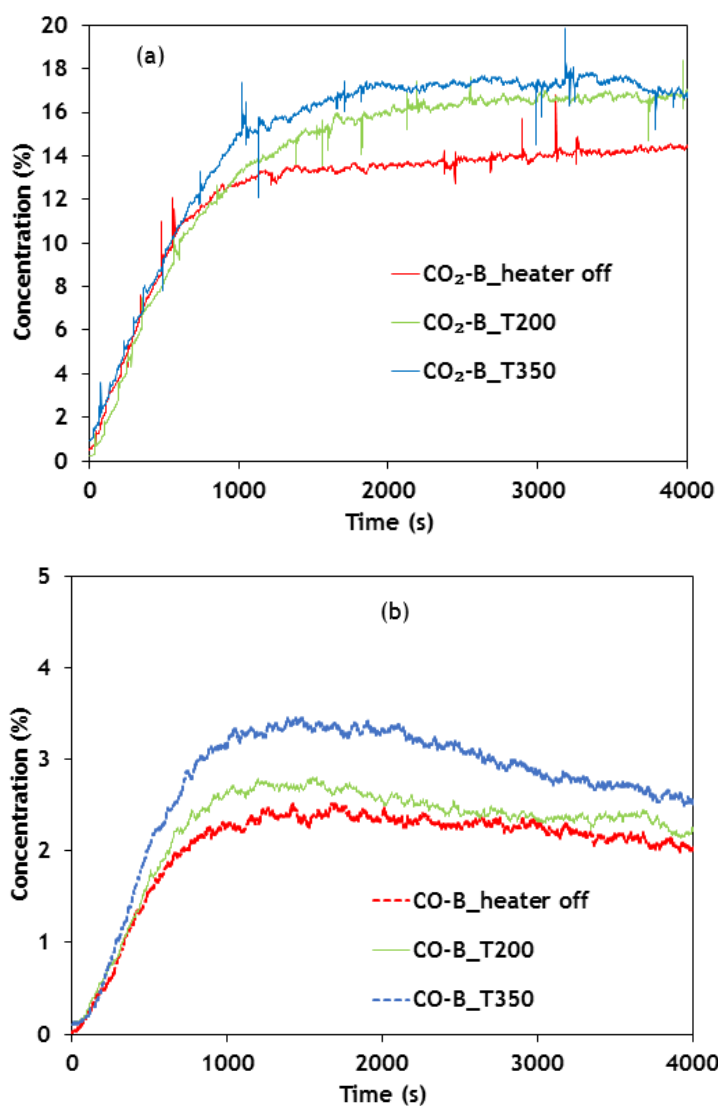


Figure 6-19. Gas products of coal B at various temperatures (a) CO₂, and (b) CO.

6.4.3 Investigation of the effect of air flowrate variation

A particle packed bed of coal C was prepared for the test, and it was set up with a block of coal in the reactor bed to perform the reaction. The schematic of experiment set up was shown in Figure 6-9. The temperature set at channel four constant at 350°C, and the test was performed for about 4000s. The detail of performance test scenario can be seen in Table 6-5.

After about 60minutes, the picture and gas product measurements of each test were compared in order to identify the behaviour. The results of the reaction front propagation were measured with the length of ash formation of each flowrate, and can be seen in Figure 6-20.

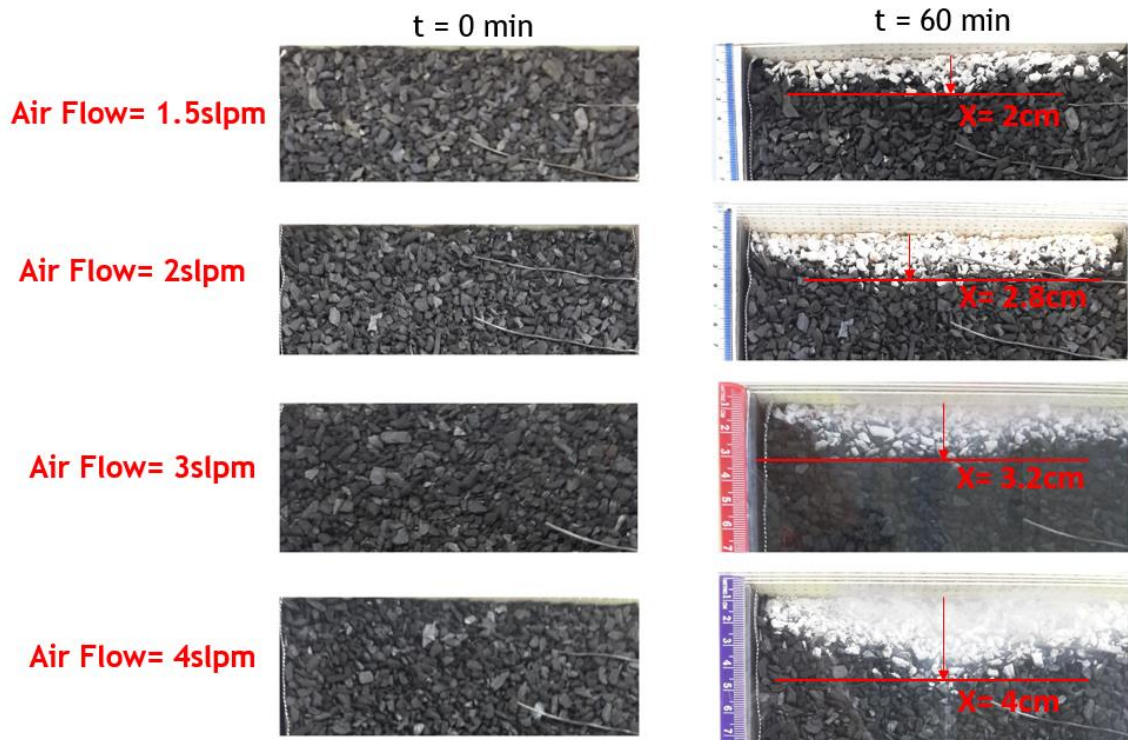


Figure 6-20. Reaction propagation of coal C in different air flowrates

Figure 6-20 shows the coal bed at its initial condition and after 60 minutes. There were differences of length reaction front shown with ash formation. The length of reaction front obtained for each flowrate variation was 2cm, 2.8cm, 3.2cm, and 4cm for test with a flowrate of 1.5slpm, 2slpm, 3slpm and 4slpm, respectively. This indicates that the greater flowrate provides a longer area on surface bed reactor.

Other information for the investigation comes from the gas products' measurements and the result of gas products' observation during the test, can be seen in Figure 6-21. The CO_2 and CO have similar trends of formation as seen in Figure 6-21(a) and (b), and they initially increase until they reach stability. Meanwhile, the CH_4 formation initially increases and goes down after some time, indicating the discontinuity of formation. However, this result indicates that the increment in air flowrate increases the gas products for each species. Nevertheless, in order to get greater understanding of the reaction behaviour, the excess oxygen can be identified. The excess oxygen measurement for each flowrate condition can be seen in Figure 6-22.

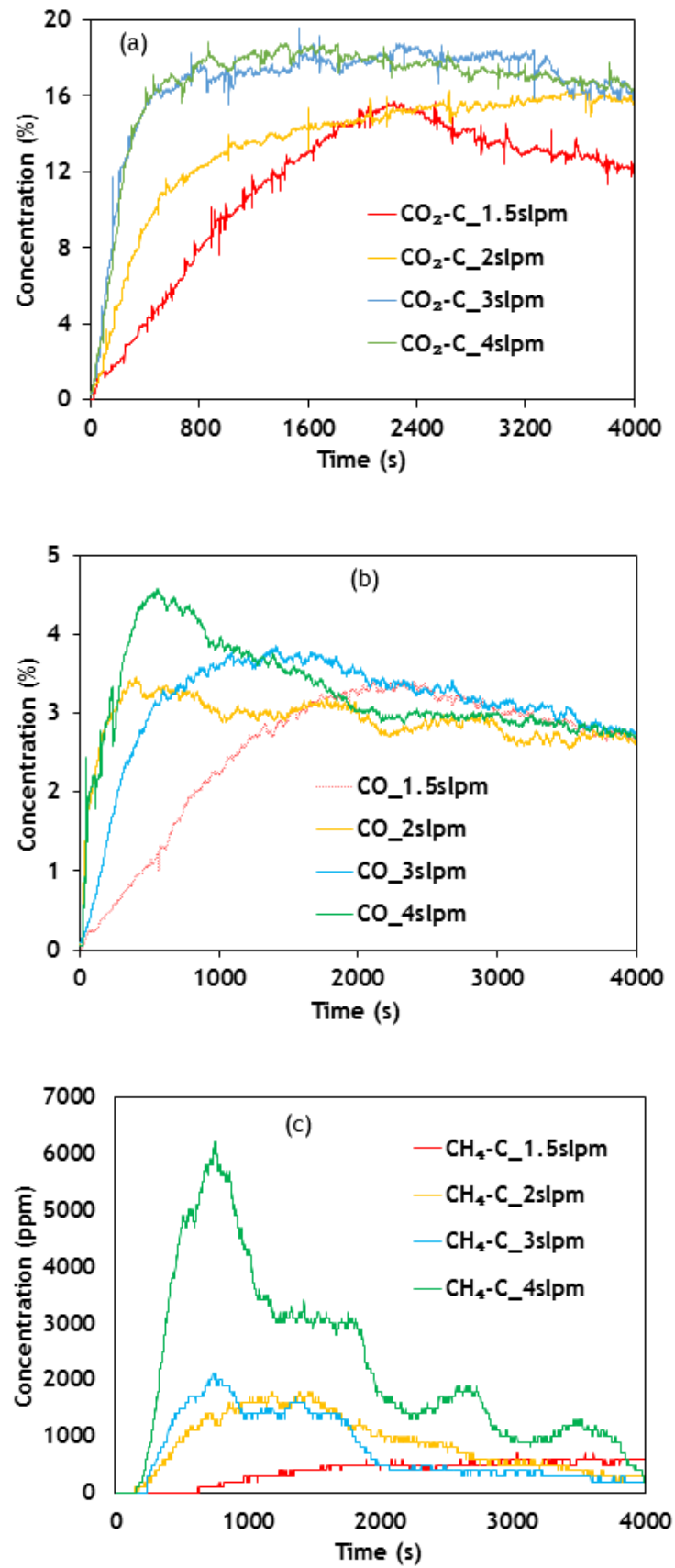


Figure 6-21. Gas products of coal C in various flowrates (a) CO₂, (b) CO, and (c) CH₄.

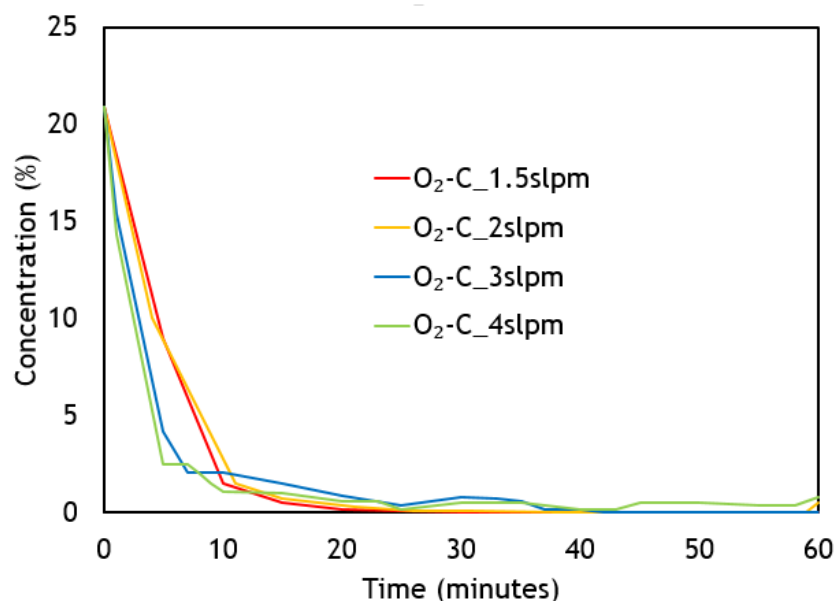


Figure 6-22. Excess oxygen concentration for each flowrate condition.

Figure 6-22 shows the excess oxygen during the test and the trend was similar for each flowrate case. The oxygen level drops because of the coal reactions. At conditions of air flowrate 1.5slpm, 2slpm, and 3slpm, they drop and reach a level of 0%, while at condition of air flowrate 4slpm the excess oxygen appears slightly above zero. This indicates that the greater flowrate potentially increases the excess oxygen of the coal bed reaction.

6.5 Possible results that relevant with UCG application

The experiment was developed with the aim of supporting the investigation of UCG through the coal particle gasification method approach. From the experiments, there were some results can be considered to develop an understanding in UCG application.

The coal's pore, or porosity, is a parameter that influences the reactions in UCG application. It was stated by *Wang et al.* [27] that the pores affect oxygen transport then participating in the chemical reactions during the oxidation process. The similar arguments also supported by *Campbell* [139] and *Merrick* [140], which stated the coal with more porous has a more permeable of a solid substance called char to be combusted and gasified by injected oxidant agents and exhausted gases from the previous steps. The pores itself can be formed during the drying and devolatilization process. At this stage, an inherent water and volatile matter content evolve their phase, and therefore the gasification agent replaces, flows through the pores. The behaviour caused by the effect

of porosity to the coal reactions can be observed through the experimental. The particle size variations identify the different of coal porosity. It was obtained that the excess oxygen at the bed reactions with coal A was higher than coal B and C (see Figure 6-13). It indicates that at the smaller porosity, the air and coal reactions occurred more at the channel surface. Meanwhile, the coal with greater pores could have more air reactions within the pores, and therefore their excess oxygen less. It also can be confirmed through the gas products (see Figure 6-12), which showed that the CO and CO₂ at coal B and C was higher than at coal A, because of they had more porosity.

Temperature and air injection pressure have an important role in the application of UCG. As stated by *Yang* [29], the drop of temperature causes the decrease of CO, and the increase of CO₂. This behaviour potentially occurred in the reduction zone of gasification reactions. Of all reactions in the reduction zone, mostly were endothermic reactions. Especially at *Boudouard* reaction that potential to convert the CO₂ into CO, as it preferable obtained in gasification process. Meanwhile, in the oxidation zone reactions, the increase of reactor temperature potentially increases both products, CO and CO₂. This result is shown in the experimental with temperature variations, which indicates the more gas products (CO and CO₂) obtained at higher temperature.

The role of air pressure explained by *Blinderman et al.*[21] was to meet the air with the coal stock during the reactions. In the channel of UCG, an air was injected and need sufficient pressure to provide continues reactions with coal stock sources. The better way on providing air to react with the coal stock, potentially provide better efficiency in the process of reactions and energy consumption, as described in Chapter 1 [8, 20]. The information obtained from the experiments of air flow variation can be correlated to describe the important role of air pressure. Insufficient air pressure could cause the discontinuity of reactions, as it shown in Figure 6-21(a) for parameter CO₂. The drop of CO₂ possible caused by the less sufficient of air pressure into the rig. It was affirmed by the decrease of gas CO as well. However, it shows on how important the injection air pressure for maintaining the reactions occurred continuously in UCG application.

6.6 Conclusion

The coal particle packed bed was provided in the reactor in order to perform the coal reactions. The further investigation was conducted to correlate the results of the model

simulation and the results of experiment study. No results were provided for direct comparison, but they can provide important information that suits the development of coal particle models for UCG application. The experiments obtained some key information on the process reactions;

The first relates to the identification of the effect of particle size on the reactions. In the condition of sufficient oxygen for the coal to have a reaction, the smaller coal particle size has a rate of reactions faster than the bigger size. However, when particles are packed to form a block, the role of porosity becomes very important. In a coal block, the appearance of porosity will help the oxygen to access the greater area of the coal surface to perform the reaction.

The second is with regards to the role of temperature for the coal reactions. The results of the experiment agree with the results from the simulation model that states that the higher temperature provides the greater number of gas products of the reaction. In the case of gasification, a high temperature is required to perform reactions and the experiment performance indicates less need for the temperature to support the reactions in the reduction zone. However, the current results have sufficiently informed the role and effect of temperature for the coal reactions.

The third is on the effects of the flowrate air injection on the coal reactions behaviour. In the simulation study, the expected cavity formation was caused by the coal mass shrinkage because of the reactions. The ash formation behaviour is part of the cavity formation because of the coal reactions. The experiment initiated a simple investigation on the effect of air flowrate on the coal reactions. The test results agree with a reference mentioned that a higher pressure injection was needed to provide air into coal stock downstream.

Further observation to identify the flowrate level that needed to maintain the coal reactions last for 60minutes can be seen in Figure 6-20. This figure showed that at air flowrate 1.5slpm, the length of reaction front was far below at air flowrate 2slpm. With defining the ratio of the increase of the reaction front length with the increase of air flowrate as (dx/dQ) , hence the ratio of the flowrate increase from 1.5slpm to 2slpm; and 2slpm to 3slpm were 1.6 and 0.4, respectively. It indicates that from the flowrate of

1.5slpm to 2slpm, the significant increment has occurred. Therefore, with 2 slpm air flowrate should be sufficient to provide coal bed reactions last for 60minutes.

Overall, the experiment results have performed, and further experimental set up needed to investigate deeper for UCG application.

Chapter 7 Final conclusions and recommendations for future work

The work presented in this thesis has investigated coal combustion and gasification behaviour using a coal particle model. This model was proposed because it can present the coal reaction mechanisms more properly compared with the existing model, and the further application of the model gasification is for UCG modelling. An experimental study of coal particle reactions was also conducted to support the investigation. In this case, the coal particles were collected and packed into a bed inside the reactor, and the reaction process was carefully observed. The findings of the study are summarised in section 7.1, with a recommendation for future work in section 7.2.

7.1 Conclusions

The coal combustion model was initially introduced to perform the reaction mechanisms and afterwards the gasification reactions were applied. The model was properly obtained and studied through simulation and coal combustion and gasification were the main results. They are presented as follows.

In Chapter 4, the study of coal particle combustion, also known as an oxidation process in a stage of gasification, was developed. The kinetic parameter study was the main key for this development. This study was initiated with the work on coal particle combustion conducted by *Blaid et al.* [93], and the variety of kinetic parameter values provided in the study conducted by *Zogala* [53]. This study was successful in developing the model of coal combustion.

The suit of set kinetic parameter values to perform a proper evaluation of coal particle combustion was identified through the validation procedures. From this investigation, it was identified that the char with exothermic reactions (R2 and R3) had a significant role in carrying the suit particle burn out time and maximum temperature in good agreement with the experimental results conducted by *Levendis et al.* [105].

The study of kinetic parameters for coal particle combustion performance also identified the combustion behaviour of two different coal types; bituminous (PSOC 1451) and lignite (PSOC 1443). Their differences were identified through the study of kinetic parameters of devolatilization reaction. For the co-efficient rate of the devolatilization reaction, the lignite coal has a higher value than the bituminous coal, and therefore their ignition delay time is shorter. This is in agreement with the experiment conducted by *Khatami et al.* [106].

In Chapter 5, the coal particle gasification performance was developed. The study of kinetic parameters was conducted mostly for homogeneous reactions. The model simulation was carried out to distinguish between the coal combustion and gasification. This identification is in agreement with the study conducted by *Yoshiie et l.* [136] and through the performance of coal gasification simulation, the importance of char and oxygen control in the gasification reactions was identified.

The reactions' behaviour was provided through the performance of syngas productions. The simulation results have identified the syngas productions at each reactions zone. Gas CO and CO₂ were dominant in the oxidation zone reactions, while H₂ was dominant in the reduction zone reactions. The effects of particle size and reactor temperatures were also identified to provide the information for the better gasification products obtained.

Various environments for reactions were also provided in the reactor and a simulation was performed to investigate their effect on the syngas productions. The addition of steam (H₂O), potentially to increase the H₂ productions, was in agreement with the results stated by *Kuiper et al.* [71], while, the additional CO₂ potentially increased the H₂ and CO productions. However, the addition of H₂O and CO₂ into the reactor could decrease the temperature of the coal particle.

In Chapter 6, the experiment with coal particles in the reactor bed was performed. The effect of porosity was investigated by varying the particle size on each bed reaction performance. The results indicated that the porosity has an important role in delivering the oxygen to the surface of the coal for the reaction process which is in agreement with *Bhutto et al.* [5]. Greater porosity means more pores can be passed by the oxygen to reach the coal surface. Therefore, the coal with greater porosity has more gas productions than the others.

Experiments of coal particle bed reactions in various temperatures of reactor were also carried out. The temperature helped the reactions to perform better and therefore more gas products were obtained at the higher temperature. In the UCG application, there are some important reactions for producing syngas and they were identified as endothermic reactions. These reactions need heat to perform and also caused a decrease in temperature reactions. Therefore, the higher temperature at the oxidation zone would be better for gasification reactions.

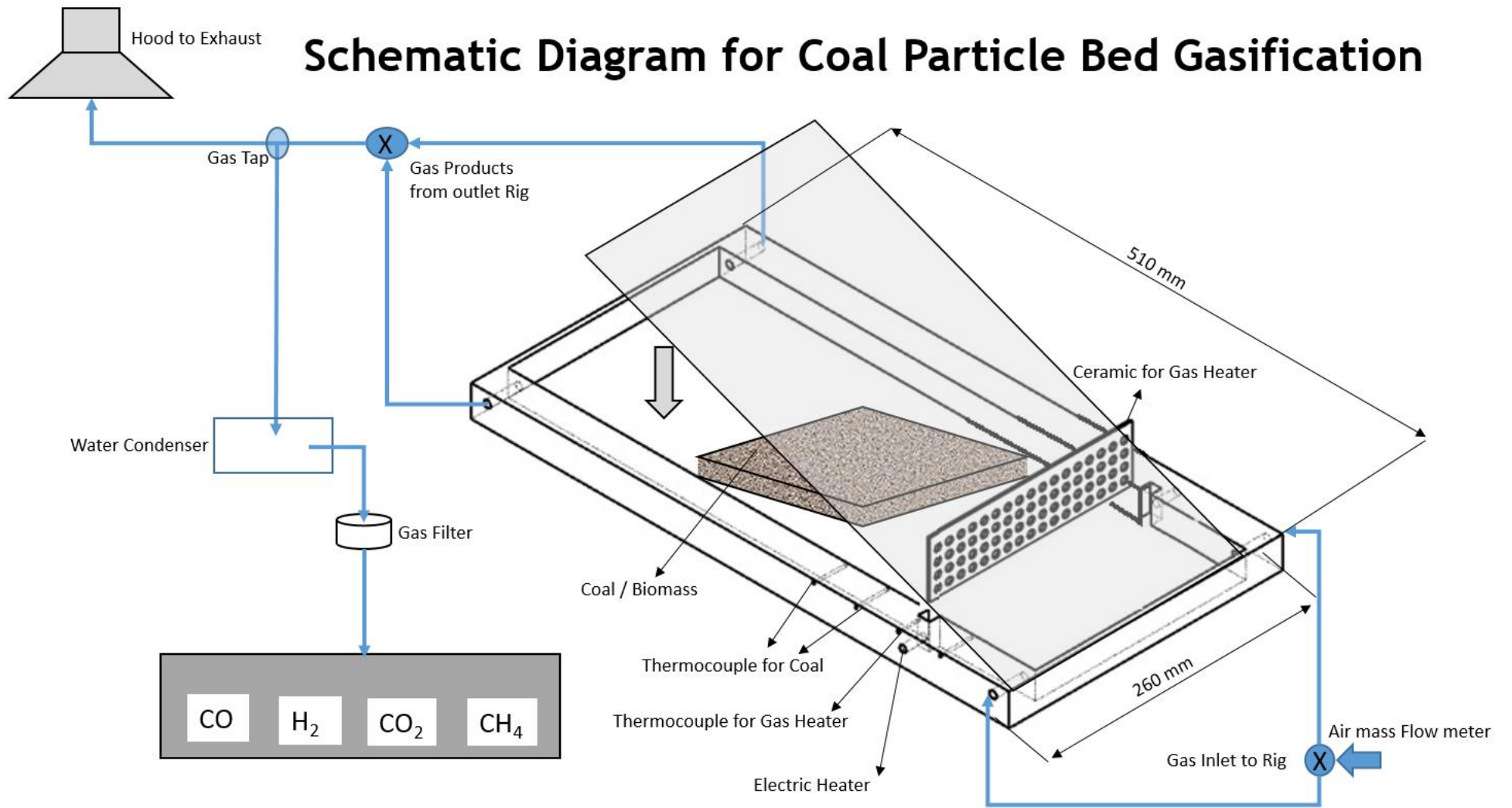
Another set of experiments was conducted to identify the effect of the flow rate of gas injection. The gas injection as an agent of gasification was needed in order to continuously maintain the coal reactions. In one of the linking methods for UCG application Forward Combustion Linking (FCL) was used because a higher pressure of gas injection was needed to make the gas reach further into the coal stock [21]. This is because the coal stocks in the UCG application, over time, move downstream. Therefore, a higher pressure of gas injection was needed to reach the coal stock. However, the experiments indicated that a higher flow rate was obtained in the greater area of coal surface reactions and there was also a higher concentration of gas products.

7.2 Recommendations for future work

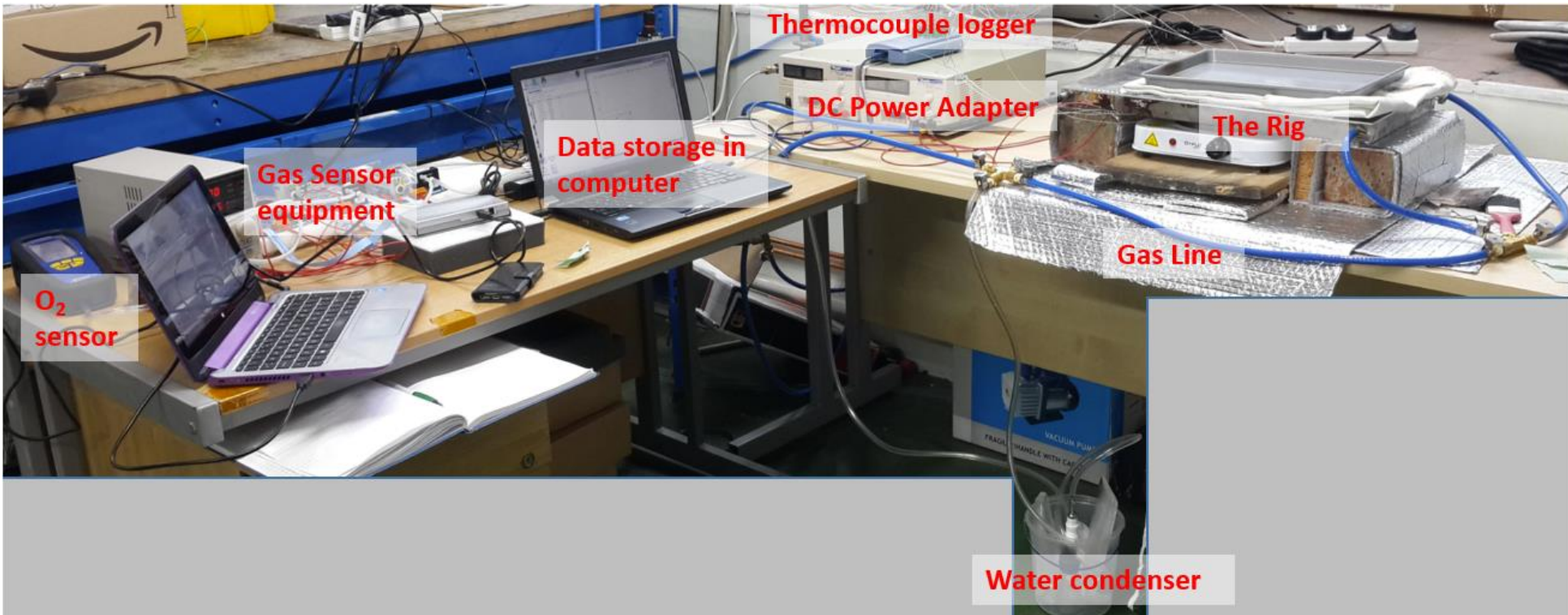
The coal particle gasification model was developed and performed to identify the reactions' behaviour. The model could potentially be developed further with a scope to examine the coal particle gasification performance while the gas flows in the reactor. For this, a coal particles' simulation needs to be carried out as a block so the reaction processes are studied more closely in seam coal environment for UCG application. Therefore, this study recommends the following research scopes and work to be possibly conducted in future:

- The development of a coal block model that will consist of particles packed.
- Applying the gasification reactions developed in the study into the particle block, to investigate the gasification performance further.
- Further development of coal particle gasification through experimental performance, allowing the further validation and study between the coal particle block modelling and experiment.

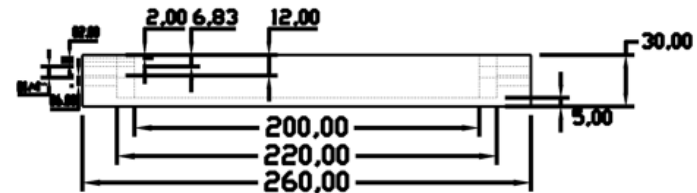
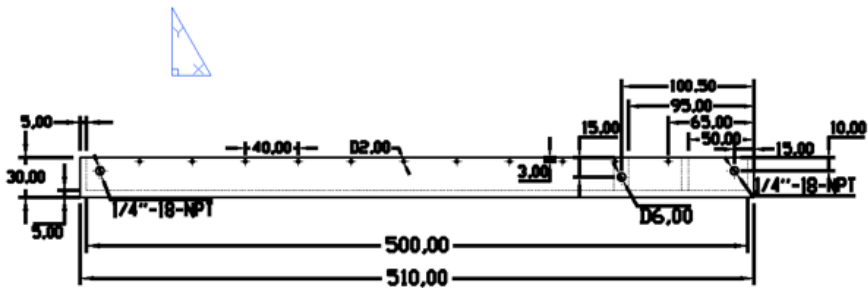
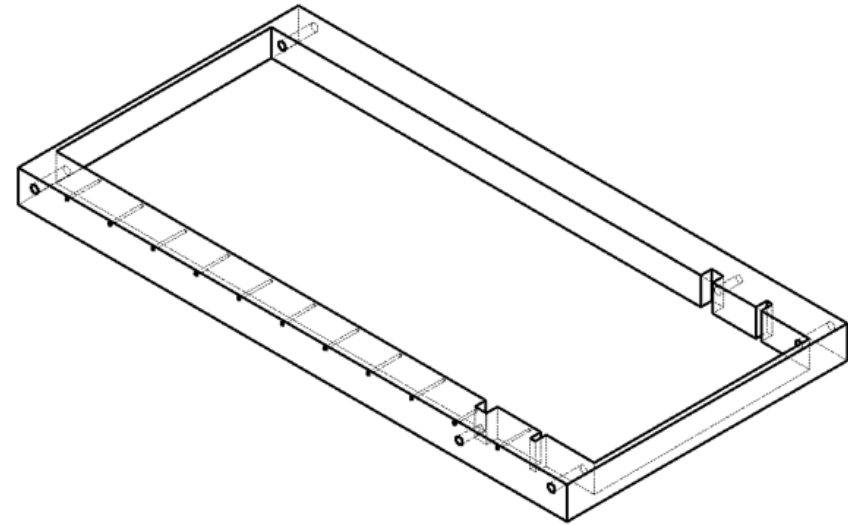
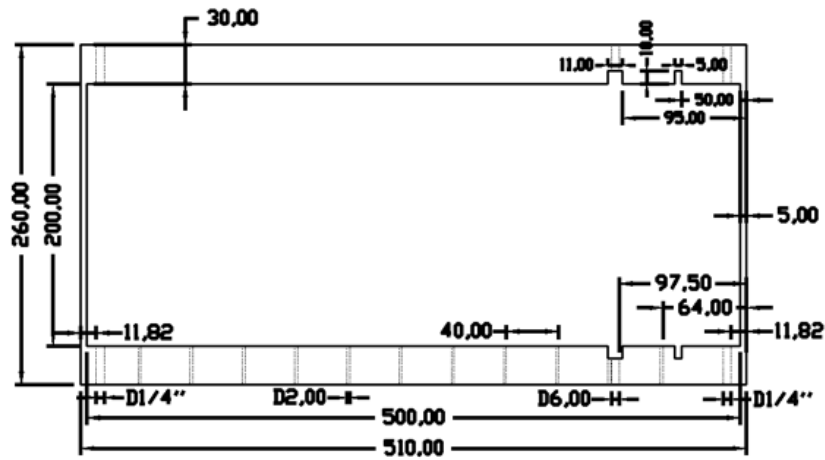
Appendix A Equipment and Instruments

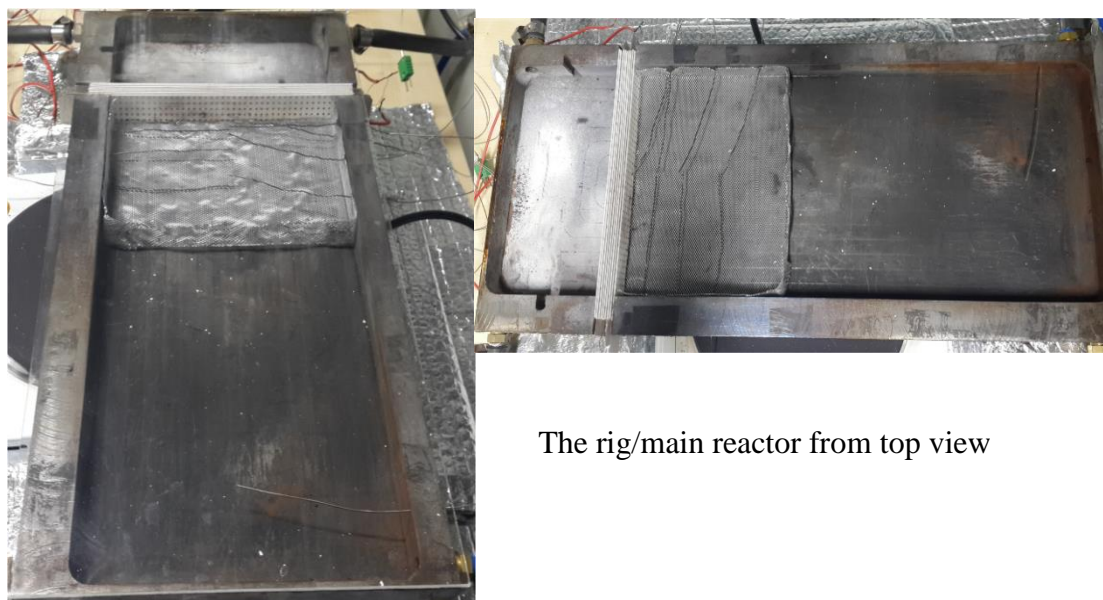


The Equipment assembly



Design for the main Rig/Reactor





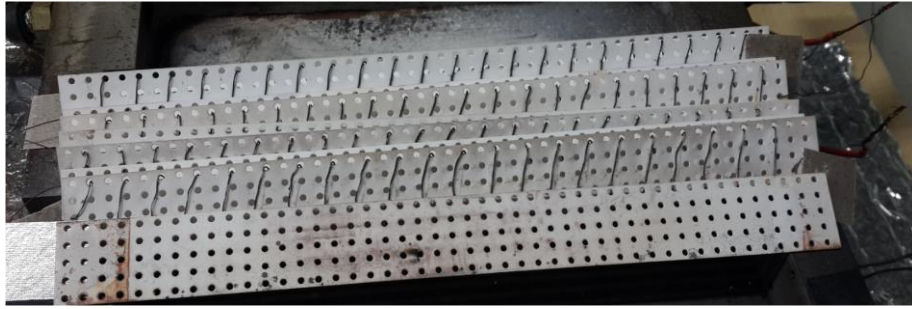
The rig/main reactor from top view



The rig during performance test without additional heater



The rig during performance test, and with external heater



Ceramic and heater wire with the specification as seen in the figure



DC Power Supply, (Rapid-85-1706) (2 unit)

Output 0 - 30 V ; 5V with 500 mA ; and 12 V with 500 mA



Anton Sprint V1 Combustion Analyser,
Oxygen sensor 0 -25%, Callibrated due 13/06/2019



Gas Flowmeter controller, (Alicat Scientific)

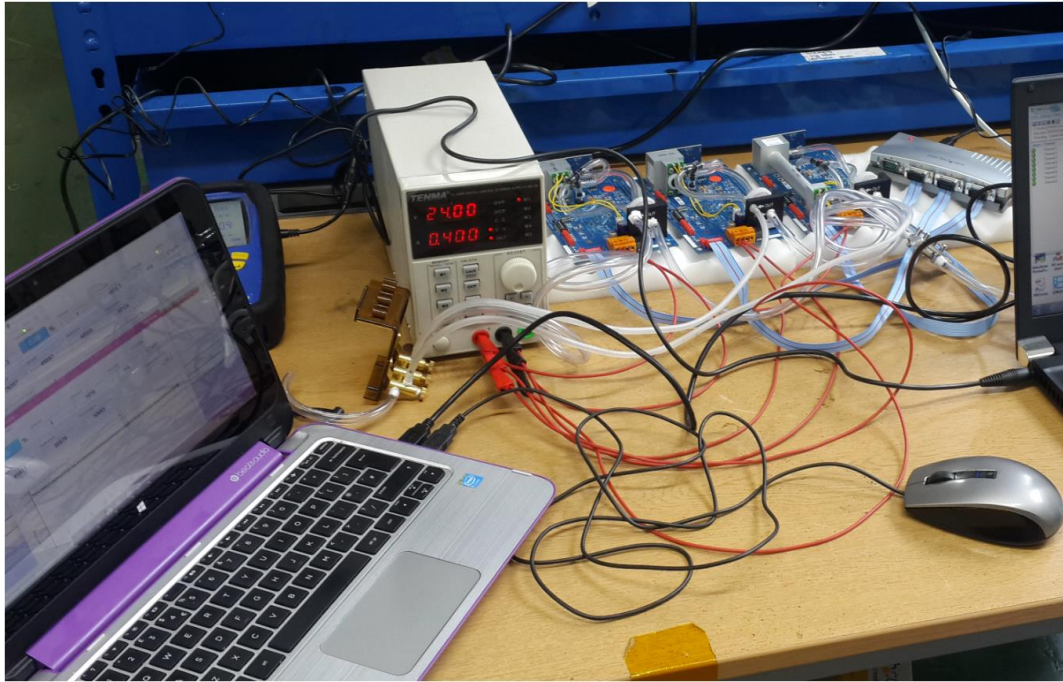
Flow 0 – 20slpm



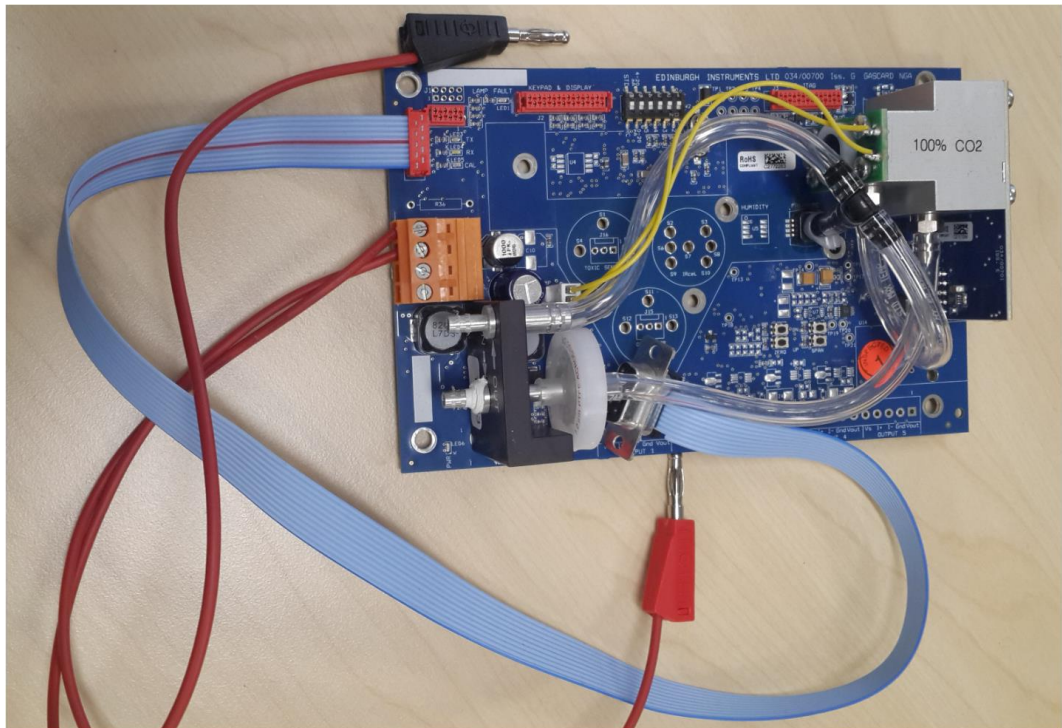
Thermocouple Type K

Temperature data Logger (Picolog - TC 08)
8 miniature input, with USB cable data

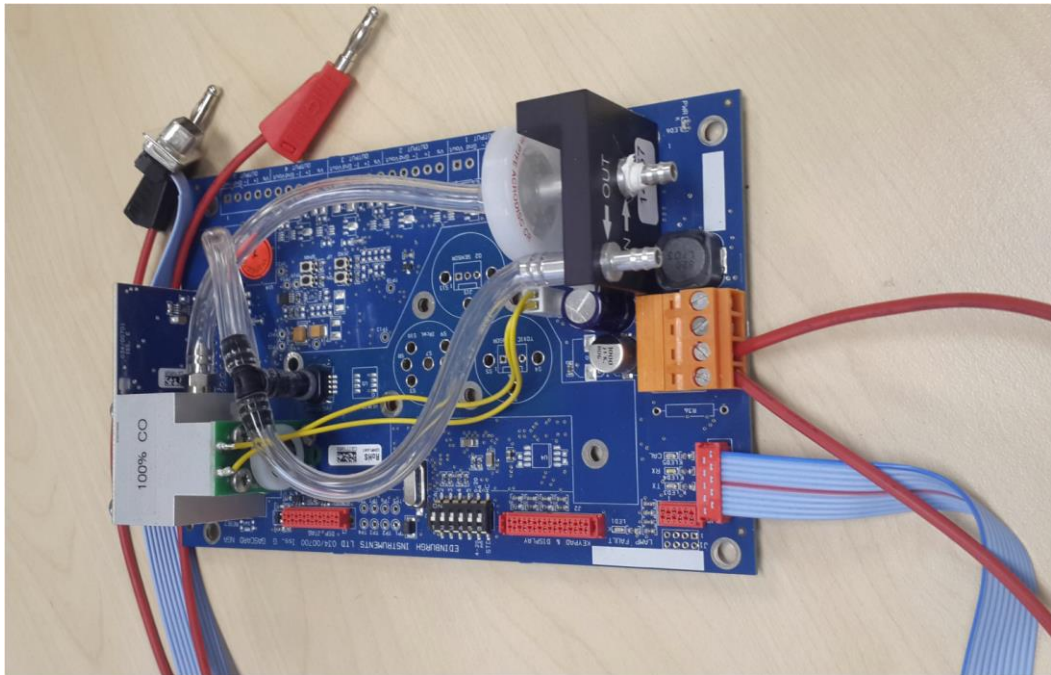
Fire blanket



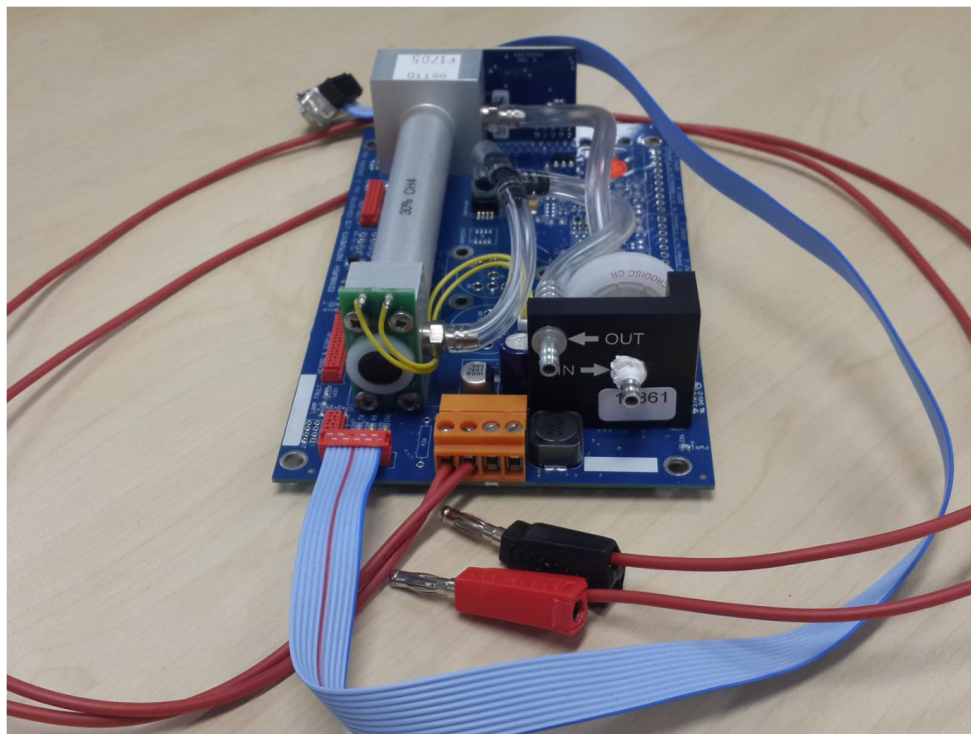
Gas Sensor and logging system



Gas Card NG for CO₂ (S197760-S) with range 0 - 100%, Accuracy 2%
RS232 NG Cable (S75212-S), 10 way micro match, 10 way ribbon, & 9 way IDC



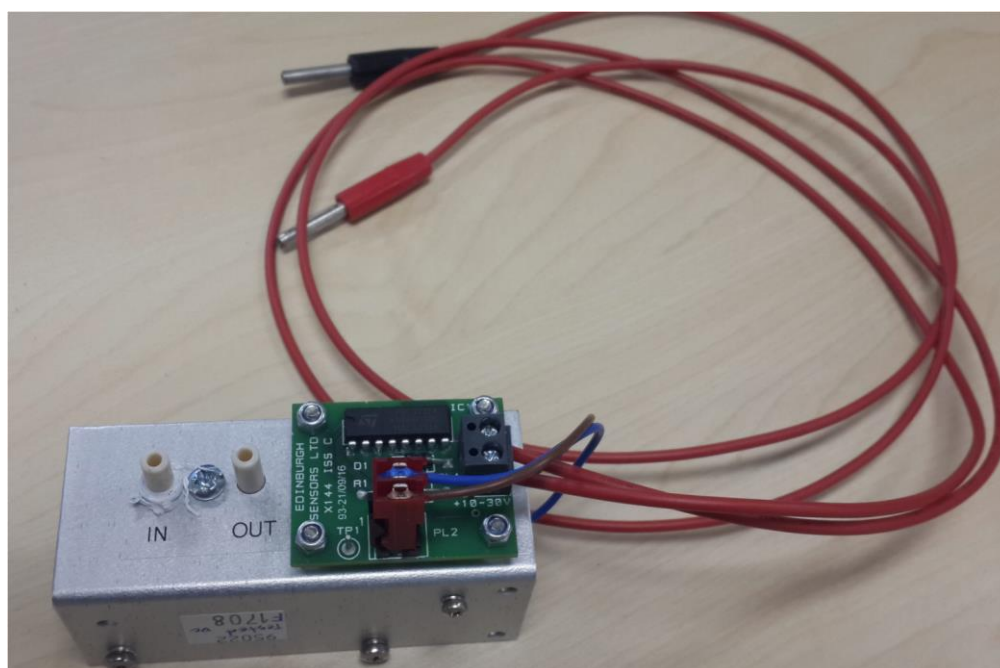
Gas Card NG for CO (S197902-s), with range 0 - 100%, Accuracy 2%
RS232 NG Cable (S75212-S), 10 way micro match, 10 way ribbon, & 9 way IDC



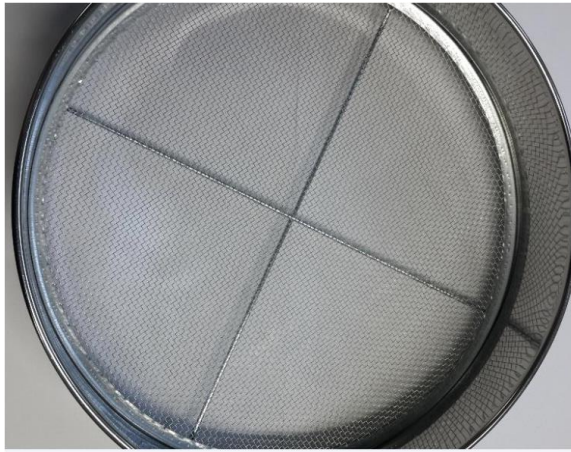
Gas Card NG for CH4 (S197850-s), with range 0 - 30%, Accuracy 2%
RS232 NG Cable (S75212-S), 10 way micro match, 10 way ribbon, & 9 way IDC



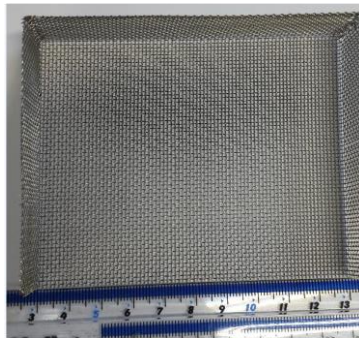
Data hub for gas card, 4 port, RS232 to USB



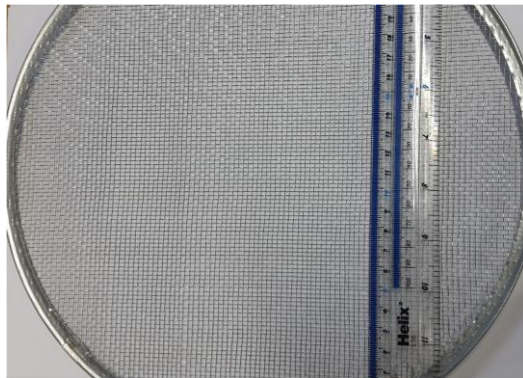
Gas card 24v dc pump (S95022-S), flow rate 1 lpm



Coal Sieve



Screen 1 x 1 mm²



Screen 2 x 2 mm²



Screen 4 x 4 mm²

Appendix B Microanalysis

MICROANALYSIS

90747

Name: TATA SUTARDI		Dept./Room No.	
Sample No. 1		Telephone:	
Elements Present: Char Coal		Stable Hygroscopic M.P. >100°C Toxic	
Elements Required: C-H-O-N		Supervisor: Dr. Manosh C. Paul	
Molecular Formula:		Other Comments:	
Element	Result	Theory	
C	66.21 65-95		
H	3.00 2.89		
N	1.04 0.98		

E-Mail: t.sutardi.1@research.gla.ac.uk

NOTE 1. Please ensure that all samples are completely free of solvent and moisture.

Bibliography

- [1] World Energy Council, 2013 "*World Energy Resource - 2013 Survey*," in *Report - Survey*. pp. 1-2.
- [2] BP, 2017 "*World Energy 2017*," in *BP Statistical Review*. p. 36.
- [3] DOE/EIA, 2016 "*International Energy Outlook 2016*," in *US Energy Information Administration*. vol. 0484. pp. 61-78.
- [4] Dongmin Yang, Yong Sheng, and Michael Green, 2014 "*UCG: Where in the world*," in *The Chemical Engineer (872)*. vol. 38-41.ISSN 0302-0797. pp. 38-41.
- [5] Abdul Waheed Bhutto, Aqeel Ahmed Bazmi, and Gholamreza Zahedi, 2013 "*Underground coal gasification: From fundamentals to applications*," in *Progress in Energy and Combustion Science*. vol. 39. pp. 189-214.
- [6] Dongmin Yang, Nikolaos Koukouzas, Michael Green, and Yong Sheng, 2015 "*Recent Development on Underground Coal Gasification and Subsequent CO₂ Storage*," in *Journal of the Energy Institute* vol. 89 (4). pp. 469-484.
- [7] Alexander Y. Klimenko, 2009 "*Early Ideas in Underground Coal Gasification and Their Evolution*," in *Energies*. vol. 2. pp. 456-476.
- [8] Harish Kumar RN, Devamanokar Lakshmanan Udayakumar, Alex Stojcevski, and Amanuallah Maung Than O, 2014 "*Underground Coal Gasification: an alternate Economical and Viable Solution for future Sustainability*," in *International Journal of Engineering Science Invention*. vol. 3. pp. 57-68.
- [9] Md M. Khan, Joseph P. Mmbaga, Ahad S. Shirazi, Japan Trivedi, Qingxia Liu, and Rajender Gupta, 2015 "*Modelling Underground Coal Gasification—A Review*," in *Energies*. vol. 8. pp. 12603-12668.
- [10] E Burton, J Friedmann, and R Upadhye., 2007 "*Best Practices in Underground Coal Gasification*," in *Lawrence Livermore National Laboratory, University of California, Draft*.
- [11] J.J. Nitao, D.W. Camp, T.A. Buscheck, J.A. White, G.C. Burton, J.L. Wagoner, et al., 2011 "*Progress on a new integrated 3-D UCG simulator and its initial application*," in *In: Proc. Int. Pittsburgh Coal Conf., Pittsburgh, September*. pp. LLNL-CONF-50055.
- [12] Yuteng Xiao, Jihang Yin, Yifan Hu, Junzhe Wang, Hongsheng Yin, and Honggang Qi, 2019 "*Monitoring and Control in Underground Coal Gasification: Current Research Status and Future Perspective*," in *Sustainability*. vol. 11. p. 217.
- [13] Dongmin Yang, Nikolaos Koukouzas, Michael Green, and Yong Sheng, 2015 "*Recent Development on Underground Coal Gasification and Subsequent CO₂ Storage*," in *Journal of the energy institute*. vol. 89(4). pp. 469-484.
- [14] CouchG, 2009 "*Underground coal gasification. London, United Kingdom*," in *IEA Clean Coal Centre, Report*. p. Contract No.:CCC/151.
- [15] Cluff Natural Resources Plc, 2015 "*Economic Impact Assessment of UCG*," in *Report : Index: AIM*. p. Epic: CLNR / Sector: Natural Resources.
- [16] Fei Mao, 2016 "*Underground coal gasification (UCG): A new trend of supply-side economics of fossil fuels*," in *Natural Gas Industry B*. vol. 3. pp. 312-322.

- [17] Company Eskom Holding Limited, 2016 "*UCG – Eskom's Experience and Future Projects*," in *Presentation in SAUCGA Workshop*. p. 2.
- [18] S. Pershad, M. van der Riet, J. Brand, J. van Dyk, D. Love, J. Feris, *et al.*, 2018 "*SAUCGA: The potential, role, and development of underground coal gasification in South Africa*," in *The Journal of the Southern African Institute of Mining and Metallurgy*. vol. 118. pp. 1-12.
- [19] Greg Perkins and Veena Sahajwalla, 2005 "*A Mathematical Model for the Chemical Reaction of a Semi-infinite Block of Coal in Underground Coal Gasification*," in *Energy & Fuels*. vol. 19. pp. 1679-1692.
- [20] Ltd Portman Energy, 2012 "*UCG - the 3rd way : Lower Capex, Smaller Footprint and Higher Productivity*," in *Presentation*. pp. 1-8.
- [21] M. S. Blinderman, D. N. Saulov, and A. Y. Klimenko, 2008 "*Forward and reverse combustion linking in underground coal gasification*," in *Energy*. vol. 33. pp. 446-454.
- [22] Hill RW, 1981 "*Burn Cavity Growth during the Hoe Creek No. 3 Underground Coal Gasification Experiment*," in *Report of US - DOE*. pp. No. UCRL-85173, .
- [23] CB Thorsness, RW Hill, and JA Britten, 1988 "*Execution and performance of the CRIP process during the rocky mountain I UCG field test.*," in *CA: Lawrence, Livermore National Laboratory (LLNL) Report*. pp. Contract No.: UCRL-98641.
- [24] L. Yang, 2003 "*Clean coal technology—Study on the pilot project experiment of underground coal gasification*," in *Energy*. vol. 28. pp. 1445-1460.
- [25] The National Mining Association, 1995 "*Facts about Coal*."
- [26] RY Wu, 1988 "*Coal gasification*," in *Xuzhou: China University of Mining and Technology Press*. pp. 68-73.
- [27] H Wang, BZ Dlugogorski, and EM Kennedy, 2003 "*Coal oxidation at low temperatures: oxygen consumption, oxidation products, reaction mechanism and kinetic modelling*," in *Progress in Energy and Combustion Science*. vol. 29(6). pp. 487-513.
- [28] Yang LH and Song DY., 2001 "*Study on the method of seepage combustion in underground coal gasification*," in *Xuzhou, China: China University of Mining and Technology Press*. pp. 61-63.
- [29] LH Yang, 2008 "*A review of the factors influencing the physicochemical characteristics of underground coal gasification*," in *Energy Sources, Part A: Recovery, Utilization, and Environmental Effects*. vol. 30(11). pp. 1038-1049.
- [30] Krzysztof Stańczyk, Krzysztof Kapusta, Marian Wiatowski, Jerzy Świądrowski, Adam Smoliński, Jan Rogut, *et al.*, 2012 "*Experimental simulation of hard coal underground gasification for hydrogen production*," in *Fuel*. vol. 91. pp. 40-50.
- [31] L Yang, 2008 "*Coal properties and system operating parameters for underground coal gasification*," in *Energy Sources, Part A: Recovery, Utilization, and Environmental Effects*. vol. 30(6). pp. 516-528.
- [32] LH Yang, X Zhang, and S Liu, 2009 "*Characteristics of temperature field during the oxygen-enriched underground coal gasification in steep seams*," in *Energy Sources, Part A: Recovery, Utilization, and Environmental Effects*. vol. 32(4). pp. 384-393.
- [33] L Yu and SQ Liu, 2003 "*Thoughts on commercialization of the LLTS-UCG new technique*," in *Journal of Science & Technology Review*. pp. 2-51.
- [34] SQ Liu, J Liang, and L Yu, 2000 "*Reaction character and influence factor of CO₂ in underground coal gasification.*," in *Journal of China University of Mining and Technology*. vol. 29. p. 606.

- [35] L Yang, 2003 "Model and calculation of dry distillation gas movement in the process of underground coal gasification," in *Numerical Heat Transfer, Part B: Fundamentals*. vol. 43(6). pp. 587-604.
- [36] GW Paul, 1999 "Simulation on the methane storage in the coal layer," in *Coal Layer Gas*. vol. 4. p. 76.
- [37] X Wang, H Wang, and MH Shi, 2001 "Study on the coupling effect in the process of the quick drying of porous media," in *Journal of Engineering Thermophysics 2001*. vol. 22. p. 344.
- [38] GR King and TM Ertekin, 2000 "Review of methane-related mathematical models (part one): experiment and the model on balanced absorption," in *Coal Layer Gas*. vol. 25. p. 13.
- [39] Alina Zogala, 2014 "Critical analysis of underground coal gasification models. Part I: equilibrium models – literary studies," in *Journal of Sustainable Mining*,. vol. 13(1). pp. 22–28.
- [40] Marcio L. de Souza-Santos, 2004 "Solid Fuels Combustion and Gasification," in *Textbook and Reference Books*.
- [41] Lanhe Yang, 2003 "Study on the model experiment and numerical simulation for underground coal gasification," in *Fuel*. vol. 83. pp. 573-584.
- [42] G Perkins and V Sahajwalla, 2006 "A numerical study of the effects of operating conditions and coal properties on cavity growth in underground coal gasification," in *Energy & Fuels*. vol. 20(2). pp. 596-608.
- [43] P. Basu, 2010 "Biomass Gasification and Pyrolysis: Practical Design and Theory," in *Elsevier*.
- [44] Ftwi Yohaness Hagos, Abd Rashid Abd Aziz, Shaharin A. Sulaiman, and Bahaaddein K. M. Mahgoub, 2016 "Low and Medium Calorific Value Gasification Gas Combustion in IC Engines," in *INTECH*. pp. 234-264.
- [45] Zhang X Yang LH, Liu S, 2009 "Underground Coal Gasification Using Oxygen and Steam," in *Energy source, part A ; Recovery, Utilization and Environmental Effect*. vol. 31(20). pp. 1883-1892.
- [46] DN Saulov, OA Plumb, and AY Klimenko, 2010 "Flame propagation in a gasification channel.," in *Energy*. vol. 35(3). pp. 1264-1273.
- [47] TF Wall, G-S Liu, H-W Wu, DG Roberts, KR Benfell, and S Gupta, 2002 "The effects of pressure on coal reactions during pulverised coal combustion and gasification," in *Progress in Energy and Combustion Science*. vol. 28(5). pp. 405-433.
- [48] Lanhe Yang, 2004 "Three-dimensional non-linear numerical analysis on the oxygen concentration field in underground coal gasification," in *Fuel Processing Technology*. vol. 85. pp. 1605-1622.
- [49] R.D. Gunn and W.B. Krantz, 1987 "Underground Coal Gasification: Development of Theory, Laboratory Experimentation, Interpretation, & Correlation with the Hanna Field Tests," in *Final report; U.S. Department of Energy: Morgantown, WV, USA*.
- [50] LK Walker, 2007 "Commercial development of underground coal gasification," in *Proceedings of the Institution of Civil Engineers (ICE)-Energy 2007*. vol. 160(4). pp. 175-180.
- [51] R.D. Gunn, 1977 "Problem Solved and Problem not Solved in UCG," in *Laramie Energy Research Center, Laramie, Wyoming. Preprints of Papers—American Chemical Society. Div. Fuel Chem. 1977*. vol. 22. pp. 64–75.
- [52] Ali Arshad Uppal, Aamer Iqbal Bhattib, Erum Aamirb, Raza Samarb, and Shahid Ahmed Khana, 2014 "Control oriented modeling and optimization of one

- dimensional packed bed model of underground coal gasification," in Journal of Process Control. vol. 24(2014). pp. 269-277.*
- [53] Alina Zogala, 2014 "Critical Analysis of Underground Coal Gasification Models. Part II: Kinetic and Computational Fluid Dynamics Models," in *Journal of Sustainable Mining. vol. 13(1). pp. 29-37.*
- [54] Alina Żogała and Tomasz Janoszek, 2015 "CFD simulations of influence of steam in gasification agent on parameters of UCG process," in *Journal of Sustainable Mining. vol. 14. pp. 2-11.*
- [55] G.H. Higgins, 1976 "A New Concept for in-Situ Coal Gasification," in *Report No. UCRL-51217; Lawrence Livermore National Laboratory: Livermore, CA, USA, 1976.*
- [56] C.B. Thorsness and R.B. Rosza, 1976 "In-Situ Coal Gasification Program: Model Calculations and Laboratory Experiments," in *Report No. UCRL-78302; Lawrence Livermore National Laboratory: Livermore, CA, USA.*
- [57] B. Dinsmoor, J.M. Galland, and T.F. Edgar, 1978 "The Modeling of Cavity Formation during Underground Coal Gasification.," in *J. Petroleum Technol. 1978. vol. 30. pp. 695-704.*
- [58] A.N. Khadse, M. Qayyumi, S. Mahajani, and P. Aghalayam, 2006 "Model for the Underground Coal Gasification (UCG) Channel Reactor," in *Int. J. Chem. React. Eng. 2006. vol. 4. pp. 1-25.*
- [59] M.J. Shannon, C.B. Thorsness, and R.W. Hill, 1980 "Early Cavity Growth During Forward Burn," in *Report No. UCRL-84584.*
- [60] A. M. Winslow, 1976 "Numerical Model of Coal Gasification in a Packed Bed," in *Report No. UCRL-77627.*
- [61] C.B. Thorsness, E.A. Grens, and A.A. Sherwood, 1978 "One Dimensional Model for in Situ Coal Gasification," in *Report No. UCRL-52523; Lawrence Livermore National Laboratory: Livermore, CA, USA.*
- [62] C.B. Thorsness, S.W. Kang, and Lawrence, 1985 "Further Development of a General-Purpose Packed Bed Mode for Analysis of UCG Process," in *Report No. UCRL-92489, Lawrence Livermore National Laboratory: Berkeley, CA, USA.*
- [63] A.A. Abdel-Hadi Eed and Hsu T.R., 1987 "Computer Modeling of Fixed Bed Underground Coal Gasification Using the Permeation Method.," in *J. Energy Resour. Tech. 1987. vol. 109. pp. 11-20.*
- [64] D.W. Gregg and T.G. Edgar, 1978 "Underground Coal Gasification," in *AIChE J. vol. 24. pp. 753-781.*
- [65] W.D. Batenburg, N.J. Biezen, and J. Bruining, 1994 "A New Channel Model for Underground Coal Gasification of Thin, Deep Coal Seams," in *In Situ 1994. vol. 18. pp. 419-451.*
- [66] R.A. Kuyper, T.H. van der Meer, and J. Bruining, 1996 "Simulation of Underground Gasification of Thin Coal Seams," in *In Situ 1996. vol. 20. pp. 311-346.*
- [67] S.Y. Schwartz, T.L. Eddy, K.H. Mehta, S.A Lutz, and M.B. Binaie-Kondoloyj, 1978 "Cavity growth mechanisms in UCG with side wall burn gasification," in *In Proceedings of the SPE Annual Fall Technical Conference and Exhibition, Houston, TX, USA, 1-3 October 1978.*
- [68] T.L. Eddy and S.H. Schwartz, 1983 "A Side Wall Burn Model for Cavity Growth in Underground Coal Gasification," in *J. Energy Resour. Tech. 1983. vol. 105. pp. 145-156.*
- [69] Y. Luo, M. Coertzen, and S. Dumble, 2009 "Comparison of UCG Cavity Growth with CFD model predictions," in *In Proceedings of the 7th International*

- Conference on CFD in the Minerals and Process Industries CSIRO, Melbourne, Australia, 9–11 December 2009.*
- [70] P. Pirlot, J.P. Pirard, A. Coeme, and M.A. Mostade, 1998 "Coupling of Chemical Processes and Flow in View of the Cavity Growth Simulation of an Underground Coal Gasifier at Great Depth," in *In Situ* 1998. vol. 22. pp. 141–156.
- [71] R.A. Kuyper, T.H. van der Meer, and C.J. Hoogendoorn, 1994 "Turbulent Natural Convection Flow due to Combined Buoyancy Forces during Underground Coal Gasification of Thin Seams," in *Chem. Eng. Sci.* 1994. vol. 49. pp. 851–861.
- [72] G. Perkins and V. Sahajwalla, 2007 "Modelling of Heat and Mass Transport Phenomena and Chemical Reaction in Underground Coal Gasification," in *Chem. Eng. Res. Des.* 2007. vol. 85. pp. 329–343.
- [73] T.H.T. Tsang, 1980 "Modeling of Heat and Mass Transfer during Coal Block Gasification," in *Ph.D. Thesis, University of Texas at Austin, Austin, TX, USA.*
- [74] J.G.M. Massaquoi and J.B. Riggs, 1983 "Mathematical Modeling of Combustion and Gasification of a Wet Coal Slab—I: Model Development and Verification," in *Chem. Eng. Sci.* 1983. vol. 38. pp. 1747–1756.
- [75] J.G.M. Massaquoi and J.B. Riggs, 1983 "Mathematical Modeling of Combustion and Gasification of a Wet Coal Slab—II: Mode of Combustion, Steady State Multiplicities and Extinction," in *Chem. Eng. Sci.* 1983. vol. 38. pp. 1757–1766.
- [76] T.A. Wellborn, 1981 "Linear Burning Rates of Texas Lignite," in *Master's Thesis, University of Texas, Austin, TX, USA, 1981.*
- [77] T.H. Tsang and T.F. Edgar, 1983 "Modeling of Drying and Pyrolysis during Underground Coal Gasification—I," in *In Situ* 1983. vol. 7. pp. 237–264.
- [78] S.J. Hsia, T.A. Wellborn, and T.F. Edgar, 1978 "Measurement of Combustion Rates of Texas Lignite with Application to Underground Coal Gasification," in *In Proceedings of the Fourth UCC Symposium, CO, USA, 17–20 July 1978.*
- [79] K.Y. Park and T.F. Edgar, 1987 "Modeling of Early Cavity Growth for Underground Coal Gasification," in *Ind. Eng. Chem. Res.* 1987. vol. 6. pp. 237–246.
- [80] Ahad Sarraf Shirazi, Shayan Karimipour, and Rajender Gupta, 2013 "Numerical Simulation and Evaluation of Cavity Growth in In Situ Coal Gasification," in *Industrial & Engineering Chemistry Research.* vol. 52. pp. 11712–11722.
- [81] Tata Sutardi, Manosh C. Paul, and Nader Karimi, 2019 "Investigation of coal particle gasification processes with application leading to underground coal gasification," in *Fuel.* vol. 237. pp. 1186–1202.
- [82] Star-CCM+, Documentation 2018 "Particle Reactions," in <https://documentation.thesteveportal.plm.automation.siemens.com>.
- [83] M. M. BAUM, 1971 "Predicting the Combustion Behaviour of Coal Particles," in *Combustion Science and Technology.* vol. 3. pp. 231–243.
- [84] Oleg Zikanov, 2012. ISBN :978-81-265-3497-5 "Essential Computational Fluid Dynamics," in *Textbook and Reference Books, Wiley-India Edition.*
- [85] H K Versteeg and W Malalasekera, 1995 "An Introduction to Computational Fluid Dynamics," in *A Book of reference, Longman Scientific & Technical.* vol. ISBN 0-582-21884-5.
- [86] Star-CCM+, Documentation 2018 "RANS Turbulence Models," in <https://documentation.thesteveportal.plm.automation.siemens.com/starccmplus/latest/en/index.html#page/STARCCMP%2FGUID-14F1432B-B915-42FE-9862-71D1B53BEA6B%3Den%3D.html%23>.

- [87] T. J. Coakley, 1983 "Turbulence modeling methods for the compressible Navier-Stokes equations," in *16th AIAA fluid and plasma dynamics conference*, Danvers, MA,.
- [88] S. Peng, L. Davidson, and S. Holmberg, 1997 "A modified low-reynolds number $k-\omega$ model for recirculating flows," in *Journal of Fluids Engineering*. 1997. vol. (119):4. pp. 867-875.
- [89] S. Zeierman and M. Wolfshtein, 1986 "Turbulent time scale for turbulent flow calculations," in *AIAA Journal*. 1986. vol. (24):10. pp. 1606-1610.
- [90] B. E. Launder and D. B. Spalding . 1972 "Lectures in Mathematical Models of Turbulence," in *Academic Press, London, England, 1972*.
- [91] D. C. Wilcox, 1998 "Turbulence Modeling for CFD," in *DCW Industries, Inc., La Canada, California, 1998*.
- [92] J. O. Hinze, 1975 "Turbulence," in *McGraw-Hill Publishing Co., New York, 1975*.
- [93] Blaid Alganash, Manosh C. Paul, and Ian A. Watson, 2015 "Numerical investigation of the heterogeneous combustion processes of solid fuels," in *Fuel*. vol. 141. pp. 236-249.
- [94] V. Yakhot and S. A. Orszag, 1986 "Renormalization Group Analysis of Turbulence: I. Basic Theory," in *Journal of Scientific Computing*. 1986. vol. (1):1. pp. 1-51.
- [95] T. H. Shih, W. W. Liou, A. Shabbir, Z. Yang, and J. Zhu, 1995 "A new $k-\epsilon$ eddy-viscosity model for high reynolds number turbulent flows - model development and validation," in *Computers Fluids*. 1995. vol. (24):3. pp. 227-238.
- [96] T.-H. Shih, Liou, W.W., Shabbir, A., Yang, Z. and Zhu, J., 1994 "A New $k-\epsilon$ Eddy Viscosity Model for High Reynolds Number Turbulent Flows -- Model Development and Validation," in *NASA TM 106721*.
- [97] Star-CCM+, Documentation 2018 "Thermal Radiation," in https://documentation.thesteveportal.plm.automation.siemens.com/starccmplus/latest_en/index.html#page/STARCCMP/GUID-58217E9D-AAF2-4BEC-BFEE-B6C6D242AE29=en.html#wwID0EIJNYC.
- [98] W. P. Jones and M. C. Paul, 2005 "Combination of DOM with LES in a gas turbine combustor," in *International Journal of Engineering Science*. vol. 43. pp. 379-397.
- [99] S. C. Paul and Manosh C Paul, 2010 "Radiative heat transfer during turbulent combustion process," in *International Communications in Heat and Mass Transfer*. vol. 37. pp. 1-6.
- [100] Star-CCM+, Documentation 2018 "Reacting Flow," in https://documentation.thesteveportal.plm.automation.siemens.com/starccmplus/latest_en/index.html#page/STARCCMP%2FGUID-F057047C-0E4F-4E91-8A1C-DAB17F993E95%3Den%3D.html%23.
- [101] STAR-CCM+, Documentation 2018 "Reaction-Species Transport-Eddy Break-Up," in https://documentation.thesteveportal.plm.automation.siemens.com/starccmplus/latest_en/index.html#page/STARCCMP/GUID-D427B894-CFEE-4C43-A850-498FF878F086=en.html.
- [102] Rajesh Rawat Piyush Thakre, 2010 "Setting up Coal Combustion in STARCCM+5.04."
- [103] Linwei Wang, Nader Karimi, and Manosh C Paul, 2018 "Gas-phase transport and entropy generation during transient combustion of a single biomass particle

- in varying oxygen and nitrogen atmospheres," in International Journal of Hydrogen Energy.* vol. 43(17). pp. 8506-8523.
- [104] Linwei Wang, Nader Karimi, Tata Sutardi, and Manosh C. Paul, 2018 "Numerical modelling of unsteady transport and entropy generation in oxy-combustion of single coal particles with varying flow velocities and oxygen concentrations," in *Applied Thermal Engineering.* vol. 144. pp. 147-164.
- [105] Yiannis A. Levendis, Joshi Kulbhusan., Khatami Reza, and Adel F. Sarofim, 2011 "Combustion behavior in air of single particles from three different coal ranks and from sugarcane bagasse," in *Combustion and Flame.* vol. 158. pp. 452-465.
- [106] Reza Khatami, Chris Stivers, Kulbhusan Joshi, Yiannis A. Levendis, and Adel F. Sarofim, 2012 "Combustion behavior of single particles from three different coal ranks and from sugar cane bagasse in O_2/N_2 and O_2/CO_2 atmospheres," in *Combustion and Flame.* vol. 159. pp. 1253-1271.
- [107] Tiziano Maffei, Reza Khatami, Sauro Pierucci, Tiziano Faravelli, Eliseo Ranzi, and Yiannis A. Levendis, 2013 "Experimental and modeling study of single coal particle combustion in O_2/N_2 and Oxy-fuel (O_2/CO_2) atmospheres," in *Combustion and Flame.* vol. 160. pp. 2559-2572.
- [108] Paula A. Bejarano and Yiannis A. Levendis, 2008 "Single-coal-particle combustion in O_2/N_2 and O_2/CO_2 environments," in *Combustion and Flame.* vol. 153. pp. 270-287.
- [109] Reza Khatami and Yiannis A. Levendis, 2011 "On the deduction of single coal particle combustion temperature from three-color optical pyrometry," in *Combustion and Flame.* vol. 158. pp. 1822-1836.
- [110] Javier Ballester and Santiago Jiménez, 2005 "Kinetic parameters for the oxidation of pulverised coal as measured from drop tube tests," in *Combustion and Flame.* vol. 142. pp. 210-222.
- [111] A.M. Carpenter and N.M. Skorupska, 1993 "Coal Combustion— Analysis and Testing," in *IEACR/64, IEA Coal Research, London, 1993.*
- [112] J. Tomeczek, 1992 "Spalanie węgla [Coal combustion]," in *Politechniki Śląskiej.*
- [113] Z.Q. Li, Wei, F., & Jin, Y. , 2003 "Numerical simulation of pulverized coal combustion and NO formation.," in *Chemical Engineering Science.* vol. 58(23-24). pp. 5161–5171.
- [114] E.A. Boiko, & Pachkovskii, S.V.A. , 2004 "Kinetic Model of Thermochemical Transformation of Solid Organic Fuels.," in *Russian Journal of Applied Chemistry.* vol. 77(9). pp. 1547–1555.
- [115] A. Silaen, & Wang, T., 2009 "Comparison of instantaneous, equilibrium, and finite-rate gasification models in an entrained-flow coal gasifier," in *In Proceedings of the 26th International Pittsburgh Coal Conference.* pp. 1–11.
- [116] C.J. Chen, Hung, C.I., & Chen, W.H. , 2012 "Numerical investigation on performance of coal gasification under various injection patterns in an entrained flow gasifier.," in *Applied Energy.* vol. 100. pp. 218–228.
- [117] A. Silaen, & Wang, T. , 2010 "Effect of turbulence and devolatilization models on coal gasification simulation in entrained-flow gasifier.," in *International Journal of Heat and Mass Transfer.* vol. 53(9-10). pp. 2074-2091.
- [118] H. Watanabe, & Otaka, M. , 2006 "Numerical simulation of coal gasification in entrained flow coal gasifier.," in *Fuel.* vol. 85(12-13). pp. 935–943.
- [119] A M Mayers, 1934 "The rate of reduction of carbon dioxide by graphite," in *Am Chem Soc J.* vol. 56. pp. 70–76.

- [120] Williams GC Howard JB, Fine DH. Fine., 1973 "*Kinetics of carbon monoxide oxidation in postflame gases*," in *Proceedings of 14th symposium (Int.) on combustion*. pp. 975–986.
- [121] Reza Khatami, Chris Stivers, and Yiannis A. Leventis, 2012 "*Ignition characteristics of single coal particles from three different ranks in O₂/N₂ and O₂/CO₂ atmospheres*," in *Combustion and Flame*. vol. 159. pp. 3554-3568.
- [122] Star-CCM+, Documentation 2018 "*Lagrangian Multi Phase*," in https://documentation.thesteveportal.plm.automation.siemens.com/starccmplus/latest_en/index.html#page/STARCCMP%2FGUID-93159E9C-B0AF-4A70-BB07-A33DEEF15727%3Den%3D.html%23.
- [123] Robert H.Essenhigh, Mahendra K.Misra, and David W.Shaw, 1989 "*Ignition of coal particles: A review*," in *Combustion and Flame*. vol. 77. pp. 3-30.
- [124] Li Guo, Ming Zhai, Zhentong Wang, Yu Zhang, and Peng Dong, 2018 "*Comparison of bituminous coal and lignite during combustion: Combustion performance, coking and slagging characteristics*," in *Journal of the Energy Institute 2018*.
- [125] Ahmed M. Salem, Umesh Kumar, Ainul Nadirah Izaharuddin, Harnek Dhani, Tata Sutardi, and Manosh C. Paul, 2017 "*Advanced Numerical Methods for the Assessment of Integrated Gasification and CHP Generation Technologies*," in *Coal and Biomass Gasification, Recent Advances and Future Challenges*, De. Santanu et.al (editor), Springer, ISBN: 978-981-10-7334-2. pp. 307-330.
- [126] Philip G. Sweeny, Dana T. Grow, and Donald P. McCollor, 1988 "*Studies On Ignition Of Coal: The Effects Of Rank, Temperature, Volatile Content, And Lithotype*" in *University of North Dakota Energy and Mineral Research Center*. pp. 853-861.
- [127] S Bandyopadhyay and O Bhaduri, 1972 "*Combustion and Flame*." vol. 18. p. 411.
- [128] J.H. Harker and N.S. Mellor, 1986 "*J. Inst. Energy*." vol. 59. p. 154.
- [129] B.C. Young and S. Niksa, 1988 "*Fuel*," in *Fuel*. vol. 67. p. 155.
- [130] D.J. Smoot and P.J. Smith, 1985 "*Coal Combustion and Gasification*," in *The Plenum Chemical Engineering series, New York*.
- [131] Tata Sutardi, Manosh C. Paul, Nader Karimi, and Paul L. Younger, 2017 "*Identifying Kinetic Parameters for Char Combustion of a Single Coal Particle*," in *European Combustion Meeting*. vol. ISBN 978-953-59504-0-0. p. 247.
- [132] Tata Sutardi, Manosh C. Paul, N. Karimi, and P. L. Younger, 2017 "*Numerical Modelling for Process Investigation of a Single Coal Particle Combustion and Gasification*," in *Lecture Notes in Engineering and Computer Science: Proceedings of The World Congress on Engineering 2017, July 5-7, 2017, London, U.K.* pp. 946-951.
- [133] Tata Sutardi, Linwei Wang, Manosh C. Paul, and Nader Karimi, 2018 "*Numerical Simulation Approaches for Modelling a Single Coal Particle Combustion and Gasification*," in *Engineering Letters*. vol. 26:2. p. 09.
- [134] Tata Sutardi, Manosh C. Paul, and Nader Karimi, 2019 "*Investigation of Coal Particle Gasification Process with Application Leading to Underground Coal Gasification*," in *Fuel*. vol. 237. pp. 1186-1202.
- [135] Z. Sun, Wu, J., Wang, Y., Zhang, D. , (2009)"*A kinetic study of CO₂ gasification of a Chinese coal char during combined coal gasification and CH₄ reforming*,"In: *Journal of Fuel Chemistry and Technology*, vol. Vol. 37, No. 4, 2009, pp. 410-415.,

- [136] Ryo Yoshiie, Yukihiro Taya, Taro Ichiyanagi, Yasuaki Ueki, and Ichiro Naruse, 2013 "*Emissions of particles and trace elements from coal gasification*," in *Fuel*. vol. 108. pp. 67-72.
- [137] Wang Z Jing X, Zhang Q, Yu Z, Li C, Huang J, et al., 2013 "*Evaluation of CO₂ gasification reactivity of different coal rank chars by physicochemical properties*," in *Energy Fuels*. vol. 27. pp. 7287–7293.
- [138] Pooya Lahijani, Zainal Alimuddin Zainal, Maedeh Mohammadi, and Abdul Rahman Mohamed, 2015 "*Conversion of the greenhouse gas CO₂ to the fuel gas CO via the Boudouard reaction: A review*," in *Renewable and Sustainable Energy Reviews*. vol. 41. pp. 615-632.
- [139] John H. Campbell, 1978 "*Pyrolysis of subbituminous coal in relation to in-situ coal gasification*," in *Fuel*. vol. 57.
- [140] D. Merrick, 1983 "*Mathematical models of the thermal decomposition of coal: 1. The evolution of volatile matter.*," in *Fuel*. vol. 62(5). pp. 534-539.